Development of New Self-centring Friction-based Damage Avoidant Systems for Earthquake-prone Reinforced Concrete Buildings

Sajad Veismoradi

A thesis submitted to
Auckland University of Technology in fulfilment of the requirements for the degree of Doctor of Philosophy (PhD) in Structural/Earthquake Engineering,

Supervisors:
Dr. Pouyan Zarnani
Prof. Pierre Quenneville

School of Future Environments, Department of Built Environment Engineering Auckland University of Technology (AUT), New Zealand
December 2022

Abstract

The slip friction devices have been investigated and tested in several research studies. Due to the lack of self-centering feature, such dampers might show residual deformation after moderate to severe earthquake actions. To address this shortcoming, self-centering friction-based dampers were introduced that can preserve the advantages of friction damper while introduce self-centering feature to the system. The Resilient Slip Friction Joint (RSFJ) is among the available self-centering devices that combines translational friction sliding with self-centering feature in one compact device and has proven its capability in various structural applications. Inspired by the RSFJ concept, through this study, initially a new self-centering friction damper is introduced named as the Rotational-Resilient Slip Friction Joint that combines the rotational friction with self-centering capability. The Rotational-RSFJ can provide remarkable flexibility in both the damper component design as well as various structural applications. The force-deformation principles of this new damper were provided, along with its numerical verification using finite element analysis. The performance of the damper was experimentally investigated, and the numerical outcomes were validated by the experimental data. The results highlight the damper capability for a stable and repeatable energy dissipation with no requirement for post-event maintenance, than can be utilized for both new design and retrofit purposes.

As the major focus of this study, the possible applications of RSFJ dampers have been investigated for improving the seismic performance of current earthquake-prone buildings (on both local and global levels). As for the local retrofitting, the RSFJ was utilized as a haunch element for strengthening of deficient RC beam-column joints. The proposed system can preserve the benefits of conventional haunch retrofitting system while offering the benefits of RSFJ damper (reliable energy dissipation and recentering force) to weak RC frames. On this basis, a numerical nonlinear model was developed and a design procedure was provided for proper retrofit design of the haunches for beam-column joints of the RC frames. Two beam-column joints (one interior and one exterior) were then selected as a case study for retrofit design and their improved performance demonstrated their enhanced behaviour in terms of energy dissipation, stiffness and strength improvement, along with minimal residual deformation.

As for the global retrofitting of deficient RC frames, the RSFJ-toggle bracing system is introduced and investigated numerically and experimentally. The RSFJ-toggle bracing system can be activated within small drift values of the structure and preserve the frame from excessive damage. Two scaled deficient RC frames representing typical pre-1970s RC moment resisting frames were constructed and tested to investigate the performance of such retrofitting system, as compared to the bare frame. Material testing of the concrete and steel rebars as well as the damper component testing were conducted to gain accurate data for numerical modelling. Recommendations regarding the proper design of various aspects of this retrofitting system were provided in the thesis, including the brace buckling design, instability consideration for the damper, as well as the overall system, connection detailing and gusset plate design requirements. The experimental observations demonstrate the improved behaviour of the frame in terms of energy dissipation and enhanced stiffness and strength for the upgraded RC frame. The numerical model could also capture the behaviour of the system with an acceptable accuracy. As per the findings of this study, the proposed retrofit solution can strengthen the non-ductile RC frames within a limited drift and replace the pinching behaviour of the deficient RC frames with a repeatable reliable semi-flag shape hysteresis performance.

Attestation of Authorship

I hereby declare that this submission is my own work and that, to the best of my knowledge and belief, it contains no material previously published or written by another person (except where explicitly defined in the acknowledgements), nor material which to a substantial extent has been submitted for the award of any other degree or diploma of a university or other institutions of higher learning.

Signature: Sajad Veismoradi

Date: December 2022

Acknowledgement

This study has been financially supported by the Ministry of Business, Innovation and Employment of New Zealand (MBIE). The financial support provided by this institution is greatly appreciated.

I would like to express my deepest respect and gratitude toward my first supervisor, Dr. Pouyan Zarnani for offering me this wonderful PhD opportunity in the first place and all of his continuous help and motivation, during this journey. It was indeed a pleasure and honour for me to work with him and none of these outcomes would have been possible without his mentorship and support. I also learned invaluable lessons from my second supervisor, Prof. Pierre Quenneville, a true gentleman whose guidance helped me throughout this research. Thank you both, for accepting me in your incredible research team, taking me under your wings and teaching me how to fly.

I would like to thank the professional technicians and mentors in AUT structural lab, Dave Croft, Allan Dixon, Andrew Virtue and Stephen Hartley, as well as Dr. sherif beskhyroun and his PhD student, Kelly (Hui) who helped me during the experimental testing and setting up the data acquisition systems.

I am also very grateful to two expert examiners of my thesis, Prof. Marjan Popovski (University of British Columbia, Canada) and Dr. Mustafa Mashal (Idaho State University, United States of America) who devoted their time and carried out the review of my work with patience, enthusiasm and scrutiny. Their valuable feedback and comments have definitely elevated the thesis.

Special thanks to all my friends and colleagues from the AUT PhD office and the university of Auckland, Hamed, Farhad, Mohamad, Kaveh, Nick and Mohsen who were there for me during the hard times and defined the terms “friendship” a new meaning. I owe it to you all, for the good memories we had at the university.

Finally, I would like to express my deepest gratitude and love toward my family in Iran, my father, mother, my siblings (especially my younger brother, Sam) for their emotional support and encouragement. It is indeed because of you that I have reached to this stage in my life, and for that, I am truly grateful. This thesis is dedicated to you.

Table of Contents

Abstract i

Attestation of Authorship iii

Acknowledgement iv

Table of Contents v

List of figures viii

List of tables xiv

Declaration of Contribution: xv

1. Chapter 1: Introduction 1

1.1. Seismic design for new and existing buildings 1

1.2. Damper types 2

1.2.1. Fluid Viscous (FV) dampers 2

1.2.2. Metallic (or yielding) dampers 4

1.2.3. Friction dampers 5

1.3. Damper geometrical configuration 9

1.4. Self-centering slip friction connections 11

1.5. Objectives and Motivations of the research 15

1.6. Organization of the thesis 17

2. Chapter 2: Research Background 19

2.1. Introduction 19

2.2. Various Concepts for retrofit of RC buildings 22

2.3. Previous works 24

2.3.1. Conventional Strengthening 24

2.3.2. Added damping to the system 28

2.3.3. Using base isolation systems 30

2.3.4. Partial selective weakening 31

2.3.5. Full selective weakening 33

2.4. Summary and Conclusion 36
3. Chapter 3: Rotational Resilient Slip Friction Joint 38
3.1. Introduction 38
3.2. SC-RF damper 40
3.2.1. friction plates performance 42
3.2.2. Damper assembly performance 47
3.2.3. Finite Element Analysis of the damper 50
3.3. Experimental testing 51
3.3.1. Disk Spring testing 52
3.3.2. Damper testing 54
3.4. Damper's parameter effects 57
3.5. Summary and Concluding Remarks 59
4. Chapter 4: Seismic Strengthening of Deficient RC Frames Using RSFJs as Haunches 61
4.1. Introduction 61
4.2. Seismic behaviour of deficient RC beam-column joints 63
4.3. RSFJ haunch performance and design considerations 64
4.4. Retrofit Design and Recommendations 68
4.5. Numerical Modelling 72
4.5.1. Joint modelling 72
4.5.2. Bar-slip model 73
4.5.3. Joint shear model 74
4.5.4. RSFJ haunch modeling: 77
4.5.5. RC beam-column joint model validation 78
4.6. Retrofitting Case studies 79
4.7. Summary and Concluding Remarks 85
5. Chapter 5: Seismic Retrofitting of RC Frames Using RSFJ-toggle Bracing Systems: Analytical, Numerical and Experimental Studies 87

5.1. Introduction 87
5.2. RSFJ Toggle-bracing system 89
5.3. Preliminary numerical analysis 91
5.4. Characteristics of the Deficient RC frame 94
5.5. Material properties and testing 99
5.6. RSFJ damper design 103
5.6.1. Damper characteristics 104
5.6.2. Damper Component testing 107
5.7. Retrofit Design considerations 109
5.7.1. Brace Design 109
5.7.2. Stability Criteria 111
5.7.3. Frame restraints and connection considerations 116
5.7.4. Gusset plate design 119
5.8. Experimental testing of the RC frames 122
5.8.1. Instrumentation and Cyclic testing protocol 123
5.8.2. Discussion of the gravity loading accuracy 126
5.8.3. Results and discussion 129
5.9. Summary and conclusion 135
6. Chapter 6: Conclusions and Future Studies 136
6.1. Summary and concluding remarks 136
6.2. Proposed future studies 138
References 140
Appendix 1: Structural Drawings of the test setup and RC Frame 160

List of figures

Figure 1-1 The common passive energy dissipation devices and their hysteretic behaviour [4] 2
Figure 1-2 The Pall Friction damper in cross bracing configuration and diagonal bracing 6
Figure 1-3 Components of the first introduced rotational Friction damper; Implementation of the rotational friction damper in a three-story steel building for shake table test 7
Figure 1-4 (a) Longitudinal section of CFD; (b) Assembled CFD 8
Figure 1-5 Schematic view of AFD: (a) longitudinal section; (b) Cross section 8
Figure 1-6 (a) The proposed wall-type frictional damper; and (b) retrofit of R/C frame using the wall-type friction damper 9
Figure 1-7 Examples of using dampers with toggle-bracing arrangement: (a)Viscous Damper in a building in Boston, USA; and (b) Rotational friction damper in toggle bracing arrangement for retrofitting a school in Seoul, South Korea. 11
Figure 1-8 Some of the possible installation layouts for scissor-jack damping system[32] 11
Figure 1-9 (a) RSFJ components, (b) Assembled RSFJ, (c) to (f) RSFJ in different loading steps, and (g) flag-shape hysteresis 14
Figure 1-10 Single friction Rotational-RSFJ (top) and Rotational-RSFJ in series assembly of two friction disks (bottom) 15
Figure 1-11 Rotational-RSFJ in parallel assembly of four, six and eight friction disks . 16
Figure 1-12 Application of Rotational-RSFJ for Haunch retrofit of RC beam column joint 17
Figure 2-1 Examples of failure of poorly reinforced columns in past earthquakes 20
Figure 2-2 Poor transverse detailing example of columns 20
Figure 2-3 building collapse during 1999 Kocaeli earthquake in Turkey 21
Figure 2-4 The formation of soft-story mechanism for a RC building after 1999 Kocaeli earthquake in Turkey 22
Figure 2-5 ADRS illustration of different retrofit strategies: 23
Figure 2-6 examples of Reinforced Concrete jacketing retrofit for RC frame 25
Figure 2-7 Cast in place shear wall for the retrofit of RC frames 25
Figure 2-8 Conventional Strengthening of RC frame using EBF (Massey University Library, Wellington) 26

Figure 2-9 Lateral force versus storey drift hysteretic curves of test frames (bare frame vs retrofitted frame) 27
Figure 2-10 The effect of added damping on the ADRS curve 29
Figure 2-11 Exterior view of a 17-story building and the installed FVD 30
Figure 2-12 The increasing trend of designing structures with seismic isolation in New Zealand 31
Figure 2-13 Roof displacement numerical results of an 8-story building during Lucerne earthquake (the whole plot, left and zoomed-in plot, right) 31
Figure 2-14 Selective Weakening strategy for improving frame ductile behaviour (a) Existing RC frame; (b) cutting a few or all of the bottom longitudinal rebars in the beam to reduce joint shear stress; and (c) full selective weakening by adding post-tensioning cables 33
Figure 2-15 Experimental testing comparison of a pre-1970s shear wall and retrofitted shear wall with full selective weakening technique 34
Figure 2-16 The schematic photo of RC shear wall with combination of regular and self-centering friction connectors, and the ADRS curve obtained for the retrofitted building (ζ=13%) 35
Figure 2-17 The experimental results comparison of RC beam column joint 36
Figure 3-1 The SC-RF damper and its components, including cap and middle plates, disk springs, high strength bolt or rod 41
Figure 3-2 Some examples of installation scheme for the SC-RF damper in bracing frames 41
Figure 3-3 Symmetric friction plate 44
Figure 3-4 Free body diagram for symmetric friction plates: (a) at initial slipping; (b) at ultimate loading; (c) at ultimate unloading (restoring); and (d) at restored position 45
Figure 3-5 The FEM analysis of a single friction plate: (a) stress distribution; (b) comparison between analytical equations and FEM outcomes 46
Figure 3-6 Simplified damper model for implementing in SAP2000 48
Figure 3-7 The influence of initial adjustment of friction disks for equal deflection: I: Non-adjusted damper in its initial (a), closed stage (b) and opened stage (c); II: Adjusted damper in its three initial (d), closed (e) and opened stage (f). 48
Figure 3-8 Comparison of the analytical formulation with Numerical model (SAP2000) and FE analysis (Abaqus) 50
Figure 3-9 Finite element analysis of the damper assembly: Von-Mises stress counter at ultimate tension and compression 51

Figure 3-10 The utilized sleeve for testing of disk springs 53
Figure 3-11 Cyclic testing of disk springs: (Left) Sample test of stack of 11 disk springs up to the flattening load, and (Right) The obtained average deflection capacity of the disk springs 53
Figure 3-12 The SC-RF damper components: (a) The stack of disk springs, (b) The cap and middle plates, (c) a closer look of the friction plates 55
Figure 3-13 SC-RF damper, at its resting, open and close position 56
Figure 3-14 The Force–Deflection hysteresis comparison of Experimental vs. Finite Element Analysis for the SC-RF damper with different pre-stressing force scenarios: (a) 0kN, (b) 18kN, (c) 40kN, and (d) 55kN 56
Figure 3-15 ideal load-deflection graph for different stack of disk spring arrangement 58
Figure 3-16 Numerical study on damper parameters' effects: (a) Number of disk springs, (b) Number of parallel stacks, (c) Friction plates outer groove angle, and (d) Coefficient of friction 59
Figure 3-17 Progressive stacking of disk springs: (a) An example stack of single, double and triple parallel set in series; (b) The multi-linear self-centering hysteresis M-θ behaviour of friction plate 59
Figure 4-1 Schematic view of RSFJ Haunch retrofitting system with various configurations: a) Interior joint assembly with four haunches, b) Exterior joint with double haunches, and c) single haunch 62
Figure 4-2 Typical rebar detailing for deficient RC joints: (a) Interior joint, (b) Exterior joint with bar bent-in, (c) Exterior joint with bar bent-out, (d) Exterior joint with insufficient anchorage, and (e) Exterior joint with end hook anchorage 64
Figure 4-3 The RSFJ damper: (a) The comprising components of the RSFJ and the damper assembly, (b) The joint behaviour, and (c) The effect of pre-stressing 65
Figure 4-4 The geometry of the joint tested 66
Figure 4-5 The effect of restraining plates on the cyclic performance of the pined-pined RSFJ: (a) the stiffness drop due to axial-rotational behaviour of the RSFJ, (b) a photo of the axial rotational behaviour of the RSFJ during compression load, (c) the effect of restraining plate on the cyclic performance of the RSFJ, and (d) a photo of RSFJ with restraining plate during compression load 67
Figure 4-6 The symmetric cyclic flag-shape behaviour of joint with added restraints ... 68
Figure 4-7 Different retrofit solutions with RSFJ haunches: (a) Interior joint with quadruple haunch subassembly (QHS), (b) Exterior joint with double haunch subassembly (DHS), and (c) Exterior joint with single haunch subassembly (SHS) 69

Figure 4-8 Shear and moment diagrams: (a) non-retrofitted subassembly (NRS), (b) Double Haunch Subassembly (DHS), and (c) Single Haunch Subassembly (SHS).....70
Figure 4-9 OpenSEES model for Interior and exterior beam-column joint assembly....73
Figure 4-10 Bar-slip rotation behaviour in RC joint.....74
Figure 4-11 Constitutive model of Pinching4 material for simulation of joint rotation .76
Figure 4-12 SMA material for modeling RSFJ haunches: (left) the required parameters, and (right) Calibration validation with experimental data 78
Figure 4-13 Comparison of the force-deformation hysteresis curve of numerical model and experimental outcomes of non-seismically designed RC joints: (a) PEER14 Interior joint[156], (b) Experimental test Exterior joint BS-L[157], (c) Interior Specimen E-03[158], and (d) Exterior joint testing unit 6 79
Figure 4-14 Selected test specimens for RC joint retrofit with RSFJ haunch: PEER14 (left)[156] and BS-L (right) 81
Figure 4-15 The displacement-controlled loading protocol applied for testing: (a) Interior joint, and (b) Exterior joint 83
Figure 4-16 Comparison of force-displacement cyclic behaviour of the retrofitted joints against the non-retrofitted assembly: (a) Interior joint, and (b) Exterior joint 83
Figure 4-17 The cyclic performance of RSFJ haunches in the retrofitted beam-column joint assemblies: (a) Interior joint, and (b) Exterior joint 84
Figure 4-18 Comparison of cumulative energy dissipation for the cyclic loading: (a) Interior joint, and (b) Exterior joint.....85
Figure 5-1 Schematic view of different toggle-bracing arrangement, as compared to common bracing systems 91
Figure 5-2 Section and reinforcement detail of the RC frame tested by Al-Sadoon et al.[172, 173] 92
Figure 5-3 Comparison of the pushover results with the experimental hysteretic load-displacement of the frame 94
Figure 5-4 Performance of the retrofitted RC frame with RSFJ-toggle bracing system : (a) Flag-shape behaviour of the RSFJ adopted in the toggle-brace system (F_{slip}=56.6, F_{ult}=113.1, $F_{restoring}$=12.9, F_{res}=6.4, μ=0.18, and Deflection capacity=49.1mm); and (b) Cyclic pushover of the retrofitted frame up to 36mm lateral displacement.....94
Figure 5-5 The RC frame rebar detailing and section geometry dimension: (a) Overall height and length of the frame, and (b) to (c) frame beam and column section 95

Figure 5-6 The Fibre-based moment curvature analysis of the sample RC-frame using SAP2000 software: (a) Column section, (b) Equivalent bilinear moment-curvature of the column, and (c) Beam section 97
Figure 5-7 Definition of beam and column moment strength for calculation of sway index 98
Figure 5-8 The RC frame tested: (a) Actual frame, (b) Overall height, (c) Placement of Reid eye anchors on top of columns, (d) Foundation pads dimentions, (e) Placement of drossbachs for the connection of foundation and RC frame 100
Figure 5-9 Concrete cylinder Sample testing of the RC frame: (a) nine samples for the frames and foundation, (b) testing the samples using UTM, (c) Obtained results for the samples 102
Figure 5-10 The tensile strength testing of the reinforcements employed in the RC frame: (a) testing the rebars using UTM, (b) results of M10 rebars, and (c) results of M16 rebars 103
Figure 5-11 RSFJ flag shape force-deformation relationship 105
Figure 5-12 Equivalent prismatic column concept for the RSFJ 107
Figure 5-13 RSFJ dampers component test: (a) Cap and middle slotted plates, (b) Assembly test setup 108
Figure 5-14 RSFJ damper performance result: (a) calculated hystersis behaviour for the first tuning, (b) Observed load-deformation behaviour for the first tuning, (c) calculated hystersis behaviour for the second tuning, and (d) Observed load-deformation behaviour for the second tuning 109
Figure 5-15 Parameter definition of the toggle-bracing forces 110
Figure 5-16 The RC RSFJ-toggle bracing test setup: (a)The overall view of the test-setup, (b) the pinned connections for the braces, (c) constraint naming for the test setup; and (d) the RSFJ damper-brace assembly 112
Figure 5-17 Stability of a general column: (a) General end-restrained column with length L, (b) Equivalent pin-pin column with Effective length KL; (c) Theoretical K factor for the isolated columns with idealized end conditions 113
Figure 5-18 Compressive performance of steel braces and their potential failure modes 115
Figure 5-19 Results obtained from the stability analysis of the Damper-brace assembly 115

Figure 5-20 Common failure modes of the post-installed anchors (ACI-318-19): (a) tensile rupture, (b) concrete break-out in tension, (c) bond failure, (d) anchor shear rupture, (e) concrete breakout in shear, and (f) anchor pry-out in shear.....116
Figure 5-21 RC Frame restraints: (a) top view, (b) lateral support provided for the RC frame test setup (shown with red arrow); and (c) shear key that prevents frame sliding (shown with black arrow).....117
Figure 5-22 Concrete restraints detailing: (a) top brace to frame connection using stud bars, (b) bottom brace to frame using floor high strength bars and stud bars, (c) maximum avaliable space for anchor design, and (d) prestressed rods for connecting the frame to the floor.....118
Figure 5-23 Gusset plate tension and compression failure design criteria: (a) net section fracture, (b) gross section yielding failure, (c) block shear combined tension failure and shear) (d)pureshear tear out (e) compression member considered for gusset plate design 120
Figure 5-24 Finite Element analysis of gusset plate connections of the (a) damper brace, (b) top brace, and (c) bottom brace 122
Figure 5-25 Instrumentation layout of the test setup 124
Figure 5-26 Lateral loading history of the benchmark bare frame 124
Figure 5-27 Sample photos of physical damages (cracks) on the benchmark frame....125
Figure 5-28 Crack patterns of the bare frame in different drift levels: (a) 0.5%, (b) 1.0%, (c) 1.5%, and (d) 2.0% 126
Figure 5-29 The rope effect contribution on the recorded base shear of the frame 128
Figure 5-30 Comparison of the initial and corrected backbone curve for the benchmark bare RC frame 129
Figure 5-31 Hysteretic lateral load-lateral deformation of the bare frame up to 1.5% drift 131
Figure 5-32 Retrofitted frame performance results: (a) Sample photos of RSFJ damper in the retrofitted frame (b) the comparison of the cyclic behaviour of retrofitted frame (Fslip=12.2 kN) against the benchmark bare frame.....132
Figure 5-33 Numerical model results of the retrofitted frame (Fslip=12.2 kN) 133
Figure 5-34 Experimental results for the second retrofit test vs. the first retrofit test ..134
Figure 5-35 Energy dissipation of the reference frame and retrofitted frames for each drift ratio 134

List of tables

Table 1-1 The common geometrical configurations of the dampers in braced frames...10
Table 3-1 Parameters for friction plate modelling 46
Table 3-2 Summary of the damper characteristics.....50
Table 4-1 The summarized empirical stress strain behaviour for the interior and exterior joints.....77
Table 4-2 Summary of the selected experimental tests for OpenSEES model validation 78
Table 4-3 Calculated and assumed parameters for retrofitting of interior and exterior RC joints using RSFJ haunches.....81
Table 4-4 The RSFJ haunches utilized for retrofitting of interior and exterior joint subassemblies.....81
Table 5-1 Amplification factor for different bracing system 91
Table 5-2 Tuning characteristics of the RSFJs for the experimental testing 108
Table 5-3 Changes in the rods prestressing forces due to drift 128
Table 5-4 Recorded damper displacement during cyclic testing of the retrofitted frame 131

Declaration of Contribution:

Manuscript 1 (Chapter 3): Development and parametric study of a new self-centering rotational friction damper (Published in Engineering Structures)

Manuscript 2(Chapter 4): Seismic strengthening of deficient RC frames using self-centering friction haunches (Published in Engineering Structures)

Manuscript 3 (Chapter 5): Seismic Retrofitting of RC Frames Using RSFJ-toggle Bracing Systems: Analytical, Numerical and Experimental Studies (To be Submitted soon).

Authors	Manuscript 1 Contribution		Manuscript 2 Contribution		Manuscript 3 Contribution	
	(%)	Description	(%)	Description	(%)	Description
Sajad Veismoradi	82	Main research, paper writing	82	Main research, paper writing	82	Main research, paper writing
Pouyan Zarnani	6	Assist with test, Review	6	Review	6	Assist with test, Review
Pierre Quenneville	6	Review	6	Review	6	Review
Mohamad Mahdi Yousef-beik	6	Assist with test, Review	6	Assist with test, Review	6	Review

The author/co-authors hereby declare that their contributions in the mentioned research papers is as mentioned in the table above:

Sajad Veismoradi	Date:	26/04/2023	Signature
Pouyan Zarnani	Date:	26/04/2023	Signature
Pierre Quenneville	Date:	26/04/2023	Signature
Mohamad Mahdi Yousef-Beik	Date:	26/04/2023	Signature

Chapter 1: Introduction

1.1. Seismic design for new and existing buildings

The current conventional building design codes rely on dissipating the seismic energy through introduction of some inelastic deformation in specific regions or structural components of the buildings. As for the steel moment resisting frames, usually the connections and beam plastic hinges will experience the inelastic deformation, while in braced frames, the inelastic behaviour is accumulated in braces. The same philosophy is also applicable for the reinforce concrete frames where plastic hinges would occur due to rebar yielding in the RC beams and shear walls and thus the seismic energy dissipation occurs [1]. By using structural dampers, one can concentrate the input seismic energy at predefined locations and protect the gravity load-resisting system from inelastic behaviour [2, 3].

As a primary lateral load resisting system or in combination with other systems (dual systems), dampers dissipate the seismic energy in structures and usually are being designed as an off-the-shelf connector that can be checked or replaced in case of extreme seismic events. This can make them suitable for design of the new building or even seismic strengthening of the existing buildings. This can facilitate the post-earthquake inspection and maintenance of damper-equipped buildings, after strong seismic events.

While different types of damping systems have been introduced by researchers and engineers, one can subdivide the dampers into three main categories of passive, active and hybrid systems [2]. As compared to the passive dampers, active and semi-active damping systems can change their properties based on the load demand or other parameters. However, they require external energy source to be activated, which has made them less common than passive systems, although other factors such as economical and reliability constraints could also be effective in this regard. Here, the focus of this thesis is devoted to the passive dampers (with an emphasis on the friction-type systems). In general, two aspects for implementing a damping system in a structure could be the selection of a suitable and efficient damper among the available options for the seismic strengthening of the structure and adopting a preferable geometrical configuration for damper installation.

Figure 1-1 shows the common three different types of dampers in the construction industry, with the common force-deformation (hysteresis) curve. Each of them will be explained below, with more emphasise on the friction dampers.

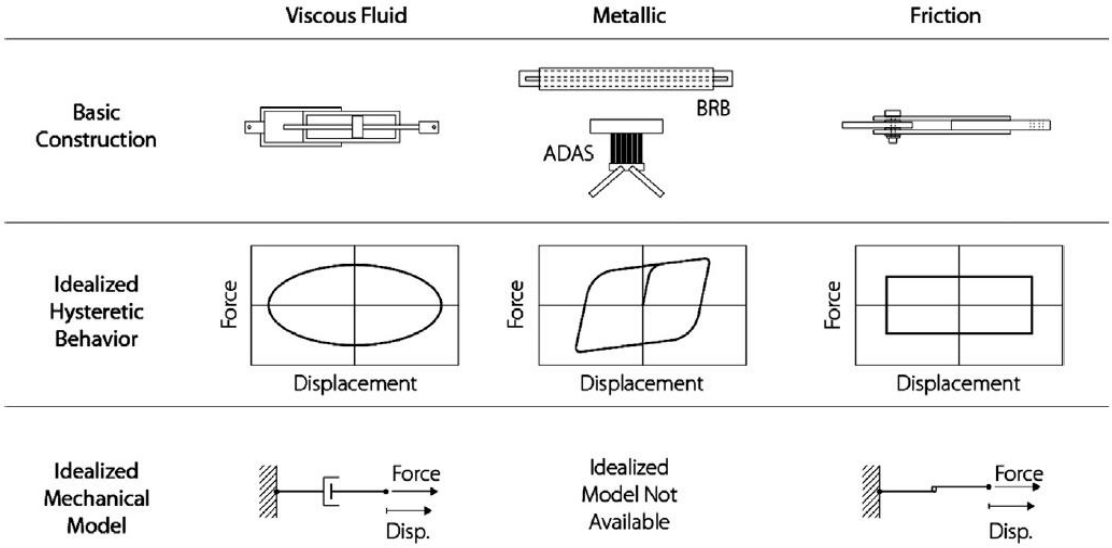

Figure 1-1 The common passive energy dissipation devices and their hysteretic behaviour [4]

1.2. Damper types

As stated in the previous section, there are several types of dampers in the industry that fall into three main categories namely viscous dampers, yielding dampers and friction dampers.

1.2.1. Fluid Viscous (FV) dampers

The FV damper is basically a central piston inside a fluid-filled tube which can dissipate the energy by pushing the fluid through orifices and piston head. The energy is converted into heat through the action of viscous friction stresses in the fluid. While friction and yielding are displacement-dependent dampers (their force depends on the damper displacement), viscous dampers are classified as velocity-dependent energy dissipaters, which means that the force induced in the damper, is a function of the velocity of the seismic load:

$$F = C * V^{\alpha} \quad (1)$$

In this equation, F represents the damper force, C is the damping constant and α denotes the damping exponent parameter, having a value between 0.2 to 2.0 depending on specific applications[5]. The damper can be activated at low displacement and requires minimal restoring force with temperature-independent properties. The fluid would resist the force only when the damper is moving, therefore the damper does not add stiffness to a structure. On this basis, it is possible to increase the damping ratio of a structure without significant alteration of the structure inherent stiffness. This advantage could result in less trial-and-error design that might be needed for other dampers such as yielding dampers[6].

Another advantage of using viscous dampers is related to their capability of generating forces that are out-of-phase displacement. In simpler terms, during a seismic event, the maximum damper forces happen when their displacement demands are zero (structure passing its initial position with greatest velocity). On the other hand, when the structure reaches its greatest deflection stress, the velocity reduces to zero which translates into zero damper force[5].

While FV dampers could provide additional damping for the structure, they cannot be considered as the main lateral load resisting system given the velocity dependency (i.e., absence of sufficient resistance at low activation speed). Also, possible fluid leakage is one of the reliability concerns for the viscous damper [4], which can necessitate the health monitoring and inspection of the dampers during their service life and strong seismic events. Another limitation is related to the fixed and unchangeable properties of the viscous damper. While this cannot be considered as drawback for viscous dampers, yet having a damping system which can be adjusted, even after its production, would provide more flexibility for the designers and engineers, in case of any calculation errors or design changes.

It is worth noting another type of dampers known as Visco-Elastic (VE) dampers which act in between velocity dependent and displacement dependent devices. They are capable of providing velocity dependent viscous damping, as well as displacement-dependent elastic restoring force[7]. On this basis, their behaviour can be modelled using a simple Kelvin solid model (a parallel summation of spring and a dashpot). The VE dampers have the capability of activating at low displacements and adding damping to the system, making them a suitable option for frequent wind events with small deflection demands.

As compared to earthquakes, the wind events might last for longer times, therefore they are manufactured to be durable against fatigue and aging. Readers can find more info about VE dampers in the related references[2, 7]. As for the limitations of the VE dampers, it can be referred to its limited deformation capacity. Moreover, due to their temperature and frequency-dependent behaviour, it might be necessary to consider an upper bound and lower bound temperature for the analysis of such dampers under the frequency range of interest within the recommended strain limits provided by the damper manufacturers[8, 9].

1.2.2. Metallic (or yielding) dampers

As their names implies, the yielding dampers dissipate the seismic energy through cyclic yielding of steel components (or other materials). The yielding occurs via axial loading (like in BRB braces [10, 11]), bending deformation (such as yielding plates in TADAS system[12], YBS connector[13, 14], or U-Shaped Flexural Plates[15]), shear deflection (like in Slit dampers[16]) or a combined action where in all the cases, the seismic energy is dissipated by the plastic deformation. The metallic dampers can provide ductile hysteresis behaviour with reasonable price, as well as long-term reliability. Moreover, the materials and behaviours of such dampers is known to practicing engineers[2]. However, inelastic deformation means permanent damage and residual displacement on the system which could necessitate the inspection of the condition of the damper after the event. The replacement of the damper would be required in case of extreme deformation or possible rupture (due to low cycle fatigue). For seismically active zones with high probability of multiple aftershocks and limited time intervals, the inspection and replacement of the dampers could be a challenge and a costly process. As an illustration, after 2011 Great Tohoku earthquake in Japan, 588 aftershocks with magnitude greater than M5.0 were recorded in which 60 of the aftershocks were bigger than M6.0 and three of them were bigger than M7.0[17]. The accumulated damage due to consecutive earthquakes in the buildings equipped with yielding dampers would increase the risk of structural collapse[10]. Some of the steel yielding dampers like YBS[13] benefit from easy inspection, and present stable strength without significant degradation (such as U-Shaped flexural plate[15]), while others like BRB are more challenging in terms of inspection, since the steel core cannot be checked visually[10].

1.2.3. Friction dampers

The friction dampers dissipate the energy via sliding of two rigid bodies. The configuration of frictional components can take different shapes, which results in different types of friction damping systems. However, almost all of the friction dampers present certain advantages such as high level of initial stiffness and energy dissipation, with stable cyclic behaviour. In general, friction dampers are damage-free, insensitive to temperature changes and can present their hysteresis behaviour over many cycles. They are designed not to be activated during service loads and wind. Hence, there is no possibility of failure due to fatigue, before an earthquake[18]. Moreover, most of the dampers are tuneable, which means their slipping force can be adjusted via tightening the clamping bolts or changing other features of the damper. This can be considered as an advantage over viscous dampers or metallic fuses with fixed force-deformation characteristics. However, the sliding interface condition might change over time (for example, the sliding surfaces must be protected from corrosion) and although they remain elastic after their performance, the permanent displacement in the device could be considered as a major drawback for these dampers [4, 19].

During the past decades, several different types of friction devices and connections were developed and tested by researchers. One of the famous and pioneer devices in this field is the Pall Friction Damper (PFD) which was introduced in 1980s[20], and has been employed in different forms of sliding, including rotational and linear friction in cross-braces and diagonal braces as well[18, 21]. Figure 1-2 shows some of the applications of the Pall Friction Dampers. Wu et. al[22] introduced an improved version of Pall damper, by changing the shape of the core plate. The result was a more economical damper with simpler configuration.

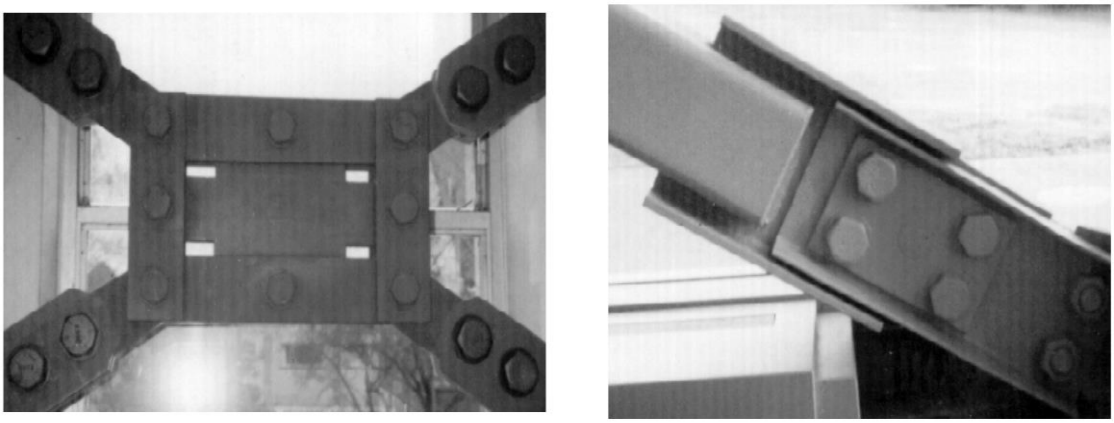

Figure 1-2 The Pall Friction damper in cross bracing configuration (Left) and diagonal bracing (Right)[21]

Mualla and Belev[23] introduced the Rotational Friction (RF) damper and experimentally analysed the performance of the damper at the Technology University of Denmark (See Figure 1-3). The shaking table test of a three-story steel building equipped with RF-damper further demonstrated the performance of structures using this type of dissipator. The rotational friction damper has been utilized with various configurations, on a number of new and existing buildings by Damptech[24]. It is worth noting that unlike linear friction dampers with constant rectangular hysteresis curve, the rotational friction dampers present nonlinear curve, due to the second order geometric effects of the damper in high deflection[25]. This nonlinear behaviour has been witnessed by other researchers as well[26, 27].

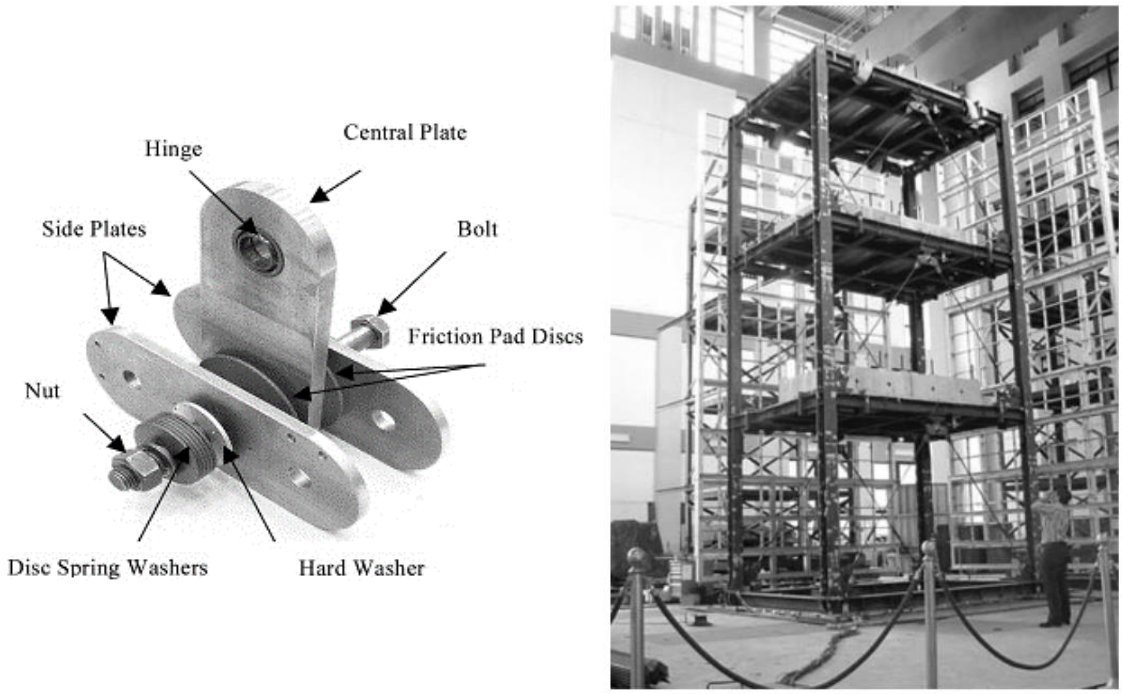

Figure 1-3 Components of the first introduced rotational Friction damper[23] (Left); Implementation of the rotational friction damper in a three-story steel building for shake table test[28] (Right)

Mirtaheri et. al[29] introduced a Cylindrical Friction Damper (CFD), consisting of two main parts (inner shaft and outer cylinder) (See Figure 1-4). The two parts were assembled such that the inner shaft was shrink fitted into the outer cylinder using external force. Compared to other frictional dampers, the CFDs did not use high-strength bolts to induce friction between contact surfaces; thereby it was more efficient in terms of construction costs, simplified design computations and increased reliability as compared to the other types of frictional dampers. In another study[30], they introduced a semi-active adjustable friction damper (AFD) which utilizes adjustable hydraulic pressure as a clamping force (Figure 1-5). One of the benefits of such a damper, is that the re-centering of the structure can be assisted, after severe earthquakes.

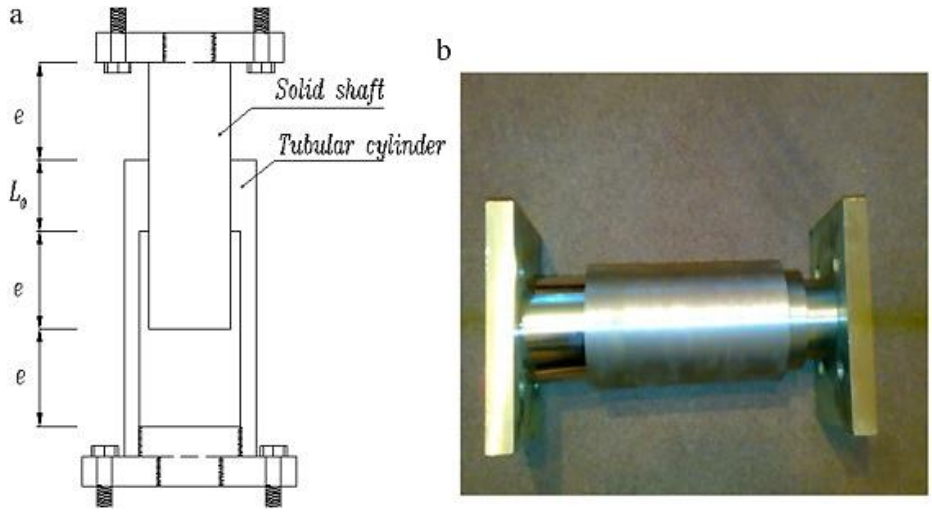

Figure 1-4 (a) Longitudinal section of CFD; (b) Assembled CFD[29]

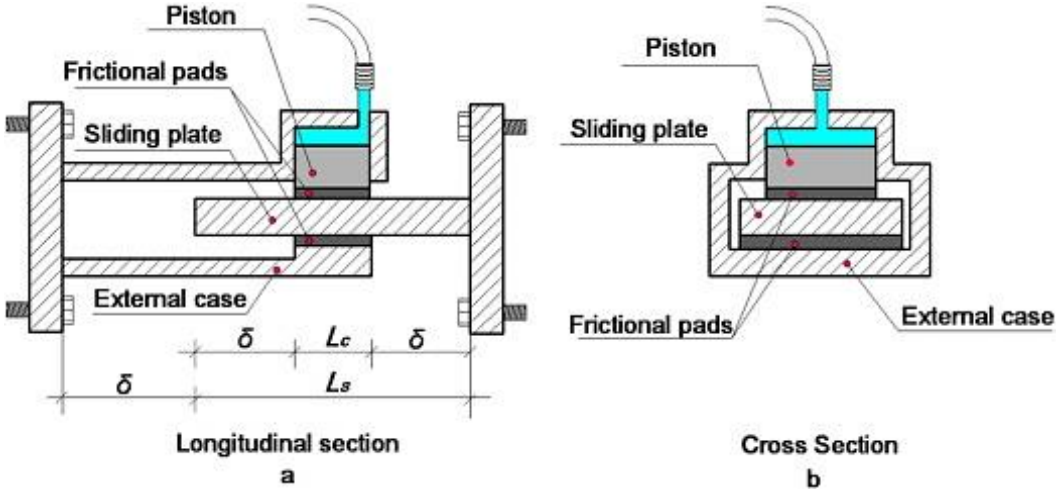

Figure 1-5 Schematic view of AFD: (a) longitudinal section; (b) Cross section [30]

Cho and Kwon[31] invented a frictional wall damper, to improve the performance of existing RC frames (Figure 1-6). At first, the damper was developed as a brace-type element; however, due to the local damages in the frame, they decided to focus on the wall-type damper concept with a Teflon slider. Their numerical outcomes showed that increasing the normal pressure acting on the frictional sliders could reduce the imposed seismic damage on the RC fame elements.

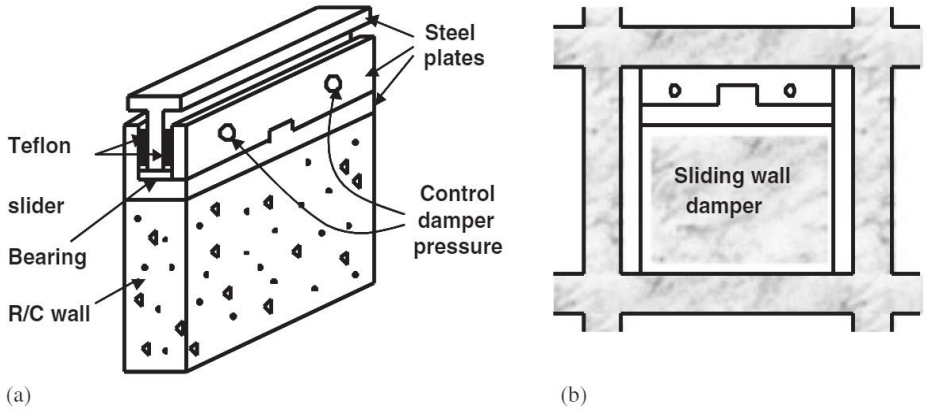

Figure 1-6 (a) The proposed wall-type frictional damper; and (b) retrofit of R/C frame using the wall-type friction damper[31]

As can be noticed, different types of friction devices are being introduced by researchers and practitioners. Almost all of the friction devices can be considered damage-free and some of the dampers can also be adjusted after their manufacturing, meaning that their force-deformation behaviour can be modified.

1.3. Damper geometrical configuration

Regarding the geometrical configuration of the dampers, one should pay attention to the definition of structural dampers. A seismic damper is a structural component that dissipates seismic energy when it experiences relative motion (velocity or displacement) at its both ends. Therefore, the most effective locations for installation of dampers is where building motions are the largest. While building motions are needed to activate the dampers, it is worth noting that large building movements can affect the occupants' comfort. Therefore, the design of the damping system is a combined effort to amplify the building motion for activating the damper, while keeping the movement in the acceptable range for the occupants. While dampers can be designed to be activated with different levels of deflection, researchers have also explored the possibility of using the damper in various geometrical configuration as well. The common geometrical configuration for the braced frames is listed in the Table 1-1. While diagonal and chevron configuration are very common in the construction industry, the toggle and scissor bracing configurations are also available. As illustrated by Taylor on viscous dampers, the Toggle brace damper system can magnify the relatively small displacement in the buildings to provide the opportunity for the damper to be activated[32]. This can be beneficial for increasing the damping of stiff framing systems. Figure 1-7 shows some of the real application of toggle-

bracing system with viscous and rotational friction dampers. It is worth to note that the toggle bracing system requires intricate modelling and design which should consider proper out-of-plane constraints for the damper system. Moreover, the experimental and theoretical results of Zhang[33] shows that the magnification factor changes with loading and is different when the force is applied in the pull or push direction. The other configuration, known as Scissor-Jack Damping System, introduced and patented by Constantinou[34] (see the Figure 1-8), can also magnify the effect of damping device, with the added advantage of being more compact, as compared to the toggle bracing system. For more information about the performance of scissor-jack damping systems and the experimental test results, it can be referred to[35].

Table 1-1 The common geometrical configurations of the dampers in braced frames[19]

Geometrical Configuration	Advantages	Disadvantages
Diagonal	• Simple distribution of damping along height	• Limited relative deformation • Architectural freedom issues
Chevron	• Full horizontal movement transfer from structure to damper	• Less efficiency due to constraints of attainable stiffness under small motion • Architectural freedom issues
Toggle	• Good efficiency due to amplification of small motions (could reach to about 2-3 times)	• More complex design and manufacturing • More difficult modeling of toggle system • Greater space requirement
Scissor	• More compact than toggle system (space saving) • Simpler installation between columns with less distance	• Less efficiency compared to toggle system

(a)

(b)

Figure 1-7 Examples of using dampers with toggle-bracing arrangement: (a)Viscous Damper in a building in Boston, USA (Taylor Devices)[2]; and (b) Rotational friction damper in toggle bracing arrangement for retrofitting a school in Seoul, South Korea (Damptech)[24].

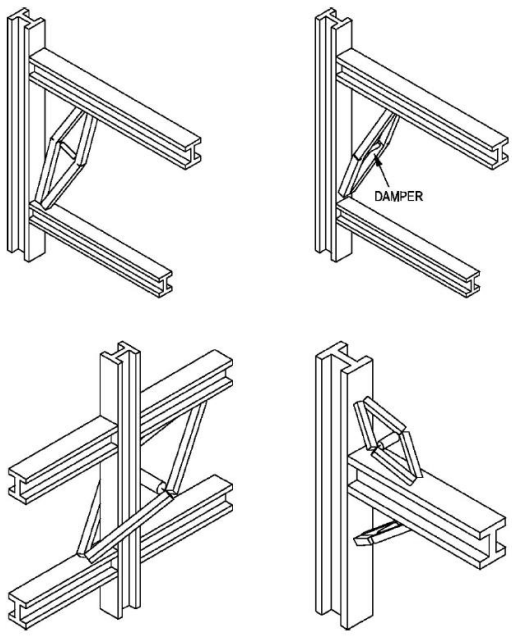

Figure 1-8 Some of the possible installation layouts for scissor-jack damping system[35]

1.4. Self-centering slip friction connections

The majority of world's populations are living in the cities and most of the economic activities depends on functionality of cities. Therefore, sustainable and resilient cities has become one of the most important research directions for scholars and engineers to design structures and building them in a way that can be quickly repaired and restored to their

normal function[36]. One of the key parameters that can reflect the difficulty in restoring the earthquake-hit structures and highlight the economic costs is the residual deformation of the structure. As an illustration, the studies of Erochko, Christopoulos and Tremblay [37] showed that for the buildings with residual drift higher than 0.5%, the cost of repairing and realignment of the damaged building could surpass the cost of rebuilding a new one. As a result, self-centering solutions and devices have found their way in the construction industry to tackle the residual drift issues of the buildings after severe events. Readers are referred to the review work of Zhong and Christopoulos[38], for a state of the art review of the self-centering seismic resistant structures.

In general, self-centering dampers have two main aspects: The restoring force and the energy dissipation [36]. The energy dissipation aspect could be provided by any of the three different types of dampers (viscous, metal yielding and friction) which was briefly explained in the previous section. The restoring force aspect can be provided by various elements and techniques such as Shape Memory Alloy (SMA) materials (see for example [39, 40]), synthetic Fiber materials such as glass, carbon or aramid (refer to the works of Christopoulos, Tremblay and Erochko [41, 42] for further details), prestressed steel strands (such as self-centering steel moment frames with post-tensioned connections[43]), post-tensioned bars (see the works of Mashal, Palermo and Chegini[44] for the introduction of Accelerated Bridge Construction employing precast bridge bents with self-centering and energy dissipation[44]) and prestressed disk spring (or any other type of component with spring action)[45, 46]. While the prestressed cables have already been utilized in post-tensioned timber structures[47, 48], precast concrete walls[49], moment frames[50], bracing members[41] and other structural systems, it is worth noting that noticeable tendon force losses could occur during the service life of the structure which would affect the efficiency of the system and necessitates re-tensioning the cables[51] (in particular, in case of timber given the creep). Moreover, the humidity conditions could also affect the level of this loss [52]. As for the utilization of SMA for recentering force, the general self-centering characteristics of SMA are quite promising and they offer excellent fatigue life and high durability against corrosion; albeit their higher costs as compared to other construction materials, might limit their usage[1]. It should be pointed out that the price of SMA has dropped noticeably in the last decade and it is expected to decrease even more in the near future. As for the disk springs, their compactness and various sizes available for different force range, displacement

capacities, and flexibility in terms of different arrangement for the stack of disk springs can bring various options for engineers and researchers to provide self-centering to their systems[53]. Such flexibility advantage will be explained in section 3-4 of the thesis.

As stated above, self-centering systems combine the energy dissipation and recentering force aspects to minimize the earthquake damage on the structure. One of the recent innovative damping systems that has combined energy dissipation and self-centering is the Resilient Slip Friction Joint (RSFJ) which can resolve the potential residual drift issues in structures after severe earthquake events. Invented by Zarnani and Quenneville in 2015[54], the damper is comprised of grooved middle plates with slotted holes and cap plates with regular holes that have been clamped by stacks of pre-stressed disk springs. Given the clamping force demand, high strength bolts or rods are being used for the assembly. The load-deformation of the RSFJ is a tuneable flag-shape behaviour which is repeatable, damage-free and full self-centering (See Figure 1-9[55]). It is worth to note that such a flag-shape behaviour has been witnessed and investigated in the previous works of Nims et al. [56] (Energy Dissipating Restraint (EDR) device), Kar et al.[57] (Ring-Spring damper), Filiatrault et al.[58] (Shapia Damper or friction springs damper[7]).

The RSFJ damper has been investigated in different applications, including Rocking timber shear walls[46, 59] and rocking RC shear walls with RSFJ as hold-downs[60], Rocking shear walls or braced frames with RSFJs as shear links[61, 62], steel and timber bracings[63, 64], steel moment resisting frames with RSFJs[65], tension-only steel braces [66, 67], etc. It has also been successfully implemented in real-life projects in New Zealand and overseas such as the Nelson airport new terminal, Hutt Valley new medical hub and Fast & Epp HQ Office in Vancouver [68]. Readers can find more info in the mentioned references.

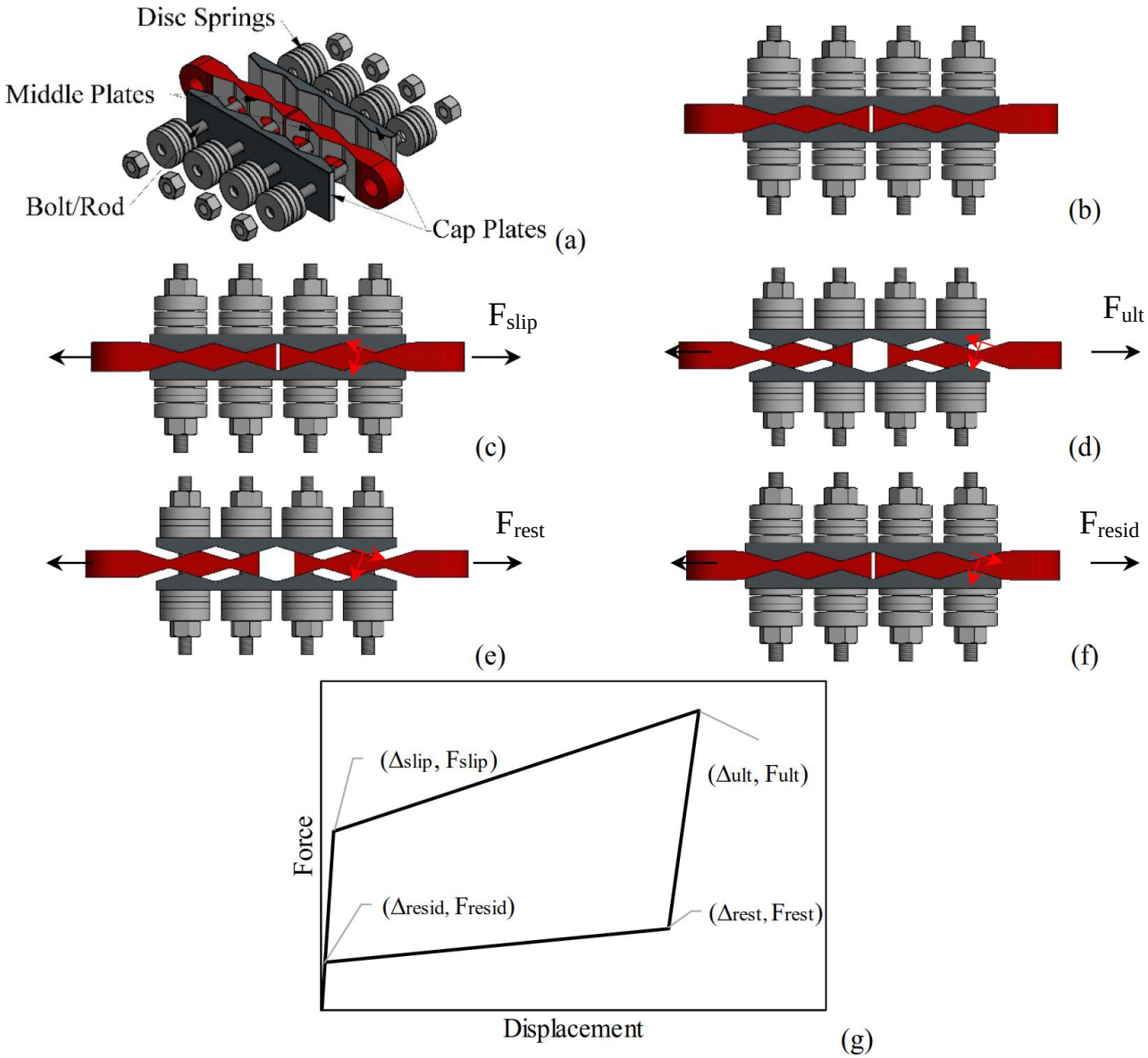

Figure 1-9 (a) RSFJ components, (b) Assembled RSFJ, (c) to (f) RSFJ in different loading steps, and (g) flag-shape hysteresis [55]

This thesis is devoted to resilient self-centering connections that combine friction sliding for dissipation of seismic energy and prestressed disk spring for restoring force. First, a new self-centering damper named Rotational-Resilient Slip Friction Joint (Rotational-RSFJ or R-RSFJ) is introduced which is basically a self-centering rotational friction (SC-RF) damper and can integrate the recentering behaviour and energy dissipation, all in one compact device, with a simple arrangement. The introduced joint is flexible, both in design and applications and utilizes friction for energy dissipation, while benefits from prestressed stack of disk spring to provide recentering behaviour. While the development of the Rotational-RSFJ is complete, it can be employed for designing of new structures or retrofitting the existing buildings. Since the number of references and studies available

for designing of new structures with self-centering dampers and connections (including the available references for applications of RSFJ for new buildings), it was decided to promote the novelty of the thesis even further by focussing the applications of such self-centering connections for retrofitting of current existing buildings, due to a limited studies conducted for this purpose.

1.5. Objectives and Motivations of the research

Two main objectives were considered for this thesis:

The first objective was to see if it is possible to improve the capabilities of the current RSFJ, in terms of damper deflection capacities for specific applications which requires larger deflection. The Rotational-RSFJ which is the first self-centering rational friction damper was introduced to answer such requirements. This damper presents similar force-deformation behaviour like traditional RSFJ with advantage of larger deflection capacities. Moreover, its flexibility of design makes it more suitable for various desirable force-deformation levels. Thanks to the unique shapes of cap and middle plates, the damper does not require slotted holes for providing deflections given the relative rotation of the cap and middle plates. Moreover, it is more suited for mass production which could reduce the cost of damper even more. Figure 1-10 and Figure 1-11 show some of the possible shapes of the Rotational-RSFJ, including single friction disk, two-series friction disks, parallel four, six and eight friction disks. The damper will be investigated in Chapter 3 of the thesis.

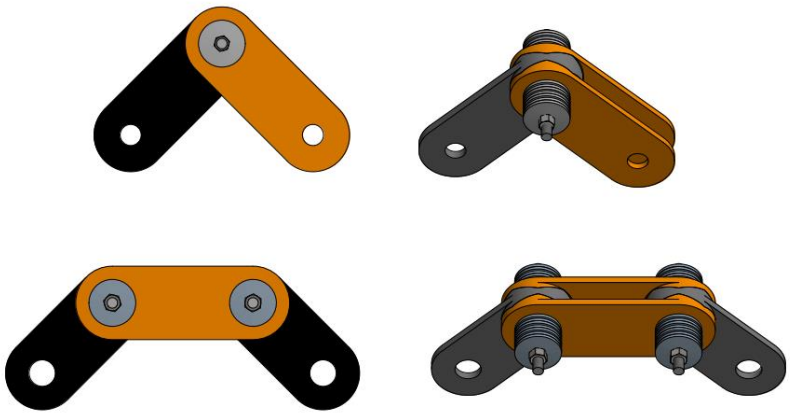

Figure 1-10 Single friction Rotational-RSFJ (top) and Rotational-RSFJ in series assembly of two friction disks (bottom)

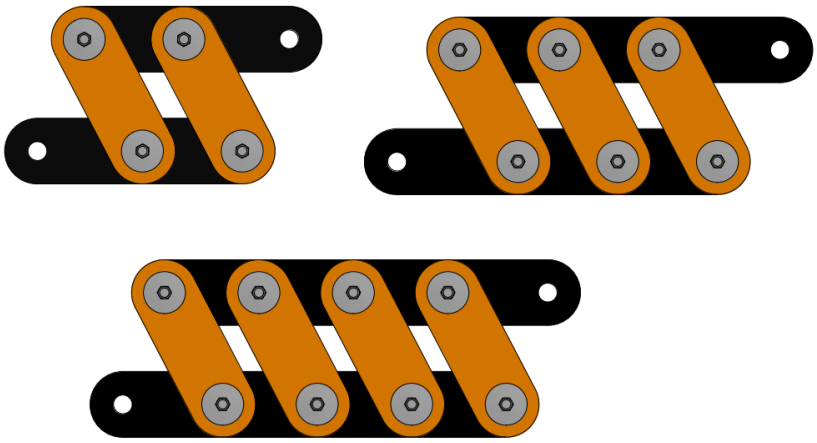

Figure 1-11 Rotational-RSFJ in parallel assembly of four, six and eight friction disks

The second objective was to explore the possibility of employing RSFJ for retrofitting and strengthening of existing buildings in local and global level. Acknowledging the fact that the RSFJ is a newly developed damper and its applications is being investigated in different potential new lateral loading systems, the industry has already accepted the damper as a resilient solution for designing seismic resilient structures. On the other hand, further opportunities exist for the existing buildings to utilize RSFJ for retrofit purposes and thus further research was required to investigate its potentials for the existing buildings as a strengthening solution. Utilizing RSFJ dampers for retrofitting purposes is a challenging subject, as it requires the proper design of the damping system for the current building to employ the capabilities of the damper while aiming to preserve the building as much as possible. This was investigated by experimental testing of a RC frame equipped with RSFJ dampers. Since the force-deformation behaviour of the RSFJ is similar to Rotational-RSFJ which is a tuneable flag-shape behaviour, it could be stated that the findings of the current thesis are applicable for both dampers. As an illustration, the results obtained for the fourth chapter of the thesis would be similar if the Rotational-RSFJ is utilized as a structural damper for beam-column connections retrofitting (Figure 1-12, as compared to Figure 4-1 in chapter 4). This is also the case for the experimental testing of RC frame equipped with RSFJ-toggle bracing. However, in order to simplify this retrofit study, it was decided to employ the RSFJ for the experimental testing of the interested deficient RC frame.

The restoring force provided by the RSFJ damper is another aspect which is quite new for the strengthening purposes and up to the author's best knowledge, only a few experimental studies have utilized self-centering dampers for retrofitting. As it will be stated in chapter 2, different methods can be implemented for retrofitting of buildings.

Such a decision is related to the current state of the target building and its surrounding, available budget, etc. If the goal of the retrofit is to minimize the residual drift of the building, then implementing a retrofit solution with restoring force mechanism would be crucial.

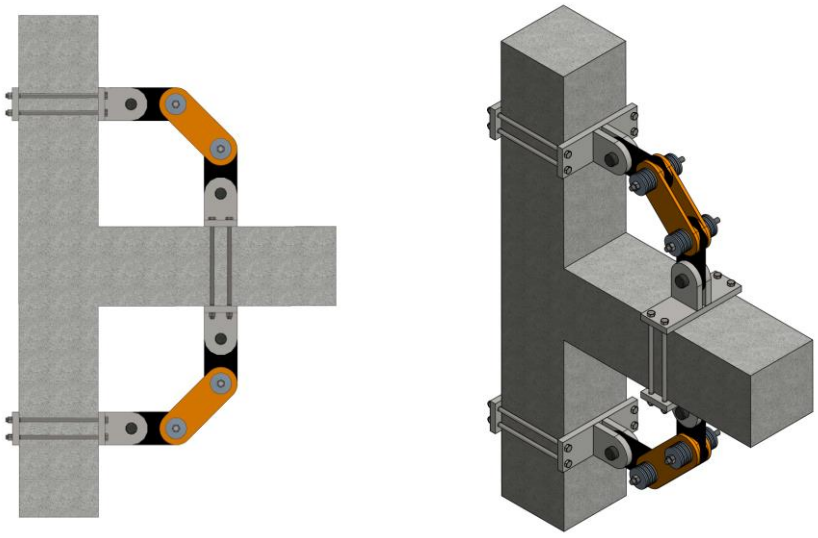

Figure 1-12 Application of Rotational-RSFJ for Haunch retrofit of RC beam column joint

1.6. Organization of the thesis

The thesis contains five chapters and two appendices as explained below:

Chapter 1 provides a short description about seismic dampers and explains the aims and objectives of the current thesis.

Chapter 2 provides a short literature review regarding the current deficiencies of old earthquake-prone RC frames and lists various seismic retrofitting techniques of these buildings, including examples of structures retrofitted with seismic dampers.

Chapter 3 introduces an innovative Rotational-RSFJ which is the first self-centering rotational friction damper. This new damper shares several benefits of RSFJ while providing some flexibility in terms of damper deflection.

Chapter 4 focuses on the applications of using RSFJ for seismic strengthening of RC frames at the local level. On this basis, the RC beam-column joint is considered for the retrofitting case study.

Chapter 5 investigates the experimental testing of RC frames equipped with RSFJ bracing system. This can be considered as RC frame retrofitting at the global level. This chapter also provides some insight and recommendations regarding the component and connection designs for the RSFJ bracing. Toggle-bracing was selected so that the damper could be activated in smaller drift demands, thus minimizing the drift on the brittle benchmark RC frame.

Chapter 6 provides a summary and conclusion.

Appendix 1 provides the structural drawings of the experimental components tested and also covers the design of the test setup.

Finally, it should be noted that since this thesis is written in the paper-based format, there would be some inevitable replication of information.

Chapter 2: Research Background

2.1. Introduction

The seismic vulnerability of existing RC buildings against strong earthquakes is one of the important topics among engineers and researchers. Many of the RC frames have been designed based on outdated codes and they fail to provide ductile behaviour as per new code requirements. Inadequacy in design and construction procedures prior to 1970s could be highlighted as a factor for potential extensive damage and failures in the RC elements [69]. The old RC buildings have traditionally utilized smooth rebars as their longitudinal reinforcement. The bond between concrete and steel rebars affects the performance of RC members. It is worth noting that plain rebars can get debonded from concrete in severe earthquakes, due to Poisson effects and thus they are considered to be vulnerable as per current seismic guidelines[70]. Apart from the employment of smooth rebars for the RC frame construction, the low-strength concrete (below 20-25 MPa and in some extreme cases, below 10 MPa) could be listed as a construction inadequacy.

Another key element for poor behaviour of RC structures is devoted to poor detailing in RC structural elements. As an illustration, the reinforcement detailing deficiencies have been identified as a main factor for the collapse of CTV building in New Zealand, during 2011 February earthquake in Christchurch[71]. Figure 2-1 presents some of the witnessed nonductile behaviour of concrete columns in historic seismic events.

While the poor detailings in columns are commonly encountered in pre-1970s buildings in New Zealand, they can also be found in relatively newer buildings designed as per NZS 3101:1982 (in other words, the buildings that were constructed between 1982 to 1995). This was due to the assumptions that some columns could be treated as Secondary Elements (gravity columns) and thereby, to be exempted from the minimum confinement requirements[72]. Although they were not considered as part of the lateral load resisting system, they must be capable of tolerating the gravity loads while undergoing lateral drifts. Unfortunately, the experimental tests performed at University of Canterbury showed high vulnerability of such columns to sustain lateral displacements[73].

Figure 2-1 Examples of failure of poorly reinforced columns in past earthquakes[72]:
Left: Indian Hills Medical Centre (1994 Northridge earthquake)
Right: Olive View Hospital (1971 San Fernando earthquake)

Another reason for observing an unacceptable RC structural behaviour could be the inadequate anchorage detailing for both longitudinal and transverse reinforcements[71]. In this regard, the relatively large spacing for the shear reinforcement in columns can be pinpointed which might trigger the buckling of longitudinal rebars, especially if the axial load in the columns is relatively high and 90-degree hooks are utilized (Figure 2-2).

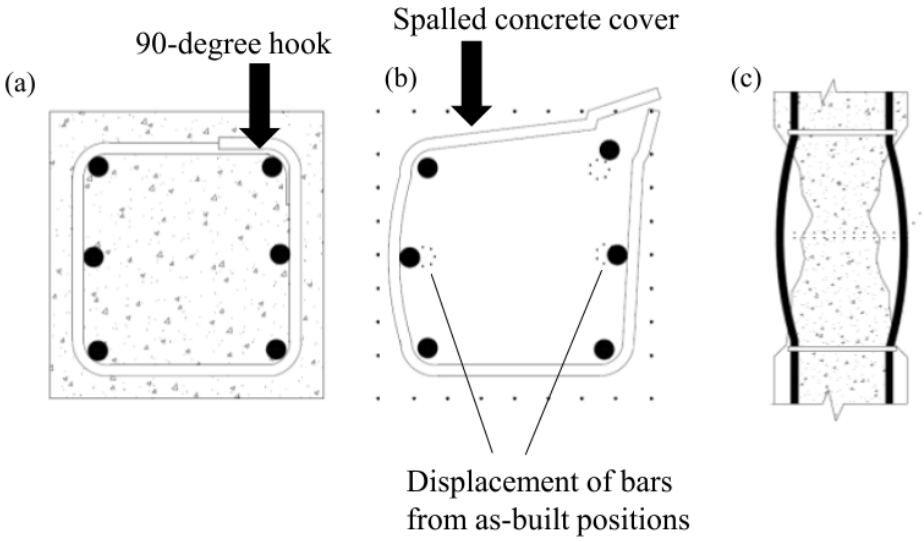

Figure 2-2 Poor transverse detailing example of columns[71]:
Inadequate shear rebar anchorage and lack of confinements for all the longitudinal bars
Lack of concrete support for the longitudinal bars after concrete spalling
Longitudinal bar buckling after concrete spalling

The inadequate anchorage of beam main rebars into the RC beam-column joints is another example of poor RC performance behaviour which has been investigated by New Zealand Assessment guidelines (C5[72]), as well as other researchers. The absence of shear rebars would indicate a lack of reliable joint shear mechanism for the beam-column joint beyond its diagonal cracking. Figure 2-3 demonstrates the failure of an RC frame after 1999 Kocaeli earthquake in Turkey[74]. As can be noted, almost all of the nonlinear behaviour of the frame is concentrated in its beam-column joint which cannot be considered as a ductile plastic mechanism. This can even result in building collapse and loss of its lateral strength. This will be investigated in detail in Chapter 4.

Figure 2-3 building collapse during 1999 Kocaeli earthquake in Turkey[74]

Finally, the lack of capacity design considerations in old RC buildings can also threaten its seismic performance. In many older RC frames, the beams are often stronger than the columns[75]. The weak-column strong-beam concept usually ends up in a non-desirable column shear failure mechanism at the local level. At the global level, one could even expect soft-story collapse mechanism. This is especially the case for the ground or lower stories in old RC buildings were functional requirements such as having more open spaces and retail spaces would result in a weak story[76]. Figure 2-4 better illustrates the soft-story mechanism in an RC frame after 1999 Kocaeli earthquake[74].

Figure 2-4 The formation of soft-story mechanism for a RC building after 1999 Kocaeli earthquake in Turkey[74]

Taking into account that the above-mentioned issues are only a few deficiencies related to existing old RC frames, more information can be found in the NZ assessment guidelines (C5)[72] as well as in the literature. In resolving such seismic deficiency of non-ductile, or limited ductile RC frames, various seismic retrofitting techniques have been introduced by researchers, to preserve the RC frames from excessive seismic damages. This will be covered in the next section.

2.2. Various Concepts for retrofit of RC buildings

To upgrade the seismic performance of RC frames, various techniques and strategies can be adopted. Based on the level of retrofit required, they could be categorized in member level upgrading of the structure (i.e. the local strengthening, such as beam-column joint strengthening which will be explained in chapter 4) or the whole structural level upgrading (global retrofitting, such as adding toggle-bracing system to an RC frame explained in chapter 5).

Figure 2-5, proposed by W. Y. Kam and his colleagues[77] better demonstrates various retrofitting options within Acceleration-Displacement Response Spectrum (ADRS) domain. The ADRS curves can be obtained using acceleration and displacement spectrum

in which the horizontal and vertical axis denotes the displacement spectrum and acceleration spectrum. A retrofit plan aims to ensure that the structure capacity spectrum reaches or surpasses the demand spectrum. As can be noted, different methods of retrofitting can be adopted for this purpose including:

1) Conventional strengthening (for example, adding shear walls or concentric braces)
2) Added damping to the system (such as adding viscous dampers)
3) Using base isolation systems (i.e., decoupling the structure from the ground and add isolators)
4) Partial selective weakening (such as cutting a few rebars from the beams to reduce the moment transferred to the column)
5) Full selective weakening (that includes both selective weakening and strengthening of the structure to improve frame ductility and resilience).

Each of these techniques will be explained briefly in the next section, with some examples from recent research studies.

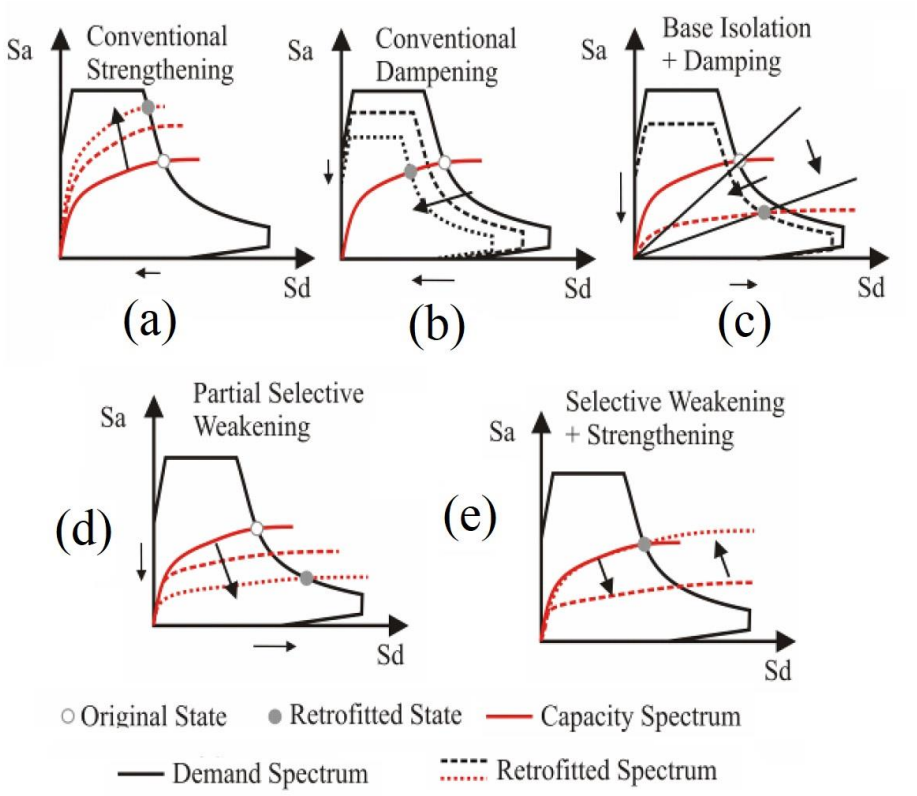

Figure 2-5 ADRS illustration of different retrofit strategies:
(a) strengthening, (b) added damping, (c) base isolation, (d) partial SW (weakening only), (e) full SW (Weakening and further enhancement)

2.3. Previous works

As stated in the previous section, the retrofitting of RC structures usually falls within one of the 5 main categories. It is worth noting that the most suited retrofitting strategy depends on various factors such as the frame structural characteristics, the importance level of the structure in terms of architectural or historical value, time, budget, the permissible levels of implementing invasive methods for retrofitting, the available gap between adjacent buildings, the soil type and geotechnical aspects of the project, etc. Therefore, different retrofit solutions can be expected for a unique case. It is not the intend of this thesis to justify a specific retrofit scheme over the other options, rather to briefly pinpoint their main features and limitations.

2.3.1. Conventional Strengthening

The typical retrofit strategy for the RC frames is mainly based on increasing the capacity (strengthening) through introduction of additional structural elements. Such strategy could cover method such as adding jackets to the RC wall, additional shear wall installation, attaching conventional braces to the RC frame. The goal here is to make sure such elements would get activated before inelastic deformation of the RC frame, thus controlling the global lateral drift of the system and reducing the damage in RC frame member.

Figure 2-6 shows the addition of RC jacketing to an existing RC frame. It should be cleared that the performance of the RC jacketing depends on couple of factors including whether the longitudinal bars are passing through the slab, how many sides of the column receive the jacketing, etc. The main advantage of the jacketing could be the uniform distribution of lateral load capacity, as compared to shear wall retrofitting or retrofit with braces where lateral load resistance is concentrated. As for the disadvantages of this technique, one could highlight the uncertainty with regard to the bonding between the jacket and the original RC member[78].

Figure 2-6 examples of Reinforced Concrete jacketing retrofit for RC frame[78]

The addition of shear wall is another common method employed by engineers (Figure 2-7). During the design process, engineers should pay attention to the distribution of walls in plan and elevation and check if the inertial forces of the diaphragms can be transferred to the wall through the connections of the wall into the existing frame. Moreover, it might be required to modify the foundation (for example, adding screw piles) to withstand the additional force introduced by the shear wall. This is also the case for the conventional strengthening with braces.

Figure 2-7 Cast in place shear wall for the retrofit of RC frames [78]

While the RC jacketing and shear wall are classified as wet retrofitting method, the application of steel bracing is a dry retrofitting method which makes it easier to apply. The steel bracing and its required connection elements can be prefabricated, thus allowing fast on-site installation. Besides, by comparing to regular shear walls, the overall weight of the structure will not increase significantly, when the steel bracing is employed for

retrofit. The bracing can provide opening which makes it more pleasing in terms of architectural flexibility[79].

Early studies investigated the performance of the RC frames with conventional braces. Moreover, the researchers also explored the possibility of utilizing Eccentrically Braced Frames (EBFs [80]) and Buckling Restrained Braces (BRBs[79]) for retrofitting of RC frames (Figure 2-8). Thanks to their stable and balanced hysteresis behaviour and improved damping, they can increase the energy dissipation of the system as well.

Figure 2-8 Conventional Strengthening of RC frame using EBF
(Massey University Library, Wellington)

While the energy dissipation of the conventional braces is only limited to their plastic elongation during tension cycles (given the buckling in the compression), the yielding of the steel core in BRBs will occur in both tension and compression cycles. As compared to steel moment resisting frames, RC frames are stiffer, and their irreversible damage initiates at their plastic deformation which is around 1% story drift[81]. The BRBs can be activated in low drifts of 0.2%[82] and increase the hysteretic damping of the system. To illustrate the effectiveness of BRBs for RC frame retrofitting, the experimental testing results of Zhang et. al[75] study is presented here. As can be noted, noticeable increase in the strength and hysteretic energy dissipation can be achieved by BRBs. It should be pointed though that the frames retrofitted by BRBs might present residual displacement after seismic events, as they fail to provide any restoring force mechanism. This is also the case for other methods of conventional strengthening.

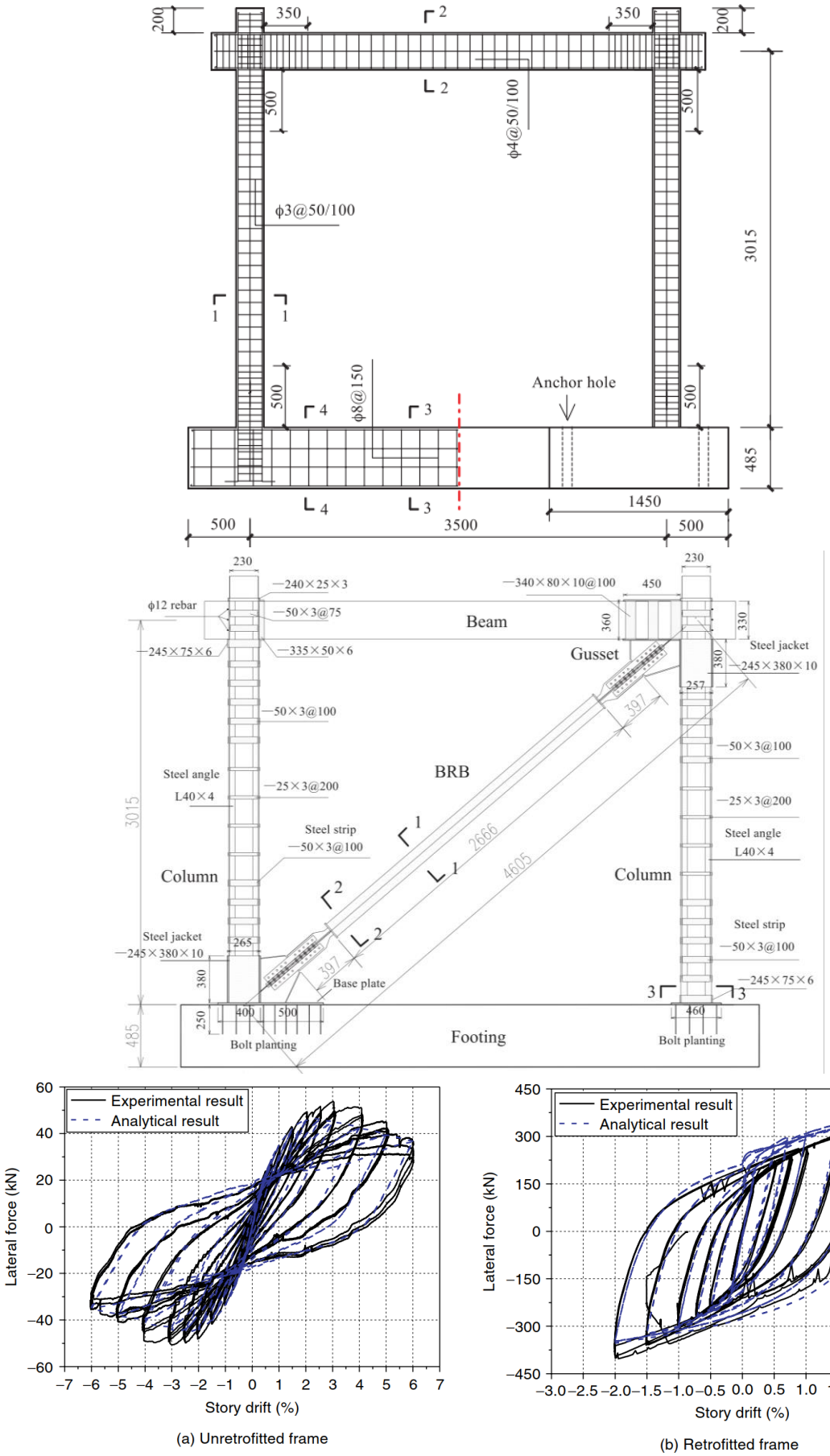

(a) Unretrofitted frame

(b) Retrofitted frame

Figure 2-9 Lateral force versus storey drift hysteretic curves of test frames (bare frame vs retrofitted frame)[75]

Another method of conventional strengthening for the RC structure is to utilize composite materials such as Fiber reinforced polymers (FRPs) in various forms (sheets, plate, rebar etc.) and different materials (carbon, glass, aramid or other synthetic fiber materials) to provide better confinement for the concrete and increase its strength and ductility[83]. Since 1980s, the FRP strengthening has gained the attention of researchers and engineers for the retrofitting of RC components, especially the columns and bridge piers. Although FRPs can be employed as a composite jacketing for both rectangular and circular columns, it provides better and more uniform confinement for the circular columns[84]. The confinement for the rectangular columns may depends on FRP reinforcement ratio, corner radius, column aspect ratio and so on[85].

As compared to concrete and steel jacketing, FRP provide some advantages in terms of speed and ease of construction. It is also lighter and more durable and requires less maintenance. However, the cost for such retrofit tend to be higher, as compared to traditional retrofitting methods [83]. Other drawbacks for such material include their low elastic modulus with elastic-brittle behaviour and poor fire-resistance[86].

2.3.2. Added damping to the system

Based on the New Zealand Engineering Assessment Guidelines (Part C2), the overall viscous damping of a system can include the inherent damping (ζ_0), the hysteretic damping (ζ_{hy}), and added damping due to supplemental viscous damping (ζ_d):

$$\zeta_{sys} = \zeta_{0+} \zeta_{hy+} \zeta_d \quad (1)$$

Therefore, any conventional strengthening that is expected to experience inelastic deformation such as adding BRBs can also be considered to increase the damping of the system. However, for added damping category (Figure 2-5(b)), we only consider the damping provided by viscous damping. Fluid Viscous Dampers (FVD) which sometimes are referred as just viscous dampers are cylindrical chambers filled with silicone fluid liquid and convert the seismic energy into dissipated heat. When added to the existing building, the damper can dissipate the input energy and shrink down the demand curve in the ADRS curve (Figure 2-10), as this curve is associated with the damped response spectrum related to the effective global damping ratio of the building. Several studies have explored the advantages of employing viscous dampers to increase energy dissipation of the building and reduce its drift[87]. A case study by Taylor Devices which

is one of the pioneer manufacturers of viscous dampers highlights the improved performance of a 17-storey brittle Pre-Northridge steel moment frame (constructed in 1970) with soft-storey issue that was retrofitted up to the ASCE 41-17 basic performance objective for existing buildings (BPOE), with drift reduction from 2.25% to 1% (Gonzalez et al[88]). Figure 2-11 shows the building view and the installed damper in the building.

The benefits of viscous dampers make them a good option for seismic retrofitting. Since the viscous dampers are a velocity-dependent component, the generated forces by dampers are out of phase with the structural forces (lowest force occurs at zero velocity, at the peak displacement of the building). Therefore, the base shear of the FVD-equipped buildings is lower than the buildings retrofitted by other types of dampers. However, it should be stated that due to velocity-dependence behaviour of such systems, more complex analyses might be required for proper design of such components. Moreover, the relatively higher costs of such dampers might limit their usage for retrofit purposes.

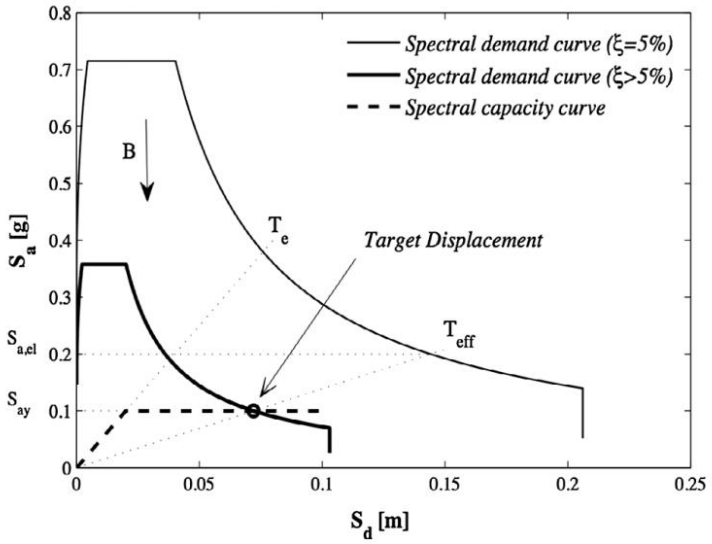

Figure 2-10 The effect of added damping on the ADRS curve[87]

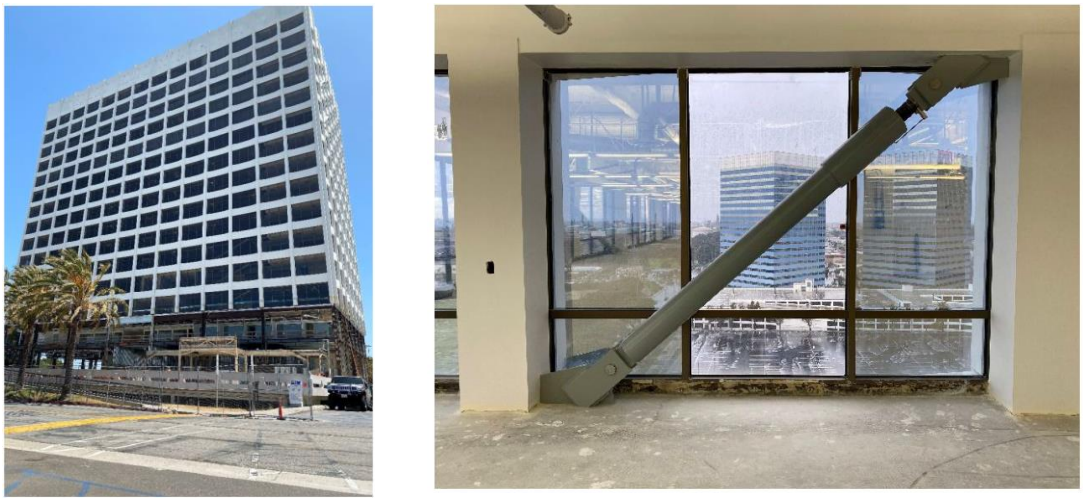

Figure 2-11 Exterior view of a 17-story building and the installed FVD[88]

2.3.3. Using base isolation systems

A research study by Whittaker highlights the growing trend of using base isolation in bridges, as well as building structures (Figure 2-12[89]). While the overall number of isolated structures remained the same during 2000s; however, after 2010-2011 Christchurch events, the number of isolated buildings increased noticeably, thanks to the life-cycle cost benefits of base isolation devices and their harmony with the emerging idea of "low-damage design" philosophy. Whether it is the Lead Rubber Bearing or friction pendulum systems, the buildings equipped with isolators are decoupled from potential earthquakes and have a longer fundamental period. Moreover, they receive lower seismic energy, as a portion of seismic energy is dissipated within the base isolation elements.

While the isolation systems can be reasonably advantageous for the short buildings by shifting their fundamental period, their effectiveness tends to decrease for the high-rise buildings which already have large periods [90]. Some of the studies also highlight that if the incoming ground motion do not follow the stylised spectra (response decreasing with increasing period), it might be possible that the isolated structure may experience even larger damage as compared to a fixed-based structure[91] (Figure 2-13). More info regarding such issue can be found in the research study by Carr and Puthanpurayil [91]. It is also worth noting that isolated buildings need separation gap to perform well and if the gap between adjacent structures would be small, the resulting buildings pounding would be even more destructive [92]. Albeit, the most important factor for utilizing seismic isolators for retrofit purposes, is the associated costs for using such systems.

Unless for the structures with special occupancy, or important historical buildings, the base isolator implementation might appear economically prohibitive than other retrofit solutions. This is due to the fact that significant intervention is required at the base level to separate the structure from ground and provide the required space for the base isolators to be installed.

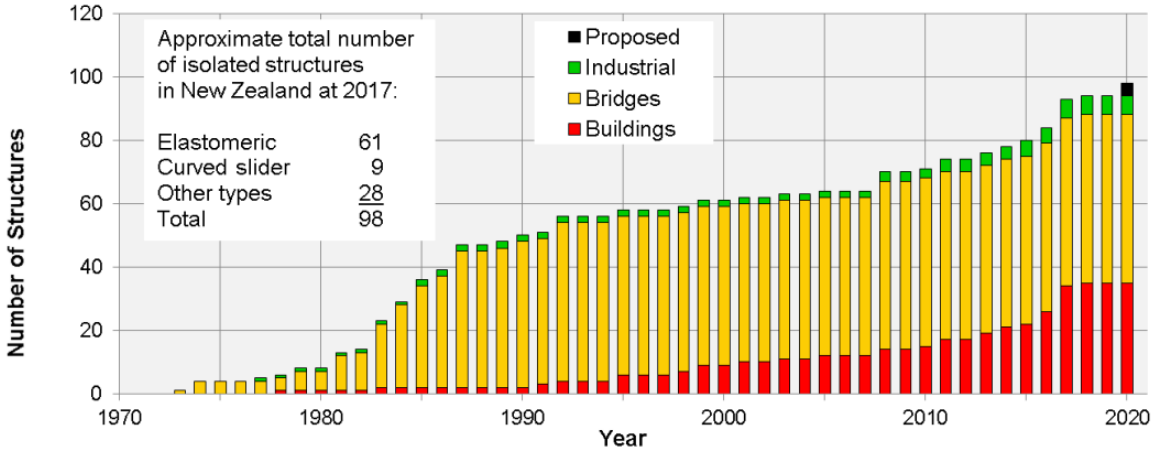

Figure 2-12 The increasing trend of designing structures with seismic isolation in New Zealand[89]

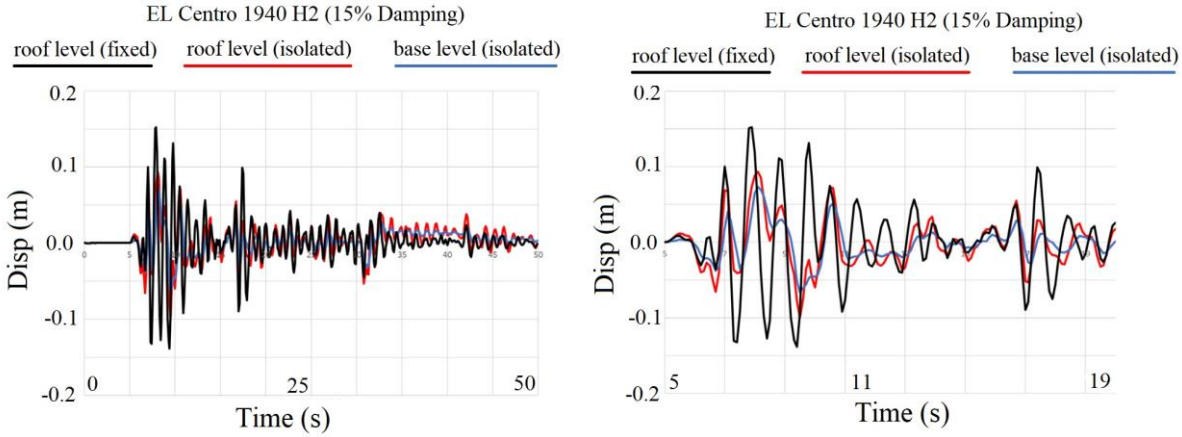

Figure 2-13 Roof displacement numerical results of an 8-story building during Lucerne earthquake (the whole plot, left and zoomed-in plot, right) (Carr and Puthanpurayil, 2021[91])

2.3.4. Partial selective weakening

Contrary to the common misconception that the retrofitting of the structure should involve strengthening of the concerned structures, the selective weakening approach would aim to improve the frame global behaviour by weakening the structure. The idea of selective weakening was first suggested by Priestley[93] and further investigated by Ireland et al.[94], Kam, Pampanin and Bull [77] and a few other studies, where their strategy aimed to change the global inelastic mechanism of the structure and achieve higher deformation (drift) capacity as a trade-off. An example in this regard is the induction of flexural hinges

in the beam by cutting a few of the bottom longitudinal rebars in the RC moment resisting frames. This can increase the frame overall ductility, especially if the frame does not follow the strong-column weak-beam design philosophy. The old-fashioned brittle RC frames with strong-beams and weak-columns can be modified in this regard and the outcome would present ductile beam hinges rather than brittle column hinges. Figure 2-14 better shows such concept for existing inadequately detailed RC frames. Possibilities are a ductile frame with reduced strength and improved ductility or a ductile frame with post-tensioned strengthening. Also, other possibilities to be briefly explained in the next section.

It should be noted that such a technique can be considered as an option for only a few special cases. For such retrofitting cases, a full selective weakening might be a better fit, as the frame would gain sufficient lateral resistance with higher deformation capacity. Albeit, this technique might not be the answer if the drift increment in the frame could bring other structural problems such as the potential pounding for close buildings, or failure for buildings with drift-sensitive flooring systems (e.g., hollow-core precast floor) [72]). Besides, the level of intrusiveness for this technique might make it not feasible if it has to be exerted all over the frame (i.e., if all of the beam longitudinal rebars need to be cut).

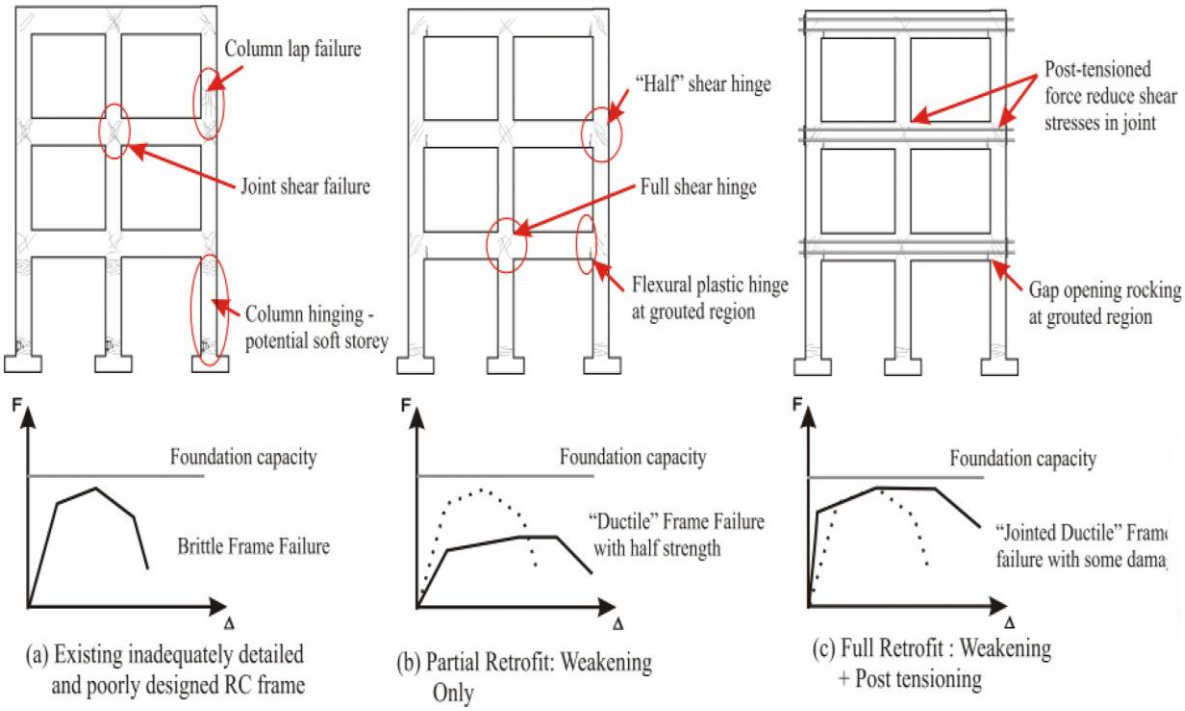

Figure 2-14 Selective Weakening strategy for improving frame ductile behaviour[77]: (a) Existing RC frame; (b) cutting a few or all of the bottom longitudinal rebars in the beam to reduce joint shear stress; and (c) full selective weakening by adding post-tensioning cables

2.3.5. Full selective weakening

Weakening the structure would improve the system ductility; but it also reduces the force demand on the system and thus additional external reinforcement, strands, plates and damping devices or FRP wrapping may be required so that the structure can meet the capacity demand. Having stated that, the literature shows that simultaneous weakening and self-centering approach seems to be promising. Ireland et al.[94] experimentally tested a weakened representative pre-1970s New Zealand RC wall with horizontal and vertical cuts and post-tensioned strands. In their research, they have cut the entire base of the wall and relied upon the energy dissipation of the external strands. Figure 2-15 shows the force-deformation behaviour of W1 wall (bare wall, benchmark) and W1R wall (horizontally cut and strengthened with post-tensioned cables). Their test also pinpointed the capability of the strengthened system to be tuneable and present desirable behaviour, depending on the retrofit aim.

(a)

(b)

(c)

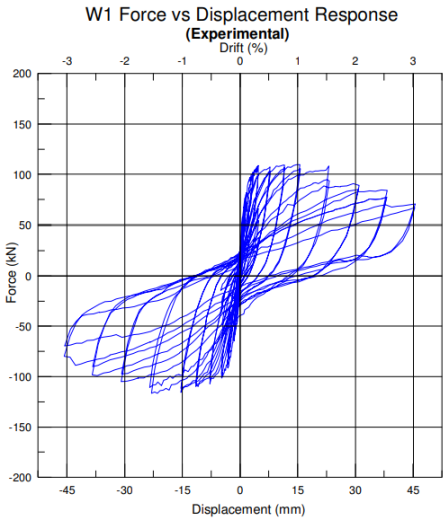

(d)

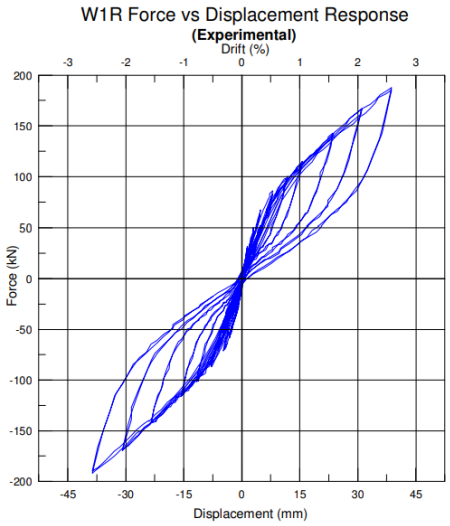

Figure 2-15 Experimental testing comparison of a pre-1970s shear wall and retrofitted shear wall with full selective weakening technique[94]

The similar concept was implemented for retrofitting of a precast shear wall RC building (13-story apartment in Christchurch). By changing the main lateral load resisting system from a traditional shear wall to a rocking shear wall with a combination of regular friction joint connections and the resilient slip friction joint connections (RSFJ hold-downs). Using such an arrangement, Hashemi et al.[95] proposed a retrofit solution for an earthquake prone building in Christchurch (with NBS rating below 34%) to increase its NBS rating up to 100% (Figure 2-16).

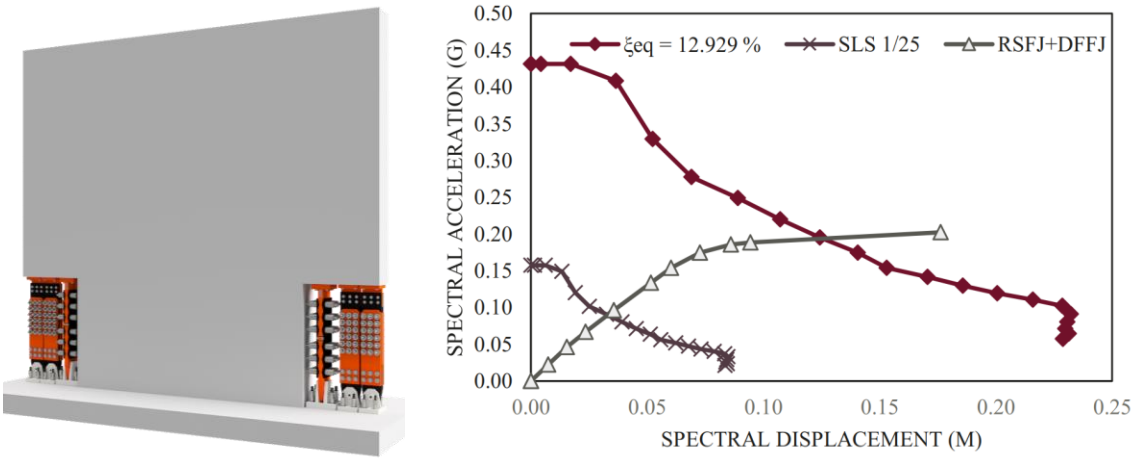

Figure 2-16 The schematic photo of RC shear wall with combination of regular and self-centering friction connectors[68], and the ADRS curve obtained for the retrofitted building (ζ=13%)[95]

In another study, the beam-column joint component of the RC frame were subjected to full selective weakening technique (Figure 2-17[77]). While the undesirable wedge mechanism of the beam column joint sub-assembly (due to hook anchorage) was witnessed in the benchmark beam joint, the retrofitted joint was able to satisfactorily improve sub-assembly deformation and energy dissipation, provided that the column has sufficient capacity.

While the selective weakening technique has the potential to be implemented in both traditional RC shear walls and moment frames, the concept for the shear wall (specifically the retrofit with resilient connections) requires less alteration to the system and thus easier to implement. Moreover, the engineers need to check that the increased ductility would not trigger other drift-related issues which was mentioned previously.

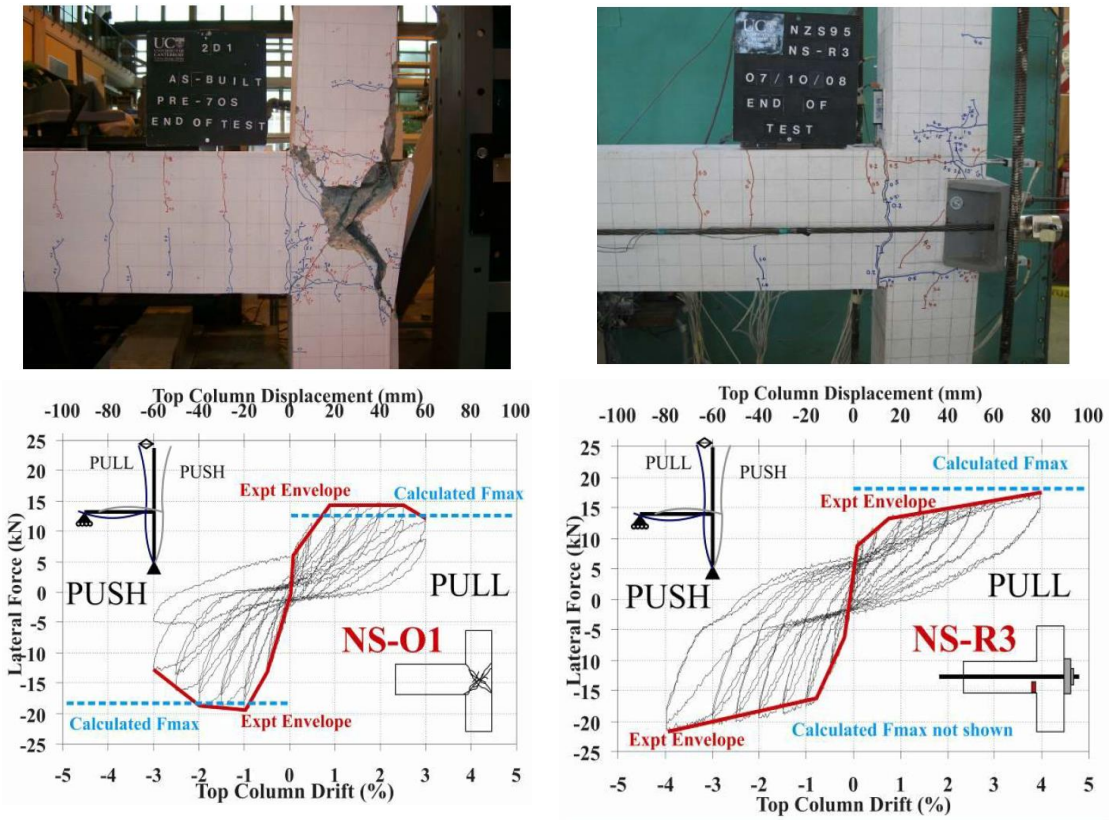

Figure 2-17 The experimental results comparison of RC beam column joint[77]:
(left) As-built beam column joint, (right) Full Selective Weakening beam column joint

2.4. Summary and Conclusion

In this chapter, some of the probable deficiencies of the old RC moment resisting frames were briefly explained and various strategies for retrofitting of RC frames were listed. Depending on the chosen strategy, the structural characteristics of deficient RC frames and permissible level of implementing invasive methods, various solutions can be used for the retrofit of these buildings.

While acknowledging the advantages and disadvantages of various retrofit techniques, for this study, it was decided to follow the conventional strengthening technique with minimal intervention to the RC frame. This is due to the fact that the deficient RC frames in New Zealand and the rest of the world have been built before 1970s (more than 50 years ago), thus they might not be a suitable candidate for invasive retrofitting method. Moreover, due to their brittle behaviour, they are more likely suffer from residual deformation and require restoring force mechanism. Another reason could be the possible pounding issue for the adjacent building, if they closely constructed to each other. For this situation, the conventional strengthening may seems more appropriate.

As for the following chapters, two retrofitting cases are investigated in the local (Chapter 4) and global levels (Chapter 5), which both fall into the conventional strengthening category. The two retrofitting techniques include the characteristics of the utilized RSFJ dampers, thus they offer reliable restoring force mechanism in case of extreme seismic events.

Chapter 3: Rotational Resilient Slip Friction Joint

3.1. Introduction

The recent earthquake events highlighted the importance of utilizing damage avoidance design (DAD) or low-damage design philosophy, to ensure structural safety and minimize the economic impact of seismic event. As for the 2010-2011 Canterbury earthquake series, with some unfortunate exceptions, the modern buildings performed as expected, based on capacity design criteria[96], by showing ductile inelastic behaviour and maintaining the gravity loading system. However, in many cases, the structures were deemed too expensive to repair, leading to no other options than complete demolition[97]. The conventional seismic-resisting frames such as concentrically or eccentrically braced frames (CBFs and EBFs) and moment resisting frames (MRFs) can provide adequate safety against seismic event, provided that the dissipative members and/or connections are designed with sufficient strength, ductility and energy dissipation. The buckling restrained braces (BRBs) can also achieve high level of confidence for the designed performance objectives[11, 14], thanks to their stable and balanced hysteresis behaviour. However, the satisfactory performance of such systems is achieved through plastic deformation in member/connections etc., which might result in residual deformation of the system. The accumulation of plastic deformation might inevitably prevent the rapid restoration of structural function, increase the post-earthquake repair cost, or even increase the risk of building collapse, in case of any upcoming aftershocks[10]. In resolve of the mentioned issues, energy dissipation devices (dampers) can be implemented in building to concentrate the input energy dissipation at pre-defined locations and protect the gravity load-resisting systems from inelastic behaviour[3]. While the performance of the damper-equipped structures depends on the energy absorption capability of the damper, as well as its cyclic behaviour, it can be stated that dampers will generally reduce the kinematic and elastic energy of the structure, which results in smaller stress in the structural members[98]. This study introduces a new damage-free self-centering rotational friction damper, which is denoted hereafter as SC-RF damper.

The frictional devices dissipate the seismic energy through utilizing dry Coulomb friction between the surfaces of two rigid bodies. The configuration of frictional components can take different shapes and forms, which will result in different types of friction damping

systems. However, almost all of the friction dampers present certain advantages such as high level of initial stiffness and energy dissipation, with stable cyclic behaviour. In general, friction dampers are damage-free, insensitive to temperature changes and can present their hysteresis behaviour over many cycles[2]. They are designed not to be activated during service loads and wind. Hence, there is no possibility of failure due to fatigue, before an earthquake[99]. Moreover, most of the friction dampers are tunable, which means their slipping force can be adjusted (for example, by tightening the bolts or changing the pre-stressing force of the damper), which could be considered as an advantage over metallic fuses with fixed force-deformation characteristics.

The friction damper utilization in the building industry dates back in 1980s, when Pall Friction Dampers (PFDs) with linear and rotational friction sliding were employed in cross braces and diagonal braced frames[99, 100]. The PFDs were improved later by Wu et. al[22] via changing the shape of the core plate. Mualla and Belev[23] introduced the Rotational Friction (RF) damper and experimentally validated its performance via one-story scaled braced frame. Since then, a number of studies have aimed to modify the damper or investigate its application for new and existing buildings (see for example, [26, 101, 102], among many others). Mirtaheri et al.[29] introduced a Cylindrical Friction Damper (CFD), by shrink fitting inner shaft into a pre-heated outer cylinder. Compared to other frictional dampers, the CFDs did not use high-strength bolts to induce friction between contact surfaces; thereby it was more efficient in terms of construction costs. In another study[30], they introduced a semi-active adjustable friction damper (AFD) which utilizes controllable hydraulic pressure as a clamping force. Among the benefits of such a damper could be that the re-centering of the structure can be assisted after severe earthquakes. Wang et al.[103] introduced a passive damper with variable saddle-shaped force-displacement behaviour called Arc-surfaced Friction damper and highlighted the capability of their damping system for protection of container crane structures. Wei et al.[104] proposed a vertical spring-viscous damper-concave Coulomb friction isolation system and utilized IDA analyses and performance-based design for seismic vulnerability assessment.

Recently, a number of self-centering (SC) friction devices were introduced and investigated by researchers, which can reduce or even eliminate the residual displacement of the structures subjected to strong earthquakes. Unlike typical friction dampers with rectangular or parallelogram shape hysteresis, the self-centering systems offer a flag-

shape behaviour that can return to its initial state upon unloading[105-107], thanks to the restoring force mechanism that works in parallel with energy dissipation system. Some of the introduced self-centering friction systems are: Energy Dissipating Restraint (EDR)[56], SC friction spring damper[108], SCFD[98], Resilient Slip friction Joint[54] and pre-stressed spring self-centering energy dissipation (PS-SCED)[107]. In this study, a new self-centering damper named Self-Centering Rotational Friction (SC-RF) Damper is introduced which can integrate the recentering behaviour and energy dissipation, all in one compact package. The energy dissipation occurs through rotational friction sliding on the especially designed groove surfaces called friction plates, while the prestressing stack of disk springs would provide the required restoring force for the damper. The SC-RF damper can offer the engineers with flexibility, both in damper design and structural applications. Here, firstly, the device is investigated at component level and the analytical equations are derived to predict the hysteresis performance of the damper, force vs deflection. Secondly, the numerical modelling of the damper is conducted and verified by finite element analysis. Then, the overall performance of the damper is evaluated by experimental tests. As for the next step, a parametric study is carried out to numerically investigate several factors influencing the performance of the system.

3.2. SC-RF damper

Figure 3-1 presents the schematic view of the SC-RF damper, which consists of cap and middle plate (the orange and black plates), clamped together by a pre-stressed stack of disk springs (conical washers) and high strength rod (or bolt). The friction sliding occurs in the circular parts of groove surfaces of the plates, denoted as friction plates, which produces a flag-shaped moment-rotation behaviour. As can be noted, the overall form of the damper is similar to a typical Rotational Friction damper introduced by Mualla and Belev[23]. The structural applications of RF-damper include base isolation systems, as well as different types of braced frame[109]. Additionally, the experimental and theoretical outcomes for RF-damper confirm its stable nearly symmetrical hysteresis over many cycles without any damages to the steel plates. Also, the flexibility in design and structural applications are some other advantages of such damper. Albeit the lack of self-centering could pinpoint the risk of residual drifts for the buildings equipped with RF-damper in active seismic areas.

The SC-RF damper can keep the benefits of RF-damper, while providing the self-centering capability for the system. As an illustration, some of the possible applications of the SC-RF damper in different bracing systems are depicted in Figure 3-2, while other structural applications such as base isolation systems, rocking shear walls, and shear links in EBF systems is possible as well[61, 110]. It is worth noting that for the chevron configuration, dampers are pin-pin connected, while the stability criteria for the diagonal bracing system requires the damper to be installed in fixed-pin condition. In the following, the analytical performance of the friction plates and damper assembly are investigated in detail.

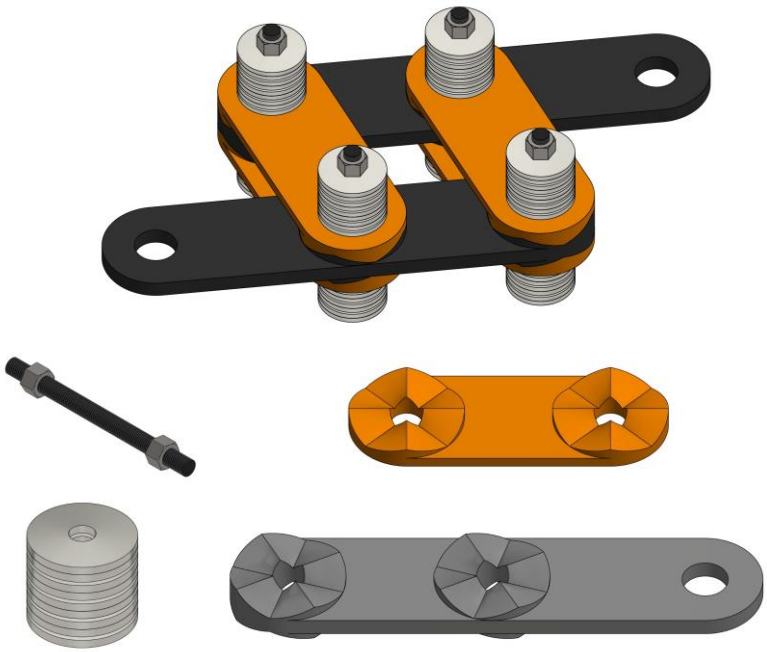

Figure 3-1 The SC-RF damper and its components, including cap and middle plates, disk springs, high strength bolt or rod

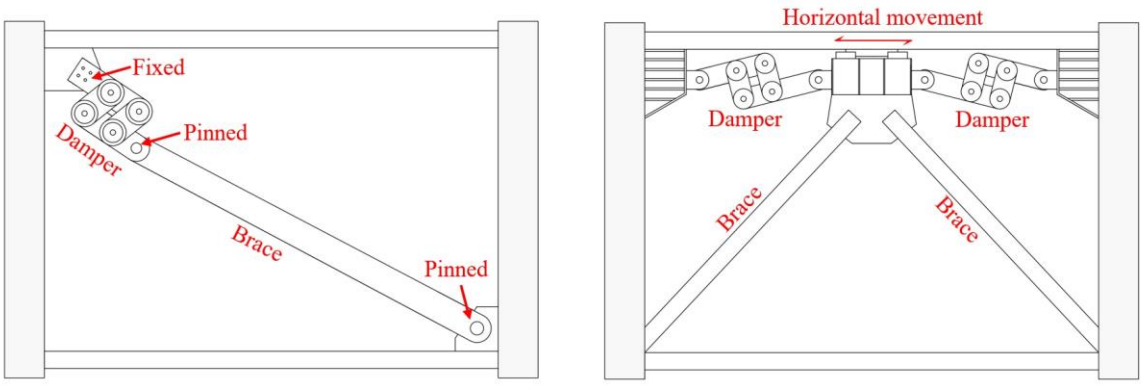

Figure 3-2 Some examples of installation scheme for the SC-RF damper in bracing frames

3.2.1. friction plates performance

The general concept and performance of the SC-RF damper is similar to RSFJ as they both comprise of especially grooved cap and middle plates, clamped by pre-stressed high strength bolt (or rods) and pre-stressed disk springs (Readers could find more information about RSFJ and its applications in [63-67, 111, 112]). As compared to RSFJ which dissipates the energy through axial friction, the SC-RF damper utilizes rotational friction in the friction plates to dissipate the seismic energy. In addition to presented 2x2 symmetric damper in Figure 3-1, other possible configurations for friction plates including asymmetric (two cap plates) and symmetric (two cap plates and one middle plate) with different number of friction plates (2x3, 3x3, etc.) are possible, based on specific force or deflection demand for each design.

Figure 3-3 represents the friction plate consisting of two cap plates and one middle plate with curved sliding surfaces. As can be seen from the top-view of the figure, the overall projected circular surface of the friction plate is divided by eight slices of ϕ=45˚ which indicates the maximum theoretical rotation capacity of the friction plate (Obviously, other angles can also be used, based on design needs). If the friction sliding surpasses the 45˚ rotations, the cap plates would jump into the next groove. However, the deflection capacity of the disk springs are designed to limit the rotation capacity of the plates and prevent such a behaviour. The figure shows that the sliding surfaces of the SC-RF damper present variable groove angle (θ) which increases constantly by moving toward the center of rotation ($\theta_{in} > \theta_{out}$). It is worth to note that such geometry can be defined by helical curves AB and A'B' which have the equal height increment L. The mentioned height increase for the helical curves AB and A'B' is depicted in the Figure 3-3. The reason for utilizing such specific form for the friction plates is to provide surface contact in the cap and middle plates and prevent any linear or point contact between the plates which might result in high stress concentration.

By dividing the friction disks using eight equal slices and concentric circles with radius increment of Δr, the whole friction surfaces can be divided into several concentric clusters with nearly constant groove angle (θ). As an illustration, in Figure 3-3, the whole friction plate is divided to 8 slices with 9 concentric clusters (the four highlighted red clusters are assumed to have constant groove angle over the length of Δr). Accordingly, the overall moment-rotation performance of the friction plate is the sum of the moments

of all clusters, acting in parallel, as they have the same rotation during sliding. When the external moment overcomes the friction resistance between the plates, the rotational sliding occurs. At the slipping motion, all the clusters initiate the sliding simultaneously and have the same rotation. By multiplying the force of each engaged cluster into the associated lever arm (r), toward the center of friction plate and summing the calculated moment for all the clusters, the M_{slip} for the friction plate can be calculated. It is worth noting that each cluster act like a translational RSFJ[52] with clamping force that is divided by the number of working clusters. If we assume that the cap plates have sufficient thickness that can uniformly distribute the bolt clamping force among the clusters, the following equations for determining the slip moment (M_{slip}) of a single symmetric friction plate can be drawn:

$$L = \phi \times R_{in} \times \tan(\theta_{in}) = \phi \times R_{out} \times \tan(\theta_{out}) \tag{1}$$

$$n = \frac{R_{out} - R_{in}}{\Delta r \times 4} \tag{2}$$

$$M_{Slip} \approx \sum_{1}^{n} F_{cluster} \times r = \sum_{1}^{n} 2\frac{F_{bolt,pr}}{n}\left(\frac{\sin\theta + \mu_s \cos\theta}{\cos\theta - \mu_s \sin\theta}\right) \times r \tag{3}$$

By substituting the Eq. 1 and Eq. 2 in the Eq. 3, we can get:

$$\begin{aligned} M_{Slip} &= \lim_{\Delta r \to 0} \sum_{1}^{n} 2\frac{F_{bolt,pr}}{R_{out} - R_{in}}\left(\frac{\sin\theta + \mu_s \cos\theta}{\cos\theta - \mu_s \sin\theta}\right) \times r\Delta r \\ &= \int_{R_{in}}^{R_{out}} \frac{2F_{bolt,pr}}{R_{out} - R_{in}}\left(\frac{L + \mu_s \phi r}{\phi r - \mu_s L}\right) r dr \end{aligned} \tag{4}$$

Where n equals to the number of clusters working in the friction plate. The factor 4 relates to the number of sliding surfaces that are experiencing frictional sliding. The restored moment can also be calculated in a similar manner:

$$M_{restored} = \int_{R_{in}}^{R_{out}} r dF_{slip} = \int_{R_{in}}^{R_{out}} \frac{2F_{bolt,pr}}{R_{out} - R_{in}}\left(\frac{L - \mu_k \phi r}{\phi r + \mu_k L}\right) r dr \tag{5}$$

Where L is the height of the groove, R_{out} is the radius of the friction plate, R_{in} denotes the radius of the bolt hole and ϕ represent the projected angle of each sliding surface. Some of the common possible choices for ϕ could be 30˚, 45˚, 60˚ or 90˚ which represents 12,

8, 6 and 4 slices, respectively. It should be noted that only half of the sliding surfaces are in contact in the clockwise rotation, while in the opposite rotational sliding of the friction plates, the other half will engage in frictional sliding.

The practical range for the θ_{out} can be in the range of 12~30 degrees. Also, the static and kinetic coefficient of friction (denoted by μ_s and μ_k, respectively) are in the range of 0.12~0.20, depending on the surface roughness and the type of steel. Previous researches highlight that the difference between the two coefficient of friction is trivial ($\mu_k=0.85\times\mu_s$ [46]). The ultimate moment upon loading and restoring moment (M_{ult} and $M_{restoring}$) can be calculated by replacing μ_s, μ_k and $F_{bolt,pr}$ with μ_k, μ_s and $F_{bolt,u}$ in the equations 4 and 5, respectively. The free body diagram for the four stages of moment-rotation behaviour of a symmetric friction plates can be seen on Figure 3-4. It is worth to note that the ultimate force in the bolt ($F_{bolt,u}$), can be calculated using the following equation where Δ_s and K_s represent the total deflection capacity of the stack of disk spring and their corresponding stiffness, when they are becoming fully flattened (conical washers become fully compressed).

$$F_{b,u} = F_{b,pr} + K_s\Delta_s \tag{6}$$

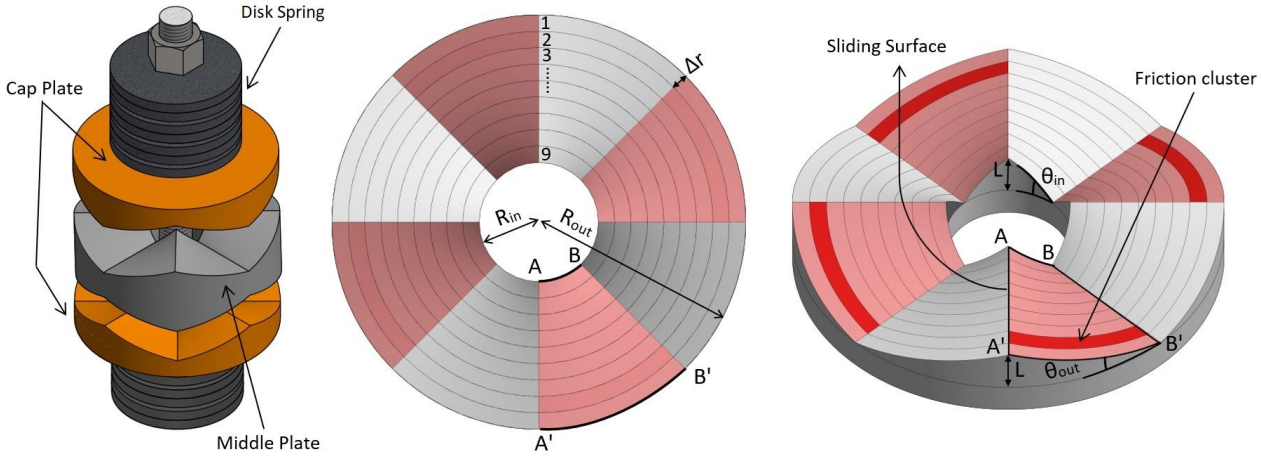

Figure 3-3 Symmetric friction plate

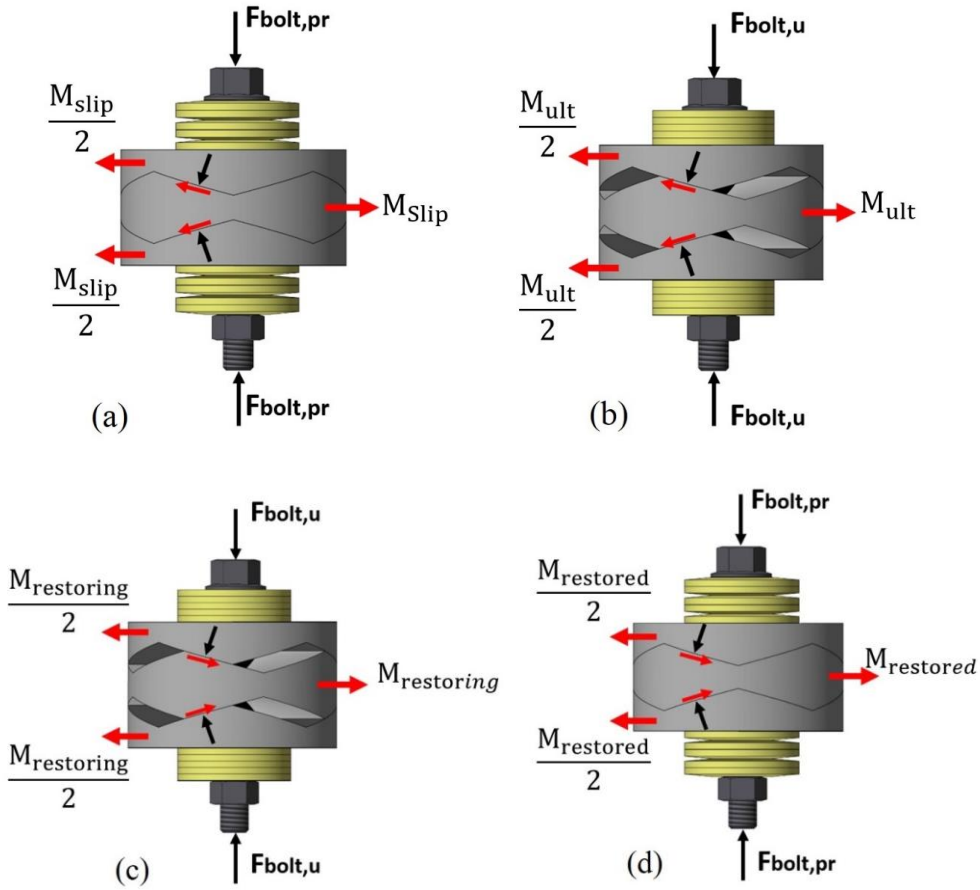

Figure 3-4 Free body diagram for symmetric friction plates: (a) at initial slipping; (b) at ultimate loading; (c) at ultimate unloading (restoring); and (d) at restored position

To verify the predicted equations, the finite element model of an asymmetric friction plate was conducted using ABAQUS software platform[113]. The friction plates were assumed to have outside groove angle θ_{out}=15˚, with overall radius of R_{out}=62.5mm and R_{in}=18mm. The disk springs were assumed to be pre-stressed at $F_{b,pr}$=66kN and provide the ultimate force of $F_{b,ult}$=132kN with Δ_s=7.875mm, representing a stack of nine disk springs placed in series with ultimate capacity of 132kN with deflection capacity of 1.75mm per disk. The assumed stack of disk springs would provide nearly 27˚ rotation for the friction plate. The slip motion was allowed utilizing a contact element with surface-to-surface discretization. The tangential behaviour of the contact was modelled by penalty method with static and kinetic friction coefficient equal to 0.18. For the normal direction, the pressure-overclosure feature of the Hard-contact was assumed for the friction model. Table 3-1 summarizes the assumed values for modelling of the friction plate and the Figure 3-5 shows the Von-Mises stress contours of a single asymmetric friction plate and compares the analytical predictions versus the obtained FE results, which are in a very good agreement.

Table 3-1 Parameters for friction plate modelling

Parameter	Unit	Value
Rin	mm	18.0
Rout	mm	62.5
Fb,pr	kN	66.0
Fb,ult	kN	132.0
Disk flattening load	kN	132.0
Disk Deflection Capacity	mm	1.75
No. of Disks	-	9
Coefficient of Friction	-	0.18

(a)

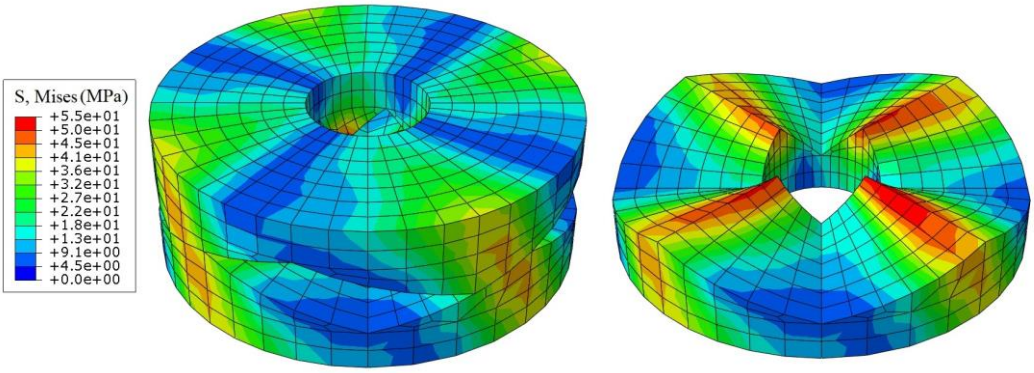

(b)

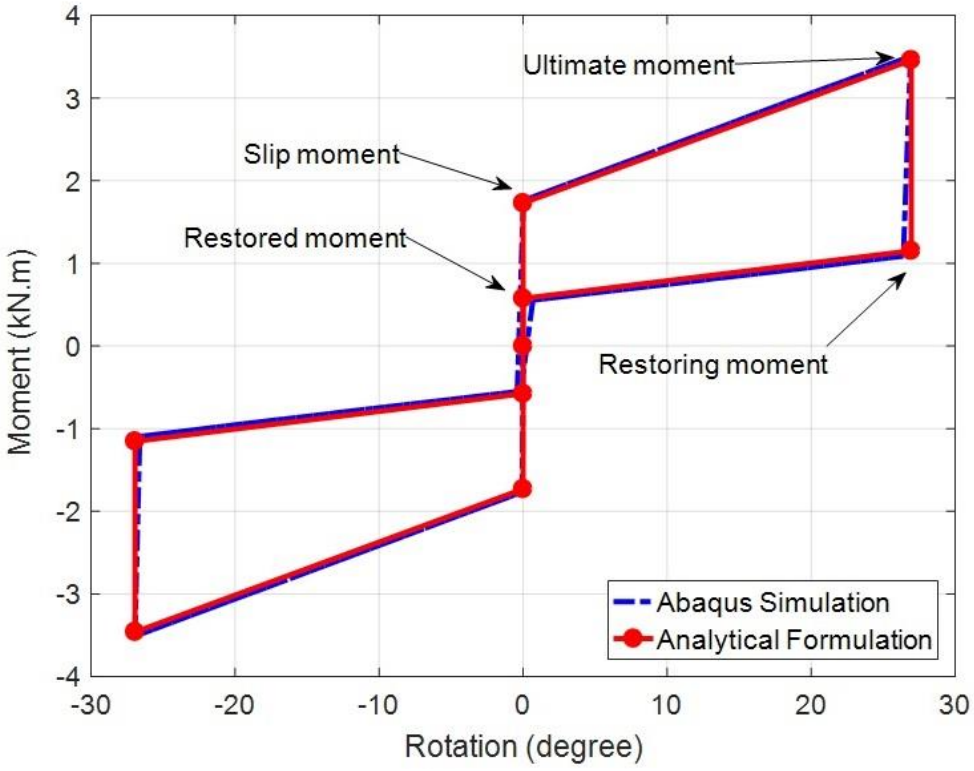

Figure 3-5 The FEM analysis of a single friction plate: (a) stress distribution; (b) comparison between analytical equations and FEM outcomes

3.2.2. Damper assembly performance

The SC-RF damper comprised of several cap and middle plates, clamped by means of bolts and pre-stressed disk springs. The friction plates can be manufactured along with the plates as a single part or be produced separately and then connected to the plates (for example, by welding), which may make it more appealing in terms of mass production. Figure 3-6 shows the damper and the simplified structural model for the device assembly, with a self-centering rotational spring connecting the cap and middle plate. The damper can be modelled in commercially available structural designing software (such as SAP2000[114]), for checking the internal forces in the cap and middle plates. In addition to the characteristics of disk springs, different length of plates could also be selected (L1, L2 and L3), based on each specific design requirement. In general, increasing the plate length would result in more deflection capacity with lower force. The effective length of the device (the distance between the two pin ends) can be calculated using the below equation:

$$Joint\ length = \frac{2L_3 + L_2 + L_1 \cos\beta}{\cos\alpha} \tag{7}$$

Where the parameter α can be obtained by:

$$\alpha = \tan^{-1}\left(\frac{L_1 \sin\beta}{2L_3 + L_2 + L_1 \cos\beta}\right) \tag{8}$$

The four friction disks act in parallel as they have equal rotation during the device performance[115]. The relation between the damper force and the moment of each friction plate is calculated using following equation:

$$F = \frac{4M}{(2L_3 + L_2)\sin\alpha} \tag{9}$$

Where M is the frictional moment provided by each friction plate. One important aspect for the damper is adjusting the orientation of the friction plates (selection of appropriate angle between cap plates and middle plates at its resting stage as denoted by β in Figure 3-6) to ensure the same amount of deflection for the damper in its open and closed position (ultimate tension and ultimate compression stage). For the bracing configurations, it is preferred for the device to show similar deflection in both tension and compression state. It should be noted that the rotation capacity of the friction plates is

equal on both clockwise and counter-clockwise direction and this is rather a geometric situation associated with the plates. Figure 3-7 better illustrate this phenomenon for a SC-RF damper having friction plate diameter=125mm with ±27˚ rotation capacity, with L_1=L_2=220mm and L_3=230mm. The Figures 3.7-a, 3.7-b and 3.7-c (case I) shows the damper with β=90 at the resting, close and open position with associated length of the device written in each stage. As for the case II, Figures 3.7-d, 3.7-e and 3.7-f demonstrates the same damper with β=180-72=108 at the resting, close and open position, which is calibrated to present equal ultimate deflection at both tension and compression. The length of the damper indicates that when β=90, the damper provides different amount of deflection for tension and compression (804.1-714.7=89.4mm in tension and 714.7-612.3=102.4mm in compression); while the second case (β=108), shows that the deflection for the same damper with similar L_1, L_2 and L_3 and modified β=108 is nearly equal for both tension and compression (almost 100mm) under 27˚ rotation.

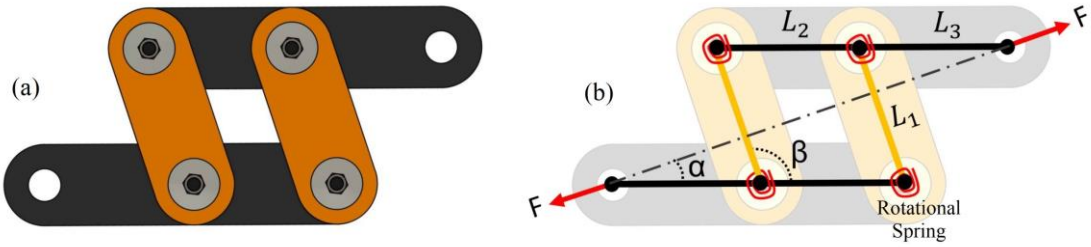

Figure 3-6 Simplified damper model for implementing in SAP2000

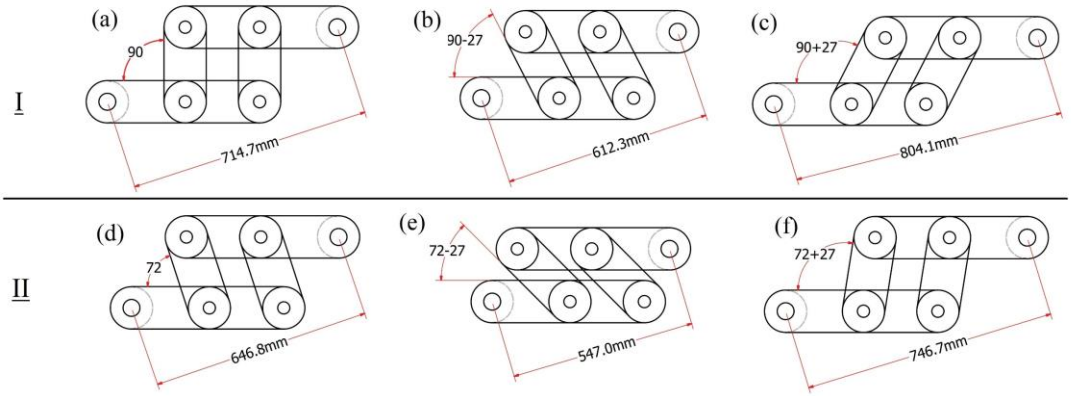

Figure 3-7 The influence of initial adjustment of friction disks for equal deflection: I: Non-adjusted damper in its initial (a), closed stage (b) and opened stage (c); II: Adjusted damper in its three initial (d), closed (e) and opened stage (f).

Based on the correlation between the force of damper and the induced moment of friction disk (eq. 10), and the overall length of the device in each value of friction plate rotation, the force-displacement curve of the device can be evaluated. On this basis, a prototype damper with 100mm deflection capacity was designed. The cyclic performance of the

prototype damper was simulated using SAP2000 software package[114]. The damper-friction link element for modelling the moment-rotation behaviour was calibrated based on the slip moment, loading and unloading stiffness of the M-θ curve. It should be noted that the nonlinear analysis model in the SAP2000 software must include geometric nonlinearities of P-Δ and large displacement, to calculate the correct force-displacement response equal to the proposed analytical equations in this chapter. Table 3-2 presents a summary of the designed prototype damper, with the assumed and required parameters. Figure 3-8 compares the calculated force-deflection behaviour from theoretical formulations and the flag-shaped hysteresis obtained from SAP2000 numerical outcome. The force-deformation value of the damper has been plotted for 0%, 25%, 50%, 75% and 100% rotation capacity of the friction plates during loading and unloading of damper). As can be noted, the post-slip stiffness of the SC-RF damper is variable and takes a slight nonlinear form. This is due to the damper's second-order geometric effects (the factor $1/\sin\alpha$ in Eq. 10). However, as the friction plates' rotation decreases, this nonlinearity tends to become more linear. Assuming that the performance of the damper is nearly linear, the equivalent viscous damping, based on the hysteretic energy dissipation can be evaluated using Jacobsen's approach[116]:

$$\xi = \frac{2}{\pi}\frac{A_1 + A_2}{A_3} \tag{10}$$

Where areas A1, A2 and A3 are shown in the Figure 3-8. The damping ratio of the damper can be adjusted by changing the surface friction (via changing the surface roughness or surface treatment), and groove angles. For the prototype damper, the calculated damping was calculated as 8.1%. Although using equivalent viscous damping concept might present some errors in the conversion of friction damping to equivalent viscous damping[117], the utilized Jacobsen's approach seems suitable for practical purposes.

Table 3-2 Summary of the damper characteristics

	Parameter	Unit	Value
Damper Characteristics	Cap plate thickness	mm	12
	Middle plate thickness	mm	20
	β	degree	108
	Friction plate diameter	mm	125
	Inner hole diameter	mm	36
	Outer groove angle (θ_{out})	degree	15
	grooves' height increment (L)	mm	13.15
	Coefficient of Friction	-	0.18
Assumed disk spring parameters	Disk spring ultimate force	kN	132
	Disk spring deflection capacity	mm	1.75
	Pre-stressing force (Fb,pr)	kN	66
	No. of disk spring per bolt per side	-	9
SAP2000 Parameters	Slipping stiffness (loading)	kN.mm/rad	7368.9
	Slipping stiffness (unloading)	kN.mm/rad	2458.1
	Pre-compression displacement (dc)	rad	-0.468
	Stop displacement (ds)	rad	0.47

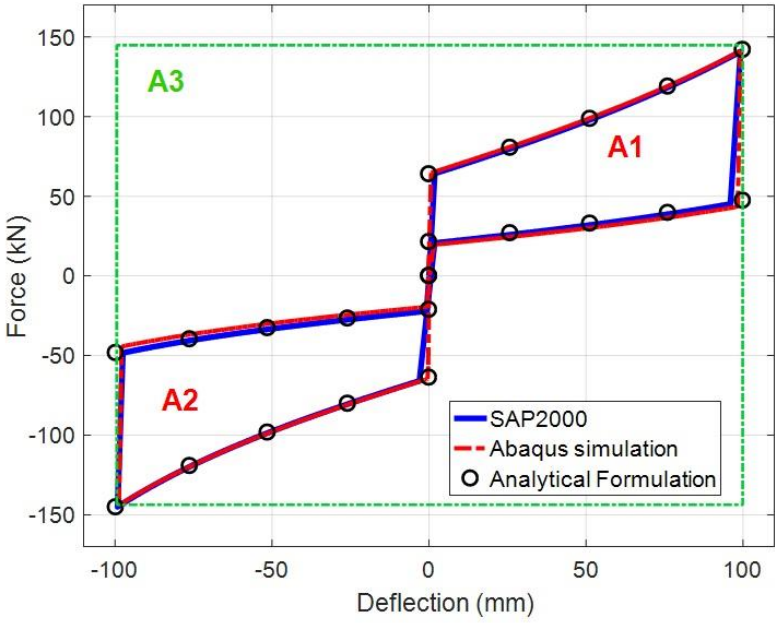

Figure 3-8 Comparison of the analytical formulation with Numerical model (SAP2000) and FE analysis (Abaqus)

3.2.3. Finite Element Analysis of the damper

To validate the analytical equations for the damper assembly and also verify the SAP2000 model, the same device was modelled in Abaqus FE analysis software. The standard solver was employed for the analysis. The high strength steel (F_y=690MPa and F_u=860MPa with 18% elongation) with isotropic hardening behaviour was considered material modelling. The cap plates and middle plates were modelled using deformable

solid parts meshed by C3D8R finite element (an 8-node linear brick with reduced integration). To lower the solution time needed by the software, only the upper half of the damper was modelled (two cap plates with half of the middle plate), with proper symmetrical boundary condition. For the contact modelling, both the "Hard contact" normal behaviour (to avoid overclosure) along with tangential behaviour with relative sliding (by assigning Coulomb friction law) was considered with single value of μ=0.18 for both static and kinetic friction coefficients. Instead of modelling the rods and the stack of disk springs, their pre-stressing effects were simulated using spring/dashpot feature of the software. The analysis was conducted considering two loading steps: (i) applying the pre-stressing force on the cap plate (to simulate the bolt clamping) and (ii) displacement history application. Figure 3-9 depicts the Von-Mises stress contour of the damper at pre-stressing stage and during 100mm compression and tension deflection, while the results of the finite element model is compared with numerical modelling (SAP2000 model), as well as analytical formulations in the Figure 3-8. As can be noted, the cap plates managed to distribute the pre-stressing force uniformly in the friction plate, where only trivial stress concentration without any plastification is witnessed at the sharp corners of the grooves near the rotation center of friction plate. Moreover, the FE outputs are in good agreement with the derived analytical and numerical modelling.

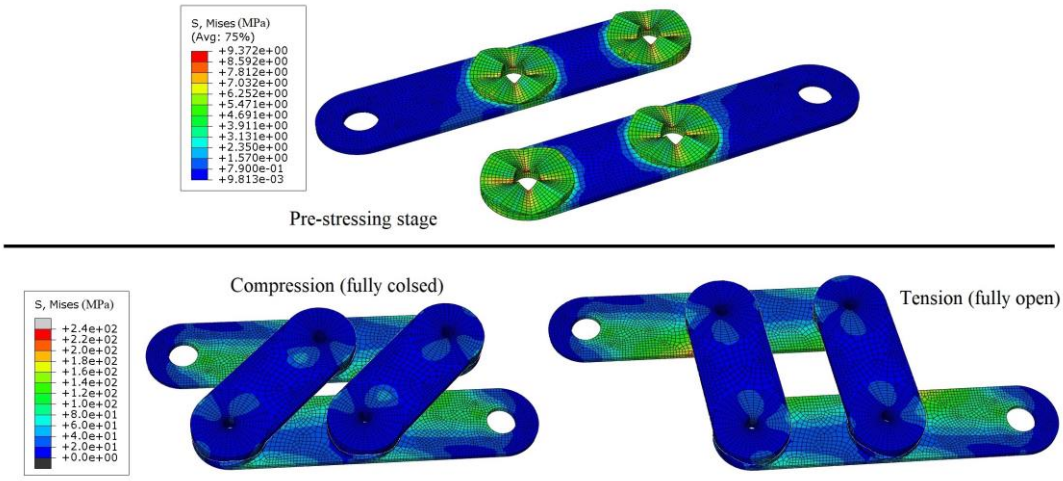

Figure 3-9 Finite element analysis of the damper assembly: Von-Mises stress counter at ultimate tension and compression

3.3. Experimental testing

In order to experimentally investigate the hysteretic behaviour of the SC-RF damper, a series of tests were conducted on the damper's components, as well as the manufactured prototype damper. It should be noted that the high strength bolts (or rods) are designed to

remain fully elastic during the expected performance of the device and their results were not included in this chapter, for brevity. Experimental tests include obtaining the performance of disk springs, as well as cyclic performance of the damper, to validate the FE model and derived equations.

3.3.1. Disk Spring testing

In general, the disk spring's performance is assumed to be linearly elastic up to its flattened load[67]. As the disk springs surpass their flattened point, their stiffness increases rapidly with small deflection. However, the experimental tests of disk springs usually do not show such a sharp flattenend point and rather shows a transition between these two phases which could differ based on the number of parameters including different number of disk springs. Moreover, based on the arrangement of disk springs, the interaction between the disk springs and bolt or rod, and also the interaction between the edges of disk springs, some variation between the calculated characteristics load curve and actual loading of the disk springs could be witnessed. Therefore, it was decided to investigate whether the resulting frictional forces can alter deflection capacity of the overall disk springs stack. To do so, a set of 3-cycle force-based test were applied on the various stacks of 1 to 21 disk springs up to their flattening load. The cyclic load ranged from 0.5kN to 135kN (slightly higher than the nominal disk spring flattening load,132kN) to make sure the disk springs are pre-set[118]. For safety reasons, an especial sleeve was utilized for test (Figure 3-10). The elastic deflection of the test sleeve (without any disk spring) at the force of 135KN, were subtracted from the overall deflection of the test to provide the gross deflection of the disk springs (including the elastic deflection of the rod). The presence of initial 0.5kN force would prevents any slackness movement in the disk springs, during the test. Such a test setup can simulate the performance of disk springs stack on a real damper, with acceptable accuracy. Figure 3-11 shows the results for a sample stack of disk spring and the average deflection capacity of the disk springs, based on their last cycle. As can be noticed, the friction forces are negligible for the stack of disk springs and the average deflection capacity remains uniform (1.56mm) for different number of disk springs, except for the stack of one to three disk spring which is in the range 0f 1.2~1.33. As for these stack of disk springs, smaller value of deflection capacity was witnessed which is mainly related to the first disk spring that has more contact surface with the top flat plate. The friction characteristics between the first disk spring and the flat plate is also different from the friction forces between two disk springs,

which can slightly change the results. However, as the number of disk springs in the stack increases, the smaller deflection capacity of the first disk spring will be distributed in the bigger stack.

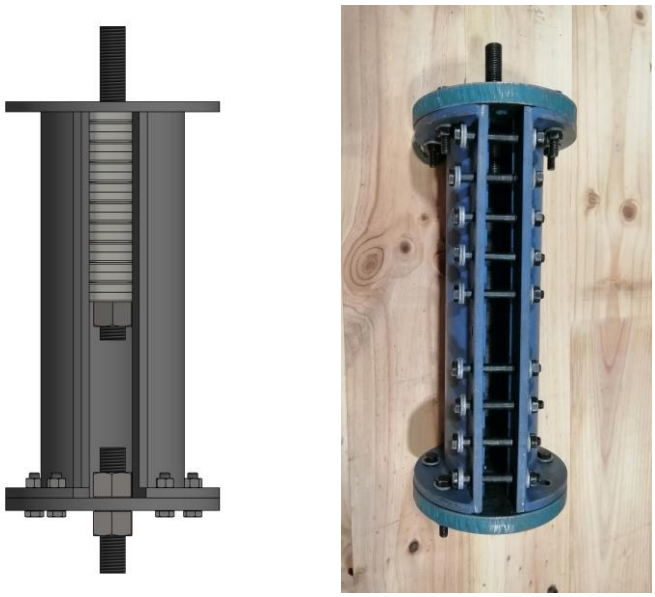

Figure 3-10 The utilized sleeve for testing of disk springs

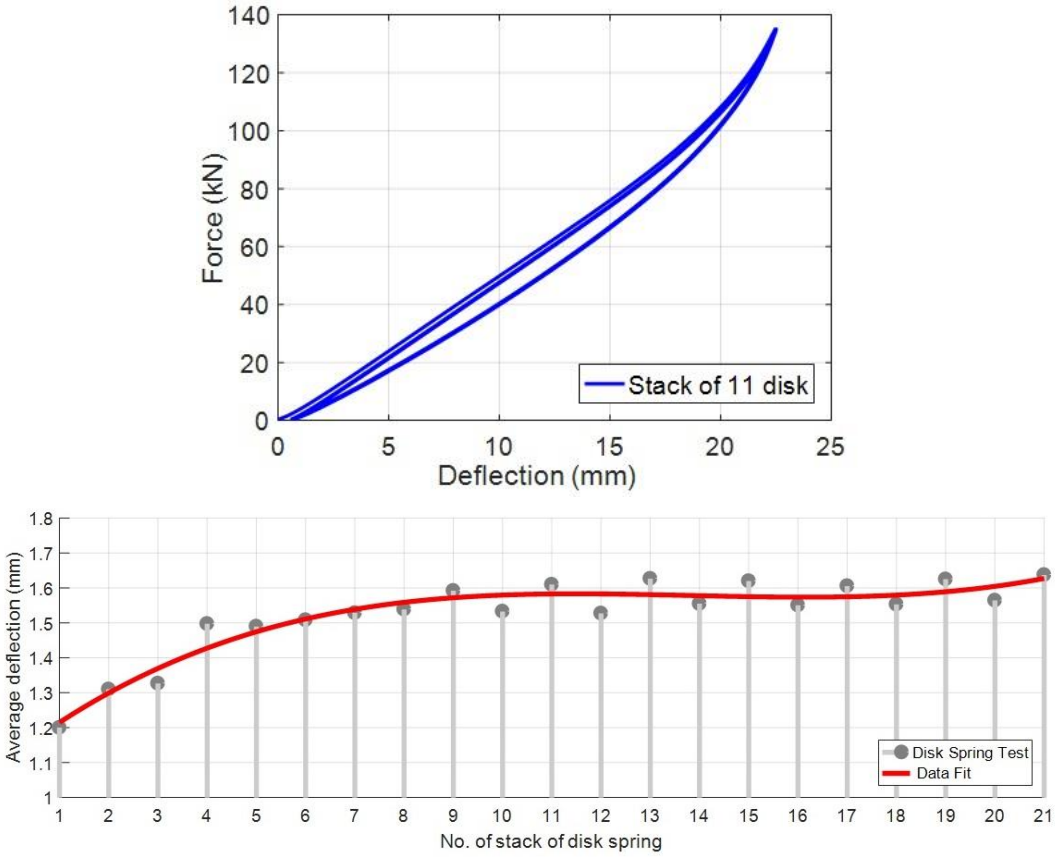

Figure 3-11 Cyclic testing of disk springs: (Left) Sample test of stack of 11 disk springs up to the flattening load, and (Right) The obtained average deflection capacity of the disk springs

3.3.2. Damper testing

The high strength steel plates (F_y=700 MPa, F_u=860MPa) were used for manufacturing the cap and middle plates of the prototype damper. Figure 3-12 shows the damper components including its cap and middle plates and a closer photo from one of the friction surfaces of the plates. It is worth noting that due to the curved surface of the friction plates, a special cutter was utilized for CNC machining, to create the friction plates, as accurately as possible. It is worth noting that the friction surfaces underwent specific surface treatment, to minimize any chance of material wearing due to high friction. The device was assembled with nine stack of disk springs on each side. The disks were preset, to eliminate any types of drop in the hysteresis curve of the device. To do so, a pre-stressing device attached to the rod to impose a flattening load to the disk springs, up to the disk spring ultimate deflection load (132KN) and then release the force.

The damper was tested with Universal Testing Machine (UTM) as shown in the Figure 3-13, with four different pre-stressing force (F_{pr}=0kN, 18kN, 40kN and 55kN), up to 100mm deflection in tension and compression as well. The loading protocol includes quasi-static progressive tension and compression displacement cycles of ±25mm, ±50mm, ±75mm and ±100mm. The loading rate were selected as 1mm/s and each cycle repeated three times to validate the performance of the system over repeated cycles. It is worth to note that the damper was initially tested without any pre-stressing, then the pre-stressing increased to minimize any failure risks and also cover the whole performance of the device with various pre-stressing as well. The results for each test are then compared with Abaqus FE model (Figure 3-14). The coefficient of friction was calibrated to 0.13, as it would fit better with experimental results. As can be noted, the experimental results are in agreement with the Finite Element Analysis. Regarding the experimental test with 55kN pre-stressing force (Figure 3-14-d), an slight jump in the experimental test can be noted, which is due to the elastic non-linear behaviour of the disk springs, when they have reached their deflection capacity and are about to be full flattened.

(a)

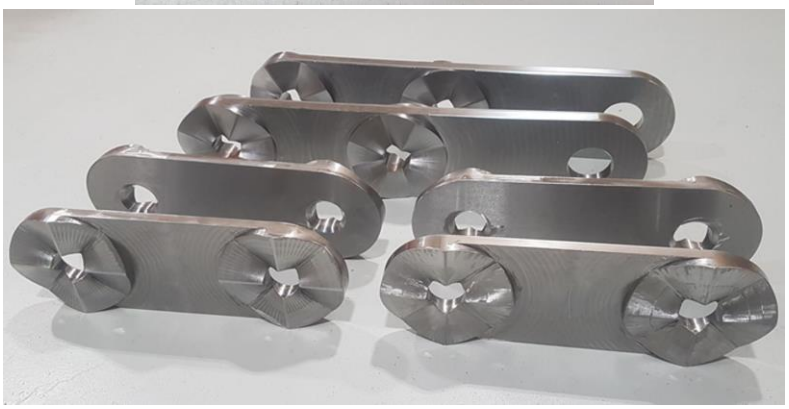

(b)

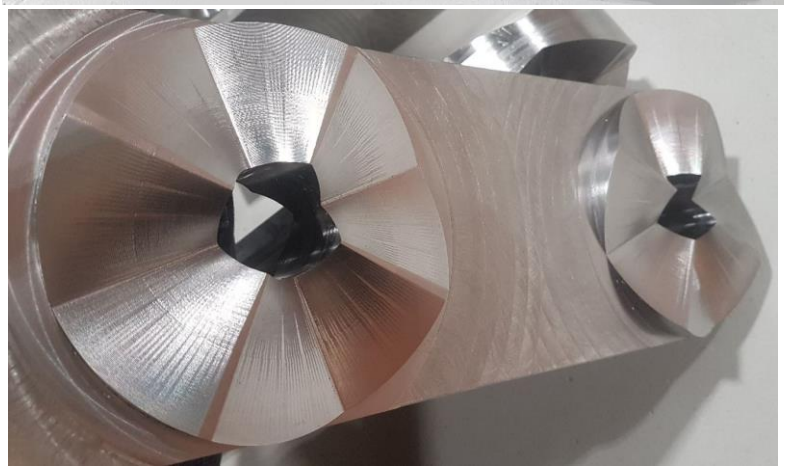

(c)

Figure 3-12 The SC-RF damper components: (a) The stack of disk springs, (b) The cap and middle plates, (c) a closer look of the friction plates

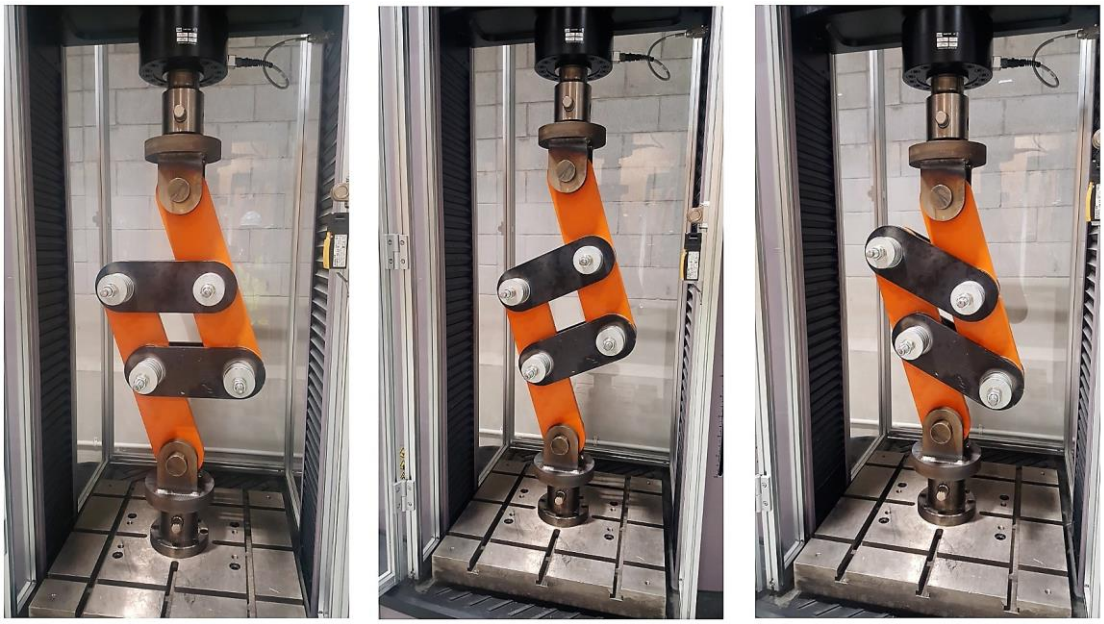

Figure 3-13 SC-RF damper, at its resting, open and close position

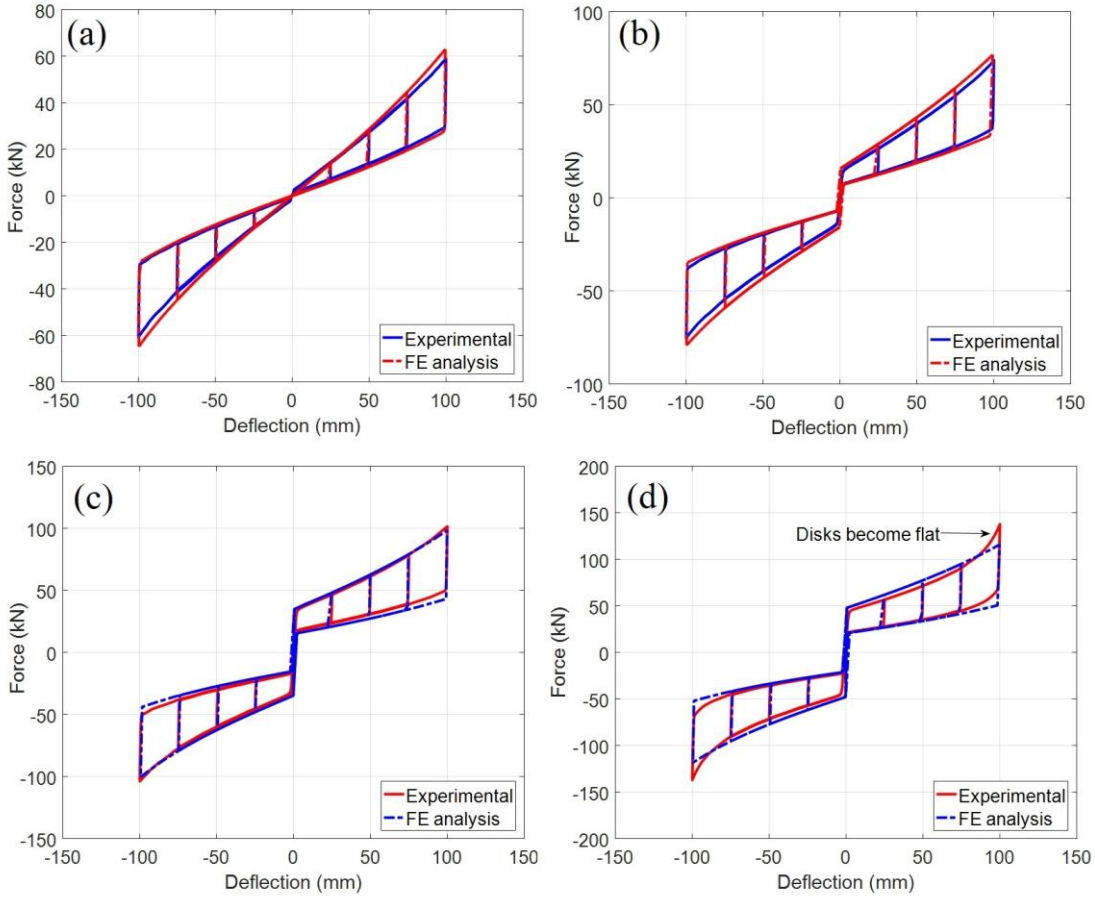

Figure 3-14 The Force–Deflection hysteresis comparison of Experimental vs. Finite Element Analysis for the SC-RF damper with different pre-stressing force scenarios: (a) 0kN, (b) 18kN, (c) 40kN, and (d) 55kN

3.4. Damper's parameter effects

As for this part of the study, some of the influencing parameter affecting the performance of the damper were investigated. Since the performance of the device is directly related to the friction plates behaviour, the parametric study is focused on the friction plates, rather than the whole damper assembly. Generally, two main categories affect the damper performance which are parameters related to disk spring arrangement (series, parallel, etc.) and characteristics related to the friction plates (coefficient of friction, and groove angle).

As for the disk spring arrangement, different stacks of disk springs can be utilized for providing wide range of force-deflections, which can offer more flexibility for the designers and researchers. Different stacking arrangements can be employed for the damper including parallel, series or combination of both. Figure 3-15 shows the ideal load-deflection graph for different disk spring arrangements. As can be seen, while putting the disk in in double and parallel stack would double and triple the ultimate load, arranging the disk in series will result in increased deflection capacity.

The effect of increasing the number of disk springs on the performance of the friction plate is shown in the Figure 3-16-a, while the effect of single vs. double stack of disk spring arrangement is depicted on the Figure 3-16-b. As can be seen from the figures, while increasing the number of series stacking does not change the Mslip and Mult, it increases the rotation capacity of the friction plates. On the other hand, doubling the stack of disks does not change the rotation capacity of the damper, whereas it can double up the Mslip and Mult of the friction plate and increase the damping of the system as well. Moreover, parallel stacks of disk springs can present some friction between the disk springs surfaces known as self-dampening within the stack of disk spring which is not included in the Figure 3-16-b and can change the actual performance of the disk springs, as compared to the calculated performance. Therefore, it is recommended to lubricate the surfaces of disks in parallel stacks and the maximum number of parallel sets be limited to four to reduce the deviation from calculated characteristics of the disk spring stack to the actual measured ones.

Regarding characteristics related to the friction plates, the coefficient of friction (COF) and groove angle are investigated. Figure 3-16-c demonstrate the effect of outer groove angles on the M-θ curve of the friction plates. It can be seen that increasing the outer

groove angles would increase the Mslip and Mult of the friction plate, with the price of lowering the friction plate rotation capacity. This is due to the increased vertical movement of the cap plate, because of larger grooves angle. Figure 3-16-d pinpoints the effect of different coefficient of friction (COF) on the M-θ curve of the friction plates. As can be seen, higher coefficient of friction means higher damping ratios (hysteresis curve) for the device. On the other hand, higher COFs require larger restoring force to ensure the self-centering of the damper.

While the most prevalent engineering applications usually utilize parallel or series stacking of disk springs, other options such as progressive stacking could also be utilized for the disk spring arrangement of friction plates. On this basis, the disks become flat consecutively and provide a progressively increasing stiffness. This can be achieved by either stacking disks of various thickness in series, or stacking single, double and triple parallel set in series, as it is shown in Figure 3-17-a. Accordingly, the pre-stressed friction plate demonstrates a progressively increasing multi-linear self-centering flag-shape (Figure 3-17-b) with distinctive post-slipping stiffnesses (zones). The single, double and triple parallel set of disk springs would reach their capacity in turn and become flat, as the load increases in the stack of disk springs. When the single parallel set becomes flat, the hysteresis curve surpasses the zone 1 and enters the zone 2 where double and triple parallel sets of disk springs have deflection capacity, while the zone 3 is provided by the remaining deflection capacity of the triple parallel set of disk springs when the single and double parallel sets have reached their ultimate force. Such a progressive self-centering behaviour might be helpful in specific applications and situations where the damper needs to be separately optimized for various seismic intensities at the same time (for example, adaptive self-centering dampers and shocking absorbers).

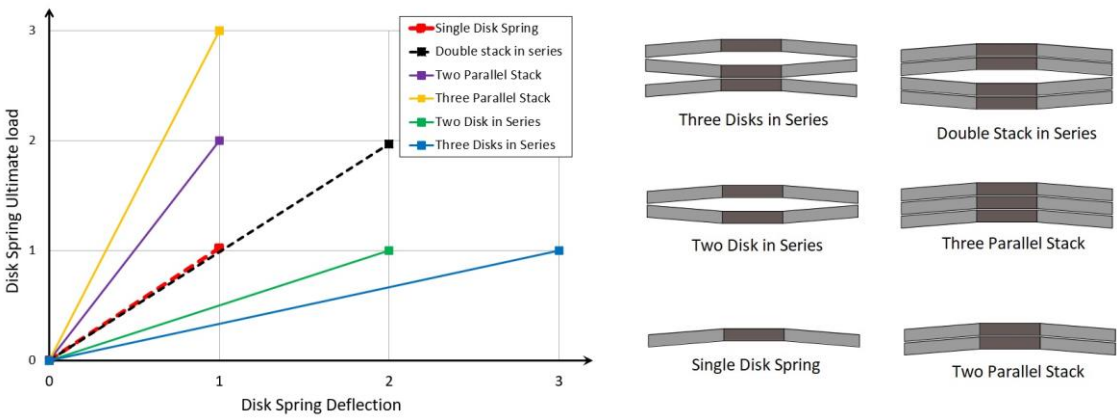

Figure 3-15 ideal load-deflection graph for different stack of disk spring arrangement

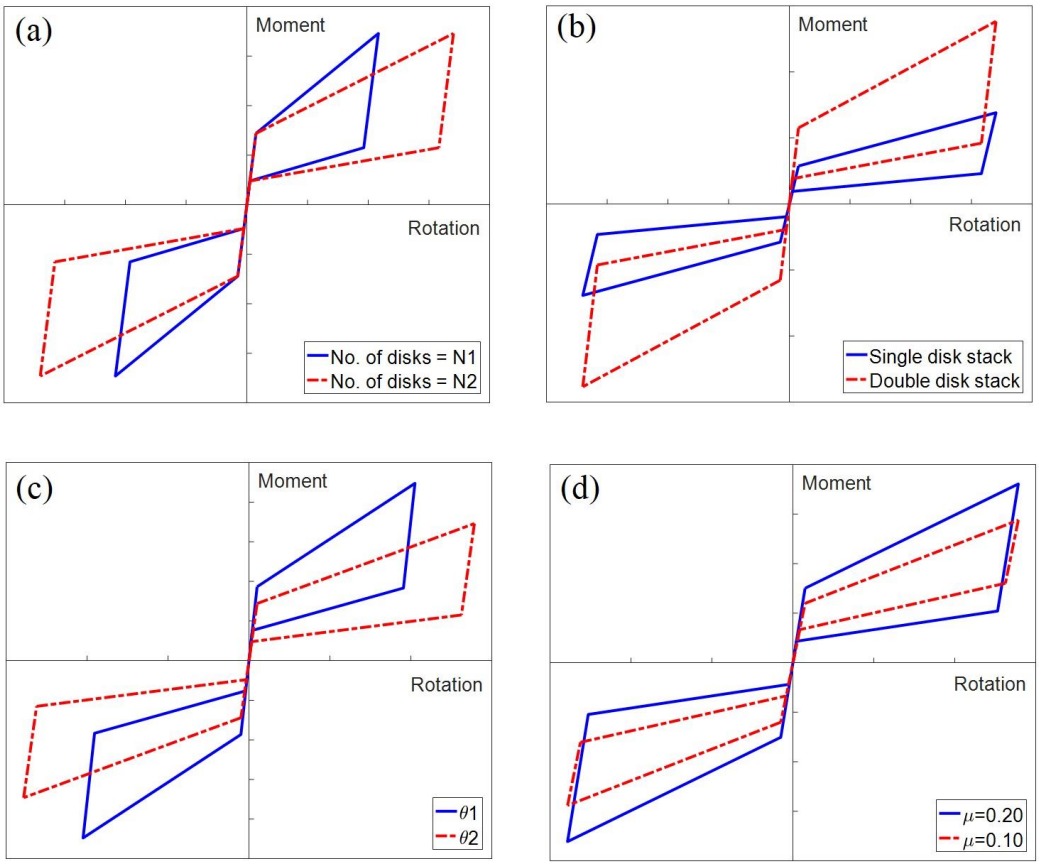

Figure 3-16 Numerical study on damper parameters' effects: (a) Number of disk springs, (b) Number of parallel stacks, (c) Friction plates outer groove angle, and (d) Coefficient of friction

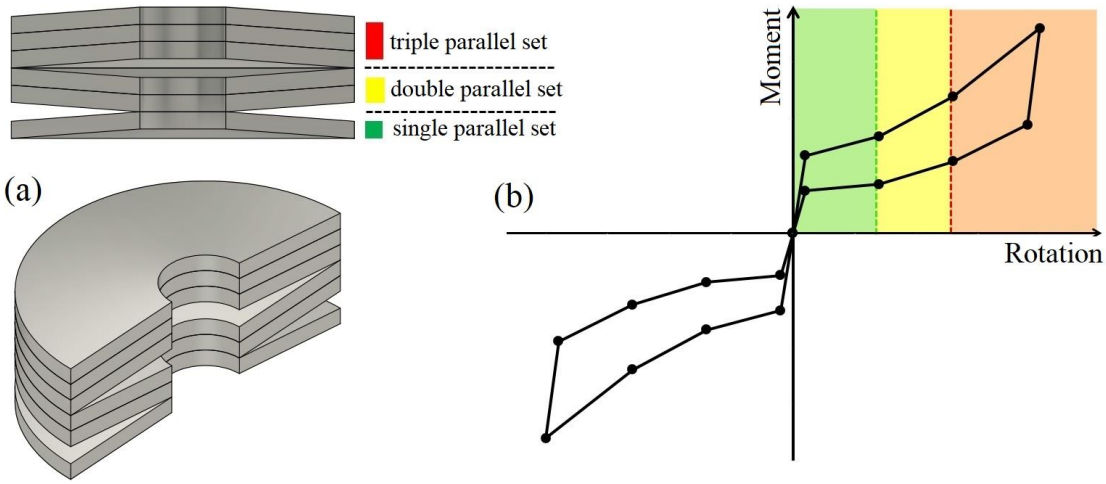

Figure 3-17 Progressive stacking of disk springs: (a) An example stack of single, double and triple parallel set in series; (b) The multi-linear self-centering hysteresis M-θ behaviour of friction plate

3.5. Summary and Concluding Remarks

In this chapter, an innovative self-centering damper named Self-Centering Rotational Friction damper (SC-RF damper) was introduced and investigated numerically and

analytically. This novel damper can be designed based on different force/deformation demands and be utilized in different structural systems as well. The flexibility of the damper regarding the length of cap and middle plates, the friction plate characteristics and arrangements and also various arrangement of disk springs can provide the designers to optimally design the damper for each specific performance.

In this chapter, the analytical equations for calculating the force-deflection behaviour of the device were derived and validated using numerical and finite element analysis. Moreover, the parameters affecting the damper's performance were thoroughly investigated. The performance of the device was experimentally tested with different pre-stressing forces and were validated by finite element model. Moreover, the performance of the disk spring stack was investigated as well. Through this new damper introduced to be used either in new or existing earthquake-prone structures, the buildings could be reoccupied quickly with minimal business interruption and repair costs after severe earthquake events.

Chapter 4: Seismic Strengthening of Deficient RC Frames Using RSFJs as Haunches

4.1. Introduction

During the past decades, seismic retrofitting and repairing of existing reinforced concrete (RC) frames has been the subject of various studies[1]. Evidence from the past earthquakes in high seismic regions (such as Christchurch, 2011 [119], Kermanshah, Iran, 2017 [120], among many others) has highlighted the necessity for strengthening and retrofitting of under-designed RC frames to improve their seismic capacity. Different retrofitting techniques can be utilized for either global retrofitting of the system (such as adding BRBs[121] or dissipative braces with dampers along the entire frame[111, 122] and use of shear walls) or local strengthening of the weak structural elements[123]. In this regard, the RC beam-column joint (defined as the region surrounded by the beam and column interfaces) has received considerable attention among the researchers, as a key-component in the frame performance. Usually, the non-seismically designed RC joints suffer from improper transverse reinforcement which might trigger the failure of the frame before formation of beam plastic hinges. Accordingly, the system would show a brittle behaviour during strong earthquakes without much warning in the form of large drifts, which could lead to serious consequences.

To improve the performance of RC joints, several techniques have been introduced and tested by researchers including use of shotcrete jackets[124], FRP laminates[125] or rebars[126], ferro-cement jackets with chamfers[127] and enlarging the RC joints[128, 129]. Recently, another attempt has been devoted to adapt the haunch retrofitting system to redirect the shear stress flow from the joint regions and impose a more ductile beam plastic hinge mechanism, instead of a brittle joint shear failure[130]. As a pioneering study, Pampanin et al.[131] demonstrated the efficiency of such system and proposed a retrofit design procedure. Various types of haunch systems have been implemented in the RC joint retrofitting such as fully-fastened haunch systems[132], reinforced concrete haunches[133], Buckling Restrained Haunches[134] and haunch viscoelastic damping braces[135].

This study introduces the Resilient Slip Friction Joint (RSFJ) haunch system for retrofitting of deficient RC beam-column joints. As a tuneable self-centering friction damper that is pin-pin connected to the beam-column connection and acts as a haunch element, the RSFJ can preserve the benefits of conventional haunch retrofitting system while offering reliable energy dissipation and recentering force for the RC frame. The schematic diagram of the RSFJ haunch retrofitting assembly is shown in Figure 4-1. While such a method can also increase the lateral stiffness of the frame, it is more suited for RC cases with inadequate shear capacity for the joints. As compared to the traditional wet retrofitting methods for RC frames (such as adding shear walls to the system, or concrete jacketing), the proposed retrofit solution is a dry construction method which is easier to implement with minimal serviceability disruption of the system. It can provide reliable energy dissipation and seismic performance during multiple seismic scenarios (main-shock aftershock events). This chapter experimentally investigates the efficiency of RSFJ with pinned end connections for haunch retrofitting. The OpenSEES software platform is utilized to develop a simple numerical model to simulate the non-seismically designed RC joints with different reinforcement details, as well as for the model retrofitted with the RSFJ haunches. With the help of the developed model, a step by step retrofit design procedure is proposed for strengthening of RC joints with RSFJ haunches. Two case studies including the interior and exterior joints of a RC frame are then retrofitted by RSFJ haunches to check the efficacy of this retrofitting system. The results highlight the improved performance of the retrofitted cases, in terms of strength, energy dissipation and residual drift, as compared to the non-retrofitted RC frame systems.

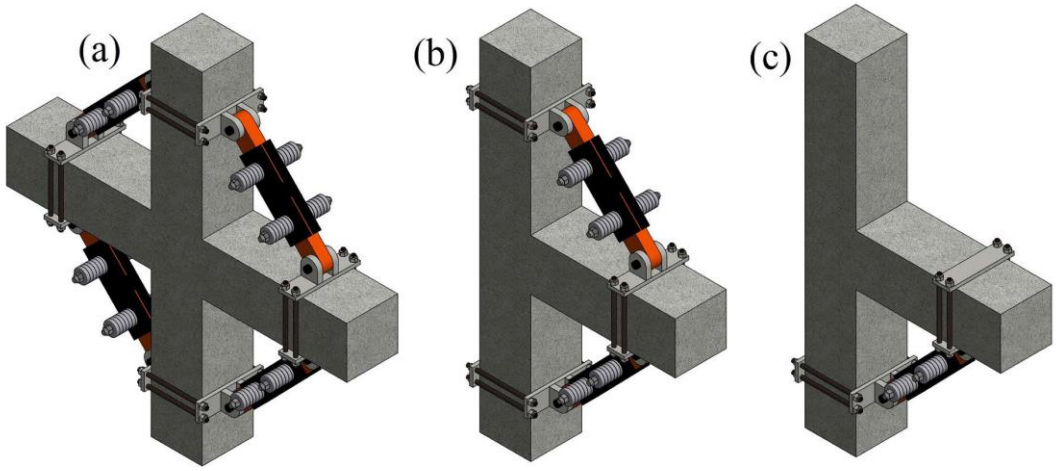

Figure 4-1 Schematic view of RSFJ Haunch retrofitting system with various configurations: a) Interior joint assembly with four haunches, b) Exterior joint with double haunches, and c) single haunch

4.2. Seismic behaviour of deficient RC beam-column joints

Different failure mechanisms can be expected in under-designed or non-seismically designed RC beam-column connections, which is mainly due to the poor reinforcement detailing in the joint region. Figure 4-2 summarizes some of the typical detailing in such weak beam-column joint regions. The lack of shear reinforcement in the RC beam column connection will adversely affect the post-cracking behaviour of the RC joint. For such joints, the compression strut mechanism of the RC beam column connection is the only source of transferring shear force in the system and its efficiency is linked to the beam longitudinal rebar anchorage[136]. While interior joints normally show a hardening behaviour after joint diagonal cracking, the exterior joints might show a potential strength degradation[131]. For example, in the joint type (b) with bar bent-in arrangement, after diagonal cracking of the joint, the diagonal strut can be preserved until the cracks open up at the hooks' region. The joint type (c), however fails to provide an effective point for developing compression strut mechanism and further the joint resistance cannot be guaranteed in such cases [137]. Regarding the joint type (d) with limited bottom bar embedment (below 150mm, as suggested by reference [138]), the bond failure prevents the formation of diagonal compressive strut, thus the joint will probably show anchorage failure during the upward load, while the shear failure happens during progressive downward loading[139]. Thereby, for the exterior joints with limited bottom bar embedment, a non-symmetrical backbone curve is expected during cyclic loading. In Figure 4-2, the last configuration for the exterior joint (type (e) with end hook anchorage), offers a brittle failure with sudden load-bearing loss, due to the expulsion of the outer face of the column through the “concrete wedge” mechanism. Therefore, after the joint shear failure, the shear resistance shows negligible hardening behaviour, with limited ductility for the beam-column connection assembly.

As for the retrofitting of the RC frames, it is essential to accurately predict the performance of the beam-column joints, to better assess the frame capacity and provide the suitable retrofitting solution. By reasonably evaluating the maximum allowable shear stress in the joint, the ultimate capacity of the connection can be calculated, which will be covered in following sections.

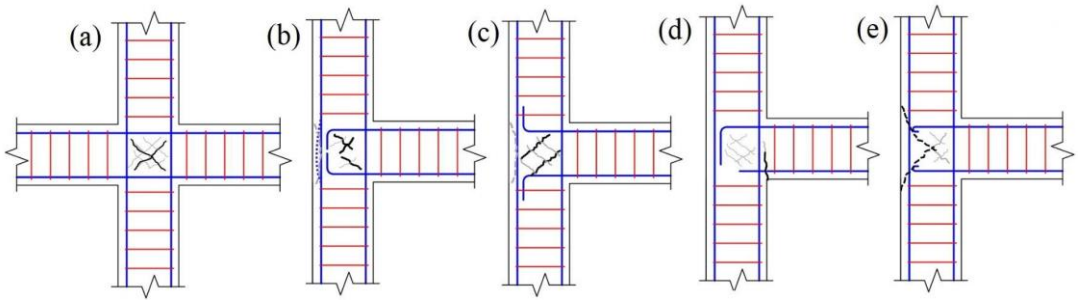

Figure 4-2 Typical rebar detailing for deficient RC joints: (a) Interior joint, (b) Exterior joint with bar bent-in, (c) Exterior joint with bar bent-out, (d) Exterior joint with insufficient anchorage, and (e) Exterior joint with end hook anchorage

4.3. RSFJ haunch performance and design considerations

The Resilient Slip Friction Joint (RSFJ)[54] is a self-centering friction damper that dissipates the input energy through the relative frictional sliding of cap and middle plates (Figure 4-3-a). The special groove shapes of the cap and middle plates, along with the stack of disk springs will provide a restoring force for the damper that can prevent the residual drift of the structure after a seismic event. Readers could find more information about the RSFJ damper and its applications in the references [61, 63, 64, 67, 112, 140, 141]. By assuming that the coefficient of friction would be constant on the sliding surfaces[117], the performance of the damper would be a flag-shape behaviour which can be tuned and adjusted with respect to different level of prestressing force in the disc springs (Figure 4-3-b and Figure 4-3-c). The flag shape behaviour of the damper with and without prestressing force is shown in Figure 4-3 which can be quantified using Eq. 1 and Eq. 2:

$$F_{ultimate} = 2n_b\left(F_{pr} + \frac{k_{st}\Delta\tan\theta_g}{2}\right)\left(\frac{\sin\theta_g + \mu\cos\theta_g}{\cos\theta_g - \mu\sin\theta_g}\right) \quad (1)$$

$$F_{restoring} = 2n_b\left(F_{pr} + \frac{k_{st}\Delta\tan\theta_g}{2}\right)\left(\frac{\sin\theta_g - \mu\cos\theta_g}{\cos\theta_g + \mu\sin\theta_g}\right) \quad (2)$$

In which, Δ shows the target axial displacement of the damper, θ_g is the angle of grooves, μ is the coefficient of friction and K_{st} is the stiffness of stack of disc springs. Parameter "n_b" indicates the number of bolts on each middle plate (Figure 4-3-a, n_b= 2), and "F_{pr}" shows the prestressing force in the disk springs. One of the advantages of the friction dampers over the ones with yielding is that the stiffness and strength of the system are decoupled and not codependent. This means that by adjusting the prestressing force, the slip resistance of the damper can be changed while the initial elastic stiffness is intact. It

is worth noting that if the prestressing force is zero, there would be no slip resistance and initial stiffness (Figure 4-3-c) while the damper can work and damp the energy with triangular flag-shape.

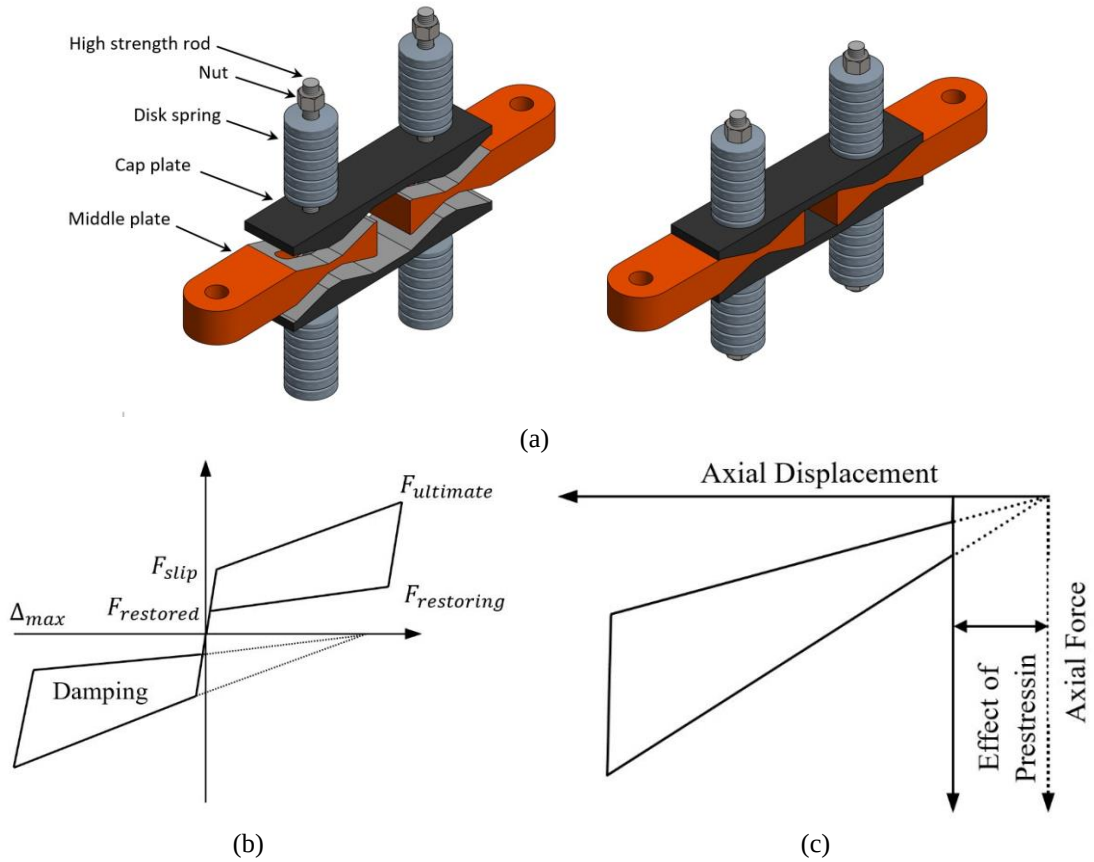

Figure 4-3 The RSFJ damper: (a) The comprising components of the RSFJ and the damper assembly, (b) The joint behaviour, and (c) The effect of pre-stressing

It is desired that the RSFJ haunches are installed and attached to the RC frame using pin end supports. This will induce only axial forces in the haunches and make the RSFJs middle and cap plates design easier and the sizes smaller. The reason is that there will be no rotational deformation compatibility requirements at the supports and as a result, there will be no extra bending and shear demands on the damper. In this manner, the following testing program is performed on the RSFJ prototype damper shown in Figure 4-4 to further investigate the feasibility of using the RSFJ with pin-pin end condition. It is worth noting that the effects of scaling errors were neglected in the experimental test [142]. For the testing program, a revered cyclic displacement-controlled test with increasing amplitude of displacement from zero to 15 mm with increment steps of 3 mm was conducted. Each cycle was repeated twice and the loading rate was equal to 1 mm/s. The number of disk springs were set to be 31 (n_d= 31), the stiffness of the stack of disc was

0.74 kN/mm, the angle of the grooves was 30 degrees, and the coefficient of friction was 0.17. The experimental results are shown in Figure 4-5.

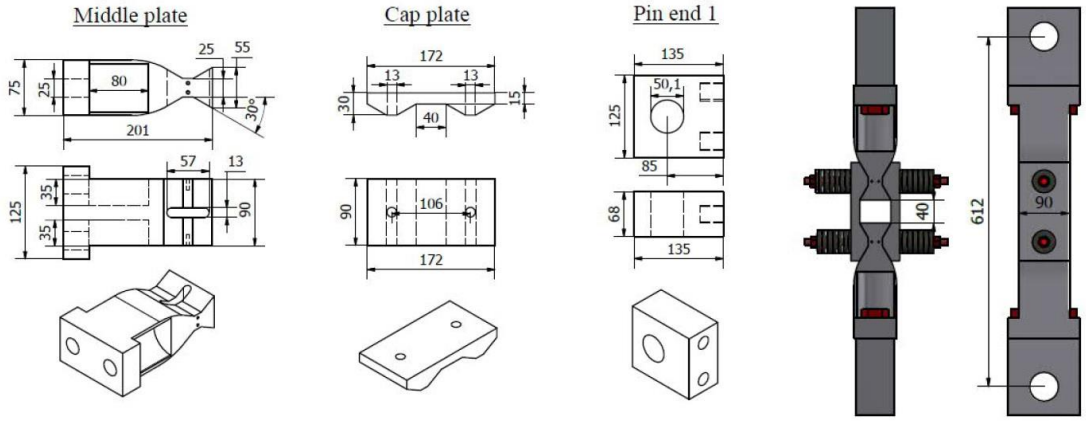

Figure 4-4 The geometry of the joint tested

Due to RSFJ rotational flexibility [63, 64, 143], the post-activation stiffness might degrade as a consequence of second-order actions. This issue is rooted in the possibility of relative rotation between the middle and cap plates when the damper is experiencing a compressive force. The reduction of post-activation stiffness can be noted in Figure 4-5-a, where the difference between the black and red lines is vivid in the compression zone (the RSFJ was exhibiting both axial and rotational movements, as shown in Figure 4-5-b). In order to tackle this issue, four additional plates were bolted to the middle plate to provide lateral supports and limit the relative rotation between the middle and cap plates. Theses plates and their attachments were designed for 2.5% of the damper ultimate axial load [144] (as the common design practice for the lateral supports required resistance). Figure 4-5-c and Figure 4-5-d demonstrate the effectiveness of the mentioned restraining plates. It is worth noting that such restraining attachments and the cap plate could be manufactured as one component.

In the above-mentioned two cases, the slip force was zero as there was no prestressing force in the discs. The disc springs were prestressed up to 10 kN to increase the slip force. Figure 4-6 shows the performance of RSFJ with slip force of 16.6 kN, where the performance in tension and compression is identical due to employment of the additional restraining plates, preventing the joint rotation.

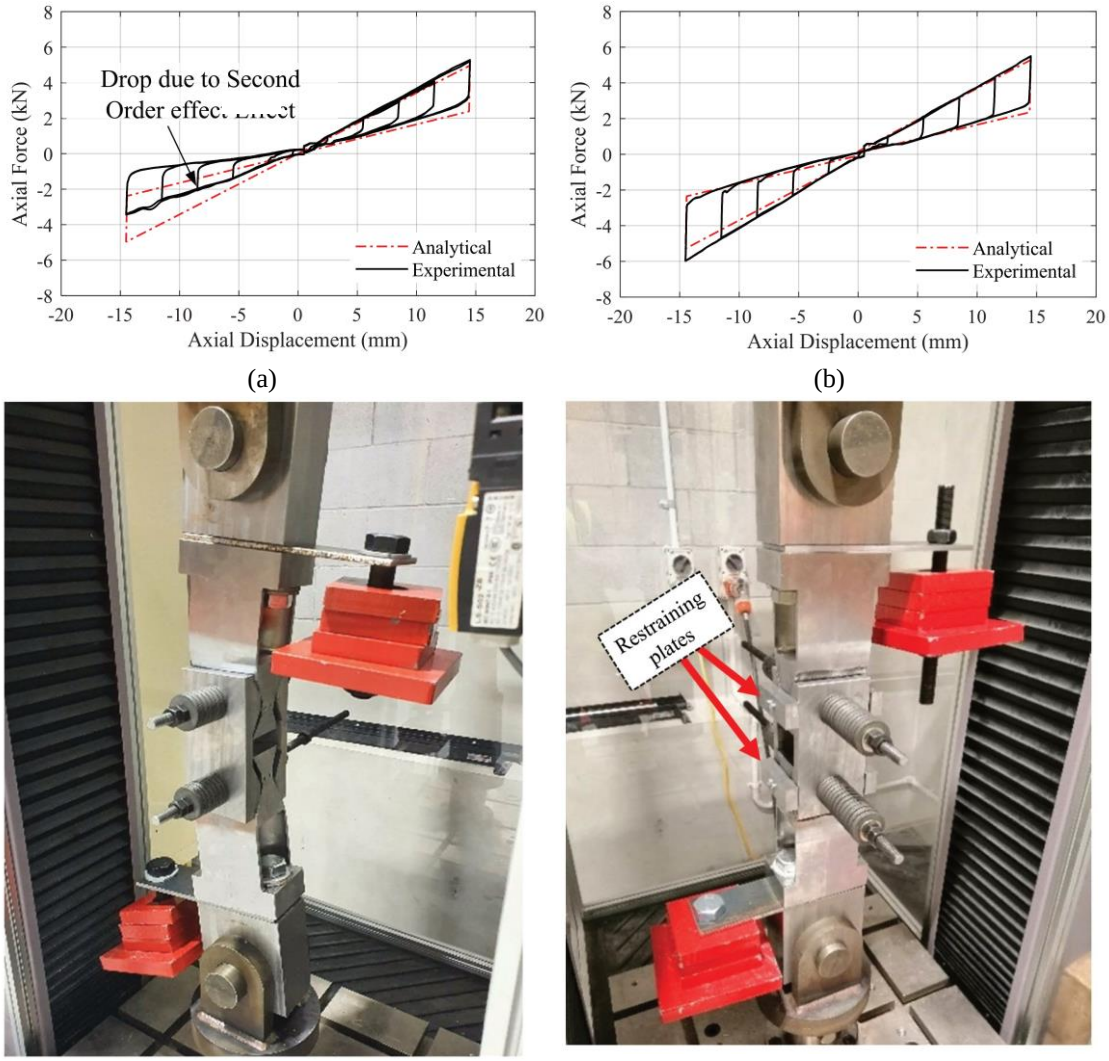

Figure 4-5 The effect of restraining plates on the cyclic performance of the pined-pined RSFJ: (a) the stiffness drop due to axial-rotational behaviour of the RSFJ, (b) a photo of the axial rotational behaviour of the RSFJ during compression load, (c) the effect of restraining plate on the cyclic performance of the RSFJ, and (d) a photo of RSFJ with restraining plate during compression load

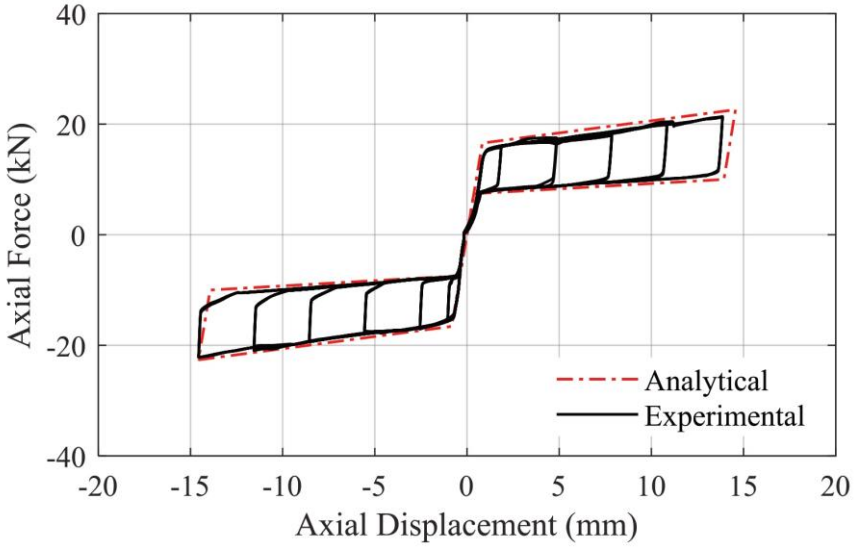

Figure 4-6 The symmetric cyclic flag-shape behaviour of joint with added restraints

4.4. Retrofit Design and Recommendations

The occurrence of shear cracking at the joint core of the old RC buildings can jeopardize the integrity of the whole frame when subjected to earthquakes. It is worth to note that by merely retrofitting the joint, the new strength associated with the joint might change the strength hierarchy of the system, leading to an adverse damage on the beams or columns. In general, an ideal retrofit solution should increase the overall seismic capacity of the system while improving the strength hierarchy of the frame in a way that during major events, the least severe damage mechanisms happen before undesirable critical failure mechanisms[120]. Readers are referred to the works of Pampanin et al.[131] for further details.

Figure 4-7 shows some of the possible arrangements for attachment of RSFJ haunches to the beam-column joint, including 4, 2 and 1 haunches for interior and exterior joints. Adding the RSFJ haunches will introduce a resisting force along its axis, which will change the force flow in the entire beam-column connection assembly. As an illustration, the schematic internal shear and moment forces in the external joints are depicted in Figure 4-8, for a Non-Retrofitted Subassembly (NRS), Double Haunch Subassembly (DHS) and Single Haunch Subassembly (SHS). The single haunch would be suitable for meeting architectural requirement, though with less efficient reduction of joint internal demands and an asymmetric force distribution. The internal shear and moment distribution in the haunch system can be calculated by either the formulas presented in the previous studies (see for example [131, 145]), or via the numerical modelling which

is described in the next section. Through their contribution of axial resistance, the haunches decrease the joint shear force and transfer the shear to beams and columns. While they alter the shear and axial forces in the beams and columns, they also relocate the maximum moment in the beam and column sections, from the beam-column interface to the point of RSFJ intersection. A bending moment reduction can be noticed in the RSFJ haunch intersection point, which is due to the offset of the haunch from the joint intersection point. Besides protecting the structures from joint shear failure and relocating the beam plastic hinges, the RSFJ haunches can offer energy dissipation and restoring force under large deformation, which can decrease the residual drifts in the RC-frame.

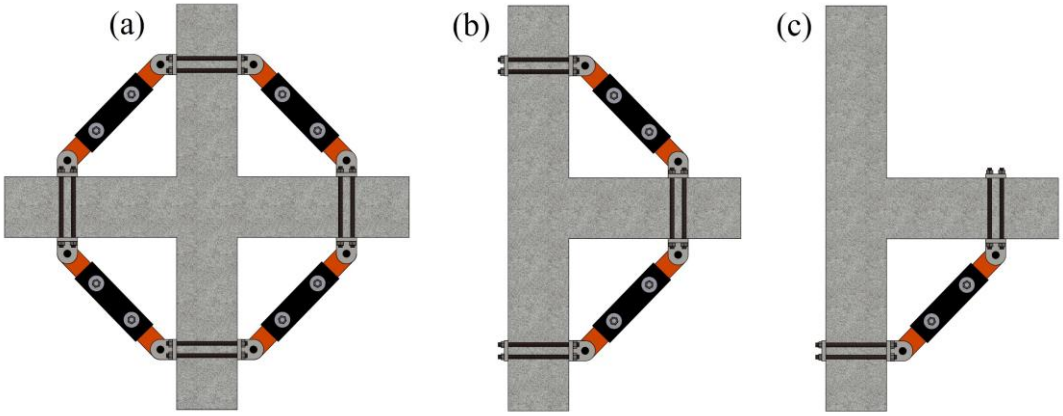

Figure 4-7 Different retrofit solutions with RSFJ haunches: (a) Interior joint with quadruple haunch subassembly (QHS), (b) Exterior joint with double haunch subassembly (DHS), and (c) Exterior joint with single haunch subassembly (SHS)

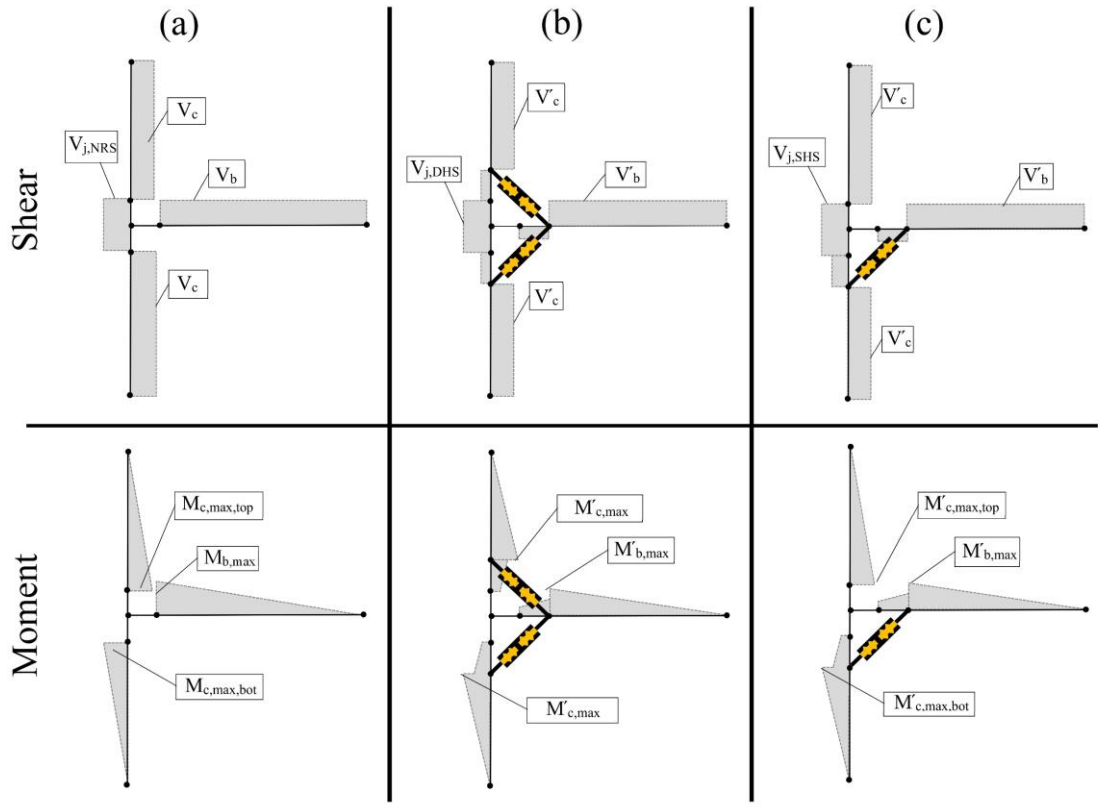

Figure 4-8 Shear and moment diagrams: (a) non-retrofitted subassembly (NRS), (b) Double Haunch Subassembly (DHS), and (c) Single Haunch Subassembly (SHS)

The following design steps are proposed to retrofit using RSFJ haunches. It should be pointed out that the proposed retrofit design procedure would prevent the joint shear failure mechanism and impose a flexural plastic hinge in the beam. Also, the added damping and restoring force of the RSFJs would improve the system performance as well as its residual drift. On this basis, the F_{slip} and F_{ult} of the joints are tuned in such a way that during high seismic events, the flexural hinge in the beam is being formed (a minimum force of F_{slip} in the RSFJ haunch is required) while the column hinge mechanism and shear failure in both beams and columns are prevented by proper tuning of the F_{ult}. The contribution of friction damping in the joint will increase the damping feature of the system while the restoring force of the damper would decrease the residual drift in the system. The following retrofitting procedure is utilized here for retrofit designing of the RC beam-column joints using RSFJ haunches:

Step 1: Determine the maximum allowable beam-column joint shear stress (τ_{max}).

Step 2: Determine the maximum shear capacities of the beam and column ($V_{b,n}$ and $V_{c,n}$), based on the following equations[146, 147]:

$$V_{b,n} = 0.17\lambda\sqrt{f_c}\,b_w d + \frac{A_v f_{yt} d}{s} \text{ , ACI318-19 (Clause 22.5.5.1 and 22.5.8.5.3)} \quad (3)$$

$$V_{c,n} = \frac{A_v f_{yt} d}{s} + \frac{0.4 A_g \lambda\sqrt{f_c}}{\left(\frac{M}{Vd}\right)}\sqrt{1+\frac{N}{0.5A_g\sqrt{f_c}}} \text{ , ASCE41-17 (Clause 10.4.2.3.1)} \quad (4)$$

In these equations, $\lambda = 1$ for normal concrete (0.75 for lightweight concrete), b_w represents the beam width, d is the effective depth of the beam section, A_v denotes the area of shear reinforcement with yielding stress of f_{yt} and spacing of s. The parameter M/Vd denotes the largest ratio of moment to shear times the effective depth of column. N is the axial compression force of the column, while Ag is the gross cross section area of the column.

Step 3: Determine the maximum flexural capacities of the beam and column ($M_{b,yield}$ and $M_{c,yield}$) using the moment-curvature method.

Step 4: Assume L and α for placement of haunches and assume the RSFJ haunch flag-shape performance behaviour (F_{slip}, F_{ult}, $F_{restoring}$, $F_{residual}$, slip and ultimate deflection capacities).

Step 5: Determine the maximum force demands in the beam (V_b, $M_{b,max}$), column ($M_{c,max}$, V_c), and joints (τ_j), through nonlinear numerical modelling.

Step 6: The following checks need to be considered for a proper retrofit:

- The joint shear stress should be lower than the joint maximum shear capacity.
- While a plastic hinge might develop in the beam ($M_{b,max}$ would reach $M_{b,yield}$), the corresponding shear force in the beam should not surpass the shear strength of beam ($V_b < V_{b,n}$).
- The corresponding column shear force should be kept below the shear strength of the column ($V_c < V_{c,n}$)
- The column maximum moment ($M_{c,max}$) should be kept below the column flexural hinge capacity ($M_{c,max} < M_{c,yield}$).

Step 7: Go back to Step 4, to revise the performance characteristics of the RSFJ haunches and the orientation angle, to satisfy the desired strength hierarchy.

For the RSFJ haunches, it is recommended to have sufficient travel distance to provide the beam-column joint rotation up to 4%. This is to prevent the yielding of the RSFJ haunch components and haunches interlocking up to Collapse Prevention (CP) limit state of the frame[67, 148]. For this purpose, a numerical model is developed (will be discussed in next section) to check the performance of the haunches, as well as optimal design of the RSFJ haunches in terms of deflection capacity. The numerical model also helps to check the current performance of the retrofitted RC beam-column joint and identify the current level of RC joint shear deformation. Checking the current performance of the overall retrofitted system, as well as the haunches and RC beam-column joint is a try-and-error procedure until the desired performance for the whole system is reached. Also, the design could aim to reduce or eliminate the residual displacement of the whole system, owing to the restoring force provided by the RSFJ haunches.

4.5. Numerical Modelling

The brittle behaviour of the old-fashioned RC frames usually initiates from either the failure of the beams and columns, or joint failure mechanism. The joint failure might occur before or after yielding of the beam (or column). Besides the shear failure in the joint, usually the failure mechanism involves the anchorage damage as well resulting in the beam bottom pull-out. Here, a 2-dimensional model is developed in the OpenSEES[149] software package, to simulate the performance of the beam-column connection, and also to check the joint maximum shear stress in the system. The OpenSEES model could also be utilized for optimal design of the RSFJ haunches in terms of deflection capacity. The overall modelling of interior and exterior joints is described, followed by modelling techniques for simulation of the joint performance, bar-slip behaviour, as well as the RSFJ haunches. Then, the modelling is validated through some experimental test results available from literature.

4.5.1. Joint modelling

Figure 4-9 shows the numerical model utilized for modelling of the interior and exterior joints. Such interior and exterior joint assemblages are common in experimental tests. The beams and columns were modelled using fiber-type force-based beam-column element with 5 integration points, to consider material nonlinearity along the length and cross section area of each member. The confinement model proposed by Mander et al.[150] with confinement factor of 1.3 was adopted to calculate the characteristic

parameters of confined and unconfined concrete. To describe the shear behaviour of the joint, a nonlinear panel zone consisting of four rigid links was utilized. The rigid links represent the joint dimensions and are connected in the center by a nonlinear rotational spring. The “Pinching4” material was utilized for rotational spring (which will be discussed in section 5-3). The assembled four rigid links with the rotational spring (known as the scissor model) simulates the joint shear behaviour.

The unconfined and confined concrete were modelled using “Concrete02” material, which includes the tensile strength of the concrete. The steel02 material with assumed hardening ratio of 0.01 was considered for modelling the longitudinal reinforcements. The steel02 material presents a bilinear curve, based on Giuffre-Menegotto-Pinto’s model[151], with smooth transition from elastic to inelastic region. A zero-length rotational spring was considered at the end of beams and columns to simulate the flexibility related to the bar-slip effects, which will be discussed in the next section. The RSFJ haunches are acting in pure axial behaviour and can be added to the system, using rigid links that are connected to the beams and columns. An elastic member with very large Young's modulus can be utilized for creating the rigid links. The uniaxial SMA material (available on OpenSEES version 2.1.0) was utilized to model the behaviour of the RSFJ haunches.

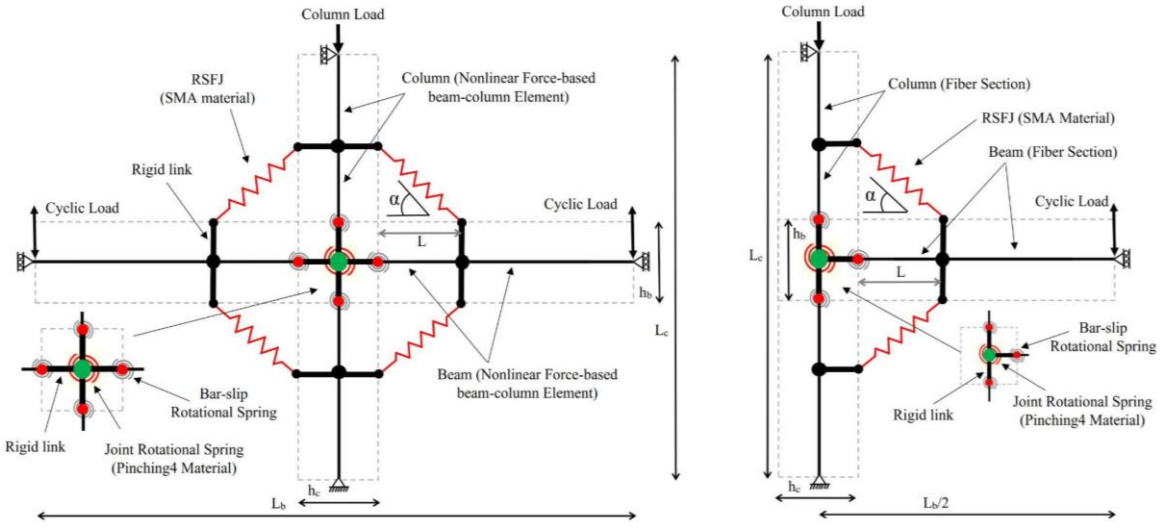

Figure 4-9 OpenSEES model for Interior and exterior beam-column joint assembly

4.5.2. Bar-slip model

Beside the rotation caused by the RC joint deformation, the rotation resulting from the bar-slip deformation could also affect the accuracy of the modelling. In this manner, the moments at the end of the beam (or column) sections tend to apply tension forces T_s on

the longitudinal rebar, as depicted in Figure 4-10. Such forces are being resisted by a bond stress between rebar and joint concrete. Assuming that the bond stress remains constant along the anchored length of the reinforcement bar, the following rotational stiffness (k_{slip}) can be considered for modelling the bar-slip deformation[152]:

$$EI_{flex} = \frac{M_{0.004}}{\phi_y} \tag{5}$$

$$u = (0.5 \sim 1.0) \times \sqrt{f_c}\ (MPa) \tag{6}$$

$$k_{slip} = \frac{8u}{d_b f_s} \frac{M_{0.004}}{\phi_y} = \frac{8u}{d_b f_s} EI_{flex} \tag{7}$$

Where, u denotes the uniform bond stress (here, taken as $0.8\times \sqrt{f_c}$), d_b is the diameter of the longitudinal reinforcement (mm), and f_s is the steel stress on the tension rebar (MPa). The parameter $M_{0.004}$ represents the flexural moment at the concrete maximum compressive strain of 0.004, ϕ_y is the curvature at yield, and EI_{flex} represents the effective flexural rigidity. Further details can be found in the reference[152].

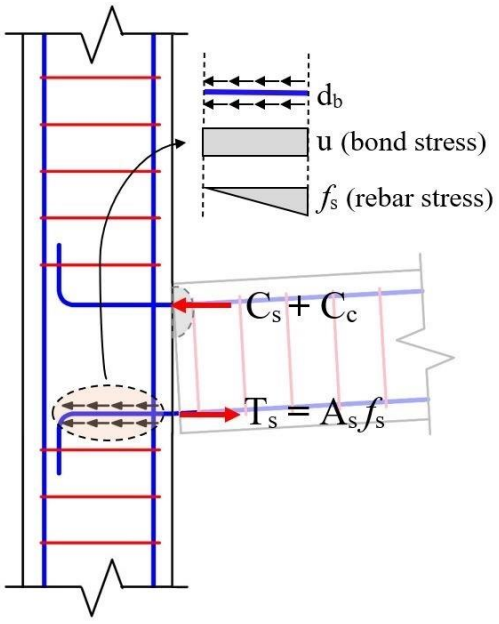

Figure 4-10 Bar-slip rotation behaviour in RC joint

4.5.3. Joint shear model

The beam-column joint response was simulated using a zero-length rotational element connected to two nodes, at the same node coordination as the beam-column intersection. The Pinching4 material was designated to the element to simulate the joint response using

a moment-rotation behaviour. Figure 4-11 shows the response envelope provided for the rotational element. As can be noted, the backbone curve contains four distinct points denoted as crack strength, yield strength, ultimate strength, and residual strength. While the joint rotational spring can be calibrated with experimental data, a suite of analytical and empirical equations has also been developed and suggested by researchers. Table 1 provides the empirical equations for the stress-strain behaviour of non-seismically designed exterior and interior RC joints (the reference for each model is provided in the table). Using the equation provided by Celik and Ellingwood[153], the joint moment-rotation relationship can be computed from joint shear stress-strain:

$$M_j = \frac{\tau_j A_j}{\lambda} \tag{8}$$

$$\lambda = \frac{\left(1 - \frac{h_c}{L_b}\right)}{jd_b} - \frac{1}{L_c} \text{ for interior and exterior joints} \tag{9}$$

$$\lambda = \frac{\left(1 - \frac{h_c}{L_b}\right)}{jd_b} - \frac{2}{L_c} \text{ for interior and exterior top floor joints} \tag{10}$$

$$\theta_j = \gamma_j \tag{11}$$

Where, M_j=joint rotational moment, h_c=depth of the column, L_b=total length of the left and right beam (for the exterior joint, the length of one beam is considered), and d_b represents the effective depth of the beam. The parameter A_j (joint effective area) is calculated as the product of joint depth and effective joint width (ACI318-19[146], Clause 15.4.2.4), while j denotes the internal moment arm factor (taken as 0.875[154]); θ_j = joint rotation; and γ_j = joint shear strain.

The shear strength of the joint (τ_{max}) is needed to predict the seismic capacity of the beam-column connection. Here, the utilized shear strength model is based on the principal tensile stress concept, which includes the column axial load, as well as the joint aspect ratio[155] (Eq. 15):

$$F_v = \sqrt{1+\frac{P_j}{\sigma_1}}, \quad P_j = \text{Joint average axial stress (MPa)} \tag{12}$$

$$F_{AR} = \frac{\cos\theta}{\cos(45°)}, \quad \theta = \tan^{-1}\left(h_b/h_c\right) \tag{13}$$

$$\tau_{max} = \sigma_1 \times F_v \times F_{AR} = \sigma_1 \times \sqrt{1+\frac{P_j}{\sigma_1}} \times \frac{\cos\theta}{\cos(45°)}, \quad \sigma_1 \text{ is calculated from Table 1} \tag{14}$$

On this basis, to calculate the joint shear strength (τ_{max}), the maximum principal tensile stress (σ_1) is increased by the factor of F_v for inclusion of column axial load[134], while the effect of joint aspect ratio, is included by the factor of F_{AR}. The influence of joint aspect ratio on the joint shear strength can be described via the Strut and Tie method[155]. As such, the joints with high aspect ratio will produce steeper diagonal strut, which is less efficient to counterbalance the horizontal shear force in the joint. The stress-strain related to crack point, yield point and residual point, can be also evaluated by Table 1. Regarding the exterior joint with end-hook, a limited ductile elasto-plastic behaviour without any hardening performance is expected. Therefore, no yielding point and ultimate point can be expected for such joints. It is worth noting that for the beam-column joint cases where nonlinearity is focused on the joint and experimental data are available, a calibrated model based on the available data would provide a more accurate result for retrofitting.

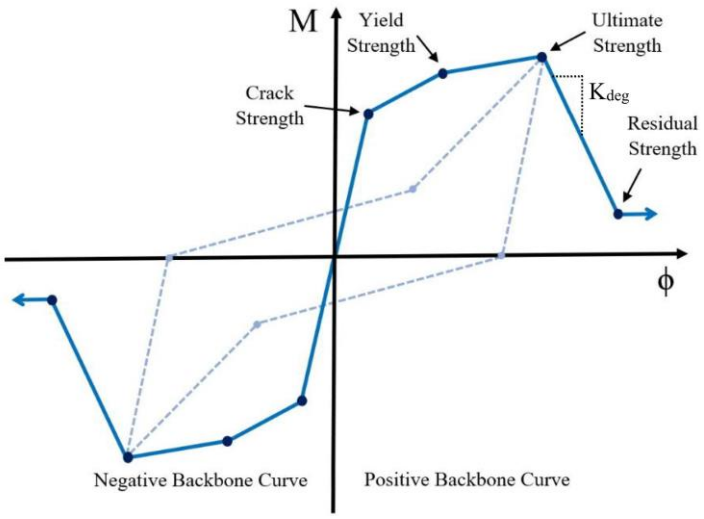

Figure 4-11 Constitutive model of Pinching4 material for simulation of joint rotation

Table 4-1 The summarized empirical stress strain behaviour for the interior and exterior joints

Joint type		Cracking Point		Yielding Point		Ultimate Point		Residual Point	
		stress	strain	stress	strain	σ_1	strain	stress	strain
Interior	I: Typical interior[134]	$\min(0.6\times\tau_{max}, 0.48\sqrt{f_c})$	0.00043	$0.9\times\tau_{max}$	0.005	$0.84\sqrt{f_c}$	0.020	$0.2\tau_{max}$	*[1]K_{deg} = -80
Exterior	II: bar bent-in[156]	$\min(0.6\times\tau_{max}, 0.48\sqrt{f_c})$	0.00043	$0.9\times\tau_{max}$	0.005	$0.42\sqrt{f_c}$	0.015	$0.2\tau_{max}$	K_{deg} = -75
	III: bar bent-out[156]	$\min(0.6\times\tau_{max}, 0.48\sqrt{f_c})$	0.00043	$0.9\times\tau_{max}$	0.005	$0.29\sqrt{f_c}$	0.015	$0.2\tau_{max}$	K_{deg} = -75
	IV: insufficient anchorage*[2][138]	shear $\rightarrow 0.29\sqrt{f_c}$	≤0.002	$0.42\sqrt{f_c}$	0.002	$0.42\sqrt{f_c}$	0.005	0.0	0.025
		anchorage $\rightarrow 0.13\sqrt{f_c}$	≤0.002	$0.19\sqrt{f_c}$	0.002	$0.19\sqrt{f_c}$	0.005	0.0	0.015
	V: end hook anchorage*[3][137]	$0.20\sqrt{f_c}$	0.0002	-	-	-	-	0.0	0.025

*[1]Note: k_{deg} (MPa/rad) is the gradient shear strength from ultimate point to the residual point[154].

*[2]Note: The proposed backbone curve is non-symmetrical, and it depends on the embedment length of bottom rebar.

*[3]Note: The proposed behaviour for the end hook anchorage, is an elastic-perfectly plastic behaviour, with limited ductility and no distinct point for the yielding and ultimate point.

4.5.4. RSFJ haunch modeling:

RSFJ haunches are self-centering components by themselves, which means they can provide a repeatable flag-shape hysteresis behaviour without any yielding or residual plastic deformation. To model such behaviour, the self-centering material with zero residual deformation is required. OpenSEES material library contains two material for modelling self-centering flag-shape behaviour: “SelfCentering” material (available on the recent versions) and “SMA” (Shape Memory Alloy) material (available on version 2.1.0). Since the SelfCentering material cannot offer RSFJ flag-shape behaviour with different stiffness during loading and unloading, it was decided to utilize SMA material, which can be easily calibrated using four points of flag-shape behaviour and the plateau length (joint deflection). The SMA material was originally developed to capture the flag-shape behaviour of shape memory alloys [157]. Figure 4-12 shows the parameters needed for calibration of SMA material and the comparison between numerical model and the experimental data for the same RSFJ in section 4.3.

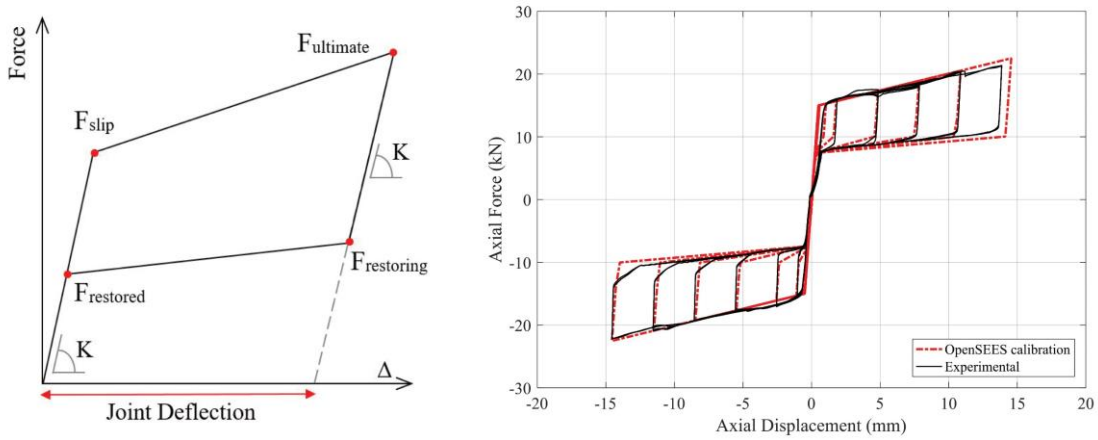

Figure 4-12 SMA material for modeling RSFJ haunches: (left) the required parameters, and (right) Calibration validation with experimental data

4.5.5. RC beam-column joint model validation

To check the efficiency of the OpenSEES model to predict the cyclic performance of deficient RC joints, four experimental tests (two interior joints and two exterior joints) from literature were considered for numerical modelling. Table 2 lists the selected experimental test characteristics, while Figure 4-13 compares the numerical outcomes with experimental data. Due to the uncertainties associated with the employed joint shear models as per Table 1, the simulated response of the RC joint in the testing unit 6 (Figure 4-13-d) might differs from the experimental data. Such difference is coming from using empirical stress-strain behaviour suggested by previous researchers which include some level of uncertainty and difference between actual response and the predicted response[154]. As for the rest of the experimental outcomes, however, the model can fairly capture the joint behaviour with good accuracy. The numerical results for the joint assemblage include its peak strength and loading/unloading behaviour, as well as its pinching performance.

Table 4-2 Summary of the selected experimental tests for OpenSEES model validation

ID	Test name		Ref.	Compressive strength (MPa)	Joint type	Axial load	Beam section	Column section
a*	Interior	PEER14	[158]	34.0	I	0.10 f_cA_g	406×508	457×406
b*	Exterior	BS-L	[159]	38.6	II	0.15 f_cA_g	260×450	300×300
c	Interior	E-03	[160]	46.1	I	0.30 f_cA_g	300×300	300×300
d	Exterior	Test unit 6	[161]	31.7	II	0.25 f_cA_g	406×406	406×406

*Note: The experimental tests PEER14 (a) and BS-L (b) will be used for retrofit case study

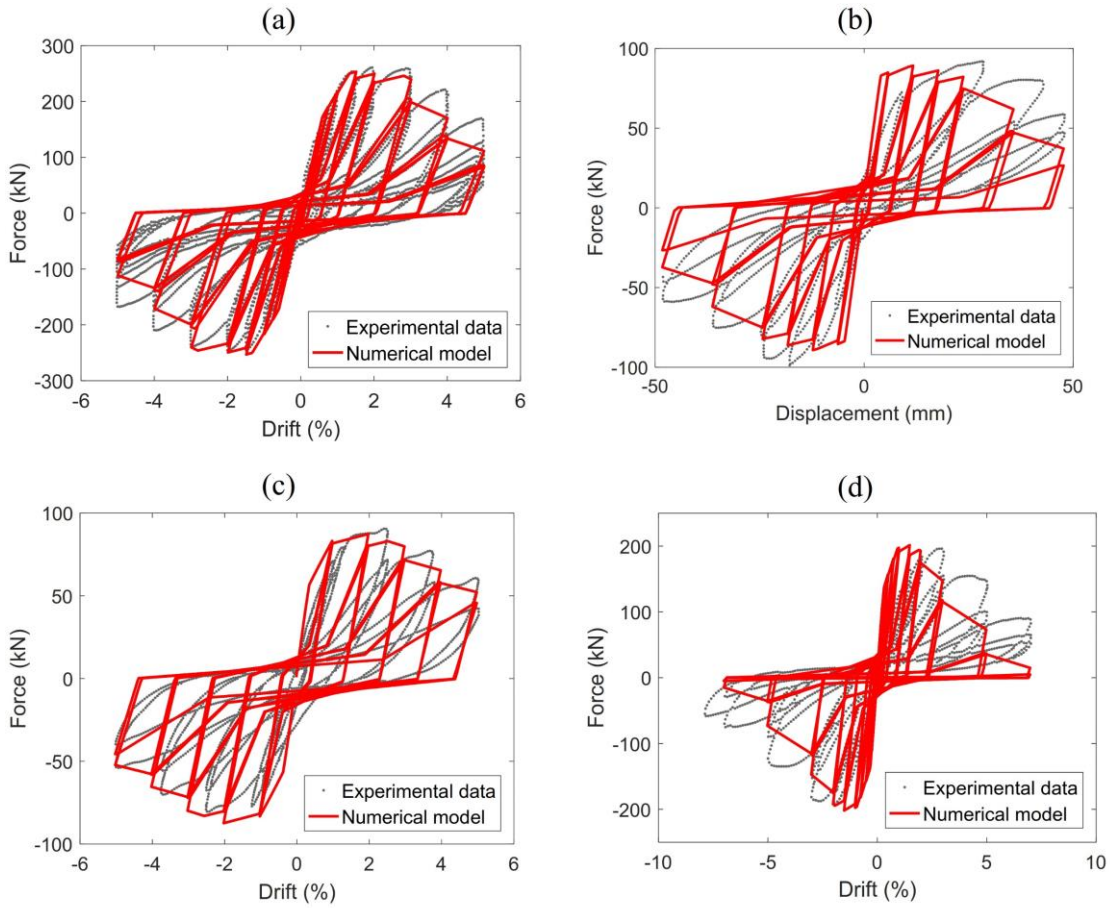

Figure 4-13 Comparison of the force-deformation hysteresis curve of numerical model and experimental outcomes of non-seismically designed RC joints: (a) PEER14 Interior joint[158], (b) Experimental test Exterior joint BS-L[159], (c) Interior Specimen E-03[160], and (d) Exterior joint testing unit 6[161]

4.6. Retrofitting Case studies

To investigate the performance of RSFJ haunch retrofitting system, an Interior and an Exterior RC joint (experimental tests a* and b* in Table 4-2, shown in Figure 4-14) were considered. The retrofit design will be briefly covered for the both joints with the help of numerical model. The interior joint was retrofitted with 4 RSFJ haunches (quadruple haunch subassembly), while the exterior RC joint was equipped with 2 RSFJs (double haunch subassembly).

The interior joint test (a*) belongs to a suite of seven interior joints, tested by Walker[158], which represents the cyclic performance of RC joint constructed before 1970s. The joints lack transverse reinforcements; thus, the capacity of the joint assembly is limited to panel zone performance. The specimen PEER14 has been selected here, for the retrofitting study. As a starting point for retrofitting, the maximum shear and moment capacities of the beam and column for the interior joint is calculated using Eq. 4 and 5,

and moment curvature method, respectively (Table 4-3). The OpenSEES numerical model of the joint subassembly has been developed as well. Assuming that the seismic loading has increased the beam moment at the yielding point, the associated internal shear in the beam should remain less than the shear capacity of the beam:

$$V_b = \frac{M_{b,yield}}{0.5\times L_b - 0.5\times h_c - L} = \frac{185.4}{1.83-0.23-L} < V_{b,n} = 1160.17kN \Rightarrow L < 1.44m$$

Accordingly, the column shear should not surpass its shear capacity, up to the hypothetical plastic hinge formation in the column at the point of haunch connection:

$$V_c = \frac{M_{c,yield}}{0.5\times L_c - 0.5\times h_b - L\tan\alpha} = \frac{304.5}{1.07-0.25-L\tan\alpha} < V_{c,n} = 1102.99kN \Rightarrow L\tan\alpha < 0.54m$$

Based on the following relationship between the column and beam maximum moments at the level of the haunch[131], we can check whether the beam would reach its yielding moment before formation of column plastic hinge:

$$\frac{M_{c(\max)}}{M_{b(\max)}} = \frac{L_b\left(L_c/2 - h_b/2 - L\tan\alpha\right)}{L_c\left(L_b/2 - h_c/2 - L\right)} \tag{15}$$

$$\Rightarrow M'_{c,\max} = M_{b,yield}\times\frac{L_b\left(L_c/2 - h_b/2 - L\tan\alpha\right)}{L_c\left(L_b/2 - h_c/2 - L\right)}$$

$$= 185.4\times\frac{3.66\times(1.07-0.25-L\tan\alpha)}{2.13\times(1.83-0.23-L)} < M_{c,yield} = 304.5kNm \Rightarrow L = 0.4,\ \alpha = 45°$$

The design parameters assumed for the haunch retrofitting of the interior joint are summarized in Table 4-4. It consists of four RSFJ haunches with slip and ultimate force of 140.2kN and 200.3kN, respectively.

Regarding the exterior joint test (b*), the experimental results of Kuang and Wong[159] are utilized here. Their study includes full-scale testing of five different exterior RC joints and investigates the effect of reinforcement anchorage of beams on the hysteretic behaviour of the exterior RC joints. The cyclic test of the BS-L specimen is selected here for retrofitting of the exterior joint. The calculated moment and shear capacities of the beam and column sections were summarized in Table 4-3. In a similar manner, the

retrofitting of the exterior joint can be conducted via installation of two RSFJ haunches with performance characteristics summarized in Table 4-4.

Table 4-3 Calculated and assumed parameters for retrofitting of interior and exterior RC joints using RSFJ haunches

Parameters	Unit	Interior Joint	Exterior joint
L_b	mm	2134	2800*
L_c	mm	3658	3100
τ_{max}	MPa	6.48	3.20
$M_{b,yield}$	kN.m	185.40	241.40
$M_{c,yield}$	kN.m	304.50	170.98
$V_{b,n}$	kN	1160.17	246.48
$V_{c,n}$	kN	1102.99	193.31
Retrofit type	-	4 RSFJs (QHS)	2 RSFJs (DHS)

*Note: The L_b for BS-L test was slightly decreased to represent the accurate length of beam where actuator was installed to the system.

Table 4-4 The RSFJ haunches utilized for retrofitting of interior and exterior joint subassemblies

Parameters	L (m)	α (deg)	Haunch Δ_{max} (mm)	F_{slip} (kN)	F_{ult} (kN)	$F_{restoring}$ (kN)	$F_{restored}$ (kN)
Interior haunch	0.4	45	12.9	156.3	223.0	94.9	66.5
Exterior haunch	0.3	50	7.4	140.2	200.3	79.6	55.7

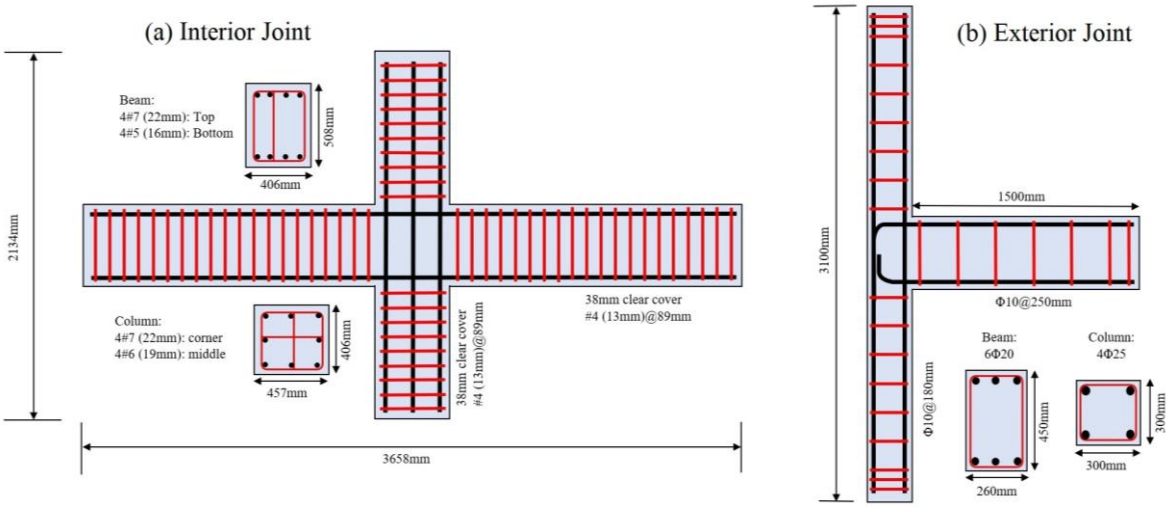

Figure 4-14 Selected test specimens for RC joint retrofit with RSFJ haunch: PEER14 (left)[158] and BS-L (right)[159]

To check the efficacy of the retrofitted system, the numerical model of the two beam-column joints with and without the RSFJ haunches were developed and subjected to the same loading protocol used in each experimental test. Figure 4-15 shows the utilized loading protocol for each experimental test, which were employed for the numerical models as well. The PEER14 was subjected to progressive increasing cyclic test up to the

5% drift of the beam-column assembly (91.4 mm deflection), while the BS-L experienced cyclic loading up to nearly 4% drift ratio (48mm deflection). The cyclic performance of the retrofitted joints was compared with behaviour of the non-retrofitted joints (Figure 4-16). As can be noted, the proposed RSFJ haunches improve the performance of the joint significantly. The yielding capacity of the RC systems were increased by a factor of 1.84 and 2.43, for the interior and exterior joints, respectively. While the cyclic performance of the non-retrofitted joints suffers from pinching behaviour and present low stiffness and load carrying capacity, the strengthened joints provide higher initial stiffness and energy dissipation, owing to the energy dissipation and load redistribution of the RSFJ haunches.

Figure 4-17 presents the force-deflection behaviour of the RSFJ haunches in the retrofitted joints. It is worth noting that a sufficient deflection capacity was assumed for the haunches to prevent damper interlocking. This can be done by using the OpenSEES macro-model and considering sufficient deflection for the haunches. In practice, the deflection capacity of the RSFJ haunches is being provided by a stack of disk spring in series. Obviously, the number of disk springs in series must be sufficient enough to provide the required deflection capacity for the haunch, to prevent the RSFJ rod yielding or interlocking [67]. In addition, the ratio of disk spring prestressing was selected to be 70% of the disk spring ultimate flattening load (i.e., $F_{slip}=0.7\times F_{ult}$). The equivalent damping ratio for both the interior and exterior joints haunches were calculated as 15%. It should be noted though, that the calculated damping is only for this specific case. The equivalent damping ratio depends on the loading protocol and the displacement level and should be evaluated for other cases accordingly.

Given the restoring force provided by the RSFJ haunches, the residual displacement of the RC joints was eliminated. Also, the pinching hysteresis responses of the bare RC frame joints were substituted with the flag-shape behaviour of the retrofitted RC beam-column joint. The haunches also enhanced the energy dissipation capability of the RC joints noticeably. Figure 4-18 depicts the cumulative cyclic energy dissipation of the RC joints in the case of the bare frames (not-retrofitted joints), against the retrofitted frames. The energy dissipation of the bare frames, which are mostly originated from the brittle shear deformation of the joints, cannot provide a reliable source for dissipating the seismic energy. As for the retrofitted frames, the energy can be dissipated mostly through frictional sliding of the RSFJ haunches, as well as the inelastic deformation of the beam. As can be noted, the energy dissipation of the retrofitted frames is almost three times and

four times of the bare frames, for the interior and exterior joints, respectively. However, it should be pointed out that the current two comparisons between the damping energy of the retrofitted frames and the bare frames, are based on the hysteretic damping of the system and the inherent damping was neglected here. Moreover, the energy dissipation of the retrofitted frames is dependent on the hysteretic damping of the RSFJ haunches which is a function of the RSFJ design parameters (including the coefficient of friction between the friction plates, as well as the angles of the grooves).

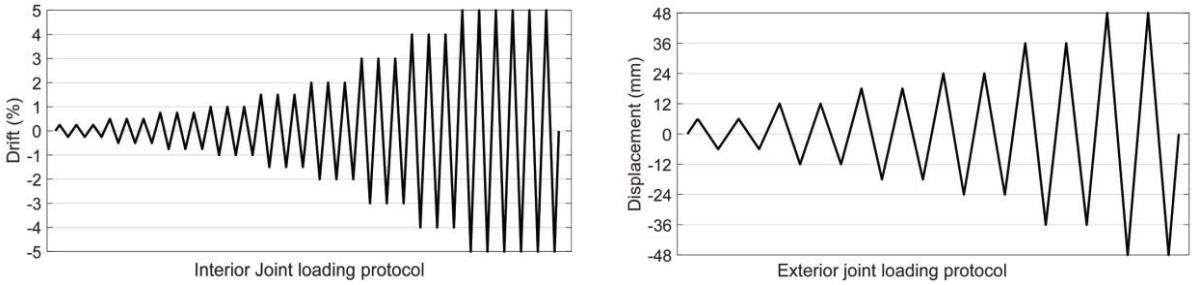

Figure 4-15 The displacement-controlled loading protocol applied for testing: (a) Interior joint, and (b) Exterior joint

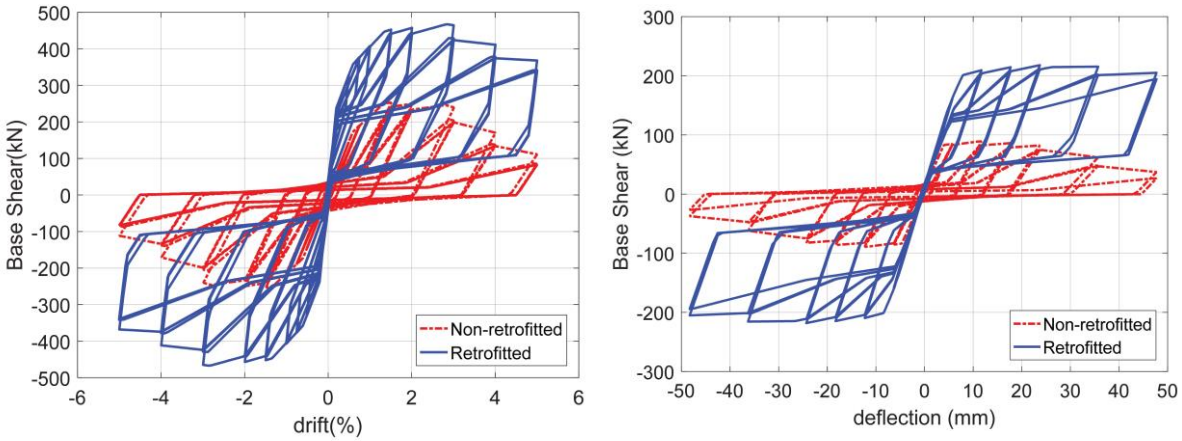

Figure 4-16 Comparison of force-displacement cyclic behaviour of the retrofitted joints against the non-retrofitted assembly: (a) Interior joint, and (b) Exterior joint

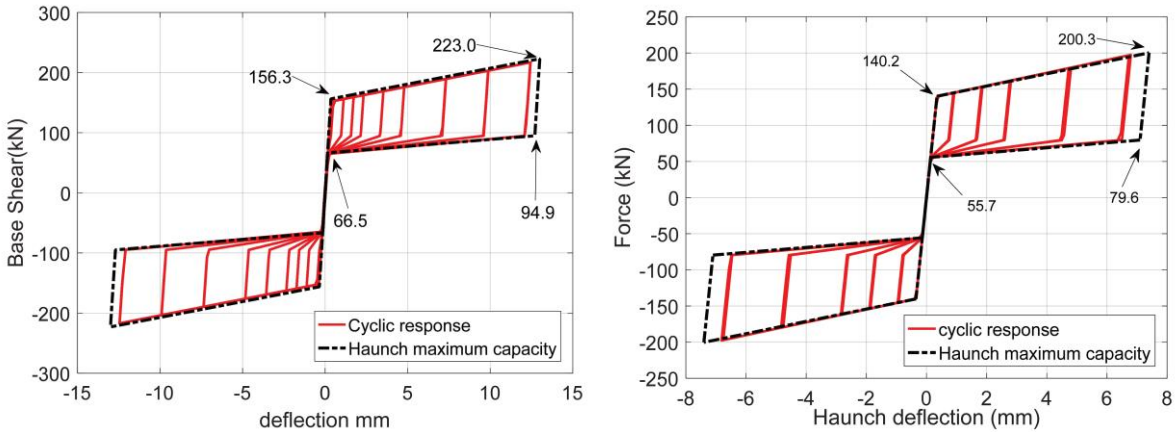

Figure 4-17 The cyclic performance of RSFJ haunches in the retrofitted beam-column joint assemblies: (a) Interior joint, and (b) Exterior joint

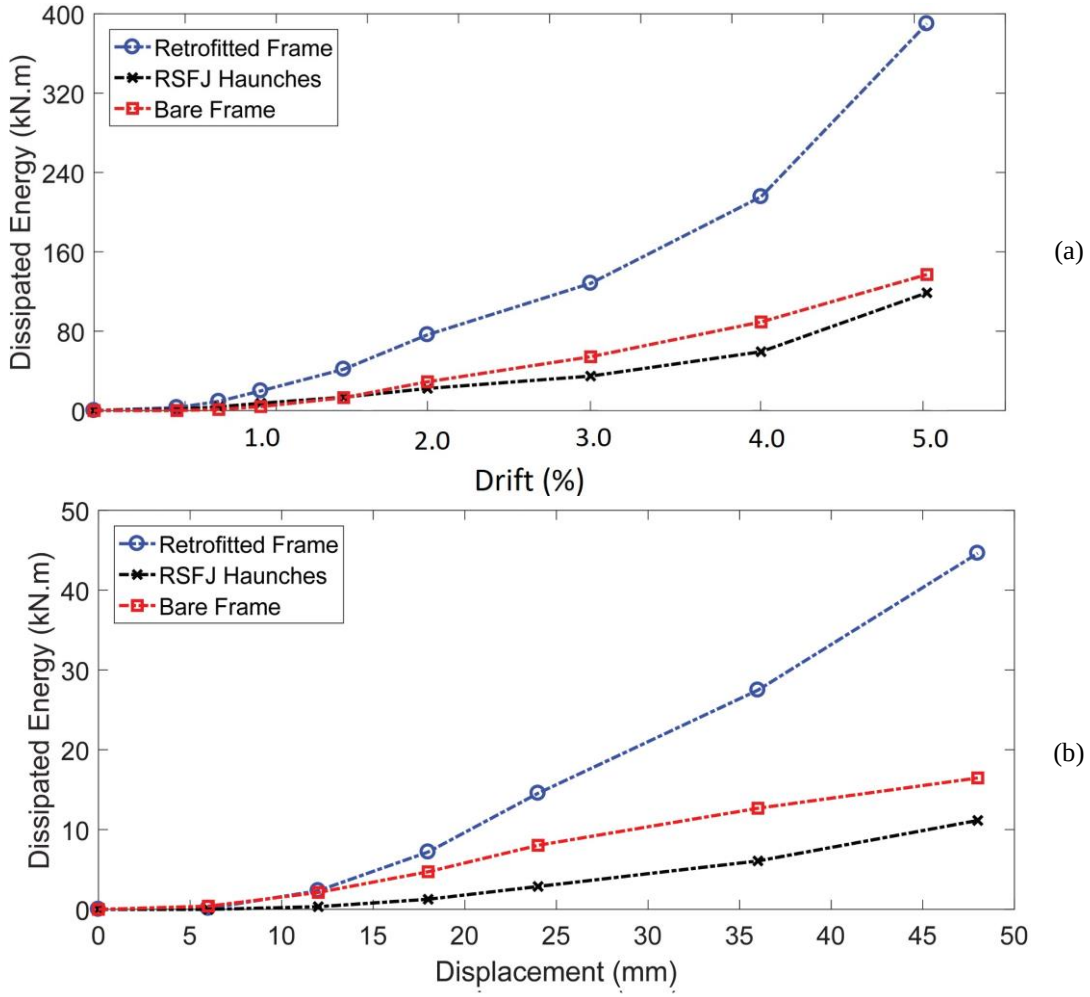

Figure 4-18 Comparison of cumulative energy dissipation for the cyclic loading: (a) Interior joint, and (b) Exterior joint.

4.7. Summary and Concluding Remarks

In this chapter, an innovative local retrofitting method for the under-designed RC joints was introduced. The Resilient Slip Friction Joints (RSFJs) were adopted as self-centering friction haunches to protect the RC frame panel zone from excessive shear deformation and redistribute the internal forces in the elements. This not only enhances the strength, stiffness and energy dissipation of the system, but also decreases the residual displacement in the frame given the restoring force provided by the RSFJs. A component test was conducted on a pin-pin end supported RSFJ to demonstrate its capability for installation as a haunch element in the RC frame. The brittle behaviour of the RC frames was simulated through macro-modelling of non-seismically designed joints via OpenSEES software package. The model was then validated by existing experimental data in the literature. A design procedure for retrofitting with RSFJ haunches was proposed for the cases of interior and exterior RC joints. The efficiency of the RSFJ

haunches was demonstrated through numerical modelling of the sample joints. The results highlight the improved strength, stiffness and enhanced energy dissipation of the system, as compared to the non-retrofitted case. Moreover, the retrofitted frames present negligible residual displacement, given the advantage of restoring force provided by the RSFJ haunches. The restoring force provided by the RSFJ haunches could be beneficial, especially on the frames that could suffer from soft-story mechanism. In summary, the findings of this chapter highlighted the potential of utilizing RSFJ haunches to significantly improve the performance of the non-ductile under-designed RC frame joints lacking transverse reinforcement. While the numerical modelling of the RC joints retrofitted with RSFJ haunches shows the better performance of the joints in terms of energy dissipation and residual drifts, further numerical studies such as time history analyses and incremental dynamic analyses and fragility assessment for structures strengthened with such retrofitting system are recommended to further quantify and investigate the performance of the introduced retrofitting system. Moreover, experimental tests are needed to further validate the performance of RSFJ haunch retrofitting. It should be pinpointed that such retrofit might increase the overall base shear of the frame which may lead to more shear demands on the structure's foundation, which may be need to be considered for a proper retrofit design.

Chapter 5: Seismic Retrofitting of RC Frames Using RSFJ-toggle Bracing Systems: Analytical, Numerical and Experimental Studies

5.1. Introduction

A reinforced Concrete (RC) building structure should have sufficient strength, stiffness and ductility to perform well during major seismic events. A high number of existing RC buildings, especially those built prior to 1970s might not satisfy the current seismic codes criteria or suffer severe earthquake damage or even collapse in case of an upcoming major seismic event. This is due to the fact that these frames are mainly designed based on allowable stress for vertical gravity load only[162], and thus lack the seismic detailing required for lateral loads and deformations imposed during high seismic events. The observations during the last three decades from the recent earthquakes such as San Fernando earthquake (1971), Northridge Earthquake (1994), Christchurch earthquake (2011) have already revealed this fact. The need for a practical, quick, safe and reliable retrofitting techniques within a reasonable budget still remains as an important topic within the structural and earthquake engineering community.

Depending on the required level of seismic retrofitting, the deficient RC structures may go through a member-level upgrading (local-retrofitting), or structural-level upgrading (global-retrofitting). Normally, the aim for local retrofitting is to improve the deformation or force capacity of a few deficient components so that they will not reach their limit state as the building responds to the overall seismic demand[163]. Examples of local retrofitting includes addition of various jackets[123, 164] or structural haunches to the beam-column joints [165]. As for the global retrofitting method, the aim is to improve both stiffness and strength of the whole system at the structural level[163]. Examples include adding shear-walls or various types of steel braces to the RC frame to reduce storey drifts and ductility demand[166]. Noting the fact that most deficient RC frames suffer from non-ductile behaviour, it is crucial to control the overall deformation demand of the building. Other reasons include (but not limited to) the risk of seismic pounding, or the presence of infill walls in the RC frame which is vulnerable to collapse, even at small drift demands. On this basis, the global retrofitting may be more popular, thanks to

its efficacy and relative ease, as well as lower overall cost for implementation, compared to local retrofitting.

Besides utilizing traditional global retrofitting methods, researchers have also explored the possibility of using seismic dampers for seismic upgrading of RC frames. Among the research relevant to this chapter are the studies by Javidan and Kim[102] who introduced a system consisting of pin-jointed steel frame with rotational-friction damper for seismic retrofitting of a fragile RC frame with soft-storey issue. Their numerical and experimental outcomes demonstrated the efficacy of the proposed system for collapse prevention of the frame and inter-story drift reduction to the code-stipulated limit states. In another study, Javidan et al. [167] presented a steel hysteretic column damper for seismic retrofitting of RC structures and tested the damper on a single-story one-bay RC frame. Such a damper has the benefits of occupying only a small space next to the column without blocking the passage of people or vehicles.

Eskandari Nasab et al.[168] employed Visco-Elastic Dampers (VEDs) with fail-safe mechanism for retrofitting of a full-scale two-story RC frame and studied the performance of such dampers in terms of inter-story and residual drift reduction. Tahamouli Roudsari et al.[169] performed an experimental testing on seven RC frames where six of them were retrofitted by chevron bracing with different numbers of ADAS and TADAS yielding dampers. Their results showed that the dampers increase the strength of the RC frames, as well as ductility, energy dissipation and strength reduction factor for all the frames. Sarno and Manfredi [121] investigated the applications of Buckling Restrained Braces (BRBs) as hysteretic energy dissipation elements for seismic retrofitting of a typical two-story RC frame that were designed for gravity loads only. Their results showed the concentration of damage in the BRBs while the existing RC frame remained elastic. Vafaei et al. [170] investigated a specific yielding damper called Tapered Strip Dampers (TSD) for the purpose of retrofitting of damaged non-ductile RC frames. For this purpose, they constructed a full-scale one bay non-ductile RC frame and subjected the frame up to its ultimate load capacity using quasi-static cyclic load. Then, they utilized the TSD to demonstrate the capabilities of the retrofitted frames in comparison with the reference frame. Their results showed that the stiffness degradation of the retrofitted frame was slower and its energy dissipation was superior. Bruschi and Quaglini[171] introduced a novel hysteretic friction damper named prestressed lead damper with strait shaft (or PS-

LED) and illustrated the damper efficacy for seismic retrofitting of out-dated RC frames, as compared to conventional steel hysteretic dampers.

This chapter presents the details of the experimental results obtained by the cyclic testing of a RC frame equipped with RSFJ-toggle bracing system. Two identical one-story single bay RC frames were tested for this purpose (one serves as a benchmark bare frame while the second frame represents a retrofitted performance). The chapter also includes the testing results for the damper components, as well as material testing of the frame and covers the criteria considered for the proper design of the retrofit scheme in this research, including the brace and gusset plate design. The objectives of this study are: (1) to investigate the performance of the proposed retrofit solution, (2) to check whether the criteria suggested by the authors can lead to an acceptable design for such retrofitting, and (3) to investigate the accuracy of capturing the performance of such retrofitted frame with a numerical model. While the design recommendations and outcomes presented here are based on a self-centering flag-shaped damper, it can also provide some basic information for retrofit designing of toggle-bracing system with other dampers including traditional friction, viscous or yielding dampers.

5.2. RSFJ Toggle-bracing system

The RSFJ-Toggle bracing can limit the story drift of the frame and increase the overall strength and stiffness of the system, while magnifying the small floor displacement for the joint to dissipate the seismic energy. Therefore, it performs as a combination of category ***a*** and ***b*** in Figure 2-5 in Chapter 2. It can also provide restoring force for the frame, in case of extreme seismic events.

RSFJ is classified as displacement-dependent devices and thus, its performance depends on the relative displacement of its two ends. While many possibilities can be considered for connecting the joint to the structure, the key locations are where the expected relative displacements are highest for the device. As for the non-seismically designed RC frame where the maximum permissible drift of the frame is limited (in the order of 1% or less), common installation of the joint such as diagonal and chevron may not provide considerable relative displacement for the joint to dissipate the seismic energy. To tackle this issue, Toggle-bracing arrangement can be employed to amplify the small deflection of the frame into a large relative motion for the joint. The concept was introduced by Constantinou et al.[172] on viscous dampers and its effectiveness was verified through

shaking table tests[173]. Figure 5-1 depicts the common different arrangements of toggle bracing systems introduced by previous studies, in comparison to the diagonal and chevron bracing system. While the amplification factor (*f*) for each system is provided in Table 5-1. The following relationships exist for the installation of the joint in the toggle-bracing system:

$$u_d = f \times u \quad (1)$$

$$F = f \times F_d \quad (2)$$

Where u_d, and F_d are the relative displacement and force along the axis of the joint, respectively. The parameters u and F denote the story displacement and horizontal component of the force exerted to the frame. The derivation of magnification factor for different arrangements of braces can be determined by considering a small deflection of the frame toward either left or right direction and assuming that all of the braces deformations are focused in the dampers (i.e. the braces axial flexibility are neglected). Although the provided equations are useful for initial estimation of the damper deflection, the software modelling can estimate the damper deflection more accurately, as they can take into account the brace axial flexibility as well. Moreover, for the arrangements outside of the cases shown below, the numerical software modelling may be utilized to compute the damper deflection against certain amount of frame drift.

Among the available arrangements, the lower toggle (Type II) (Figure 5-1-f) was adopted here for the initial analytical investigation (section 5.3), where the toggle brace system is connected to the three beam-column joints of the frame. It should be noted that the braces are assumed to be pin-connected to the beam-column joints and the designed connections can fully transfer the brace forces to the RC frame.

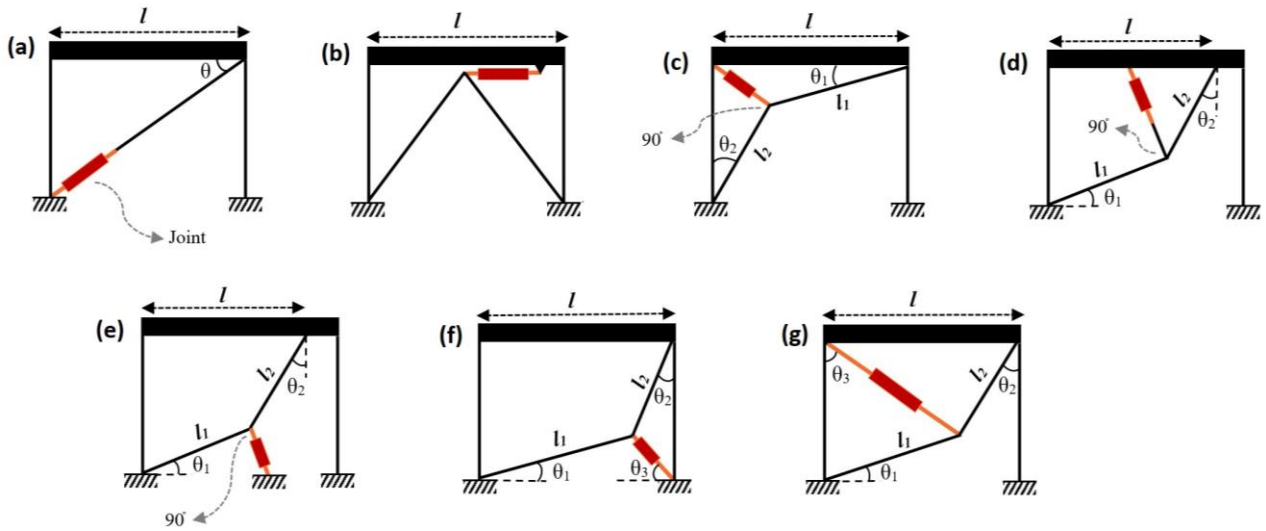

Figure 5-1 Schematic view of different toggle-bracing arrangement, as compared to common bracing systems

Table 5-1 Amplification factor for different bracing system

System ID	Name	Amplification factor (f)
a	Diagonal	$\cos\theta$
b	Chevron	1.0
c	Reverse Toggle	$\frac{\cos\theta_1}{\cos(\theta_1+\theta_2)} - \cos\theta_2$
d	Upper Toggle (Type I)	$\frac{\sin\theta_2}{\cos(\theta_1+\theta_2)} + \sin\theta_1$
e	Lower Toggle (Type I)	$\frac{\sin\theta_2}{\cos(\theta_1+\theta_2)}$
f	Lower Toggle (Type II)	$\frac{\sin\theta_2 \sin(\theta_1+\theta_3)}{\cos(\theta_1+\theta_2)}$
g	Upper Toggle (Type II)	$\frac{\sin\theta_2}{\cos(\theta_1+\theta_2)}\cos(\theta_3-\theta_1) + \sin\theta_3$

5.3. Preliminary numerical analysis

Based on the experimental works by Al-Sadoon et al. [174], a single bay non-ductile RC frame was selected to investigate the performance of the RSFJ-Toggle brace system. The selected frame (Figure 5-2) represents the exterior ground floor level frame of a 6-story RC structure, designed based on the National Building Code of Canada issued in 1965 (NBCC) which does not provide any specific seismic detailing. Such a frame can fairly represent an old-fashioned RC frame designed based on NZ RC codes in the 1960s. It needs to be pinpointed that neither the 1960s NZ codes (NZS 1900.8:1965; NZS 1900.9:1964) nor U.S codes (ACI 1971) contained any of the capacity design provisions[72], and generally no seismic detailing is provided by such codes; thus the RC

buildings designed before 1970s can be considered as gravity-only frames with minimal drift capacity.

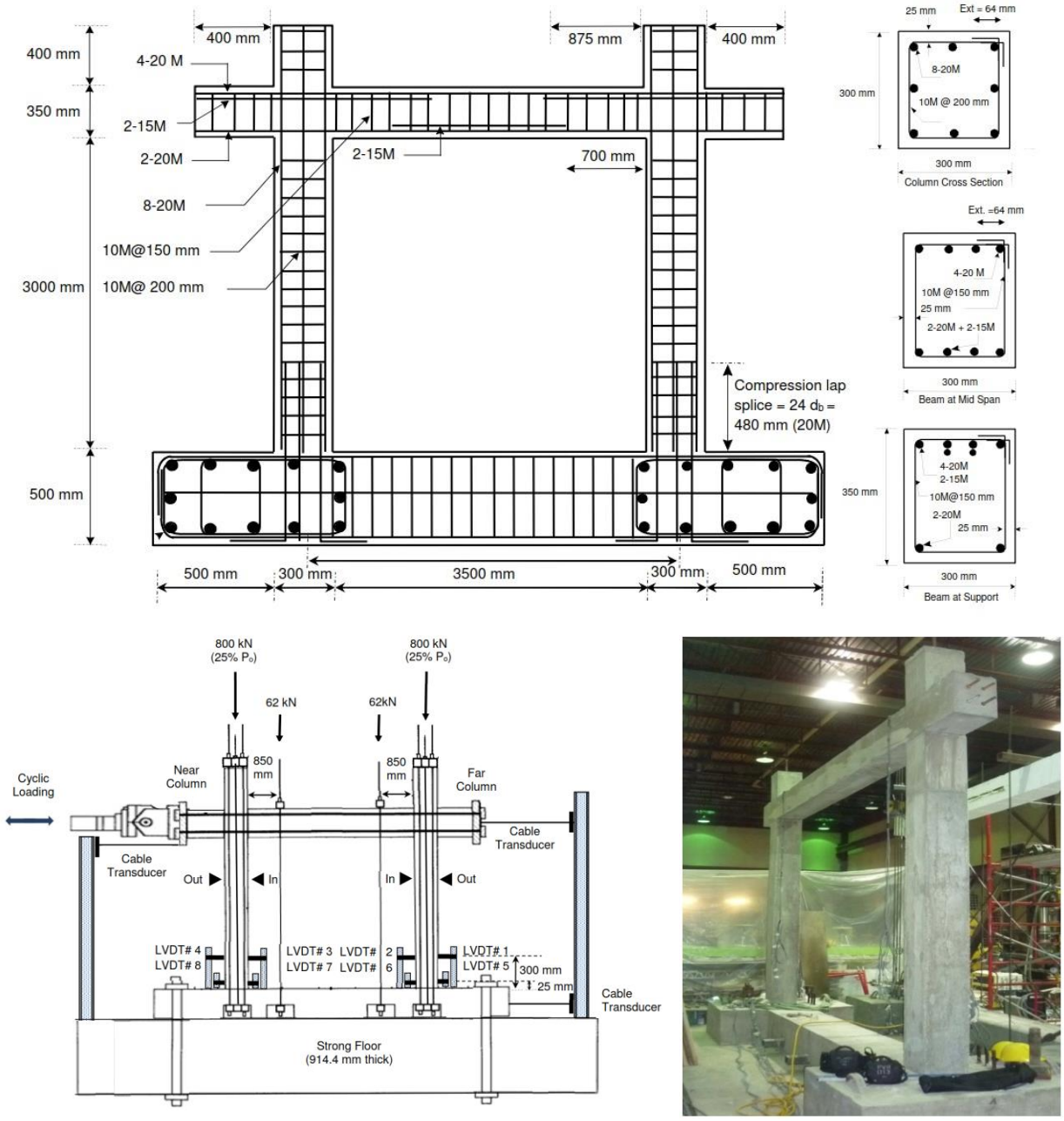

Figure 5-2 Section and reinforcement detail of the RC frame tested by Al-Sadoon et al.[174, 175]

Figure 5-3 shows the cyclic performance of the tested frame, which clearly indicates its rapid strength degradation and brittle behaviour. The same frame was modelled in SAP2000 and its nonlinearity was considered via fibre hinges at both ends of columns and beams. The comparison between backbone curve from pushover analyses with experimental cyclic performance of the frame shows good agreement between the numerical and experimental results and highlights the elastic performance of the frame

when the lateral drift is below 40mm (≈1.0% frame drift). An RSFJ-Toggle brace system with lower Toggle type II arrangement (Figure 5-1-f) was assumed for retrofit of the sample RC frame (θ1=29.6, θ2=36.6, θ3=40.0), with approximate amplification factor of 1.38. It is worth noting that the amplification factor for each toggle bracing arrangement is derived from theoretical equations that usually neglects the axial braces deformation. Therefore, the actual damper deformation is expected to be marginally less than the theoretical u_d, which can be modified after finalizing the brace design. Figure 5-4-a shows the utilized RSFJ for the modelled toggle-bracing configuration, based on the target drift of the frame (36mm ≈ 1% drift), while the cyclic pushover curve for the frame is depicted in Figure 5-4-b, for comparison. As can be noted, the damping of the system, as well as its initial stiffness is increased. It should be noted that the maximum base shear in the pull and push direction slightly differs, which is due to the fact that the magnification factor can change with loading direction. Such behaviour depends on the geometrical configuration of the system, as well as targeted drift. If the differences in the performance of the system is sensible in the push or pull direction, then the effect should be either considered in the retrofit strategy, or addressed by implementing toggle braces in two bays. Moreover, it should be pointed out that the magnification factor for the numerical model is calculated as 1.23 (equivalent to 45.93mm damper deflection in 37.34mm frame drift). Again, the difference initiates from the fact that the software can includes the brace axial flexibility into account. It is worth noting that for the experimental testing, other factors such as elastic deflection of gusset plates, the slackness and tolerances (gaps) in the pins, connections, etc. might influence the damper deflections as well.

Regarding the system overall damping, by using the Jacobsen equation for calculating the hysteretic damping[116], the added damping for the RSFJ-toggle RC frame can be calculated using the following equation:

$$\xi_{eq} = \xi_{elastic} + \xi_{hyst} \tag{3}$$

$$\xi_{hyst} = \frac{2}{\pi}\frac{(A_1 + A_2)}{A_3} \tag{4}$$

Where ζ_{eq} denotes the equivalent viscous damping, ζ_{hyst} is the hysteresis damping, and A1, A2 and A3 are shown in Figure 5-4. For the current modelled system, the ζ_{hyst} is evaluated as 8.98%, thereby the overall damping for the system can be considered as 13.98% (assuming an elastic damping of 5% for the bare frame).

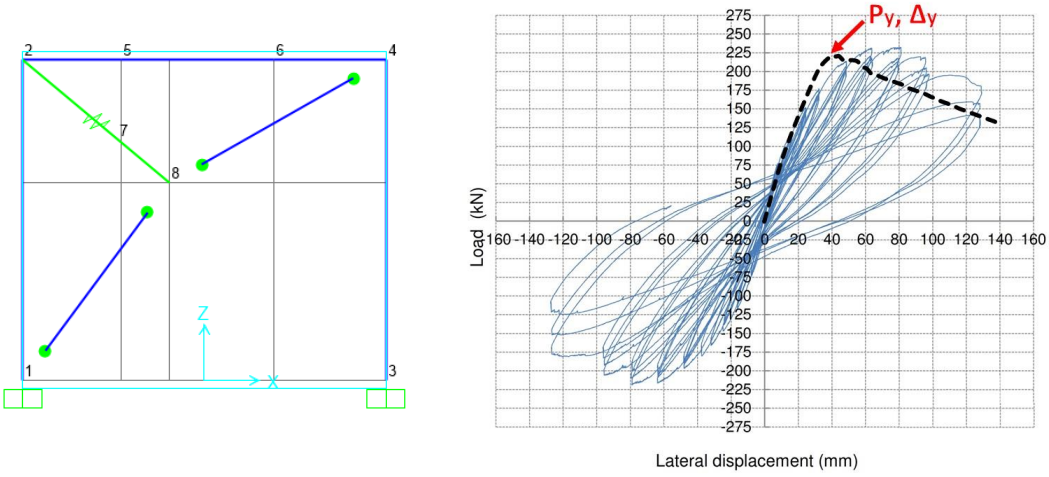

(a) (b)

Figure 5-3 Comparison of the pushover results with the experimental hysteretic load-displacement of the frame

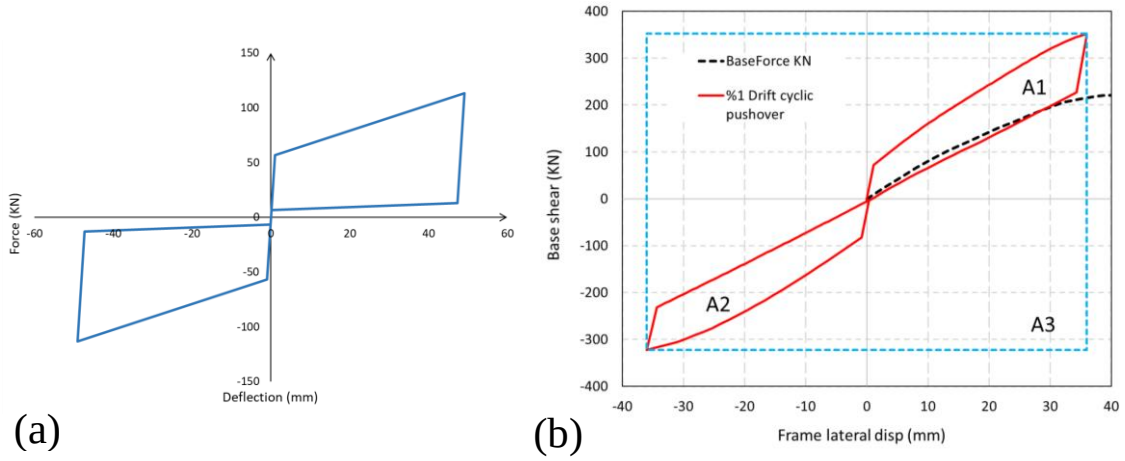

Figure 5-4 Performance of the retrofitted RC frame with RSFJ-toggle bracing system : (a) Flag-shape behaviour of the RSFJ adopted in the toggle-brace system (F_{slip}=56.6, F_{ult}=113.1, $F_{restoring}$=12.9, F_{res}=6.4, μ=0.18, and Deflection capacity=49.1mm); and (b) Cyclic pushover of the retrofitted frame up to 36mm lateral displacement

5.4. Characteristics of the Deficient RC frame

To check the efficacy of the RSFJ-toggle bracing system, two identical RC frame were manufactured for the experimental testing. The frames are similar to the ones studied by Al-Sadoon et al.[175], with scale factor of 0.6 and slight changes in dimension given the testing space limitations of the AUT Structures lab. The frame specimens can represent a good constructed pre-1970s RC moment resisting frame. The bar details and dimensions of the frame are depicted in Figure 5-5. Appendix 1 provides more details about the frame, including the shop drawings and the reinforcement detail. A few aspects were considered

for the construction of these frames so they better represent an old-fashioned deficient RC frame which will be explained in the following paragraph.

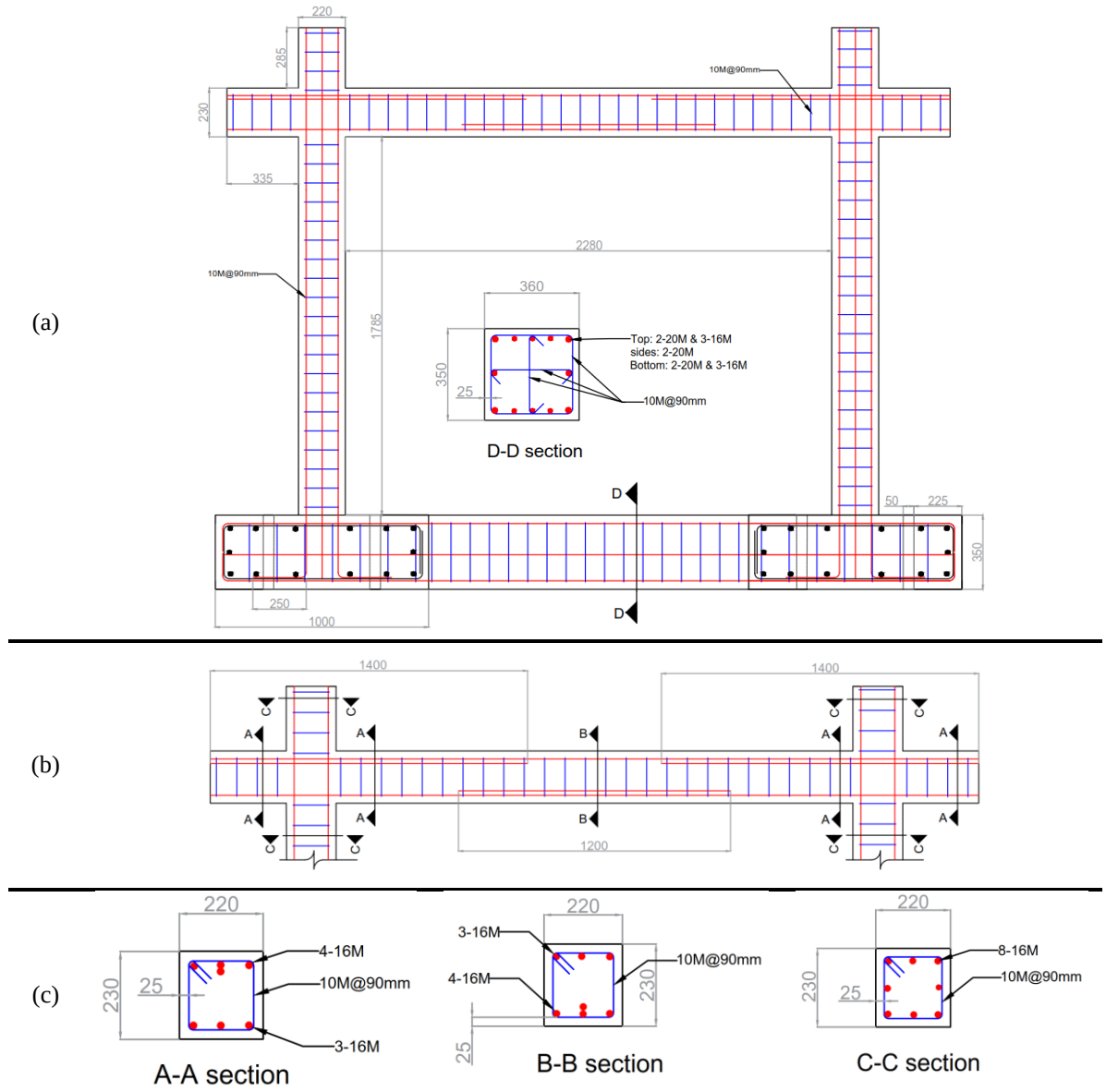

Figure 5-5 The RC frame rebar detailing and section geometry dimension: (a) Overall height and length of the frame, and (b) to (c) frame beam and column section

It needs to be stated that old-fashioned RC frames are constructed with material and rebars which may not demonstrate the quality and characteristics of today's material and their characteristics are subject to change over time. For the retrofit purposes, the probable characteristics of materials are considered for analysis. Based on Yellow-C5, the probable compressive strength for a building constructed between 1970-1980 can be considered as 1.5* f'_c (specified 28-day compressive strengths ≤ 40MPa) or 30 MPa if no information is available for the frame. For the two frames constructed here, a low value for

compressive strength of the concrete was considered (approximately 20MPa) to better demonstrate a frame with low strength concrete.

A critical aspect for the detailing of reinforced concrete members, especially the columns is the amount of transverse reinforcing provided and in particular the spacing between the adjacent rebars. The transverse rebars provide confinement for the core concrete and prevent the buckling of longitudinal bars. The performance of non-ductile concrete RC members with light shear reinforcements has been extensively investigated in the literature[176, 177]. In general, the lower shear reinforcement results in smaller drift capacity for such columns. Based on Engineering assessment guidelines (C5)[70], unconfined condition is present if at least one of the following conditions are exist in the RC frame:

- Only corner bars are restrained against buckling by bending of shear rebars.
- Having 90-degree hooks.
- Spacing of stirrups $s \geq d/2$, where d denotes effective depth of the section.

For the manufactured frames, the middle longitudinal rebars are not restrained against buckling; moreover, the s of 90mm is slightly bigger than the d/2 = 88.5mm = (220-25-10-8)/2. Therefore, two of the above conditions exist for the deficient frames and the concrete core is poorly confined for the manufactured specimen. Although it was possible to specify 90-degree hooks for the manufacturing of RC frames, it needs to be stated that 90-degrees hooks were not commonly witnessed in New Zealand. This is due to the fact that Clause 409 of NZSS 95:1935 already included 135-degree hooks for stirrups; however, no requirements were specified on this regard.

Other indicators for non-ductile behaviour of columns which was suggested by Stirrat et al.[176] is the ratio of concrete core to gross concrete area (A_c/A_g) and the ratio of axial load demand ($P/A_g f'_c$). Speaking from their experience and available literature, they state that the ratio of A_c/A_g=70% or smaller may suggest the non-ductile behaviour of the column (for the current RC frame, this ratio is calculated as 64.7%). As for the axial load demand, they proposed the ratio of 0.3, where columns with higher axial load are expected to behave in a non-ductile manner. This behaviour has been explained with the help of moment-curvature analysis of the RC frames column considering different axial load ratios (Seismic Assessment Guideline-Yellow C5[72]) and similar graphs have been calculated for the column section of the manufactured RC frame. As can be seen, while

the yield curvature (especially the equivalent yield curvature) is not greatly dependent to the axial load level, the curvature capacity as well as the drift capacity of column are strongly influenced by the axial load level.

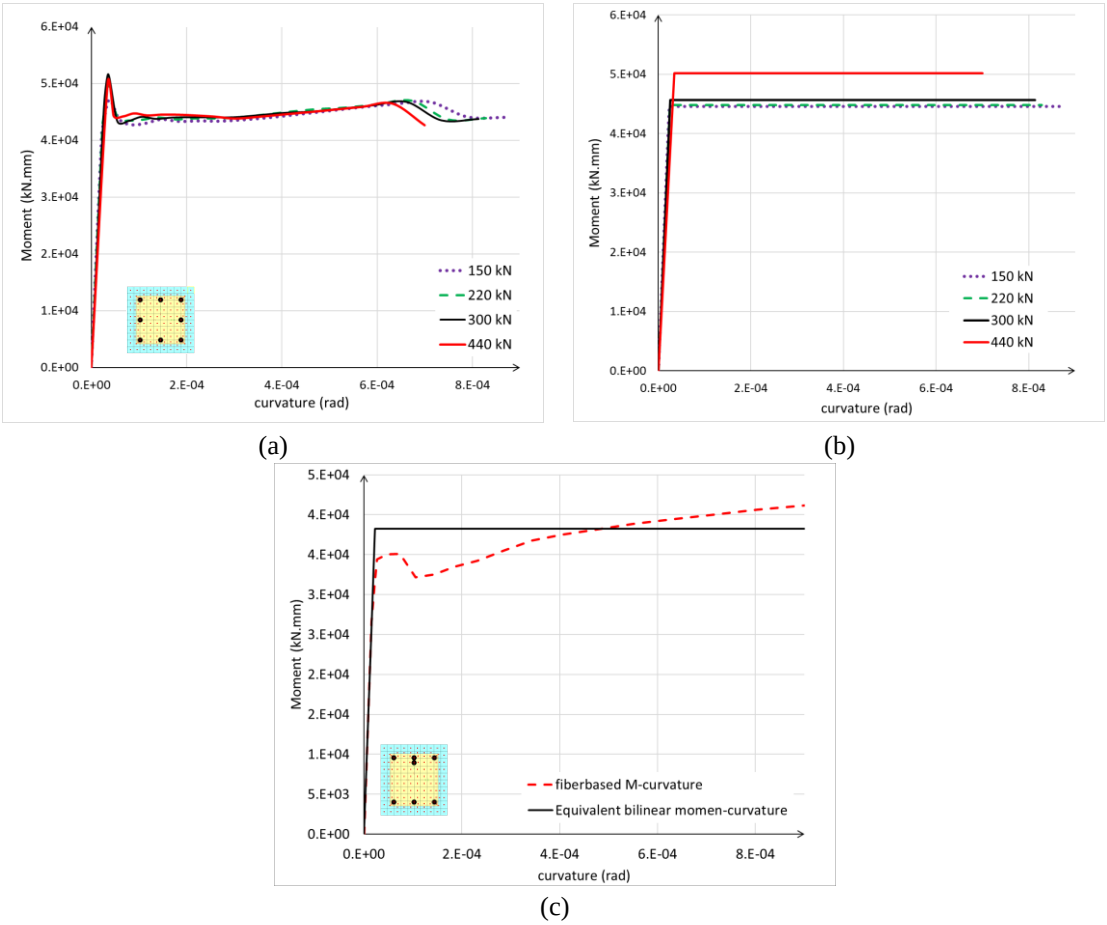

Figure 5-6 The Fibre-based moment curvature analysis of the sample RC-frame using SAP2000 software: (a) Column section, (b) Equivalent bilinear moment-curvature of the column, and (c) Beam section

It should be pointed out that for the current experimental testing, $P_{axial} \approx 220kN$ (equivalent to $0.15*P/A_g f'_c$) were applied on the columns, which can be considered as a typical loading ratio for regular RC columns. As the columns with high axial loading ratio (larger than $0.30*P/A_g f'_c$) present very limited post-elastic range of drifts, 15% axial loading seemed more suitable for the experimental testing, so that the capability of RSFJ toggle brace could be tested for re-entering force provision of the frame in its post-elastic range. Moreover, as it will be shown in section 5.8.3, for the current testing setup, the level of column axial load is affected by the rope effects which can change the results and impose higher axial load on the system.

As a final point regarding the employed RC frame tests, the design philosophy of strong-column weak-beam needs to be considered. Such a philosophy has been introduced in the

1982 version of the New Zealand concrete code of practise (NZS 3101, 1982) in the commentary section. This means that the older buildings constructed before legalization of this code may or may not follow such philosophy, depending on their beam sections and rebar detailing. The strong column weak beam philosophy ensures the formation of beam hinges before column mechanism and thereby promotes an inelastic beam sway mechanism rather than a column sway mechanism.

While the beam section of the current RC frame is slightly larger in order to identify the likely inelastic mechanism in the frame, a parameter named "Sway index" for the beam column joints can be calculated. Priestley et al.[178] defined the Sway index as the summation of beam flexural capacity (left and right side of the RC joints, or negative and positive flexural capacity of beam) divided by the column flexural capacity (top and column) for all of the beam column joints in a specific story:

$$S_i = \frac{\sum\left(M_{prob,beam}^{left,i} + M_{prob,col}^{right,i}\right)}{\sum\left(M_{prob,col}^{top,i} + M_{prob,col}^{top,i}\right)} \tag{5}$$

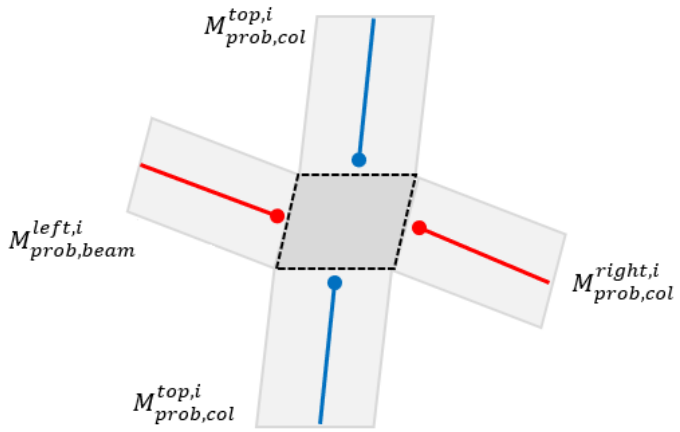

Figure 5-7 Definition of beam and column moment strength for calculation of sway index

While in theory, the value of $S_i \geq 1.00$ denotes the column sway mechanism, Priestley recommended a value of $S_i \geq 0.85$ as an indication for column sway mechanism. Such a recommendation has been accepted by codes, to ensure that there is a high likelihood of column sway mechanism to be identified in the frame considering that factors such as calculation errors, uncertainty in member geometry and material strength and higher mode effects could trigger the sway mechanism and might be missed from sway index calculations. It needs to be highlighted that the codes usually increase the negative flexural capacity of beams (in general, by 50%) to include the slab contribution in the

beam bending resistance. Another point to highlight is the axial force demand that can be developed in the beams and increase the beam flexural capacity. Based on the moment-curvature analysis, the Sway index for the current test setup RC frame is calculated as $38232/43861 = 0.85$ (1.07, if slab contribution is considered as per codes) which shows the potential column sway mechanism. As it will be explained in section 5.8, during the cyclic pushover testing of the frame, the concrete cracks were firstly and mostly developed in the columns which pinpoints the occurrence of column sway mechanism before the beam hinging.

5.5. Material properties and testing

The frames were manufactured at a precast concrete factory (Concretec Ltd.), close to Auckland city and were delivered to the AUT Structures lab. Due to the constraints regarding the structural lab entrance height and the crane weight limit (5 ton), the overall dimension and height of the frame were adjusted to make sure the largest possible frame to be manufactured and transferred to the lab for testing. The RC frame dimensions are depicted in the Figure 5-8-a. Two Reid eye anchors with 2.5 tonne capacity were included on top of the columns for the intention of cranage (shown in the Figure 5-8-b).

The concrete had a maximum aggregate size of 10mm and two different compressive strengths. The higher compressive strength was aimed for the foundation, while the lower compressive strength was allocated for the beam and columns material. Although it was specified to keep the concrete compressive strength at about 20 MPa and not surpass the 25 MPa, such a limitation was not necessary for the frame foundation. On this basis, for the foundation of the test frame, different mixture of concrete with compressive strengths of 30 MPa were utilized. The foundation dimensions, are depicted in Figure 5-8-c. Moreover, it needs to be noted that the foundation and the frame parts were manufactured separately, and then connected together using drossbachs (four per column, two on each perpendicular direction as depicted on Figure 5-8-d).

(a)

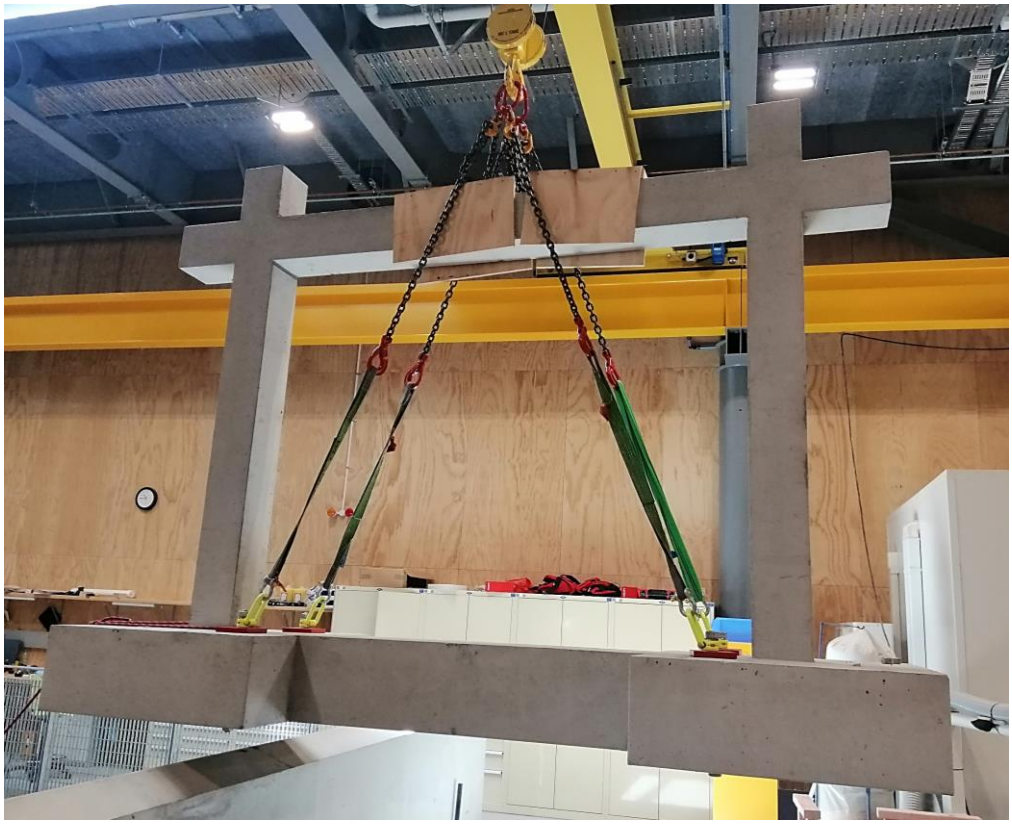

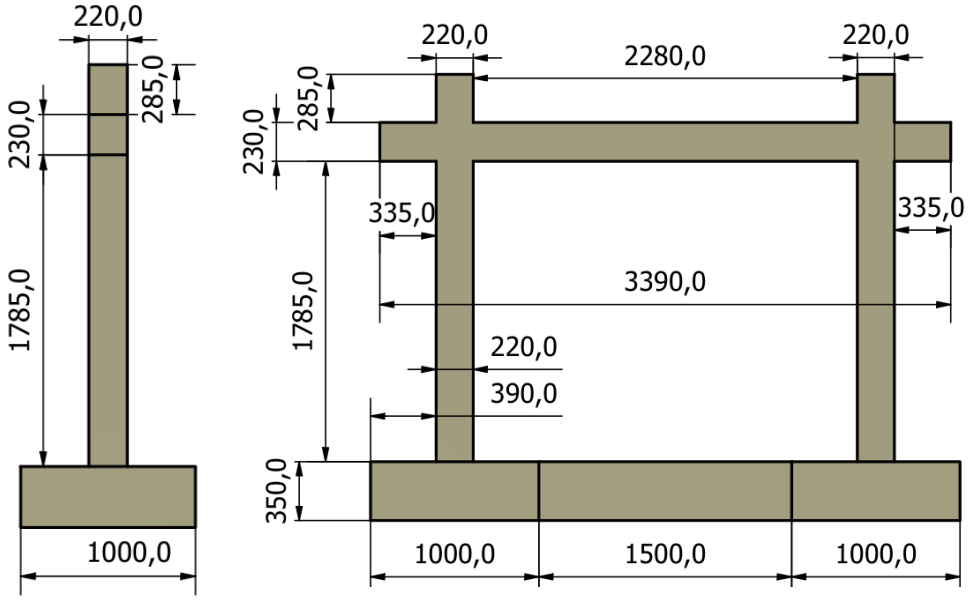

(b)

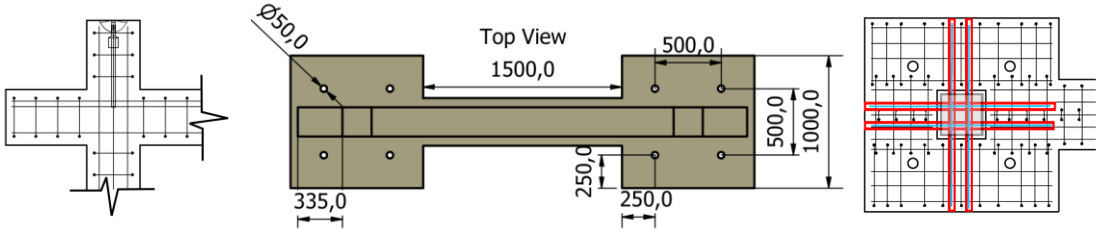

(c) (d) (e)

Figure 5-8 The RC frame tested: (a) Actual frame, (b) Overall height, (c) Placement of Reid eye anchors on top of columns, (d) Foundation pads dimentions, (e) Placement of drossbachs for the connection of foundation and RC frame

To verify the compressive strength of the concrete, three samples of standard concrete cylinders with the dimension of 100mm in diameter and 200mm height were requested from the manufacturer. Figure 5-9 shows the testing of the concrete cylinders using the UTM machine. The summary of the test results shows that the concrete compressive strengths for the benchmark bare frame, the retrofitting frame, and the foundation parts of both frames were 22.7, 19.2 and 28.0 MPa, respectively. As it can be found, the compressive strength of the concrete mix for the beams and columns of the retrofitted frame is slightly lower than the benchmark frame, however, such a small difference is not expected to alter the results significantly.

While it is unlikely that the compressive strength for the cylinders would change because of the aging effects, it needs to be cleared out that the cylinder samples for the concrete frames were tested at the exact day of cyclic testing of the real frame. As such, their compressive strength values reflect the correct compressive strength of the frame. The second frame was tested nearly a month after the first frame testing.

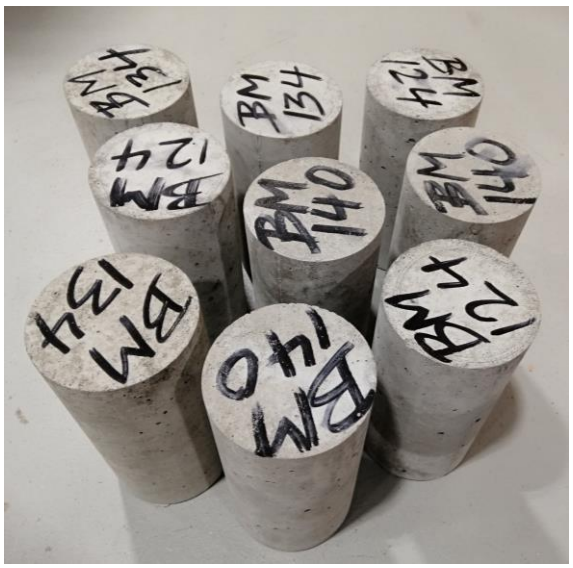

(a)

(b)

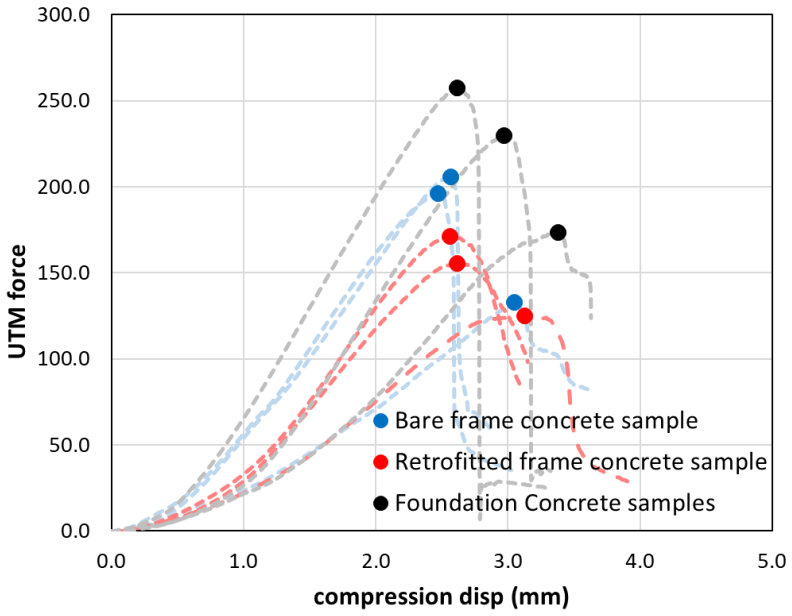

(c)

Figure 5-9 Concrete cylinder Sample testing of the RC frame: (a) nine samples for the frames and foundation, (b) testing the samples using UTM, (c) Obtained results for the samples

The employed rebars for the frames are grade 300E which follow the requirements of AS/NZS 4671:2019 code. To check the yielding and ultimate strengths of the reinforcing steel rebars utilized in the frame, three samples with length of 300mm were also requested for testing (for each size of rebar). Figure 5-10 shows the testing setup for the tensile testing of the rebars and the results obtained for each of them. The M20 rods could not be tested since the jaws on the UTM grip had a limited opening capacity. However, the M20 rods were only utilized in the foundation part of the frame, which remained intact during the testing. It is worth to note that the negligible fluctuation on the curves is due to the small slipping of the rebars in the specialized jaws of the grip in the UTM device. Based

on the test results (Figure 5-10-b), the probable yielding and ultimate strengths of the M10 rebar was 365.1kN and 497.5kN; while for the M16 reinforcement, the probable yielding and ultimate strength was 320.7kN and 460.0kN, respectively (Figure 5-10-c).

(a)

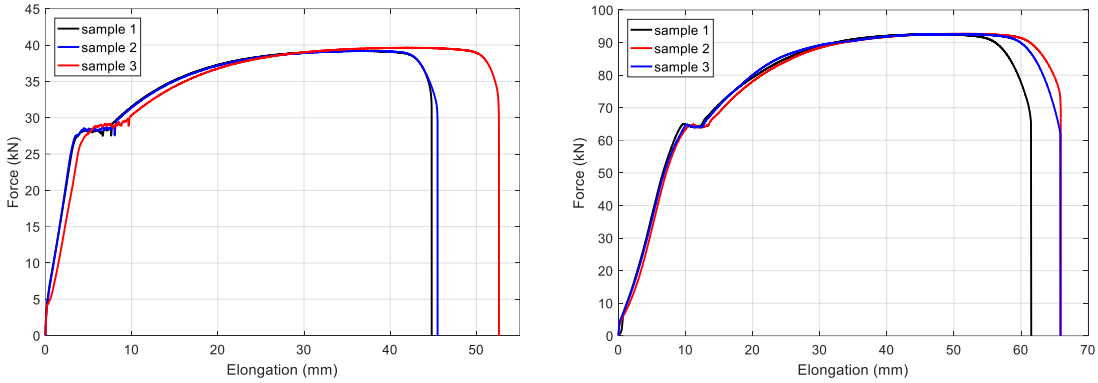

(b) (c)

Figure 5-10 The tensile strength testing of the reinforcements employed in the RC frame: (a) testing the rebars using UTM, (b) results of M10 rebars, and (c) results of M16 rebars

5.6. RSFJ damper design

The Resilient Slip Friction Joint (RSFJ)[54] was introduced to the construction industry as a self-centering friction damper which combines the performance of translational friction sliding with the restoring force provided by the prestressed disk springs. It consists of specially designed cap and middle plates which are clamped together by stack of disk springs in series and high strength bolts or rods. After assembly, the disk springs are prestressed up to a certain desired level, making sure that the activation of the damper through slippage occurs beyond the serviceability limit state (SLS) design load. Here, two RSFJ dampers which were identical in dimension, material and the utilized disk springs, were manufactured using CNC machining on high strength steel plates and tested using

the UTM to capture their force-deformation behaviour. Two different arrangements of disk springs with different prestressing forces were considered for the testing, which will be explained in Section 5.6.2.

5.6.1. Damper characteristics

As explained previously, the hysteresis behaviour of the RSFJ is a flag-shaped performance with four distinct points, which are denoted as the slipping point, the ultimate point, the unloading point, and the restored point. The slip force, ultimate force, restoring force (or unloading force) and residual force (or restored force) can be determined from the equations provided below,

$$F_{slip} = 2n_b F_{pr}\left(\frac{sin\theta + \mu cos\theta}{cos\theta - \mu sin\theta}\right) \quad (6)$$

$$F_{ult} = 2n_b F_{b,ult}\left(\frac{sin\theta + \mu cos\theta}{cos\theta - \mu sin\theta}\right) \quad (7)$$

$$F_{rest} = 2n_b F_{b,ult}\left(\frac{sin\theta - \mu cos\theta}{cos\theta + \mu sin\theta}\right) \quad (8)$$

$$F_{resid} = 2n_b F_{pr}\left(\frac{sin\theta - \mu cos\theta}{cos\theta + \mu sin\theta}\right) \quad (9)$$

where $F_{b,pr}$ is the rod clamping force, n_b is the number of bolts per each side of the damper, θ is the grooves angle, and μ is the coefficient of friction between cap and middle plates. As can be noted, by replacing the bolt prestressing force $F_{b,pr}$ with $F_{b,u}$ (bolt ultimate force where disks become completely flat), the ultimate force in loading and unloading can be calculated, respectively.

Figure 5-11 shows the force deformation behaviour of the RSFJ damper. As it can be found, the performance of the damper is a flag shape behaviour that can be tuned based on different levels of bolt prestressing, different numbers of clamping bolts (per side of the damper), the arrangement of the disk springs and their number, the groove angle of the cap and middle plates, the travel distance of the cap and middle plate, and even the surface roughness and treatment. Even the performance of the damper after it reaches to the ultimate displacement could be modified as per project design requirements. The damper could become interlocked and restrict the structure displacement or go beyond its elastic behaviour and present more deformation through the rod yielding without

compromise on its self-centring (known as secondary fuse). Readers could find more insight regarding this behaviour in the studies published by Darani et al.[140] and Bagheri et al.[67].

The translational displacement of the damper comes from the elastic deflection of the damper itself, along with the relative sliding movement of middle plates against cap plates. The ultimate displacement of the damper (Δ_{max}) comes from the movement of the cap plates before they compress the stack of disk springs up to their flattening state. Therefore, it depends on the groove angle of the cap and middle plates, and the remaining deflection capacity of the stack of disk springs on the RSFJ. On the other hand, the initial displacement of the damper, Δ_{slip} comes from the initial stiffness of the RSFJ (the elastic stiffness before F_{slip}) which is dependent on the dampers cap and middle plates dimensions and it represents the overall elastic performance of the RSFJ before mobilization of the damper plates (opening and closing). The initial stiffness is required for a numerical modelling of the damper, as well as for the retrofit design purposes. While such a stiffness can be easily derived from experimental testing, one can also utilize the following approach to approximately estimate the initial stiffness of the damper.

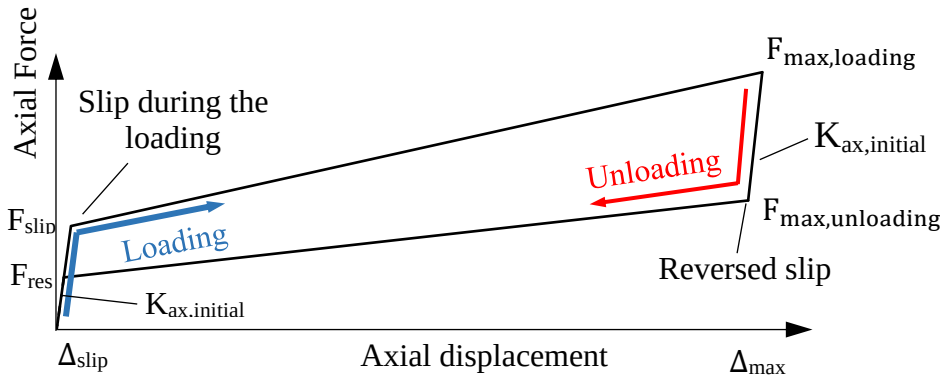

Figure 5-11 RSFJ flag shape force-deformation relationship

Figure 5-12 shows the schematic view of the RSFJ damper designed for the toggle-bracing system. The damper contains one groove at each side and the angle of grooves is 15 degrees. Thanks to its symmetric geometry, the damper can be divided into two parts carrying half of the load (Figure 5-12-b). Each of these parts can also be considered as two springs connected in series (K_1 and K_2) with an equivalent stiffness of K. Therefore, the overall stiffness of the RSFJ is the summation of the four springs shown in Figure 5-12:

$$K_{RSFJ} = 2 \times \left(\frac{K_1 K_2}{K_1 + K_2}\right) = \frac{2 \times K^2}{2K} = K \quad (10)$$

Therefore, the overall stiffness of the RSFJ is equivalent to K (stiffness associated to one of the springs shown in Figure 5-12). By assuming that each groove is acting similar to a column and then replacing the non-prismatic section of the groove with an equivalent prismatic column, a simplified geometry can be considered for calculating the damper elastic stiffness. The equivalent column has the same height as the grooves and the width of $L_3 = (L_1 + L_2)/2$. The previous studies have shown that the elastic deflection of such column comes from bending and shear deformation of the grooves. By adding the axial displacement related to one of those four springs, the summation of bending, shear and axial deformation can be calculated using the following equation:

$$\Delta_{RSFJ,elastic} = \Delta_s + \Delta_m + \Delta_{a,cap} + \Delta_{a,middle} \quad (11)$$

$$= \frac{F_{slip} h^3}{3E_m I} + \frac{1.2F_{slip} h}{AG_M} + \frac{F_{slip} L_4}{2EA_{cap}} + \frac{F_{slip} L_3}{2EA_{mid}}$$

In which the Δ_s and Δ_m are the shear and bending deflection of the equivalent column representing the damper grooves and A is the cross-section area of the equivalent column. The parameters E_m and G_m are young's modulus and shear modulus for the plates material. The third and fourth term are associated with the axial deformation of the cap and middle plates. Such a simplification was utilized previously for assessing the load distribution in case of having RSFJ with two or more bolts per each side of the damper[140]. As an illustration, for the current designed damper (F_{slip}=18.3kN), the elastic deflection was calculated by which the initial stiffness could be estimated as 937kN/mm for a single RSFJ damper.

The overall length of the RSFJ damper were measured as 446mm. Having the section SHS75x6.0 as an extension for the damper-brace assembly which is in series with the two RSFJ dampers, the overall stiffness is computed as 311.1 kN/mm (Figure 5-16 in Section 5.7.2).

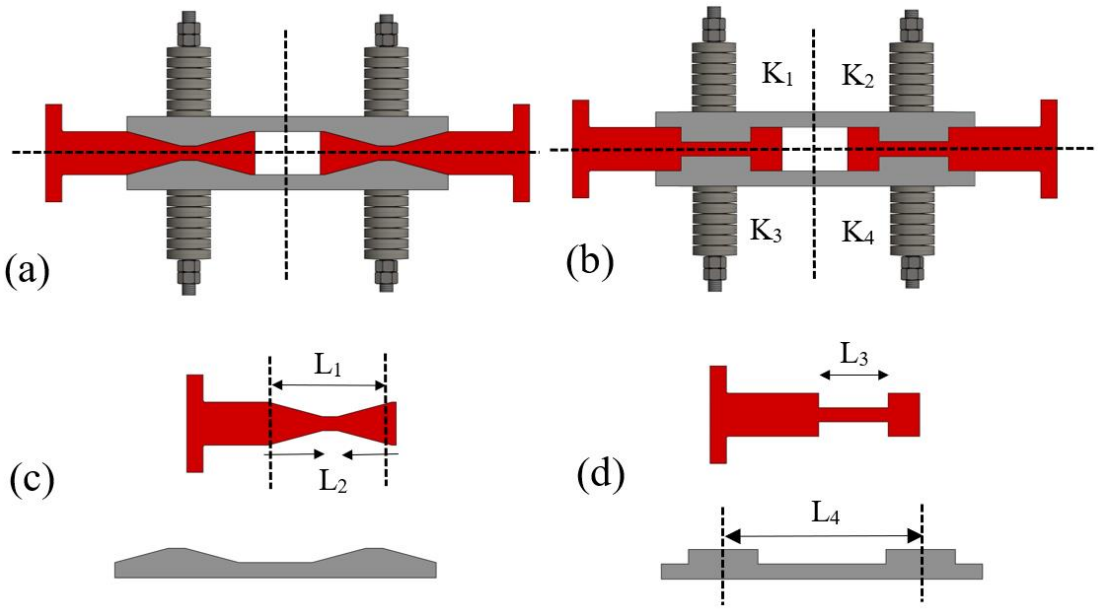

Figure 5-12 Equivalent prismatic column concept for the RSFJ

5.6.2. Damper Component testing

For the experimental testing of the retrofitted frame, two identical RSFJ dampers that have been tuned to the same force-deformation characteristics were considered. These two RSFJs were connected in parallel with a telescopic circular section that provides constraints against dampers rotation behaviour and ensure translational movement for the damper (will be explained further in section 5.7.2) Two different scenarios of prestressing with specific numbers of disk springs were employed for the tuning of the dampers, to see the influence of damper on the overall performance of the system. For this purpose, the retrofitted frame was retrofitted damper tuned with first scenario. After recording the results, the damper was tuned again with higher prestressing force and more disk springs and the test was conducted on the same frame.

Regarding the first tuning, the ratio of prestressing to ultimate force of the disk springs at flattening load (≈28.0kN, with 0.65mm deflection per disk) were considered to be 50%, whereas for the second tuning, a higher prestressing ratio was considered (75%). It was observed that for the first retrofitting test, the RSFJ dampers were not fully opened; thus, for the second retrofit testing, the ultimate deflection capacity of the dampers decreased from 45mm to 40mm (i.e., the number of disk springs were decreased). Table 5-2 presents the design parameters for the two different cases of damper tuning. The experimental results from the frame testing with both tuning scenarios will be provided in section 5.8.

(a) (b)

Figure 5-13 RSFJ dampers component test: (a) Cap and middle slotted plates, (b) Assembly test setup

Table 5-2 Tuning characteristics of the RSFJs for the experimental testing

Parameter	Unit	Tuning scenario 1	Tuning Scenario 2
Slipping force (F_{slip})	kN	12.2	18.3
Ultimate force (F_{ult})	kN	24.4	24.4
Restoring force (F_{rest})	kN	6.3	6.3
Restored force (F_{resid})	kN	3.2	4.8
Joint max deflection (Δ_{ult})	mm	46.1	40.0
Prestressing force	kN	14	21
Prestressing ratio	%	50%	75%
No. of disk spring per side	-	19	33
Hysteresis damping ratio	%	17.3%	20.3%

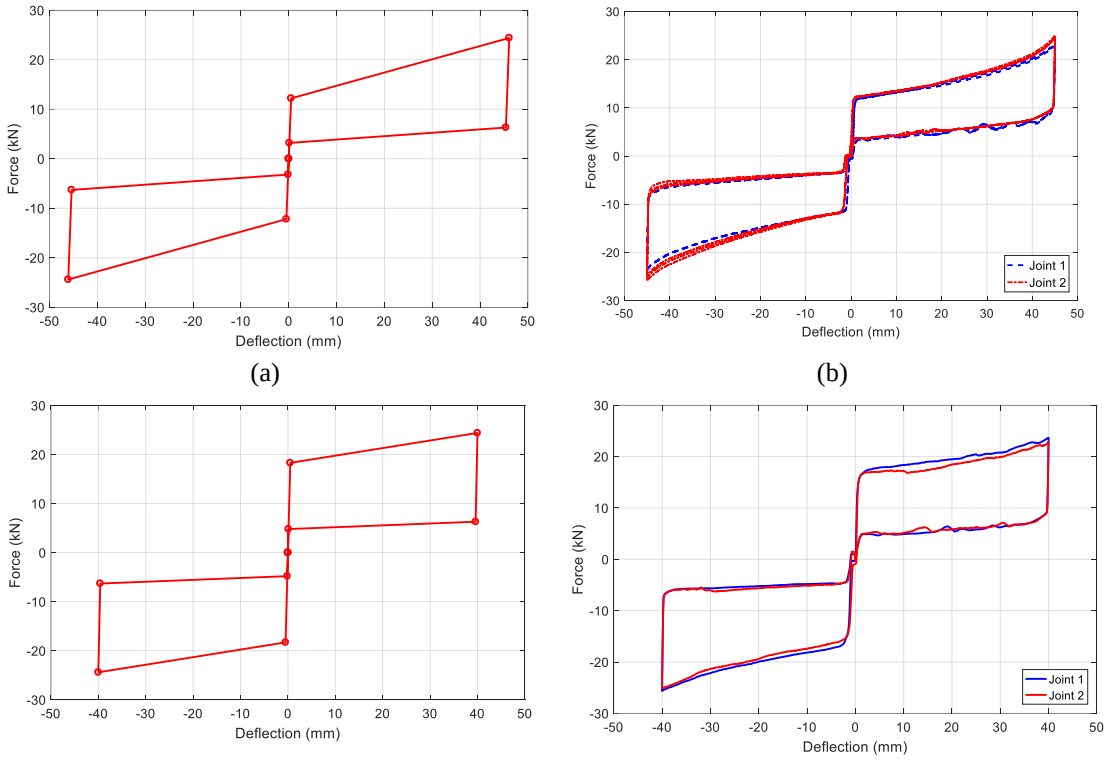

Figure 5-14 RSFJ damper performance result: (a) calculated hystersis behaviour for the first tuning, (b) Observed load-deformation behaviour for the first tuning, (c) calculated hystersis behaviour for the second tuning, and (d) Observed load-deformation behaviour for the second tuning

5.7. Retrofit Design considerations

5.7.1. Brace Design

Figure 5-15 shows the three brace members of the Toggle-bracing system that are pin-connected to their intersection point. The brace sections and dimensions are provided in the Appendix of the thesis. There are several locations for the placement of the intersection point A, however it is desired to place it above the diagonal dashed line that connects the opposite corners of the RC frame. As the frame being pushed to the right side, the tensile forces in the top brace and bottom brace would expand the damper; while the damper will go into compression as the frame drifts to the left.

The angle γ inclines to 180 degrees, as the intersection point gets closer to the diagonal line. It should be noted that sufficient distance L (shown in the figure with purple colour) should be available so that the damper can fully expand, otherwise the top and bottom forces would cancel each other when the frame drifts to the right (γ=180) and system interlocks.

If the friction in the pins is neglected, the braces will act in pure axial force and are in equilibrium at the point A. Thus, they follow the Lami's Theorem. This theorem states that when three forces acting at a point are in equilibrium, then each force is proportional to the sine of the angle between the other two forces:

$$\frac{F_{Top\ brace}}{\sin\alpha} = \frac{F_{Bottom\ brace}}{\sin\beta} = \frac{F_{damper}}{\sin\gamma} \tag{12}$$

The top and bottom brace axial forces can be derived from above equation and needs to have sufficient capacity to withstand the damper ultimate force without any buckling or yielding. For the cases where the RSFJ is expected to surpass its ultimate deflection capacity and enter its secondary fuse mechanism (where the disk springs are completely flat and the joint clamping rods start to yield), the overstrength axial force of the damper needs to be considered for the ultimate force. The overstrength factor of the RSFJ can be estimated as Ω=1.35 [67]. The buckling criteria of the braces will be explained in the next section. For the very short distance L ($\gamma \approx 180$), the small damper force would result in high top and bottom brace forces and thus uneconomical bigger sections for these two elements, while the bigger distance L would lead to smaller forces in the braces and might not justify using the toggle-bracing arrangement. For the current test setup (γ=154, β=115, α=92), the ultimate force of the damper-brace assembly was set to 48.8kN, thus the top and bottom braces need to be designed for 111.25kN and 100.9kN, respectively (in case the overstrength of the RSFJ needs to be included, the design forces would be 150.2 and 136.2kN).

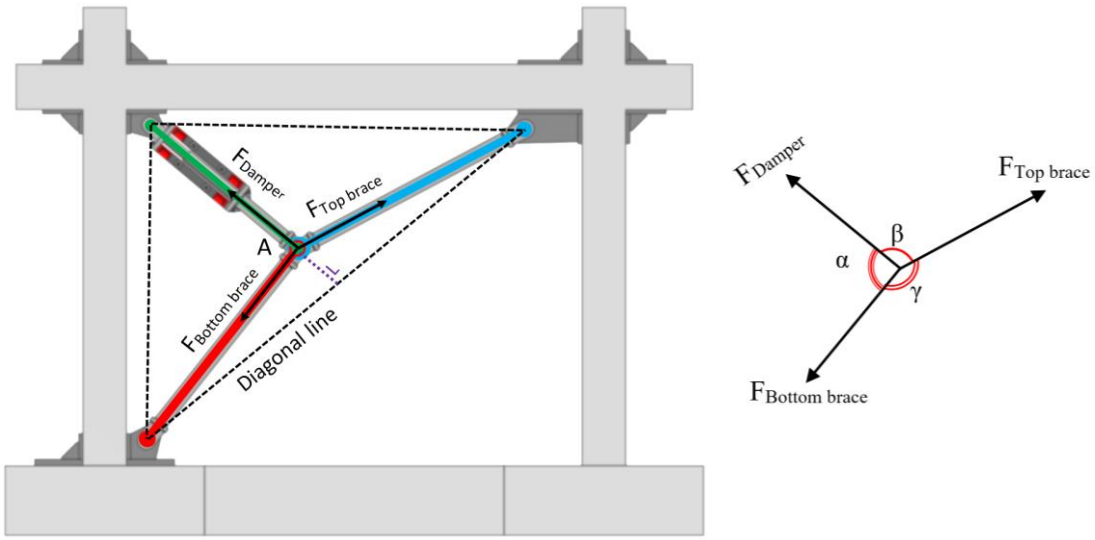

Figure 5-15 Parameter definition of the toggle-bracing forces

5.7.2. Stability Criteria

For a proper energy dissipation in the proposed bracing system, any possible buckling modes that may interrupt the performance of the braces need to be avoided. It has been shown that the compression strength of the RSFJ might drop due to its rotation flexibility[143]. Therefore, an Anti-Buckling Tube (ABT) is added to the damper-brace assembly to present a symmetric hysteresis behaviour, both in tension and compression. The ABT also prevents the global buckling of the damper-brace assembly. Readers can find further details regarding designing of RSFJ brace, reported in Yousefbeik et. al.[179]. It is worth noting that the stability analysis of the RSFJ is based on the assumption that the brace has an effective length factor of K=1 (i.e. the brace is pin-pin connected at both ends).

Contrary to regular braces where the brace is pin-connected to rigid ends, the braces in toggle bracing system (including RSFJ damper-brace) are connected to one rigid end and one restrained end as can be seen in Figure 5-16.

(a)

(b)

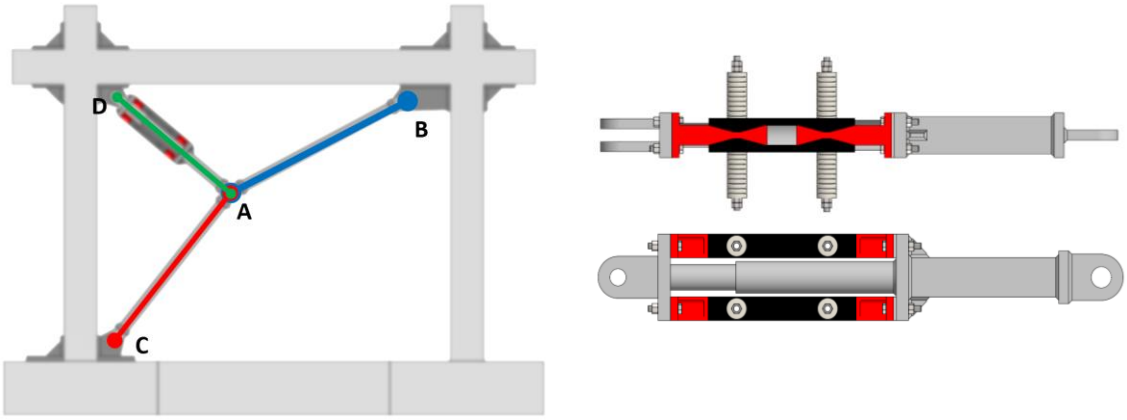

(c) (d)

Figure 5-16 The RC RSFJ-toggle bracing test setup: (a)The overall view of the test-setup, (b) the pinned connections for the braces, (c) constraint naming for the test setup; and (d) the RSFJ damper-brace assembly

From the stability theory handbooks[180], the effective length factor for a general end-restrained compressive member can be calculated based on the solution of the following equation:

$$det\begin{vmatrix} C+\frac{R_{ka}L}{EI} & S & -(C+S) \\ 0 & C+\frac{R_{kB}L}{EI} & -(C+S) \\ -(C+S) & -(C+S) & 2(C+S)-\left(\frac{\pi}{K}\right)^2+\frac{T_{ka}L^3}{EI} \end{vmatrix}=0 \quad (13)$$

Where stability functions C and S are defined as:

$$C=\frac{(\pi/K)\sin(\pi/K)-(\pi/K)^2\cos(\pi/K)}{2-2\cos(\pi/K)-(\pi/K)\sin(\pi/K)} \quad (14)$$

$$S=\frac{(\pi/K)^2-(\pi/K)\sin(\pi/K)}{2-2\cos(\pi/K)-(\pi/K)\sin(\pi/K)} \quad (15)$$

And the Parameters T_k and R_k denote the translational and rotational stiffness of the column end support (Figure 5-17).

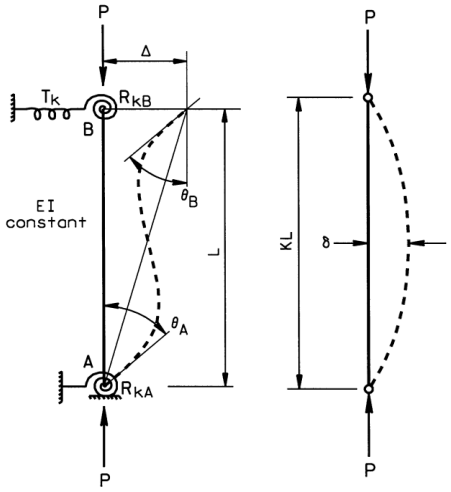

(a) (b)

Buckled shape of column is shown by dashed line	(a)	(b)	(c)	(b)	(e)	(f)
Theoretical K value	0.5	0.7	1.0	1.0	2.0	2.0
Recommended design value when ideal conditions are approximated	0.65	0.80	1.2	1.0	2.10	2.0
End condition code	Rotation fixed and translation fixed Rotation free and translation fixed Rotation fixed and translation free Rotation free and translation free					

(c)

Figure 5-17 Stability of a general column [180]: (a) General end-restrained column with length L, (b) Equivalent pin-pin column with Effective length KL; (c) Theoretical K factor for the isolated columns with idealized end conditions

The largest value of the K that can satisfy the above equation, gives the buckling load of the end-restrained element. An optimized design for the system needs to assume the sections of the braces and end support characteristics, and then calculate the buckling load for each brace and make sure that the ultimate compressive strength of the RSFJ-brace is less than the buckling load capacity of the other two braces. Since the buckling analysis

of the RSFJ-toggle bracing system is out of the scope of this thesis, here, a conservative approach was taken to size the brace sections based on the effective length factor concept.

As can be noted from Figure 5-16, the braces can be assumed to be pin-pin connected for the in-plane behaviour and connected as fixed-free for the out-of-plane behaviour. The presence of the pin at the point A and the five cleats that are connected to this point and designed to remain elastic would make the rotation of point A negligible. However, for the sake of simplicity and having a margin of safety, the influence of node A rotational and translational stiffness was disregarded for the AB and AC braces, while considering a large rotational stiffness for the point B and C (R_{kb} and R_{kc}). Therefore, both braces can be designed based on effective length factor K=2.0 (Figure 5-17c).

For the RSFJ-brace design, it can be stated that the effective length factor lies between an idealized pin-pin connection and the one with slight out-of-plane movement due to elastic out-of-plane movement of point A. Again, an effective length factor of 2 was considered for the RSFJ-brace (thus neglecting the present restraints in the middle point), to provide a margin of safety for the damper-brace assembly. It should be noted that in case of out-of-plane bending of the brace, it is unlikely that the damper experiences any damage and it would only decrease its deflection capacity (thanks to the out-of-plane flexibility of the RSFJ). However, such an out-of-plane bending would impose inelastic deformation on the ABT. It is worth noting that the ABT remained intact after the testing and no out-of-plane movement was witnessed during the test.

A tube section of SHS75x6.0 was assigned to all the three brace sections and a set of male-female telescopic circular profiles (CHS 48.3x5.4 and CHS60.3x5.4) were employed as an anti-buckling tubes for the RSFJ brace (Figure 5-17).

The final check regarding the stability of the toggle-bracing system is the buckling analysis of the damper-brace assembly itself. On this basis, the damper-brace needs to be checked against two criteria that might limit the ultimate compression capacity of the damper-brace (Figure 5-18[179]):

- The stiffness deterioration path (the effects of P-δ and initial imperfection which inclines toward Euler buckling load as the lateral deformation increases). Such failure results in elastic buckling of the member rather than pure axial movement in the damper (similar to elastic buckling of slender member).

- The strength deterioration path which provides the axial strength of the system when a plastic hinge develops in the brace body or the ABT. Such failure usually ends up in a plastic hinge development in the brace (similar to elastic-plastic buckling of stocky members)

Since it was decided to check the stability of damper-brace assembly with an effective factor k=2.0, the overall length of the body (distance from pin to pin) were doubled and the buckling analysis were conducted for overall brace length of 1922mm (2*961mm), with a joint length of 446mm. The results are shown in Figure 5-19. As can be seen, the force demand is below the Euler path and strength path which means the damper-brace would remain completely elastic during the test.

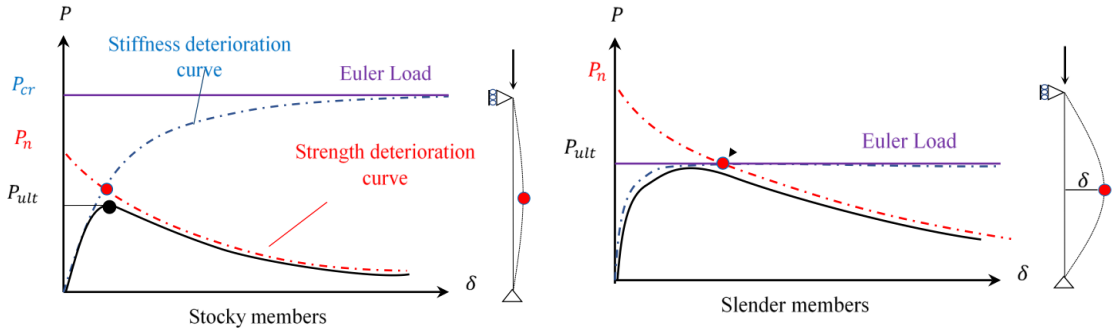

Figure 5-18 Compressive performance of steel braces and their potential failure modes

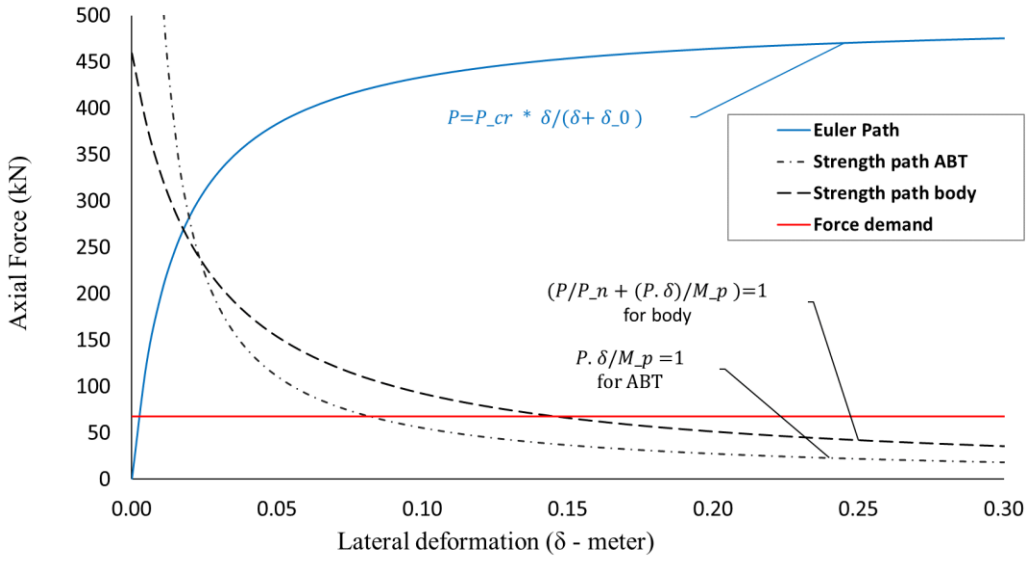

Figure 5-19 Results obtained from the stability analysis of the Damper-brace assembly

5.7.3. Frame restraints and connection considerations

Similar to the previous studies regarding RC frame retrofitting with braces[79], two main methods for connecting the RSFJ-toggle bracing system to the RC frame can be considered, namely the *direct connection* and *indirect connection*. Regarding the indirect connection, the RSFJ-Toggle bracing retrofit can be assembled as a separate steel braced frame to be continuously attached to the side face of the RC-frame via post-installed anchors. Figure 1-7-b in chapter 1 serves as an example of connecting a toggle-bracing steel frame with RF damper to an RC frame structure using the indirect method. While such a configuration might seem relatively more expensive, it may appear as less challenging for engineers since it can be separately designed and then connected to the frame and collect the RC frame force in a more distributed manner and enable using larger brace sections and dampers. On this basis, sufficient number of anchorages are required to ensure that the ultimate capacity of the system is not limited by anchor failure modes (Figure 5-20). To check the capacity of post-installed anchorages, it can be referred to the employed reinforced concrete codes (Chapter 17 of NSZ3101:2006 or ACI-318-19:2019).

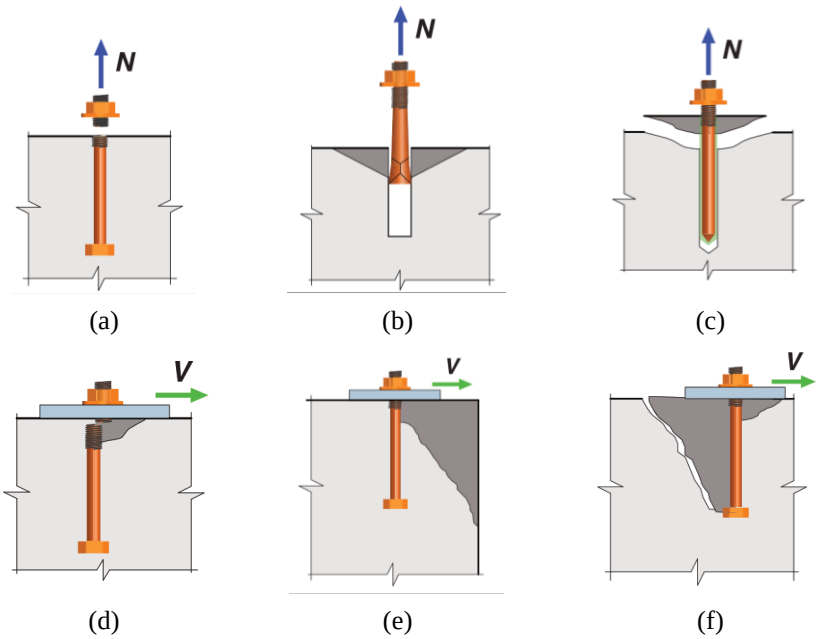

Figure 5-20 Common failure modes of the post-installed anchors (ACI-318-19): (a) tensile rupture, (b) concrete break-out in tension, (c) bond failure, (d) anchor shear rupture, (e) concrete breakout in shear, and (f) anchor pry-out in shear

Other options would be to install the toggle-bracing system directly to the RC-frame, where the RC frame is connected to the braces at discrete locations (beam-column joints for this case). The efficiency of such system depends on the ability of the connection

between RC frame and bracing member to successfully transfer the load. Owing to the fact that for the current test setup, lateral supports may be required to maintain the frame for the cyclic pushover testing (in order to keep the testing setup simple and symmetric), the direct method has been implemented for the attachment of brace to the RC frame. On this basis, three distinct connection points were considered for the toggle-bracing system (Damper-brace connection, top brace connection and bottom brace connection). The gusset plate connection details will be explained in Section 5.7.4.

As for the lateral restraints of the test setup, four adjustable timber blocks connected to a small I-section were employed to maintain the frame against out-of-plane movement (Figure 5-21-b). The surface between timber blocks and RC beam were lubricated by grease to minimize the friction force contribution from the lateral restraints to the frame test results. Also, two shear keys that were available in the AUT lab were employed in front and back of the frame to prevent the frame sliding during the cyclic loading (Figure 5-21-c). This would make sure that the draw-wire sensors would only read the frame drift, as the lateral displacement.

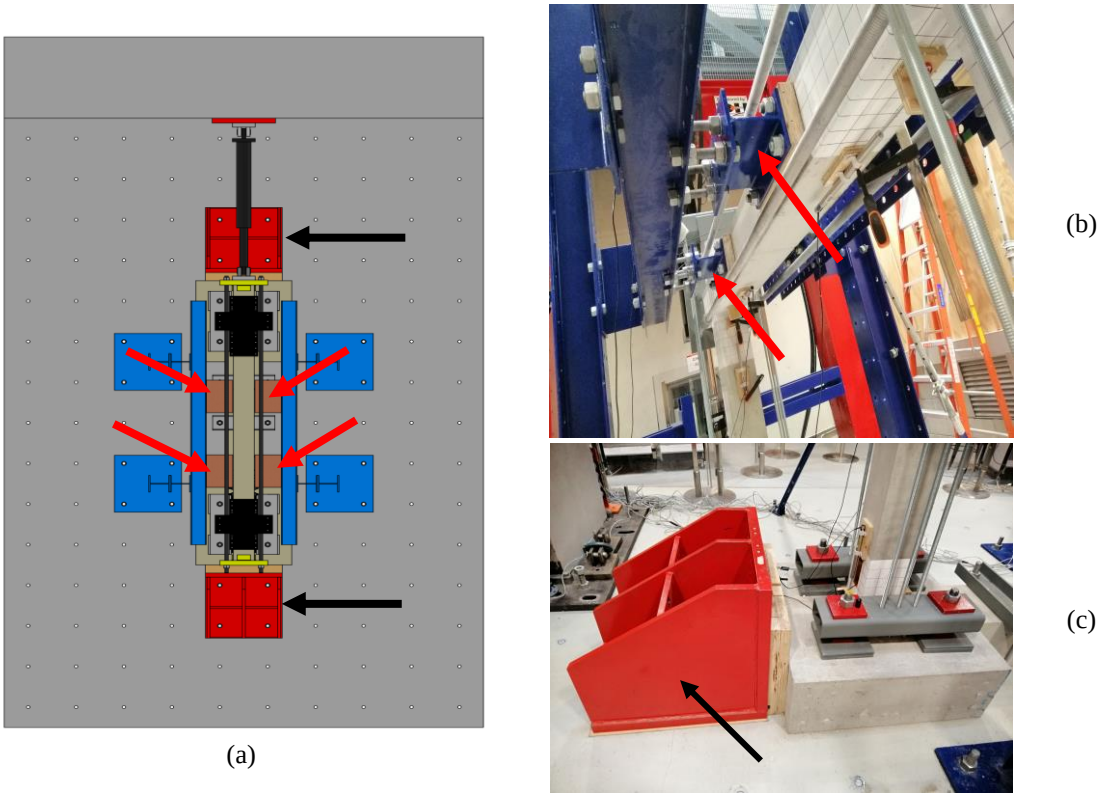

(a) (b) (c)

Figure 5-21 RC Frame restraints: (a) top view, (b) lateral support provided for the RC frame test setup (shown with red arrow); and (c) shear key that prevents frame sliding (shown with black arrow)

For the current test setup, three connections needed to be designed: the top connection (connected the top brace to the RC frame), the damper connection (connected the damper-

brace to the RC frame) and the bottom connection (connected the bottom brace to the foundation). While it was possible to connect the top and damper-brace connection directly to the RC frame via stud bars (to embrace beam-column joints), such an option was not available for the bottom brace connected to the foundation level (Figure 5-22-a,b). Although epoxy anchors could be employed for bottom brace gusset plate connection to the RC frame, the initial calculations for a group of 2x2 anchors (using Hilti Profis Engineering which is in compliance with NZS 3101) resulted in high demand with possible failure of group concrete cone breakout in tension (anchor demand to capacity equal to 165%) (Figure 5-22-c). Since the failure of anchors might jeopardize the overall results of the test, it was decided to increase the length of bottom gusset plate and connect it to the foundation using the High Strength M36 rods available in the lab (Figure 5-22-d). It is worth noting that four rods were employed per each foundation pad and prestressed up to 150kN force, making sure that the RC frame and the gusset plate remain at their position during the test.

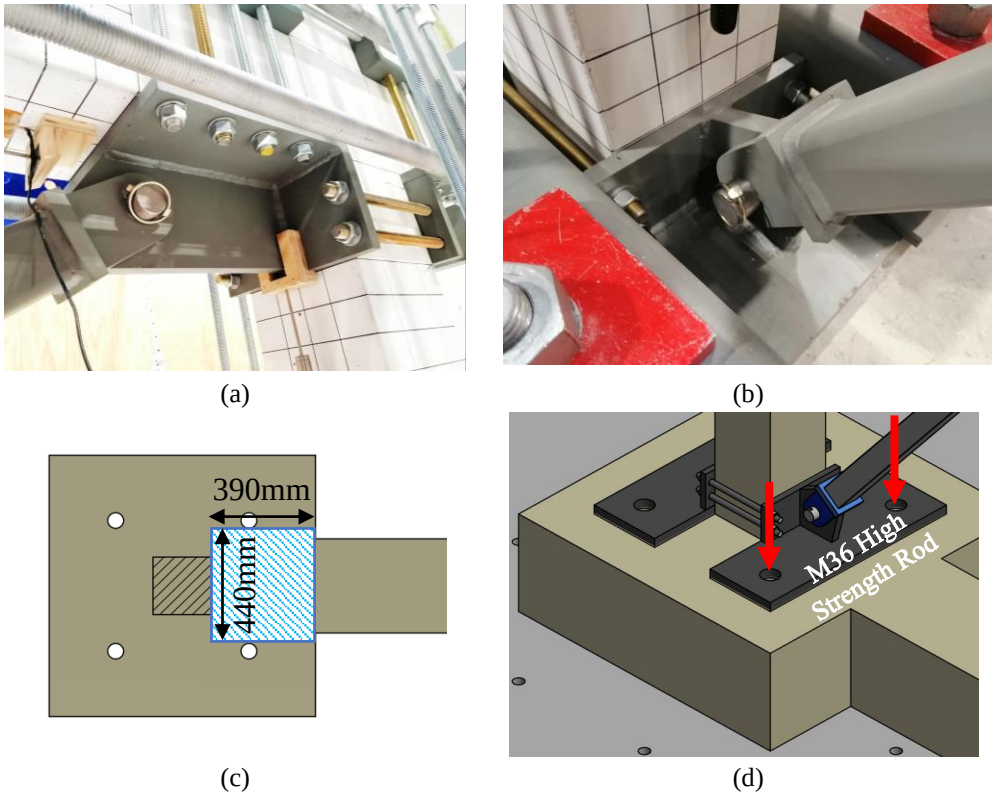

Figure 5-22 Concrete restraints detailing: (a) top brace to frame connection using stud bars, (b) bottom brace to frame using floor high strength bars and stud bars, (c) maximum avaliable space for anchor design, and (d) prestressed rods for connecting the frame to the floor

5.7.4. Gusset plate design

The next step for the test setup design was a suitable gusset plate connection to fully transfer the braces axial forces to the RC frame. The pinned connection for the braces ensures deformation compatibility of the braces as well as minimising the in-plane induced moment to the gusset plates. Similar methods for the design and sizing of the gusset plate available in the traditional steel structures can be utilized here, with one extra step for welding the gusset plate to the two corner plates which are fixed to the face of RC members at corners by stud bars. Such corner plates embrace the RC beam column joint for distributing the brace force. As for the gusset plate in tension, net section fracture, gross section yielding failure, block shear failure (combined tension and shear) and block shear failure (pure shear tear-out) were checked against the assumed tensile force in the brace (Figure 5-23-a to d).

As for the designing of the gusset plates for compression loads, it should be noted that unlike ordinary braced frames (where braces are expected to buckle for energy dissipation and gusset plates are designed for allowing this out-of-plane rotation), the RSFJ-Toggle bracing system dissipates the energy through damper component sliding. Therefore, the gusset plate should keep the braces in-plane during seismic loading. A number of methods have been introduced and explained by researchers to minimize the gusset plate out-of-plane buckling, such as using stiffeners on the gusset plate edges or using effective length factor of 2.0 for designing the gusset plates [181]. Here, a rather simplified and conservative approach was employed for the compression loading design, where a compression member with the length demonstrated in Figure 5-23-e was considered for the gusset plate buckling. Such compression member is fixed-free and has a cross section equal to gusset plate thickness and pin diameter. Such a conservative assumption will ensure the elastic performance of the gusset plate against any possible out-of-plane bending with minimal displacement.

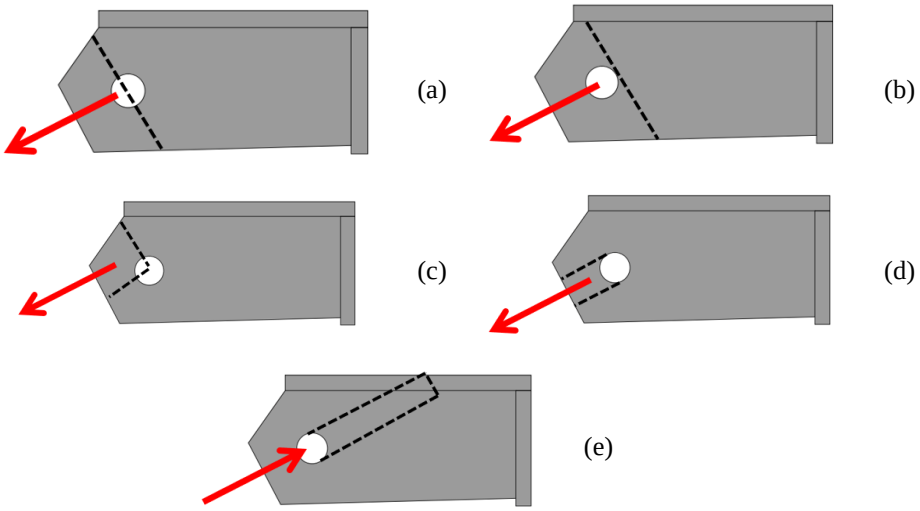

Figure 5-23 Gusset plate tension and compression failure design criteria: (a) net section fracture, (b) gross section yielding failure, (c) block shear combined tension failure and shear) (d)pureshear tear out (e) compression member considered for gusset plate design

As for the connecting plates, they can be attached to the RC beam-column joint by either anchor bolts embedded within the RC member or using stud-bars which tie the connecting plates on both sides of the beams and columns. Obviously, the second method may be more suited for retrofitting plans as it would require less modification on the RC frame and thus adopted here as well. Due to the presence of bolt hole gaps in the connecting plates, the shear forces in the stud-bars are negligible and they are working in pure tension when tensile forces are applied in the braces. By neglecting the friction between the connecting plates and the concrete surface, it can be stated that the entire horizontal and vertical components of the brace force are delivered to the associated vertical and horizontal stud-bars, respectively. As highlighted by Maheri and Yazdani[182], a linear varying normal component better represents the normal components forces in the connecting plate. The finite element (F.E.) modelling of the gusset plates verifies such distribution as well (Figure 5-24). To develop the F.E. model of the gusset plates, the obtained brace forces from the damper ultimate force (equation 12) were employed to apply the brace tensile force on the pin-hole surface of the gusset plate. It is worth noting that the ABAQUS software package[113] were used to perform the F.E. analyses and check the stress distribution. A nonlinear elasto-plastic material with isotropic hardening was designated to the gussets plate with yielding stress and ultimate stress of 350MPa and 480MPa, respectively. The finite element analyses indicated that the stress value was within the material elastic range (less than 350MPa). The model also highlighted that the stress values around the inner bolt holes were larger than the outer bolt holes. This was

the reason to employ two different rod sizes for the damper gusset plate (M12 rod for outer stud-bar and M18 rod for inner stud-bar).

Another concern regarding the gusset plate design was the risk of having undesired deformation of the gusset which is up-scaled in Figure 5-24 for better clarity. On this basis, the connecting plates in the gusset plates might get bent and deformed during the tension force and jeopardize the system performance. Obviously, such an issue can only emerge during the brace tensile force and it can be tackled by either increasing the plate thickness or welding some edge stiffeners to the gusset plate. Based on the finite element analysis of all three gusset plates, such deformation was less than 0.5mm for all the gusset plates, thus the design seemed suitable for the test.

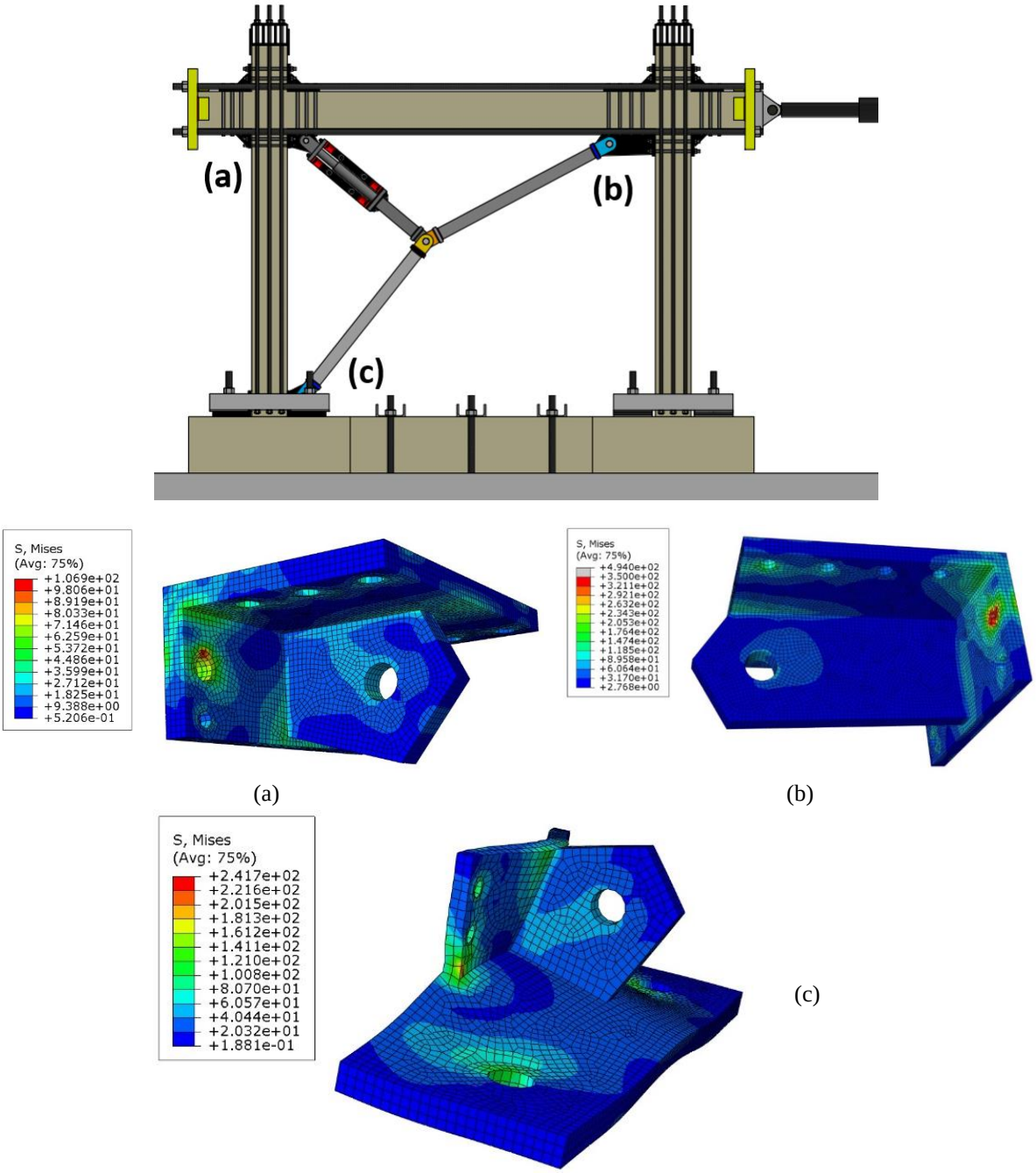

Figure 5-24 Finite Element analysis of gusset plate connections of the (a) damper brace, (b) top brace, and (c) bottom brace

5.8. Experimental testing of the RC frames

In this section, the experimental testing results and the outcomes for the benchmark bare frame and the retrofitted frame are provided. The first frame, served as a benchmark frame, was subjected to a progressive quasi-static cyclic pushover up to its failure (4.0% drift) to gain some insight about the performance of the frame without any retrofitting. Then, the second frame was retrofitted with the damper-brace system and went through

the similar lateral loading up to 1.5% drift. It was decided to tune the damper with higher prestressing force and more disk springs, and repeat the test on the frame which already pushed up to 1.5% drift. Such a testing scenario could present the benefits of having an adjustable damper that can provide some level of flexibility for the designer. It can also demonstrate the performance of an already-damaged frame retrofitted with the RSFJ damper. It should be noted that all the frame tests were applied in quasi-static cyclic pushover manner. While the performance of the RSFJ dampers is expected to remain the same for dynamic loading, the dynamic behaviour of the RC frame can differ from the static cycle. To eliminate such an effect in our study, it was decided to investigate the behaviour of the frames with quasi-static loading regime.

5.8.1. Instrumentation and Cyclic testing protocol

Figure 5-25 presents the instrumentation layout used for the RC frame. Two linear variable differential transformers (LVDTs) were placed on each end of the beams and columns to catch any displacement or sudden cracks during testing. Two LVDTs were placed on the foundation to measure any potential uplift, while two calibrated draw-wires were employed to read the frame and damper displacements. A total vertical load of 440kN was applied to the frame via six prestressed rods for each column (220kN for each column, equivalent to around 15% axial load ratio), whereas the lateral loading was exerted to the frame using a 250kN MTS actuator with ±125mm stroke capacity. The actuator was controlled in displacement mode with the loading rate of 0.5mm/s.

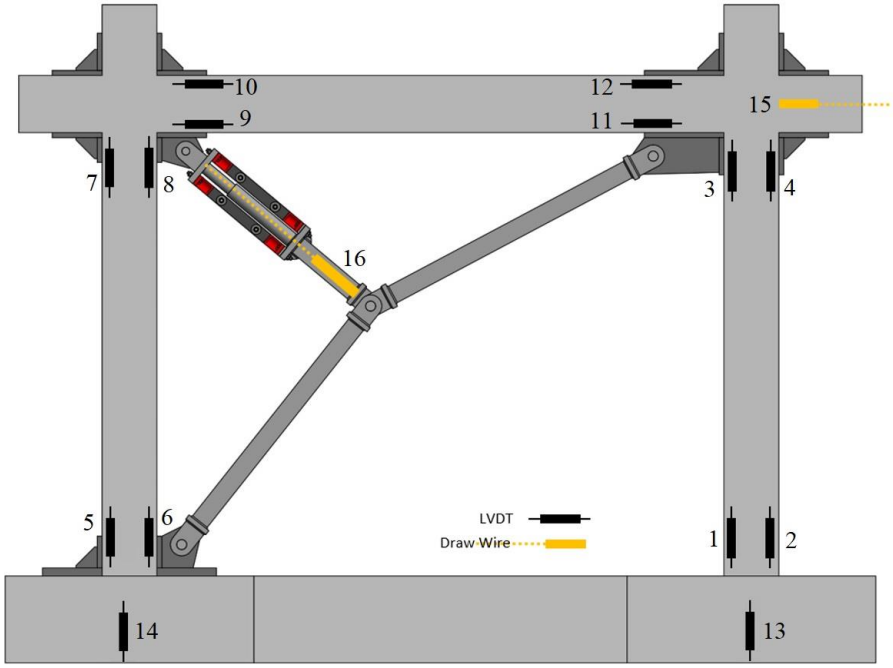

Figure 5-25 Instrumentation layout of the test setup

Figure 5-26 shows the loading protocol for the benchmark bare frame up to 2.5% drift (Δ=52.5mm). Each drift level was repeated for three cycles and at the third cycle, frame was held at the maximums of the pulling direction (towards right), so that visual damage occurred on the concrete surface to be easier to spot. Moreover, the frame was painted with thin layer of white colour at the potential cracking zones for better catching the damages during testing (Figure 5-27).

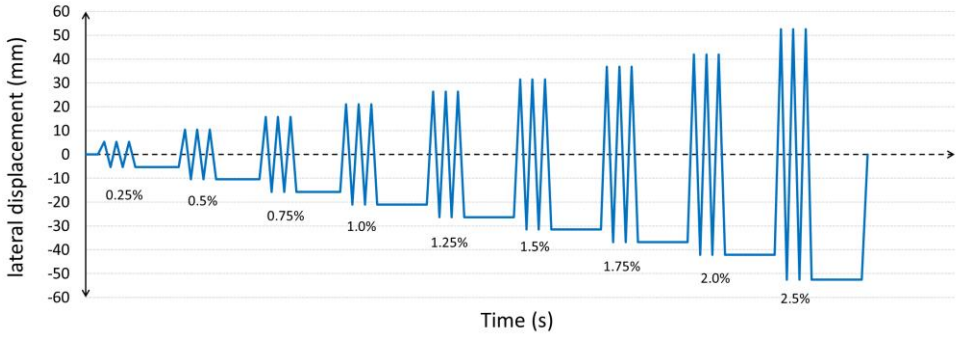

Figure 5-26 Lateral loading history of the benchmark bare frame

Figure 5-27 Sample photos of physical damages (cracks) on the benchmark frame

Four distinct crack width (C_w) limits were assumed for the observing of the evolution of crack pattern in the RC frame[183] with each limit associated with a colour for marking on the frame:

- $C_w < 0.2$mm: Representing narrow cracks on the surface (Green)
- $0.2\text{mm} \leq C_w < 1.0$mm: Visible but narrow cracks (Blue)
- $1.0\text{mm} \leq C_w < 2.0$mm: local crush of covered concrete (Red)
- $C_w \geq 2.0$mm: Remarkable crush of concrete with cover spalled off (Black)

Figure 5-28 presents the observed cracks in the RC frame during 0.5%, 1.0%, 1.5% and 2.0% lateral drifts. As can be seen, in 0.5% drift (Figure 5-28-a), only narrow flexural cracks were witnessed at the top and bottom ends of the columns. As for the 1.0% drift (Figure 5-28-b), the number and width of the cracks were increased. It should be noted that the presence of cracks in the columns were more evident than in the beam. As for the 1.5% drift, the first crack with Cw≥1.0mm was witnessed at the top and bottom of the RC frame column, with some diagonal visible narrow cracks in the beam column joint area. Regarding the observed damage in 2.0% drift, the concrete crush with crack width larger than 2.0mm was witnessed at both columns, along with large flexural cracks ($C_w \geq 2.0$mm) on the beam as well.

In general, the failure mode of the frame was the formation of flexural cracks at the end of columns. Based on the observed cracks patterns, it seemed reasonable to assume that the retrofitted frame would start to accumulate noticeable damage if the drift reaches to 1.5%. Albeit, no local crush of concrete ($C_w \geq 1.0$mm) was observed on the retrofitted RC frame (It needs to be stated that due to presence of stud bars and connection plates at the corners of the retrofitted RC frame, it was difficult to witness and mark the cracks on the

retrofitted frame). This may be due to the fact that the connection could have a confinement effect on the beam-column joints and better distribute the crack over the length of the structural member, while in the bare frame, the cracks were mostly concentrated at the beam and columns ends.

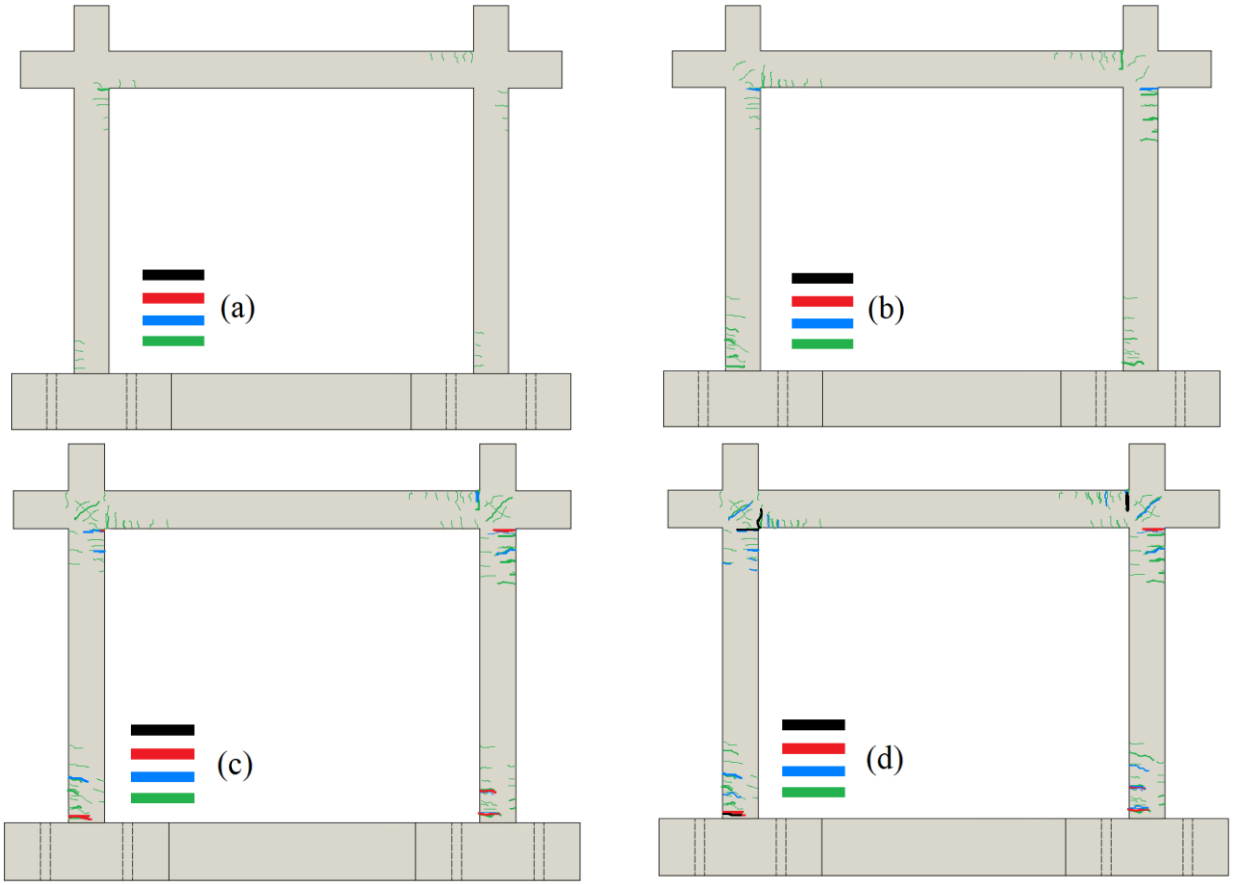

Figure 5-28 Crack patterns of the bare frame in different drift levels: (a) 0.5%, (b) 1.0%, (c) 1.5%, and (d) 2.0%

5.8.2. Discussion of the gravity loading accuracy

By taking a look at the literature, different methods have been employed to impose the dead load on the RC structural frame, such as using heavy steel blocks to represent an actual dead load, using actuators and hydraulic jacks to apply constant force on the frame, or using pre-stressed cables or rods to simulate the gravity loading. Compared to the first two method (using steel blocks or actuators), the third method seemed more convenient to implement and required less equipment and budget, and thus was adopted here for gravity loading. An especial rod holding assembly was designed to be placed on top of the columns and hold the rods. Here, the column axial load was imposed using a total number of 12*M18 high strength rods (6 rods for each column) prestressed up to

36~37kN. The yielding capacity of the rods were more than 150kN, so they remained elastic during the cyclic test.

However, it is possible that during large lateral drifts of the RC frame, the axial capacity of the rods became engaged in the lateral load resisting of the structure and contributed to the recorded base shear of the frame. Such a mechanism is denoted as the "rope effect" in structural engineering, which falsely increases the base shear of the frame. Such an effect is illustrated in Figure 5-29. Obviously, this is an error in the test results which needs to be investigated. To do so, it was decided to attach a donut load cell to each of the three prestressed rods and capture the load during different drift values (0.0%, 0.5%, 1.0%, 2.0%, 2.5% and 3.0% for this case). Thanks to symmetry of the system, it was only required to do the procedure for one set of three rods. The overall prestressing force was then calculated by summing up the rods forces and then the horizonal factor was computed for each drift value. The horizontal component was doubled to show the total contribution of the rods for both columns in the recorded base shear of the frame. For test safety reasons, interpolation values (polynomial interpolation, order=2) were utilized for 4.0% drift, rather than performing the procedure.

Table 5-3 shows the changes in horizontal and vertical forces of prestressed rod during different drift levels. As can be seen from the table, the applied gravity loading remains unchanged for the small drift and almost no contribution to the base shear is expected from the rods. As an example, the gravity loading increased by a 2.4% percent for 1.0% drift and only 4.4kN were added to the base shear. However, higher frame drifts would results in higher horizontal load contribution of the prestressed rods. While for the 2.0% frame drift, only 10kN increase was recorded, based on interpolation data, the rope effect could increase the lateral load capacity up to 24.5kN for 4.0% drift and increase the gravity loading of the system from 217.2kN to 306.2kN.

Figure 5-30 compares the new backbone curve for the bare frame and the retrofitted one. It should be stated that the new backbone curve was obtained by subtracting the rope effect contribution from the previous one. On this basis, the overall lateral force contribution from the rods is evaluated as around 7.0kN at 1.5% drift.

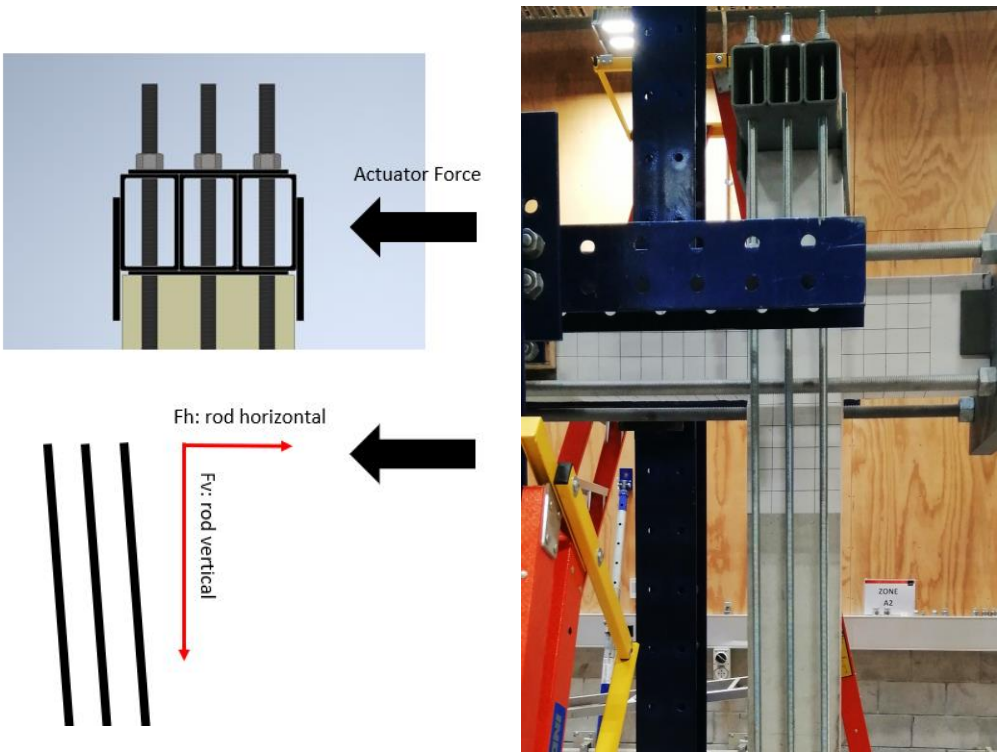

Figure 5-29 The rope effect contribution on the recorded base shear of the frame

Table 5-3 Changes in the rods prestressing forces due to drift

Parameter	Unit	Drift values						
		0.0	0.5	1.0	2.0	2.5	3.0	4.0
$F_{left\ rod}$	kN	36.1	34.8	34.0	33.4	33.8	34.8	-
$F_{middle\ rod}$ (kN)	kN	36.1	36.2	36.8	39.6	41.2	44.0	-
$F_{right\ rod}$ (kN)	kN	36.4	37.7	40.4	46.5	50.6	55.0	-
$Fv = F_{rod,total}$ (kN)	kN	217.2	217.3	222.4	239.0	251.2	267.5	306.7
changes in $F_{rod,total}$ (%)	%	0.0	0.1	2.4	10.0	15.7	23.2	41.2
$F_{h,total} = 2*F_h$	kN	0.0	2.2	4.4	9.6	12.6	16.1	24.5

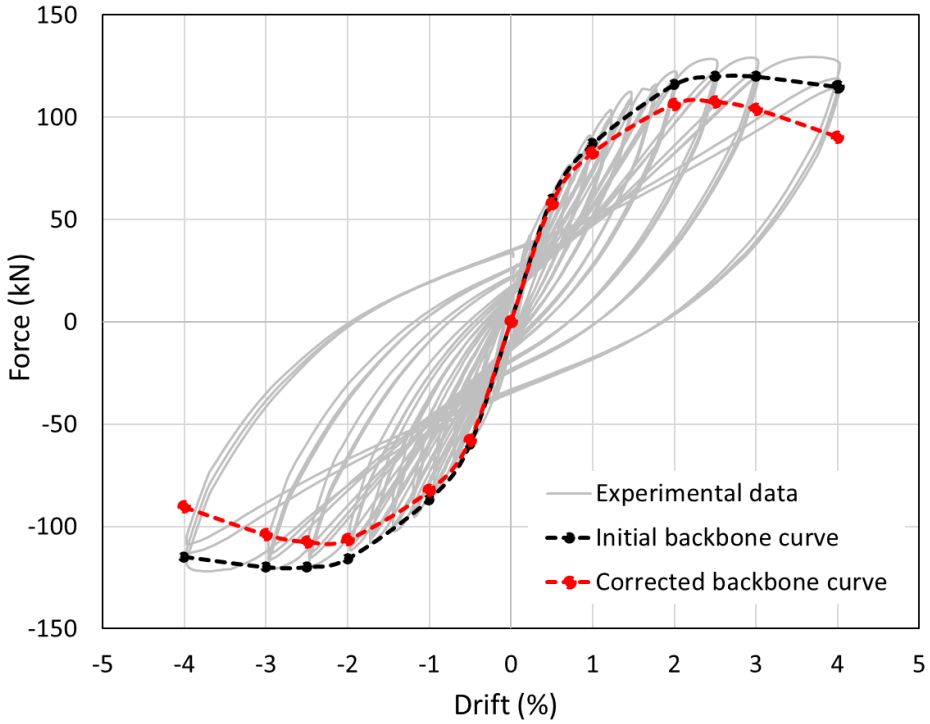

Figure 5-30 Comparison of the initial and corrected backbone curve for the benchmark bare RC frame

5.8.3. Results and discussion

In this section the obtained results from the RC frames are provided. Three distinct testing were conducted on the frames which is listed below:

- Benchmark bare frame (the first RC frame): While the bare frame was tested up to 4.0% drift, only the result up to 1.5% drift is provided, for better comparison with the retrofitted cases.
- Retrofitted frame (the second RC frame-intact), Test 1: The second frame was equipped with the toggle-bracing assembly and the dampers were tuned as per first tuning scenario in Table 5-2 (F_{slip}=12.2kN, Δ_{max}=46.1mm).
- Retrofitted frame, Test 2: Since the second frame that was already pushed up to 1.5% drift, remained in a good condition with crack width smaller than 1mm, it was decided to increase the prestressing force of the damper and the number of disk springs as per second tuning scenario in Table 5-2 (F_{slip}=18.3kN, Δ_{max}=40.0mm) and redo the cyclic testing on the second frame.

Figure 5-31 presents the lateral load response versus the lateral deformation of the bare frame up to 1.5% drift. The hysteresis behaviour reveals the gradual decrease of lateral

stiffness during the elastic range of loading, due to cracking of the concrete, however the behaviour becomes stable in the third cycle. Moreover, the numerical pushover simulation using SAP2000 is presented as well. The SAP2000 model materials were calibrated with the concrete cylinder tests and rebar tensile test results, to reduce the uncertainty between numerical and experimental results. The ultimate strength for the pull and push directions were recorded as 112kN and 100kN respectively, while the SAP2000 gives approximately the same results (96.8kN). The small difference between the numerical and the experimental results could be due to the contribution of prestressed rods which explained in previous section, along with other sources such as available friction between lateral restraints and the RC frame though minor.

Regarding the retrofitted RC frame, Test 1 (intact frame, with damper F_{slip}=12.2kN), the obtained experimental results are depicted in Figure 5-32. The experimental results highlight the improved performance of the frame, in terms of energy dissipation, increased stiffness and self-centering behaviour. The pinching behaviour of the bare frame was replaced with semi-flag shape behaviour for the retrofitted frame. The ultimate strength of the retrofitted system is recorded as 172kN and 162kN. While some levels of stiffness and strength degradation is witnessed in the retrofitted frame, such drops are associated with the concrete cracking and accumulated damage in the RC frame. Moreover, the presence of connection plates embracing the beam-column joint have helped towards distribution of concrete crack over larger area of beam and columns. Based on the performance of the toggle-bracing, the braces performed as expected without any instability issues and out-of-plane movement of the restrained node. It is important to note that while for this current test, the retrofitted frame did not show any residual drift, it is possible for the frame to present some residual displacements in higher drift demand. This indeed depends on the target level of drift for the frame, as well as the restoring force provided by the joints in the system. Such parameters need to be carefully designed by the engineers for their target drift level.

The damper displacement during the cyclic loading is summarized in Table 5-4. Based on the test results, the amplification factor in the pull and push directions of the system is evaluated as 1.16 and 0.98, respectively. The damper displacement from numerical results also provides the similar outputs. For instance, the damper displacement at 1.5% drift was recorded as 35.7mm and 29.5mm from SAP2000 which are quite close to the experimental results (36.6mm and 30.7mm for the pull and push directions). The results

shown in the table also highlights the capability of the proposed system to be activated within a small drift of the RC frame. As an illustration, for the 0.25% drift of the RC frame (5mm frame lateral deformation), the damper has already mobilized more than 2mm.

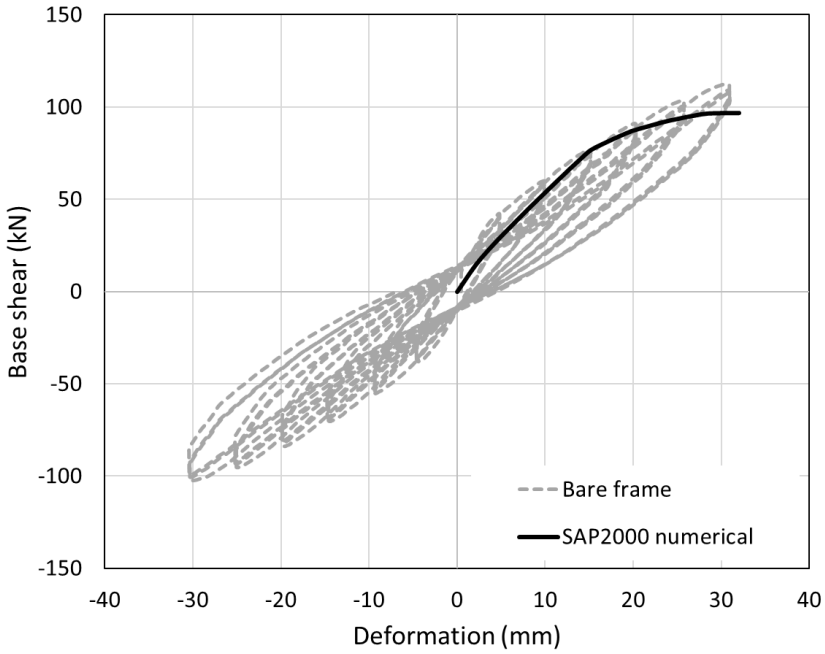

Figure 5-31 Hysteretic lateral load-lateral deformation of the bare frame up to 1.5% drift

The numerical outcomes for a cyclic pushover with 1.0% and 1.5% drifts are compared with the experimental results in Figure 5-33. While the numerical results are generally in good agreement with the experimental data, some level of difference is witnessed, especially in residual displacement results, which is slightly higher in the numerical outcomes for the 1.5% drift. This is due to the difference in true nonlinear behaviour of the frame, against the simplified mathematical model that may not consider all the aspects of RC frame. Such difference is not witnessed for the 1.0% drift case given the system is mainly behaving elastic in this drift ratio.

Table 5-4 Recorded damper displacement during cyclic testing of the retrofitted frame

Parameters	Unit	Frame lateral drift values (%)					
		0.25	0.50	0.75	1.00	1.25	1.50
Frame displacement	mm	±5.3	±10.5	±15.8	±21.0	±26.2	±31.5
damper displacement (pull)	mm	+3.2	+9.3	+16.3	+22.1	+29.1	+36.6
damper displacement (push)	mm	-2.4	-7.5	-13.0	-18.3	-23.6	-30.7

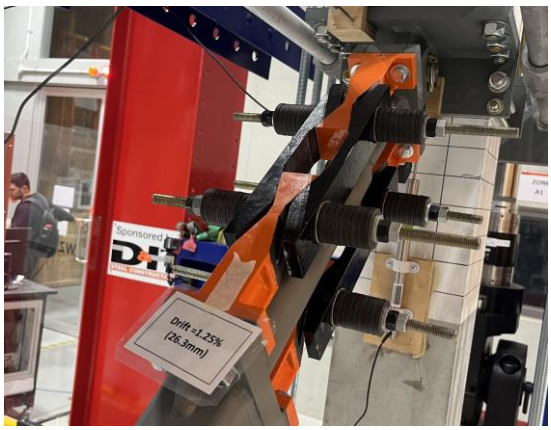

(a)

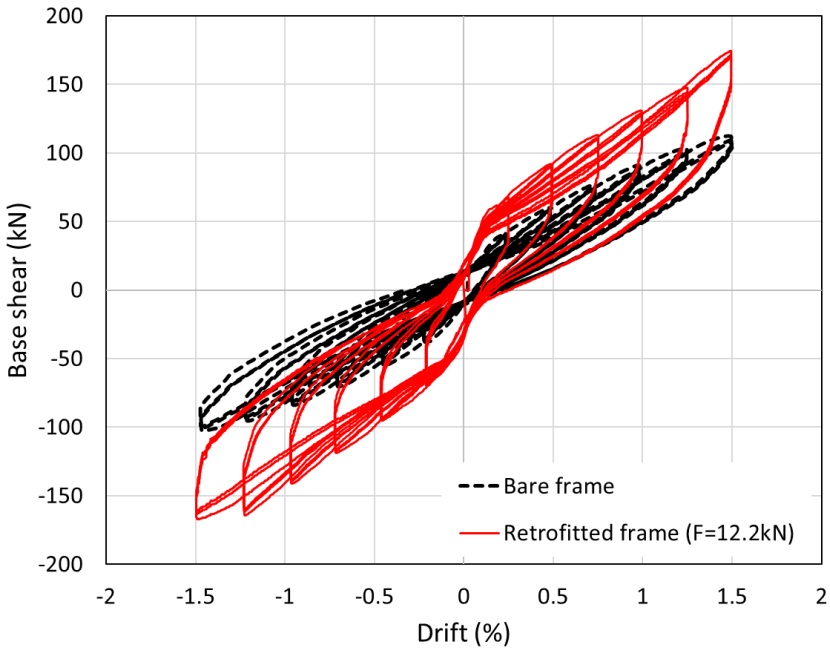

(b)

Figure 5-32 Retrofitted frame performance results: (a) Sample photos of RSFJ damper in the retrofitted frame (b) the comparison of the cyclic behaviour of retrofitted frame (Fslip=12.2 kN) against the benchmark bare frame

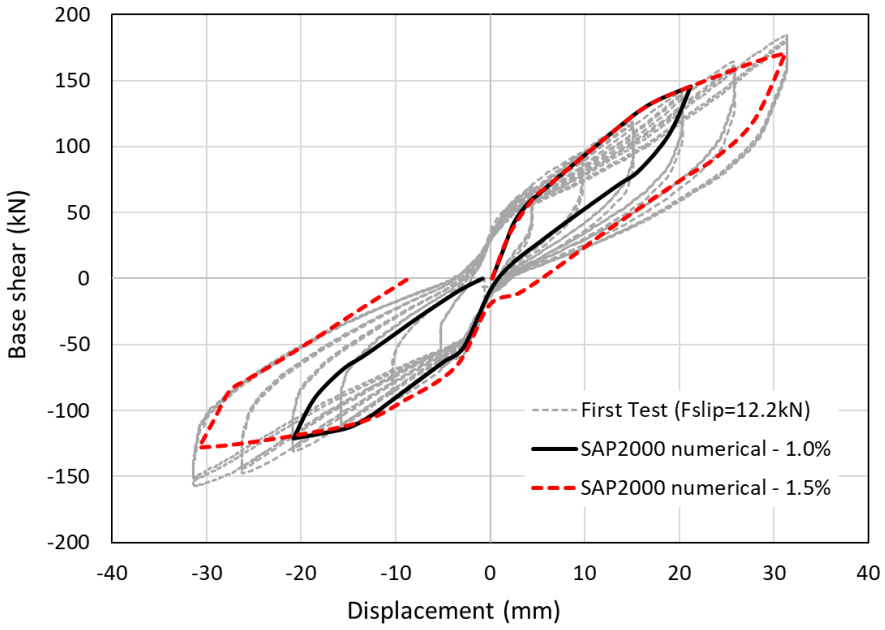

Figure 5-33 Numerical model results of the retrofitted frame (Fslip=12.2 kN)

After finishing the cyclic test on the retrofitted frame, the RSFJ dampers were tuned with higher prestressing force and more disk springs. The new force-deformation of the damper is depicted in Figure 5-14-d in section 5.6.2. The second retrofit test could represent the inclusion of retrofit for the frames that already experienced some level of earthquake demands and damage (up to 1.5% drift in this case). It should be pinpointed though, that the damage level is not critical, otherwise it might be necessary to repair the frame, then attach the retrofitting braces. The experimental data for the second retrofit testing is compared with the first test in Figure 5-34. Unlike the first test where the RC frame was intact, for the second test, the RC frame has already experienced some concrete cracking when pushed up to 1.5% drift. Therefore, no stiffness degradation was seen in the hysteresis behaviour of the second test. This also verifies the resilient and repeatable behaviour of the retrofit solution over the three cycles of testing. The ultimate strength of the frame for the second test was recorded as 164kN and 192kN for the push and pull directions, respectively. The damper displacements during the second retrofit test were the same as the first test.

The absolute energy dissipation (i.e., the area enclosed by the hysteresis curve of the RC frame) for the bare frame and the retrofitted cases are provided in Figure 5-35. As can be seen, energy dissipation capability for the second retrofit is higher than the first retrofit, considering the fact that the energy dissipation for the second test does not contain any concrete crushing or frame damage. Since the hysteretic damping ratio of the RSFJ dampers were increased for the new tuning scenario, more energy dissipation was granted

to the retrofitted frame. By accumulating the dissipated energy for all the cycles, the first and second retrofitted cases dissipated 245% and 285% of the benchmark bare frame (16% more energy dissipation for the second retrofit test, as compared to the first retrofit test). While the prestressing increment would provide some level of flexibility for the engineers to modify their design, it would increase the number of required disk springs for the joints.

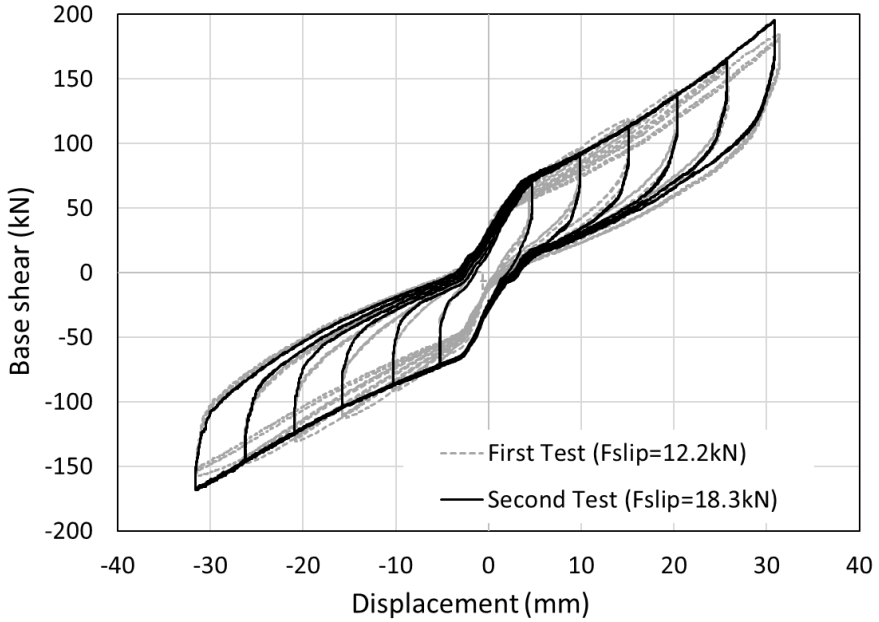

Figure 5-34 Experimental results for the second retrofit test vs. the first retrofit test

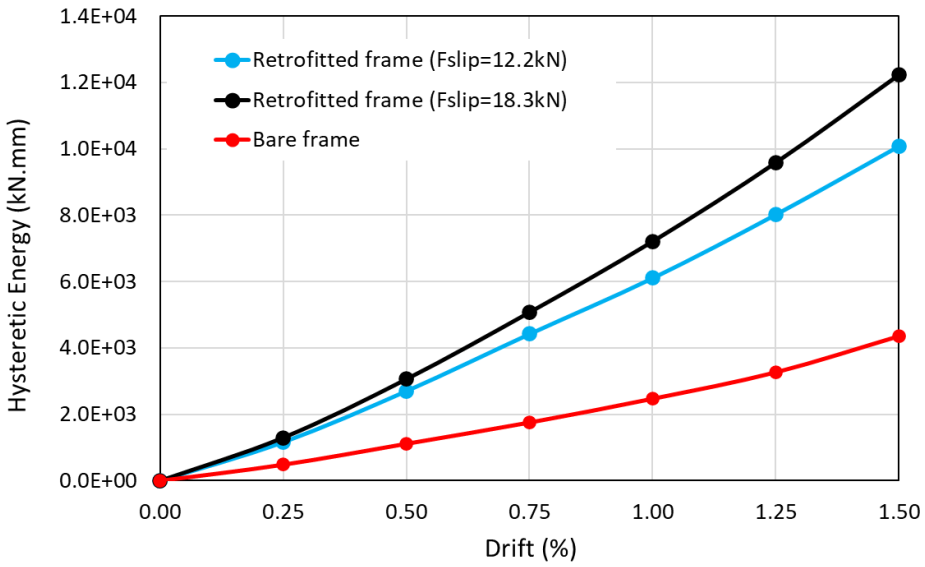

Figure 5-35 Energy dissipation of the reference frame and retrofitted frames for each drift ratio

5.9. Summary and conclusion

This chapter investigated the efficiency of the RSFJ-toggle bracing system as a global retrofitting method in seismic upgrading of deficient RC frame structures. Such a system can be added to the earthquake-prone RC frame with minimal invasiveness and little disturbance to the functioning of the building and improve strength, stiffness and damping capabilities as well as significantly minimise the residual drifts. Two small-scale identical RC frames were constructed and subjected to a quasi-static cyclic loading and the results of the benchmark frame and the retrofitted frame were compared. The design of the retrofitting components, including the RSFJ dampers, the anti-buckling tube (ABT), the gusset plate connections and the braces were explained and some recommendations were provided for the design of such elements. The successful experimental validation of the RSFJ-toggle bracing retrofit is presented in this chapter. Moreover, the experimental results were compared with the numerical model as well. The following conclusions and recommendations are drawn:

- The overall performance of the retrofitted frame improved in terms of stiffness, strength and energy dissipation features.
- The proposed retrofitting system is capable of being activated in small drift values and preserves the RC frame.
- The retrofitted braces performed as predicted without any instability issues and out-of-plane buckling.
- The connection plates were able to preserve the RC frame from concentrated damage at the beam and column ends and provide some level of confinement for the beam-column joints. This was witnessed by lesser number of concrete cracks on the retrofitted RC frame.
- The results and findings from this chapter could be used for the design of the toggle-brace retrofitting of RC frames with other types of dampers such as traditional friction dampers. Although it is expected that they would present some levels of residual displacement after the seismic events.
- Same as the previous chapter, it is worth noting that the current retrofit system can increase the overall base shear of the frame which impose higher demands on the foundation. The foundation capacity needs to be considered for a proper retrofit design.

Chapter 6: Conclusions and Future Studies

6.1. Summary and concluding remarks

Recent earthquakes have highlighted the urgent need for implementing low damage design philosophy for designing new buildings to ensure the structural safety and minimum earthquake destruction after moderate to severe seismic events. Moreover, it also brought the attention of many researchers towards local and global retrofitting of vulnerable structures with more efficient and resilient solutions that are easy to implement with little disturbance on the functioning of the building. On this basis, seismic dampers have gained the attention of engineers for both new and retrofit design purposes.

In this thesis, initially a new self-centering damage free damper was introduced for the first time, that can bring self-centering feature and energy dissipation in one structural component. The introduced damper can perform similar to RSFJ and has a tuneable flag-shape behaviour. The performance of the damper was evaluated by investigating the performance of the friction plates using analytical formulations, as well as numerical modelling. Then the performance of the damper assembly which comprises a number of friction plates connected by cap and middle plates were investigated. The force-deformation behaviour for the damper provided and verified by finite element analysis. A prototype damper was manufactured to validate the formulations and test the damper behaviour. A series of tests were also performed on the disk springs to better understand the performance of their stack. A sensitivity analysis was performed to investigate different parameters affecting the performance of this new damper.

As the major focus of the study, the possibility of using self-centering dampers for seismic retrofit of RC frame was explored. While the design of the new buildings using self-centering joints seems more convenient for engineers, the retrofit design for the current deficient RC buildings with seismic dampers may be more challenging, as it requires to include the performance of both deficient frame as well as the damper, for a proper design of these retrofit system. With the aim of developing practical retrofit solutions that are quick to implement with minimal level of invasiveness, this study explored the possibility of using RSFJ for such retrofit purposes. Two retrofitting system were introduced in this thesis to represent the local and global strengthening of the RC frame using RSFJs. As for the local retrofitting, deficient RC beam/column (B/C) joints were selected for

retrofitting and RSFJs damper were utilized as haunch system in a pin-pin connection for improving the performance of the beam column joints. First, the performance of the RSFJ damper in a pin-pin connection were investigated experimentally. Then the seismic behaviour of different B/C joints were inspected, followed by developing a nonlinear model that represents different B/C joint. A simplified retrofit procedure was utilized for retrofit of the B/C joints and some recommendations were provided for using RSFJ as a haunch system. The numerical model was validated using available experimental results from the literature. Also, two case studies were presented for the retrofitting of one interior and one exterior beam-column joint. The efficiency of the proposed retrofit system was demonstrated in terms of improved energy dissipation, stiffness and strength, as well as improving the strength hierarchy of the system.

Turning to the global retrofitting of RC frame, the RSFJ-toggle bracing system was introduced for the first time and the behaviour of such system was evaluated numerically and experimentally. First, an initial numerical model was developed and the behaviour of non-ductile RC frame was modelled in a commercially available structural engineering software. Then, the numerical model was utilized for toggle bracing retrofit analysis. Having the promising results from the numerical model, it was then decided to validate the results by doing experimental testing on deficient RC frames. On this basis, two identical small scale RC frames were constructed for testing. The frames were designed to be classified as deficient RC frames representing pre-1970s RC moment resisting frame structures. One served as a reference frame without any retrofitting, while the second frame was retrofitted with RSFJ-toggle bracing system for comparison. Material testing (concrete cylinder testing, rebar tensile failure testing), as well as damper component testing were conducted for this experimental study. Moreover, some recommendations were provided regarding the proper brace design for thiss system, instability consideration for the RSFJ-toggle braces, connections and gusset plate designs. The columns were subjected to a set of prestressed rods to simulate the gravity loading on the frame structure. The accuracy of such method for simulating gravity load on the system was investigated as well. The experimental cyclic pushover testing was performed for both the bare and retrofitted frames and demonstrated the improved behaviour of the retrofitted frame in terms of energy dissipation, strength and stiffness. The numerical model could capture the behaviour of the system with an acceptable accuracy. Moreover, system represented a semi flag-shape performance, instead of pinching behaviour, which verifies its capability for sequential seismic events.

6.2. Proposed future studies

Due to time and budget constraints, the research scopes were limited to the topics discussed in this study. Here, some of the limitations of this thesis is listed and other research subjects are proposed for future studies to further advance the topic:

1) Usually, the main strategy for retrofitting a buildings frame is to improve its damping capabilities (whether it is hysteresis or viscous damping), to lower down the demand spectrum as much as possible. Therefore, having the retrofit testing scheme with regular friction dampers could provide valuable output for comparison.
2) It is possible to combine self-centering dampers with regular friction dampers to improve the damping and reach an optimized retrofit design for deficient RC moment resisting frames. Such an approach was successfully utilized for retrofitting of RC shear walls[95] and it can be followed here as well.
3) This research introduced a new self-centering damper (Rotational-RSFJ) which has the potential to be utilized or modified for specific applications including self-centering braces, self-centering moment resisting connections, tension-only braces, self-centering shear links for rocking shear walls, EBFs or link frame systems. Obviously, each of these systems could be an interesting research topic for new seismic resisting systems that can be investigated in detail by numerical and experimental studies.
4) Thanks to the structural characteristics of Rotational-RSFJ in terms of larger displacement capacities compared to RSFJ, it is possible to utilize the damper, with flat sliding friction isolators to have an isolated building with self-centering capabilities for the super-structure. Such an isolation technique could also be investigated as another retrofit solution in future studies.
5) Due to budget limitation, it was decided to only investigate the conventional strengthening of RC frames, by comparing the behaviour of the bare frame against retrofitted frame equipped with RSFJ-toggle bracing. However, as the previous literature highlighted, the selective weakening combined with self-centering systems are promising concepts for retrofit purposes. It is suggested to perform similar tests with a RC frame that has its beam bottom rebars cut, to see the performance of weakened RC frame with RSFJ dampers as well.
6) As a general area of research, it is encouraged to investigate the effects of other structural elements such as slab and flooring systems on the retrofit performance of

the frame. Moreover, further numerical and experimental analyses is recommended for the performance of the retrofitted frame under bi-directional seismic demands.

7) It is suggested to further investigate the numerical outputs regarding the RC beam/column joint retrofitted by RSFJ as haunch element. This can be studies by experimental testing and comparison of the findings with other types of hunch elements. Moreover, the numerical study can be extended in terms of conducting time-history analysis for an entire structure equipped with such retrofitting system, or performing incremental dynamic analysis and fragility assessment for further investigations.
8) One area that needs more investigation is the stability consideration for the toggle-bracing system. While the simplified approach in this study appeared to be conservative enough, more research is required for a better optimum design of the system. As an example, the out-of-plane movement of middle pinned end in the toggle bracing might require quantitative analysis, especially if other types of dampers are being used which might be more sensitive to out-of-plane movement.
9) As a general research approach, it is necessary to suggest more affordable low-damage systems to be utilized for new and existing buildings with low to high importance levels to minimize the damage repair cost and provide quick re-occupancy after severe events.
10) Recently, the carbon foot-prints topics and sustainability have gained the attention of researchers, practitioners, building insurers and stakeholders. On this basis, the life-cycle impact of buildings which have a short life-span, or the ones that cannot be re-occupied quickly following major events is not worthwhile. Therefore, having new seismic resistant systems and retrofit solutions like RSFJ and Rotational-RSFJ that are low-damage and adaptable, is highly appreciated. More research on this area could help developing more sustainable buildings with better carbon foot-print status.

References

1. Shiravand, M., M. Nashtaee, and S. Veismoradi, Seismic assessment of concrete buildings reinforced with shape memory alloy materials in different stories. The Structural Design of Tall and Special Buildings, 2017. 26(15): p. e1384.

2. Lago, A., D. Trabucco, and A. Wood, Damping technologies for tall buildings: Theory, design guidance and case studies. 2018: Butterworth-Heinemann.

3. Bagheri, S., et al. U-shaped metallic-yielding damper in building structures: Seismic behavior and comparison with a friction damper. in Structures. 2015. Elsevier.

4. Symans, M., et al., Energy dissipation systems for seismic applications: current practice and recent developments. Journal of structural engineering, 2008. 134(1): p. 3-21.

5. Berquist, M., et al., Fluid viscous dampers-general guidelines for engineers including a brief history. USA: Taylor Devices Inc, 2019.

6. De Domenico, D., G. Ricciardi, and I. Takewaki, Design strategies of viscous dampers for seismic protection of building structures: a review. Soil dynamics and earthquake engineering, 2019. 118: p. 144-165.

7. Christopoulos, C. and A. Filiatrault, Principles of passive supplemental damping and seismic. 2006: IUSS Press, Pavia, Italy.

8. Christopoulos, C. and M. Montgomery, Viscoelastic coupling dampers (VCDs) for enhanced wind and seismic performance of high-rise buildings. Earthquake Engineering & Structural Dynamics, 2013. 42(15): p. 2217-2233.

9. Montgomery, M. and C. Christopoulos, Experimental validation of viscoelastic coupling dampers for enhanced dynamic performance of high-rise buildings. Journal of structural engineering, 2015. 141(5): p. 04014145.

10. Veismoradi, S., A. Cheraghi, and E. Darvishan, Probabilistic mainshock-aftershock collapse risk assessment of buckling restrained braced frames. Soil Dynamics and Earthquake Engineering, 2018. 115: p. 205-216.

11. Veismoradi, S. and E. Darvishan, Probabilistic seismic assessment of mega buckling-restrained braced frames under near-fault ground motions. Earthq. Struct, 2018. 15(5): p. 487-498.

12. Tsai, K.-C., et al., Design of steel triangular plate energy absorbers for seismic-resistant construction. Earthquake spectra, 1993. 9(3): p. 505-528.

13. Gray, M.G., C. Christopoulos, and J.A. Packer, Cast steel yielding brace system for concentrically braced frames: concept development and experimental validations. Journal of Structural Engineering, 2013. 140(4): p. 04013095.

14. Veismoradi, S., G.G. Amiri, and E. Darvishan, Probabilistic seismic assessment of buckling restrained braces and yielding brace systems. International Journal of Steel Structures, 2016. 16(3): p. 831-843.

15. Chen, Y., A. Palermo, and M. Mashal, Cyclic tests of an innovative seismic bracing member-multiple U-shaped flexural plates dissipater. 2020.

16. Oh, S.-H., Y.-J. Kim, and H.-S. Ryu, Seismic performance of steel structures with slit dampers. Engineering structures, 2009. 31(9): p. 1997-2008.

17. Li, Y., R. Song, and J.W. Van De Lindt, Collapse fragility of steel structures subjected to earthquake mainshock-aftershock sequences. Journal of Structural Engineering, 2014. 140(12): p. 04014095.

18. Pall, A. Performance-based design using pall friction dampers-an economical design solution. in 13th World Conference on Earthquake Engineering, Vancouver, BC, Canada. 2004.

19. Lago, A., D. Trabucco, and A. Wood, Chapter 4 - An introduction to dynamic modification devices, in Damping Technologies for Tall Buildings, A. Lago, D. Trabucco, and A. Wood, Editors. 2019, Butterworth-Heinemann. p. 107-234.

20. Pall, A.S. and C. Marsh, Response of friction damped braced frames. Journal of Structural Engineering, 1982. 108(9): p. 1313-1323.

21. Pall, R., et al. Friction-Dampers for Seismic Upgrade of Quebec Police Headquarters, Montreal. in Twelfth World Conference on Earthquake Engineering, Auckland, New Zealand. 2000.

22. Wu, B., et al., Hysteretic behavior of improved Pall-typed frictional dampers. Engineering Structures, 2005. 27(8): p. 1258-1267.

23. Mualla, I.H. and B. Belev, Performance of steel frames with a new friction damper device under earthquake excitation. Engineering Structures, 2002. 24(3): p. 365-371.

24. Damptech Earthquake Protection Inc.; Available from: www.damptech.com.

25. Veismoradi, S., P. Zarnani, and P. Quenneville, Development of self-centring Rotational Slip Friction Joint: a novel damage-free damper with large deflections, in 2019 PCEE. 2019: Auckland, New Zealand.

26. Monir, H.S. and K. Zeynali, A modified friction damper for diagonal bracing of structures. Journal of Constructional Steel Research, 2013. 87: p. 17-30.

27. Veismoradi, S., P. Zarnani, and P. Quenneville, Development of self-centring Rotational Slip Friction Joint: a novel damage-free damper with large deflections, in Pacific Conference on Earthquake Engineering 2019: Auckland, New Zealand.

28. LIAO, W.I., I. MUALLA, and C.H. LOH, Shaking-table test of a friction-damped frame structure. The Structural Design of Tall and Special Buildings, 2004. 13(1): p. 45-54.

29. Mirtaheri, M., et al., Numerical and experimental study of hysteretic behavior of cylindrical friction dampers. Engineering Structures, 2011. 33(12): p. 3647-3656.

30. Samani, H.R., M. Mirtaheri, and A.P. Zandi, Experimental and numerical study of a new adjustable frictional damper. Journal of Constructional Steel Research, 2015. 112: p. 354-362.

31. Cho, C.G. and M. Kwon, Development and modeling of a frictional wall damper and its applications in reinforced concrete frame structures. Earthquake engineering & structural dynamics, 2004. 33(7): p. 821-838.

32. Taylor, D.P., Toggle brace dampers: A new concept for structural control, in Advanced Technology in Structural Engineering. 2000. p. 1-8.

33. Zhang, R., et al., Theoretical analysis and experimental research on toggle-brace-damper system considering different installation modes. Scientia Iranica, 2012. 19(6): p. 1379-1390.

34. Constantinou, M.C., Highly effective seismic energy dissipation apparatus. 2002, Google Patents.

35. Sigaher, A.N. and M.C. Constantinou, Scissor-jack-damper energy dissipation system. Earthquake Spectra, 2003. 19(1): p. 133-158.

36. Kang, Y.-j. and L.-y. Peng, Development and analysis of the control effect of a Reid damper with self-centering characteristics. Shock and Vibration, 2018. 2018.

37. Erochko, J., et al., Residual drift response of SMRFs and BRB frames in steel buildings designed according to ASCE 7-05. Journal of Structural Engineering, 2011. 137(5): p. 589-599.

38. Zhong, C. and C. Christopoulos, Self-centering seismic-resistant structures: Historical overview and state-of-the-art. Earthquake spectra, 2022. 38(2): p. 1321-1356.

39. Eatherton, M.R., L.A. Fahnestock, and D.J. Miller, Computational study of self-centering buckling-restrained braced frame seismic performance. Earthquake engineering & structural dynamics, 2014. 43(13): p. 1897-1914.

40. Zhu, S. and Y. Zhang, Seismic analysis of concentrically braced frame systems with self-centering friction damping braces. Journal of Structural Engineering, 2008. 134(1): p. 121-131.

41. Christopoulos, C., et al., Self-centering energy dissipative bracing system for the seismic resistance of structures: development and validation. Journal of structural engineering, 2008. 134(1): p. 96-107.

42. Erochko, J., C. Christopoulos, and R. Tremblay, Design and testing of an enhanced-elongation telescoping self-centering energy-dissipative brace. Journal of Structural Engineering, 2015. 141(6): p. 04014163.

43. Shiravand, M. and S. Mahboubi, Behavior of post-tensioned connections with stiffened angles under cyclic loading. Journal of Constructional Steel Research, 2016. 116: p. 183-192.

44. Mashal, M., A. Palermo, and Z. Chegini. Quasi-static cyclic tests of half-scale fully precast bridge bents incorporating emulative and posttensioned low damage solutions. in Proc., 2nd European Conf. on Earthquake Engineering and Seismology. 2014.

45. Xu, L., X. Fan, and Z. Li, Hysteretic analysis model for pre-pressed spring self-centering energy dissipation braces. J. Struct. Eng, 2018. 144(7): p. 04018073.

46. Hashemi, A., et al., Experimental testing of rocking cross-laminated timber walls with resilient slip friction joints. Journal of Structural Engineering, 2018. 144(1): p. 04017180.

47. Iqbal, A., et al., Performance and design of LVL walls coupled with UFP dissipaters. Journal of Earthquake Engineering, 2015. 19(3): p. 383-409.

48. Granello, G., et al., Long-term performance assessment of an operative post-tensioned timber frame structure. Journal of Structural Engineering, 2019. 145(5): p. 04019034.

49. Kurama, Y., et al., Lateral load behavior and seismic design of unbonded post-tensioned precast concrete walls. Structural Journal, 1999. 96(4): p. 622-632.

50. Christopoulos, C., et al., Posttensioned energy dissipating connections for moment-resisting steel frames. Journal of Structural Engineering, 2002. 128(9): p. 1111-1120.

51. Wanninger, F., A. Frangi, and M. Fragiacomo, Long-term behavior of posttensioned timber connections. Journal of Structural Engineering, 2015. 141(6): p. 04014155.

52. Hashemi, A., et al., Seismic resistant rocking coupled walls with innovative Resilient Slip Friction (RSF) joints. Journal of Constructional Steel Research, 2017. 129: p. 215-226.

53. Darani, F.M., P. Zarnani, and P. Quenneville, Development of a New Self-Centring Structural Connector for Seismic Protection of Structures. Journal of Constructional Steel Research, 2022. 189: p. 107064.

54. Zarnani, P. and P. Quenneville, A resilient slip friction joint. Patent No. WO2016185432A1, NZ IP Office, 2015.

55. Bagheri, H., Seismic Performance of a Full-Scale Steel Structure Using Resilient Slip Friction Joints. 2022, ResearchSpace@ Auckland.

56. Nims, D.K., P.J. Richter, and R.E. Bachman, The use of the energy dissipating restraint for seismic hazard mitigation. Earthquake Spectra, 1993. 9(3): p. 467-489.

57. Kar, R., J. Rainer, and A. Lefrançois, Dynamic properties of a circuit breaker with friction-based seismic dampers. Earthquake spectra, 1996. 12(2): p. 297-314.

58. Filiatrault, A., R. Tremblay, and R. Kar, Performance evaluation of friction spring seismic damper. Journal of Structural Engineering, 2000. 126(4): p. 491-499.

59. Hashemi, A., et al., Enhanced seismic performance of timber structures using resilient connections: full-scale testing and design procedure. Journal of structural engineering, 2020. 146(9): p. 04020180.

60. Darani, F., et al. Application of new resilient slip friction joint for seismic damage avoidance design of rocking concrete shear walls.". in New Zealand Society for Earthquake Engineering (NZSEE) Conference. 2018.

61. Sahami, K., et al. Seismic performance of rocking concrete shear walls with innovative rotational resilient slip friction joints. in Pacific Conference on Earthquake Engineering (PCEE) and New Zealand Society for Earthquake Engineering (NZSEE), Auckland, New Zealand. 2019.

62. Sahami, K., P. Zarnani, and P. Quenneville, Introducing a low damage system incorporating rocking braced frame and resilient slip friction joint as a shear key. 2020.

63. Yousef-beik, S.M.M., et al., Experimental study on cyclic performance of a damage-free brace with self-centering connection. Journal of Structural Engineering, 2021. 147(1): p. 04020299.

64. Yousef-beik, S.M.M., et al., A new self-centering brace with zero secondary stiffness using elastic buckling. Journal of Constructional Steel Research, 2020. 169: p. 106035.

65. Shabankareh, M., et al., Seismic damage avoidance design of moment resisting frames with innovative resilient connection. 2020.

66. Bagheri, H., et al., New self-centering tension-only brace using resilient slip-friction joint: Experimental tests and numerical analysis. Journal of Structural Engineering, 2020. 146(10): p. 04020219.

67. Bagheri, H., et al., The resilient slip friction joint tension-only brace beyond its ultimate level. Journal of Constructional Steel Research, 2020. 172: p. 106225.

68. Tectonus, Resilient seismic Solutions. 2022; Available from: https://www.tectonus.com/projects.

69. Opabola, E.A., K.J. Elwood, and S. Oliver, Deformation capacity of reinforced concrete columns with smooth reinforcement. Bulletin of Earthquake Engineering, 2019. 17(5): p. 2509-2532.

70. Guideline, N., Part C5, Concrete Buildings, Technical Guidelines for Engineering Assessments. 2017.

71. Opabola, E. and K.J. Elwood, Comparative study on acceptance criteria for non-ductile reinforced concrete columns. Bulletin of the New Zealand Society for Earthquake Engineering, 2018. 51(4): p. 183-196.

72. Guideline, N., Part C5: Technical Proposal to Revise the Engineering Assessment Guidelines. 2018.

73. Boys, A., D. Bull, and S. Pampanin, Seismic performance assessment of inadequately detailed reinforced concrete columns. 2008.

74. Sezen, H., et al., Performance of reinforced concrete buildings during the August 17, 1999 Kocaeli, Turkey earthquake, and seismic design and construction practise in Turkey. Engineering Structures, 2003. 25(1): p. 103-114.

75. Zhang, J., et al., Experimental and analytical studies on a reinforced concrete frame retrofitted with buckling-restrained brace and steel caging. Advances in Structural Engineering, 2015. 18(2): p. 155-171.

76. Shahsahebi, A., Z. Waezi, and M.J. Hashemi. Seismic performance assessment of multi-story RC buildings with soft-story collapse mechanism equipped with gapped inclined bracing (GIB). in Structures. 2020. Elsevier.

77. Kam, W., D. Bull, and S. Pampanin, Experimental validation of selective weakening approach for the seismic retrofit of exterior beam-column joints. 2009.

78. Thermou, G. and A. Elnashai, Seismic retrofit schemes for RC structures and local-global consequences. Progress in Structural Engineering and Materials, 2006. 8(1): p. 1-15.

79. Pan, K.Y., et al., Seismic retrofit of reinforced concrete frames using buckling-restrained braces with bearing block load transfer mechanism. Earthquake Engineering & Structural Dynamics, 2016. 45(14): p. 2303-2326.

80. Ghobarah, A. and H. Abou Elfath, Rehabilitation of a reinforced concrete frame using eccentric steel bracing. Engineering structures, 2001. 23(7): p. 745-755.

81. Qu, Z., et al., Subassemblage cyclic loading tests of buckling-restrained braced RC Frames with unconstrained gusset connections. Journal of Structural Engineering, 2016. 142(2): p. 04015128.

82. Qu, Z., et al., Subassemblage cyclic loading test of RC frame with buckling restrained braces in zigzag configuration. Earthquake engineering & structural dynamics, 2013. 42(7): p. 1087-1102.

83. Wu, Y.-F., T. Liu, and D.J. Oehlers, Fundamental principles that govern retrofitting of reinforced concrete columns by steel and FRP jacketing. Advances in Structural Engineering, 2006. 9(4): p. 507-533.

84. Ali, O., et al., Numerical investigation of FRP-confined short square RC columns. Construction and Building Materials, 2021. 275: p. 122141.

85. Jiang, J., P. Li, and N. Nistico, Local and global prediction on stress-strain behavior of FRP-confined square concrete sections. Composite Structures, 2019. 226: p. 111205.

86. Lin, X., Y. Zhang, and P. Pathak, Nonlinear finite element analysis of composite and reinforced concrete beams. 2019: Woodhead Publishing.

87. Landi, L., F. Conti, and P.P. Diotallevi, Effectiveness of different distributions of viscous damping coefficients for the seismic retrofit of regular and irregular RC frames. Engineering Structures, 2015. 100: p. 79-93.

88. David Gonzalez, K.O.C., Guzhao Li, Emily McCarthy et al.,. Seismic Retrofit of a Seventeen-Story Steel Moment Frame Building. 2022 19/10/2022]; Available from: https://www.taylordevices.com/news/seismic-retrofit-101-continental/.

89. Whittaker, D., Recent developments in New Zealand in seismic isolation, energy dissipation and vibration control of structures (2017).NZSEE Conference 2017.

90. Ma, C., et al., Seismic response of base-isolated high-rise buildings under fully nonstationary excitation. Shock and Vibration, 2014. 2014.

91. Carr, A. and A. Puthanpurayil, Base isolation: the good, the bad and the ugly. 2021.

92. Amiri, G.G., et al., Effect of seismic pounding on buildings isolated by triple friction pendulum bearing. Earthquakes and Structures, 2017. 12(1): p. 35-45.

93. Priestley, M.N., F. Seible, and G.M. Calvi, Seismic design and retrofit of bridges. 1996: John Wiley & Sons.

94. Ireland, M., S. Pampanin, and D. Bull, Experimental investigations of a selective weakening approach for the seismic retrofit of rc walls. 2007.

95. A. Hashemi, S.A., P. Quenneville, T. Dawson, P. Boardman, R. Poole,, A novel solution for retrofitting concrete structures with resilient connections: a case study, in New Zealand Society for Earthquake Engineering Conference. 2022: Online.

96. Pampanin, S., Towards the “ultimate earthquake-proof” building: Development of an integrated low-damage system, in Perspectives on European earthquake engineering and seismology. 2015, Springer, Cham. p. 321-358.

97. Bruneau, M. and G. MacRae, Building Structural Systems in Christchurch's Post-Earthquake Reconstruction. Earthquake Spectra, 2019. 35(4): p. 1953-1978.

98. Westenenk, B., et al., Self-centering frictional damper (SCFD). Engineering Structures, 2019. 197: p. 109425.

99. Pall, A. Performance-based design using pall friction dampers-an economical design solution. in 13th World Conference on Earthquake Engineering, Vancouver, BC, Canada. 2004.

100. Rashmi'Tina'PALL, G.G., S. DELISLE, and A. PALL, FRICTION-DAMPERS FOR SEISMIC UPGRADE OF QUEBEC POLICE HEADQUARTERS, MONTREAL.

101. Lee, J., H. Kang, and J. Kim, Seismic performance of steel plate slit-friction hybrid dampers. Journal of Constructional Steel Research, 2017. 136: p. 128-139.

102. Javidan, M.M. and J. Kim, Seismic retrofit of soft-first-story structures using rotational friction dampers. journal of structural engineering, 2019. 145(12): p. 04019162.

103. Wang, G., et al., Modeling and experimental investigation of a novel arc-surfaced frictional damper. Journal of Sound and Vibration, 2017. 389: p. 89-100.

104. Wei, B., et al., Parameter optimization of a vertical spring-viscous damper-Coulomb friction system. Shock and Vibration, 2019.

105. Zareian, M.S., M.R. Esfahani, and A. Hosseini, Experimental evaluation of self-centering hybrid coupled wall subassemblies with friction dampers. Engineering Structures, 2020. 214: p. 110644.

106. Xu, L.-H., X.-W. Fan, and Z.-X. Li, Development and experimental verification of a pre-pressed spring self-centering energy dissipation brace. Engineering Structures, 2016. 127: p. 49-61.

107. Xu, L., X. Fan, and Z. Li, Experimental behavior and analysis of self-centering steel brace with pre-pressed disc springs. Journal of Constructional Steel Research, 2017. 139: p. 363-373.

108. Wang, W., et al., Self-centering friction spring dampers for seismic resilience. Earthquake Engineering & Structural Dynamics, 2019. 48(9): p. 1045-1065.

109. Mualla, I. and B. Belev, Analysis, design and applications of rotational friction dampers for seismic protection. Czasopismo Inżynierii Lądowej, Środowiska i Architektury, 2015. 62(4): p. 335-346.

110. Veismoradi, S., P. Zarnani, and P. Quenneville. Development of self-centring Rotational Slip Friction Joint: a novel damage-free damper with large deflections. in Pacific Conference on Earthquake Engineering (PCEE) and New Zealand Society for Earthquake Engineering (NZSEE), Auckland, New Zealand. 2019.

111. Veismoradi, S., et al., Seismic retrofitting of RC-frames using resilient slip friction joint toggle-bracing system. 2020.

112. Yousef-beik, S.M.M., et al. Seismic performance improvement of conventional timber brace using re-centring friction connection. in Structures. 2020. Elsevier.

113. Systèmes, D., Abaqus 6.14—Abaqus Analysis User's Guide. Dassault Systèmes: Vélizy-Villacoublay, France, 2014.

114. Csi, C., Analysis reference manual for SAP2000, ETABS, and SAFE. Computers and Structures, Berkeley, California, USA, 2016.

115. Chen, W. and H. Hao, Numerical study of blast-resistant sandwich panels with rotational friction dampers. International Journal of Structural Stability and Dynamics, 2013. 13(06): p. 1350014.

116. Mazza, F. and A. Vulcano, Equivalent viscous damping for displacement-based seismic design of hysteretic damped braces for retrofitting framed buildings. Bulletin of Earthquake Engineering, 2014. 12(6): p. 2797-2819.

117. Li, S., et al., Equivalence of friction and viscous damping in a spring-friction system with concave friction distribution. Journal of Testing and Evaluation, 2020. 49(1): p. 372-395.

118. Ramhormozian, S., et al., Experimental studies on Belleville springs use in the sliding hinge joint connection. Journal of Constructional Steel Research, 2019. 159: p. 81-94.

119. Kam, W.Y., S. Pampanin, and K. Elwood, Seismic performance of reinforced concrete buildings in the 22 February Christchurch (Lyttleton) earthquake. 2011.

120. Shafaei, J. and S.A. Nezami, Effect of different size of joint enlargement on seismic behavior of gravity load designed RC beam-column connections. The Structural Design of Tall and Special Buildings, 2019. 28(14): p. e1653.

121. Di Sarno, L. and G. Manfredi, Seismic retrofitting with buckling restrained braces: Application to an existing non-ductile RC framed building. Soil Dynamics and Earthquake Engineering, 2010. 30(11): p. 1279-1297.

122. Lobo, P.S., J. Almeida, and L. Guerreiro, Recentring and control of peak displacements of a RC frame using damping devices. Soil Dynamics and Earthquake Engineering, 2017. 94: p. 66-74.

123. Karayannis, C.G., C.E. Chalioris, and G.M. Sirkelis, Local retrofit of exterior RC beam–column joints using thin RC jackets—An experimental study. Earthquake Engineering & Structural Dynamics, 2008. 37(5): p. 727-746.

124. Tsonos, A.-D.G., Performance enhancement of R/C building columns and beam–column joints through shotcrete jacketing. Engineering Structures, 2010. 32(3): p. 726-740.

125. Maheri, M.R. and A. Torabi. Retrofitting external RC beam-column joints of an ordinary MRF through plastic hinge relocation using FRP laminates. in Structures. 2019. Elsevier.

126. Jiang, S.-F., et al., Experimental studies on the seismic behavior of earthquake-damaged circular bridge columns repaired by using combination of near-surface-mounted BFRP bars with external BFRP sheets jacketing. Engineering Structures, 2016. 106: p. 317-331.

127. Li, B., et al., Strengthening of non-seismically designed beam-column joints by ferrocement jackets with chamfers. Earthquakes and Structures, 2015. 8(5): p. 1017-1038.

128. Adibi, M., et al., External retrofit of beam-column joints in old fashioned RC structures. Earthquakes and Structures, 2017. 12(2): p. 237-250.

129. Shafaei, J., A. Hosseini, and M.S. Marefat, Seismic retrofit of external RC beam–column joints by joint enlargement using prestressed steel angles. Engineering Structures, 2014. 81: p. 265-288.

130. Zabihi, A., et al., Seismic retrofit of exterior RC beam-column joint using diagonal haunch. Engineering Structures, 2018. 174: p. 753-767.

131. Pampanin, S., C. Christopoulos, and T.H. Chen, Development and validation of a metallic haunch seismic retrofit solution for existing under-designed RC frame buildings. Earthquake engineering & structural dynamics, 2006. 35(14): p. 1739-1766.

132. Sharma, A., et al., Seismic Response of Reinforced Concrete Frames with Haunch Retrofit Solution. ACI Structural Journal, 2014. 111(3).

133. Akbar, J., N. Ahmad, and B. Alam, Seismic Strengthening of Deficient Reinforced Concrete Frames Using Reinforced Concrete Haunch. ACI Structural Journal, 2019. 116(1).

134. Wang, B., et al., Seismic retrofitting of non-seismically designed RC beam-column joints using buckling-restrained haunches: design and analysis. Journal of Earthquake Engineering, 2018. 22(7): p. 1188-1208.

135. Dong, Y.-R., et al., Seismic behavior and damage evolution for retrofitted RC frames using haunch viscoelastic damping braces. Engineering Structures, 2019. 199: p. 109583.

136. Calvi, G.M., G. Magenes, and S. Pampanin, Relevance of beam-column joint damage and collapse in RC frame assessment. Journal of Earthquake Engineering, 2002. 6(spec01): p. 75-100.

137. Pampanin, S., G. Magenes, and A.J. Carr, Modelling of shear hinge mechanism in poorly detailed RC beam-column joints. 2003.

138. Hofmann, I.J., Seismic behavior and retrofitting of RC frame structures with emphasis on beam-column joints–Experiments and numerical modeling. 2013.

139. Kanchanadevi, A. and K. Ramanjaneyulu, Non-invasive hybrid retrofit for seismic damage mitigation of gravity load designed exterior beam–column sub-assemblage. Journal of Earthquake Engineering, 2021. 25(8): p. 1590-1615.

140. Darani, F.M., et al. Resilient slip friction joint performance: Component analysis, spring model and anti-locking mechanism. in Structures. 2021. Elsevier.

141. Veismoradi, S., et al., Development and parametric study of a new self-centering rotational friction damper. Engineering Structures, 2021. 235: p. 112097.

142. Wei, B., et al., Scaling errors of a seismic isolation system with a shear key. Soil Dynamics and Earthquake Engineering, 2020. 139: p. 106382.

143. Yousef-beik, S.M.M., et al. Effect of second-order actions on the performance of resilient slip friction joints: Analytical and experimental investigation. in Structures. 2021. Elsevier.

144. AISC, ANSI/AISC 360-16: specification for structural steel buildings. 2016.

145. Kheyroddin, A., E. Emami, and A. Khalili, RC beam–column connections retrofitted by steel prop: experimental and analytical studies. International Journal of Civil Engineering, 2020. 18(5): p. 501-518.

146. Committee, A.C.I.A., Building Code Requirements for Structural Concrete ACI 318-19 and Commentary 318R–19. American Concrete Institute ACI Committee: Farmington Hills, MI, USA, 2019.

147. Engineers, A.S.o.C. Seismic evaluation and retrofit of existing buildings. 2017. American Society of Civil Engineers.

148. FEMA, P., Commentary for the Seismic Rehabilitation of Buildings, FEMA 356, Federal Emergency Management Agency. Washington, DC, 2000.

149. Mazzoni, S., et al., OpenSees command language manual. Pacific Earthquake Engineering Research (PEER) Center, 2006. 264(1): p. 137-158.

150. Mander, J.B., M.J. Priestley, and R. Park, Theoretical stress-strain model for confined concrete. Journal of structural engineering, 1988. 114(8): p. 1804-1826.

151. Menegotto, M. Method of analysis for cyclically loaded RC plane frames including changes in geometry and non-elastic behavior of elements under combined normal force and bending. in Proc. of IABSE symposium on resistance and ultimate deformability of structures acted on by well defined repeated loads. 1973.

152. Elwood, K.J. and M.O. Eberhard, Effective Stiffness of Reinforced Concrete Columns. ACI Structural Journal, 2009. 106(4).

153. Celik, O.C. and B.R. Ellingwood, Modeling beam-column joints in fragility assessment of gravity load designed reinforced concrete frames. Journal of Earthquake Engineering, 2008. 12(3): p. 357-381.

154. Jeon, J.-S., et al., Fragility curves for non-ductile reinforced concrete frames that exhibit different component response mechanisms. Engineering Structures, 2015. 85: p. 127-143.

155. Park, S. and K.M. Mosalam, Simulation of reinforced concrete frames with nonductile beam-column joints. Earthquake Spectra, 2013. 29(1): p. 233-257.

156. Priestley, M., Displacement-based seismic assessment of reinforced concrete buildings. Journal of earthquake engineering, 1997. 1(01): p. 157-192.

157. Fugazza, D., Shape-memory alloy devices in earthquake engineering: mechanical properties, constitutive modelling and numerical simulations. Master's Thesis, University of Pavia, Pavia, Italy, 2003.

158. Walker, S.G., Seismic performance of existing reinforced concrete beam-column joints. 2001, University of Washington.

159. Kuang, J.S. and H. Wong, Effects of beam bar anchorage on beam–column joint behaviour. Proceedings of the Institution of Civil Engineers-Structures and Buildings, 2006. 159(2): p. 115-124.

160. Au, F.T., K. Huang, and H. Pam, Diagonally-reinforced beam–column joints reinforced under cyclic loading. Proceedings of the Institution of Civil Engineers-Structures and Buildings, 2005. 158(1): p. 21-40.

161. Pantelides, C.P., et al., Seismic performance of reinforced concrete building exterior joints with substandard details. Journal of Structural Integrity and Maintenance, 2017. 2(1): p. 1-11.

162. O'Reilly, G.J., T.J. Sullivan, and R. Monteiro, On the Seismic Assessment and Retrofit of Infilled RC Frame Structures. 2018.

163. Joseph, R., A. Mwafy, and M.S. Alam, Seismic performance upgrade of substandard RC buildings with different structural systems using advanced retrofit techniques. Journal of Building Engineering, 2022. 59: p. 105155.

164. Santarsiero, G. and A. Masi, Seismic performance of RC beam–column joints retrofitted with steel dissipation jackets. Engineering Structures, 2015. 85: p. 95-106.

165. Veismoradi, S., et al., Seismic strengthening of deficient RC frames using self-centering friction haunches. Engineering Structures, 2021. 248: p. 113261.

166. Cao, X.-Y., et al., Seismic retrofitting of existing frame buildings through externally attached sub-structures: State of the art review and future perspectives. Journal of Building Engineering, 2022. 57: p. 104904.

167. Javidan, M.M., S. Chun, and J. Kim, Experimental study on steel hysteretic column dampers for seismic retrofit of structures. Steel and Composite Structures, 2021. 40(4): p. 495-509.

168. Nasab, M.S.E., et al. Experimental study on seismic retrofit of a RC frame using viscoelastic dampers. in Structures. 2021. Elsevier.

169. TahamouliRoudsari, M., et al. Experimental assessment of retrofitting RC moment resisting frames with ADAS and TADAS yielding dampers. in Structures. 2018. Elsevier.

170. Vafaei, M., A.M.O. Sheikh, and S.C. Alih, Experimental study on the efficiency of tapered strip dampers for the seismic retrofitting of damaged non-ductile RC frames. Engineering Structures, 2019. 199: p. 109601.

171. Bruschi, E. and V. Quaglini. Assessment of a novel hysteretic friction damper for the seismic retrofit of reinforced concrete frame structures. in Structures. 2022. Elsevier.

172. Constantinou, M.C., et al., Toggle-brace-damper seismic energy dissipation systems. Journal of Structural Engineering, 2001. 127(2): p. 105-112.

173. Hwang, J.-S., Y.-N. Huang, and Y.-H. Hung, Analytical and experimental study of toggle-brace-damper systems. Journal of structural engineering, 2005. 131(7): p. 1035-1043.

174. Al-Sadoon, Z.A., M. Saatcioglu, and D. Palermo, New buckling-restrained brace for seismically deficient reinforced concrete frames. Journal of Structural Engineering, 2020. 146(6): p. 04020082.

175. Al-Sadoon, Z., Seismic retrofitting of conventional reinforced concrete moment-resisting frames using buckling restrained braces. 2016, Université d'Ottawa/University of Ottawa.

176. Stirrat, A., et al. Seismic performance assessment of non-ductile columns. in 2014 NZSEE Conf.: New Zealand Society of Earthquake Engineering NZSEE. 2014.

177. Elwood, K.J. and J.P. Moehle, Drift capacity of reinforced concrete columns with light transverse reinforcement. Earthquake Spectra, 2005. 21(1): p. 71-89.

178. Priestley, M., G. Calvi, and M. Kowalsky. Direct displacement-based seismic design of structures. in NZSEE conference. 2007.

179. Yousef-beik, S.M.M., Development of A New Self-centring Low-damage Bracing System for Earthquake Resistant Structures Using Resilient Slip Friction Joints (RSFJs). 2022, Auckland University of Technology.

180. Duan, L. and W. Chen, Effective length factors of compression members. Structural engineering handbook, 1999.

181. Wu, A.C., et al., Hybrid experimental performance of a full-scale two-story buckling-restrained braced RC frame. Earthquake Engineering & Structural Dynamics, 2017. 46(8): p. 1223-1244.

182. Maheri, M.R. and S. Yazdani, Design of steel brace connection to an RC frame using Uniform Force Method. Journal of Constructional Steel Research, 2016. 116: p. 131-140.

183. Shiradhonkar, S.R. and R. Sinha, Maximum and residual flexural crack width estimation in reinforced concrete frame members under seismic excitation. Journal of Structural Engineering, 2018. 144(8): p. 04018121.

Appendix 1: Structural Drawings of the test setup and RC Frame

RC frame with RSFJ-toggle brace assembly

Overall Test setup:
A- Top brace
B- Bottom brace
C- Damper brace (female part)
D- Damper brace (male part)
E- Damper (RSFJ)
F- Top gussets
G- Bottom gussets
H- RSFJ gussets
I- Yellow plate
J- RHS 200x100x10
K- 180x75 PFC
L- Cable holding assembly
M- Pins
N- RC frame
O- Shear key
P- Lateral support system
Q- Actuator

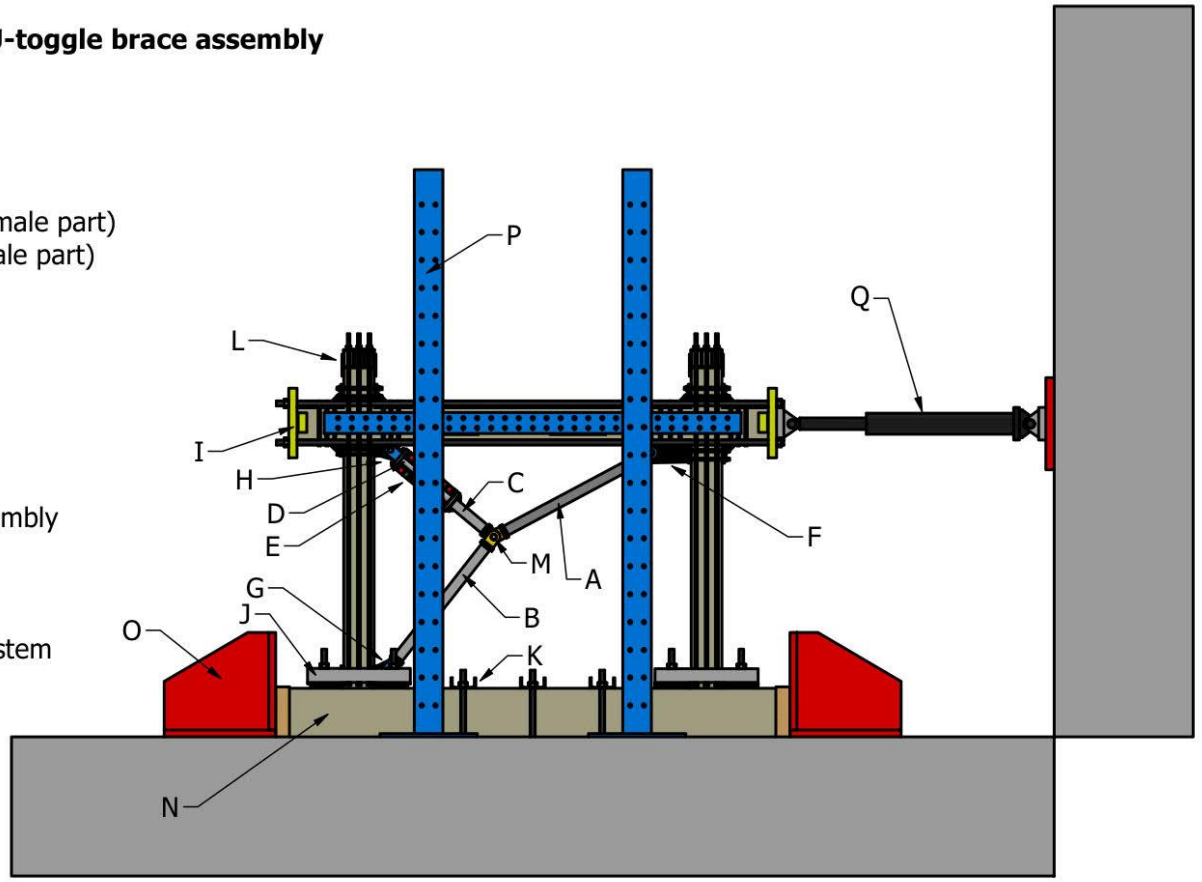

Designed by	Checked by	Approved by	Date
S. V.	P. Z.		6/25/2021

AUT University
School of Future Environment

Edition	Sheet
2	1 / 22

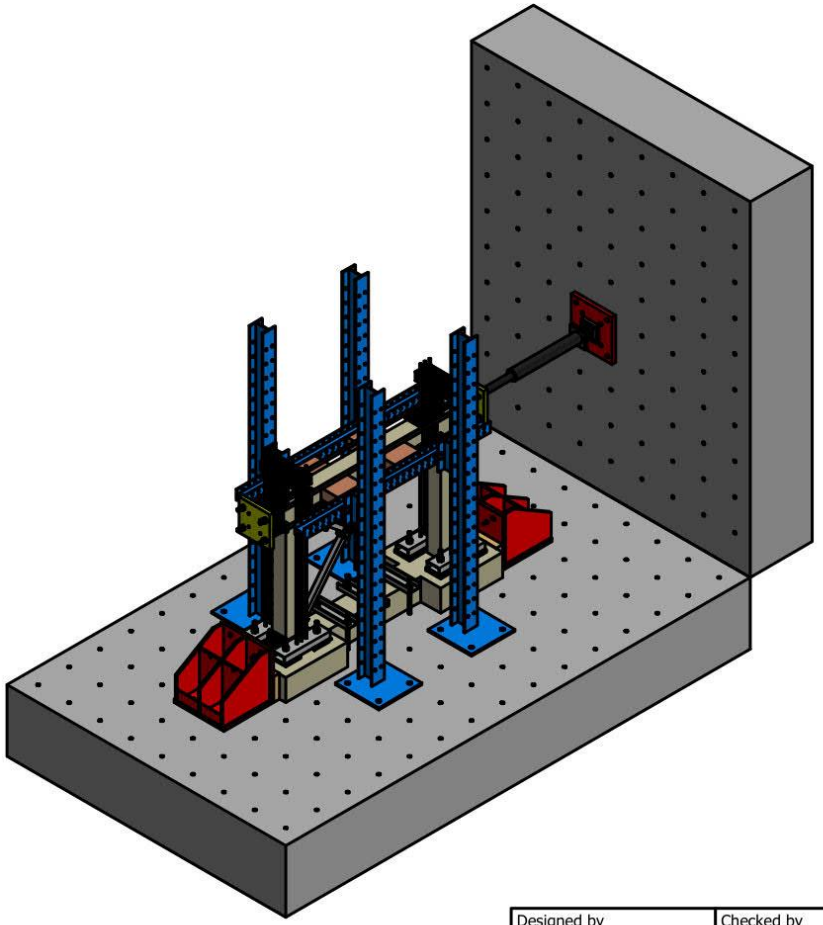

Overall Test setup Notes:

The component visible in the drawings will be made available through three main source:

1- Some of the components (such as shear keys and lateral support system) are already avaible at AUT lab. If required to be modified, the detail of the component will be provided.

2- The RSFJ dampers and the grip will be manufactored at AUT workshop.

3- The steel parts and braces will be manufactored at R&H.

4- The RC frame will be manufactored at Concretec.

Designed by	Checked by	Approved by	Date
S. V.	P. Z.		6/25/2021
AUT University School of Future Environment			
		Edition 2	Sheet 2 / 22

Cable-holding Assembly

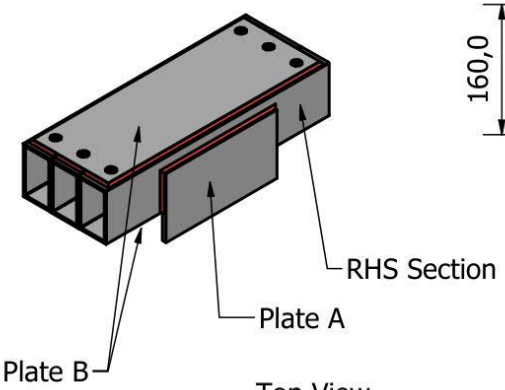

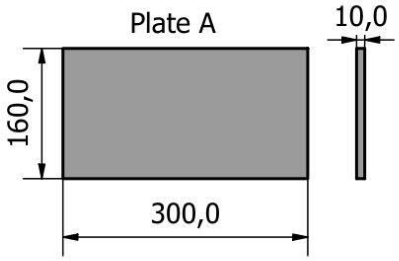

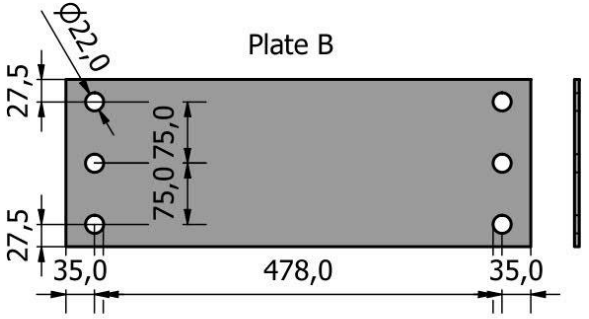

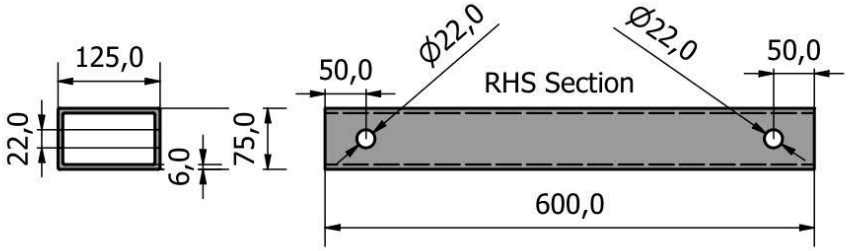

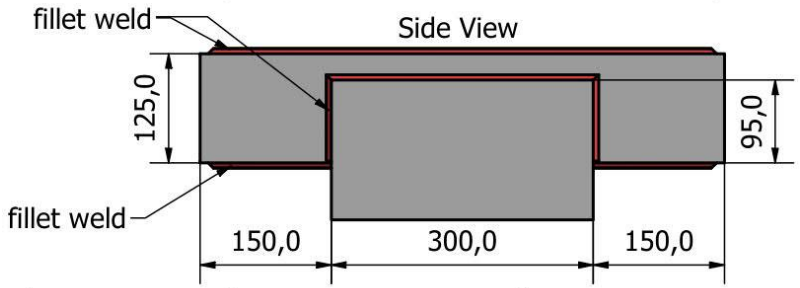

Notes:
1-Dimensions in mm with 0.1mm accuracy
2- Another Plate B is welded at the bottom of the Assembly.
3- Holes go through all the plates A and RHS sections.
4- Sections and plates have Fy=350MPa and Fu=480MPa.
5- equal leg fillet weld with leg size of 6mm is used for welding.
6- Welding is for structural purposes (SP).
7- Utilized weld metal: E48XX.
8- Required number of each part to create TWO of the Cable-holding Assembly:
Plate A: 4
Plate B: 4
RHS section 125x75x6.0: 6

Designed by	Checked by	Approved by	Date
S. V.	P. Z.		6/25/2021

AUT University
School of Future Environment

Cable-holding Assembly

No: ST-001	Edition	Sheet
	2	3 / 22

Cable-holding Assembly (continued)

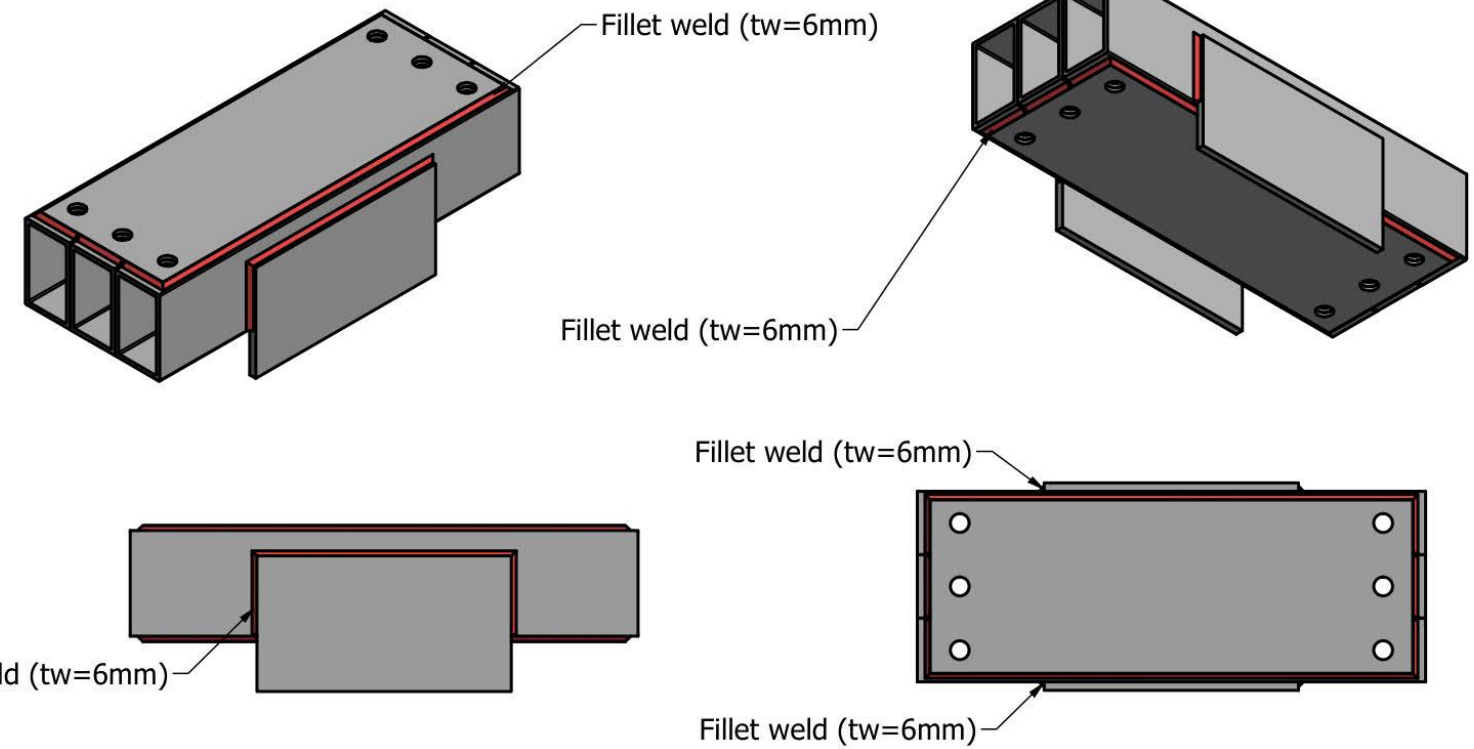

Designed by	Checked by	Approved by	Date
S. V.	P. Z.		6/25/2021
AUT University, School of Future Environment		Cable-holding Assembly	
		No: ST-001	Edition 2 / Sheet 4 / 22

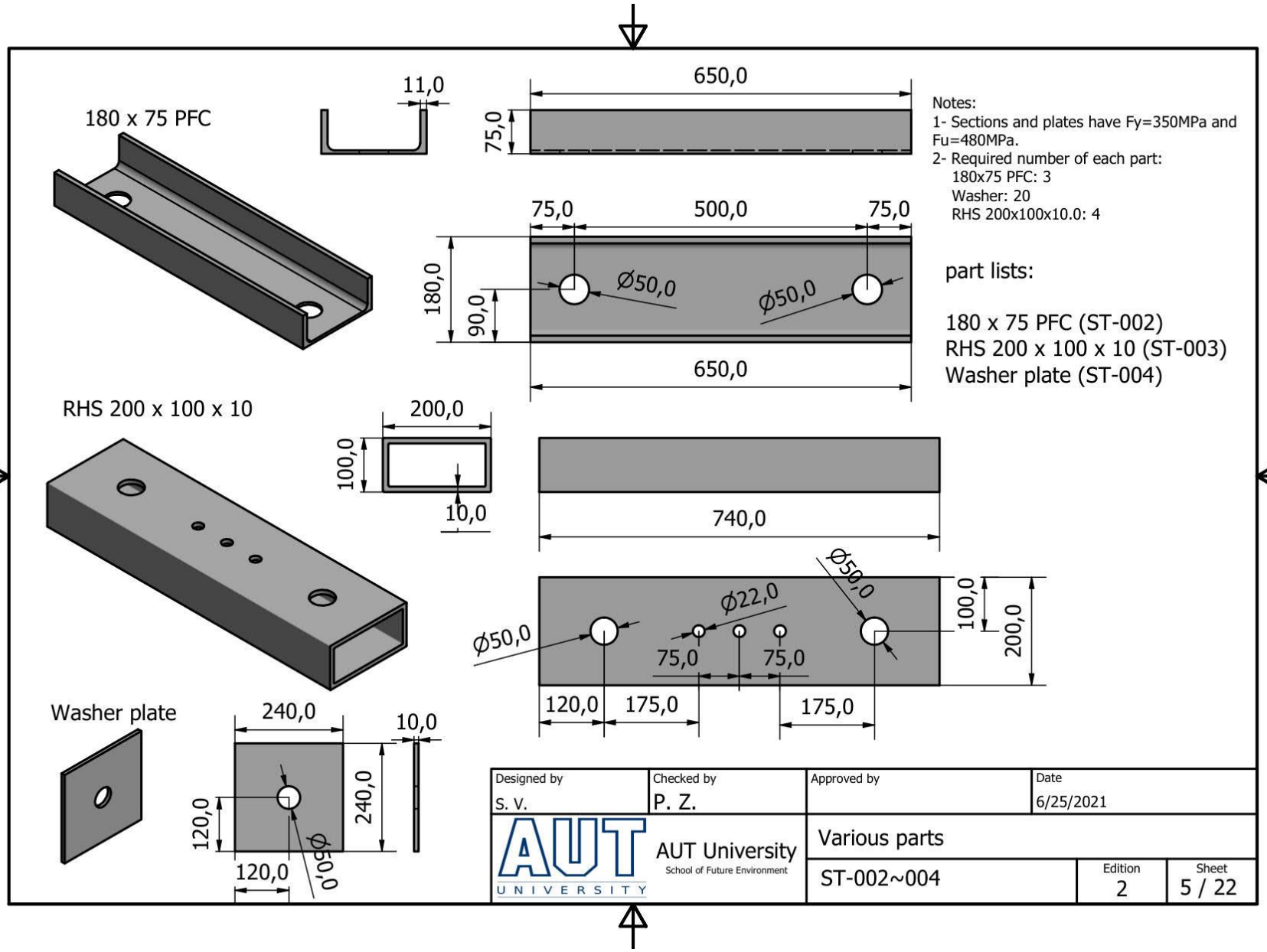
180 x 75 PFC
11,0
650,0
75,0
Notes:
1- Sections and plates have Fy=350MPa and Fu=480MPa.
2- Required number of each part:
180x75 PFC: 3
Washer: 20
RHS 200x100x10.0: 4
75,0
500,0
75,0
180,0
90,0
Ø50,0
Ø50,0
650,0
part lists:
180 x 75 PFC (ST-002)
RHS 200 x 100 x 10 (ST-003)
Washer plate (ST-004)
RHS 200 x 100 x 10
200,0
100,0
10,0
740,0
Ø50,0
Ø22,0
Ø50,0
100,0
200,0
75,0
75,0
120,0
175,0
175,0
Washer plate
240,0
10,0
240,0
120,0
120,0
Ø50,0
Designed by
S. V.
Checked by
P. Z.
Approved by
Date
6/25/2021
AUT University
School of Future Environment
Various parts
ST-002~004
Edition
2
Sheet
5 / 22

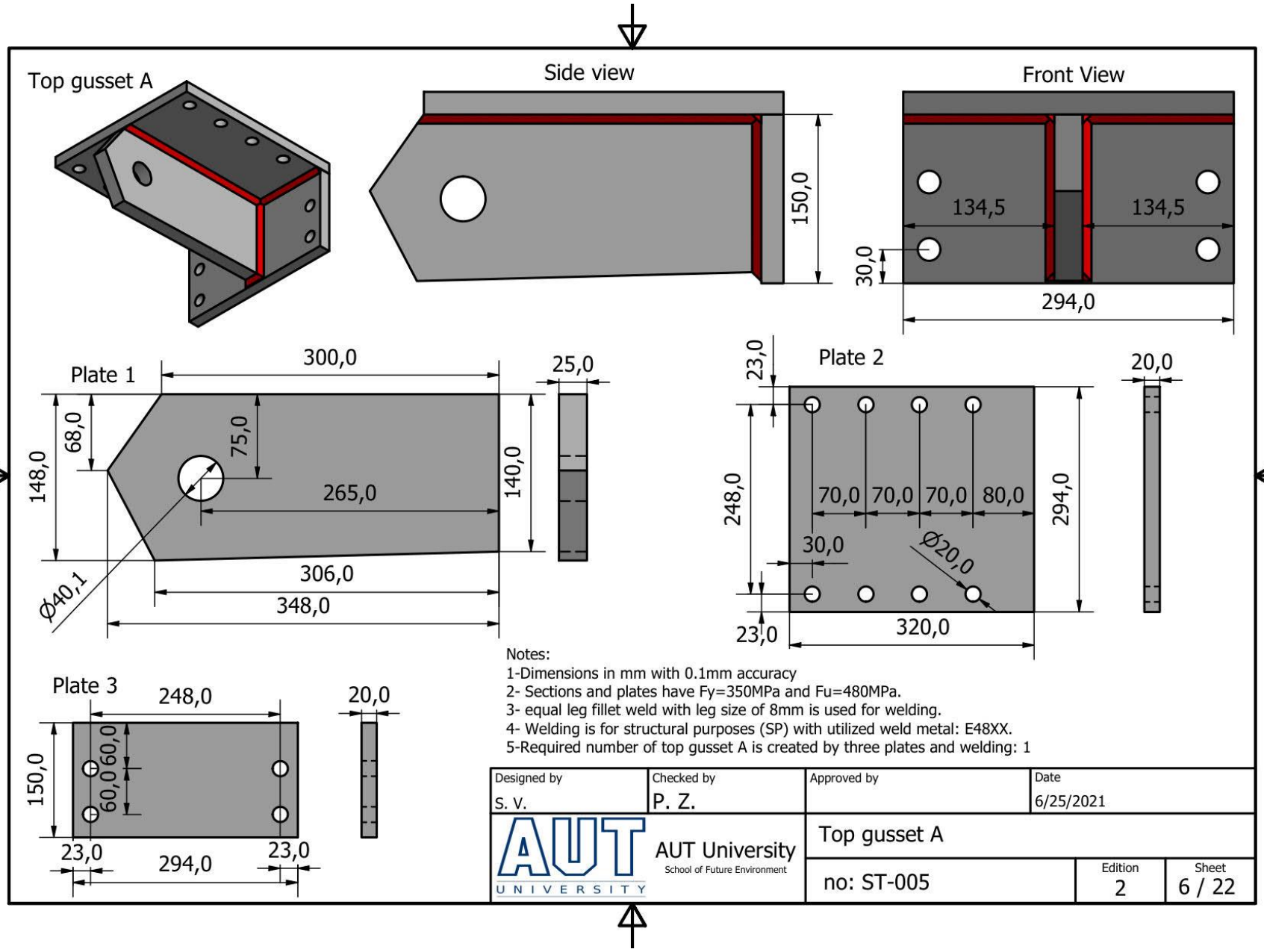
Top gusset A
Side view
150,0
Front View
134,5
134,5
30,0
294,0
Plate 1
300,0
25,0
68,0
148,0
75,0
265,0
140,0
306,0
348,0
Ø40,1
Plate 2
23,0
20,0
248,0
70,0
70,0
70,0
80,0
294,0
30,0
Ø20,0
23,0
320,0
Plate 3
248,0
20,0
150,0
60,0
60,0
23,0
294,0
23,0
Notes:
1-Dimensions in mm with 0.1mm accuracy
2- Sections and plates have Fy=350MPa and Fu=480MPa.
3- equal leg fillet weld with leg size of 8mm is used for welding.
4- Welding is for structural purposes (SP) with utilized weld metal: E48XX.
5-Required number of top gusset A is created by three plates and welding: 1
Designed by
S. V.
Checked by
P. Z.
Approved by
Date
6/25/2021
AUT University
School of Future Environment
Top gusset A
no: ST-005
Edition
2
Sheet
6 / 22

Top gusset B

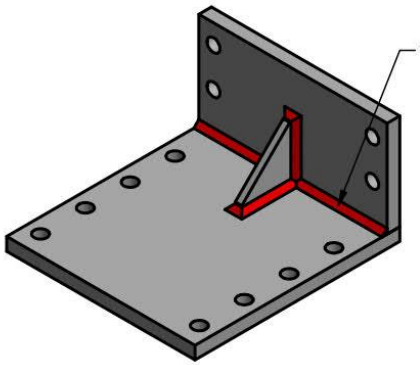

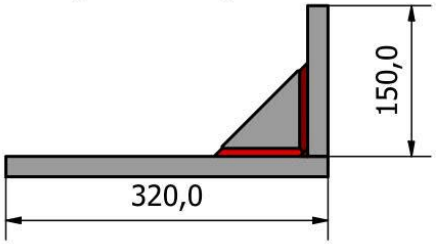

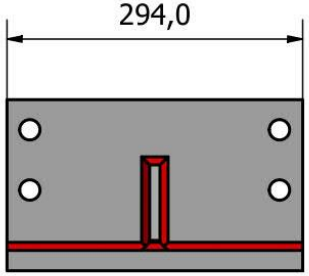

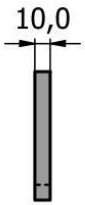

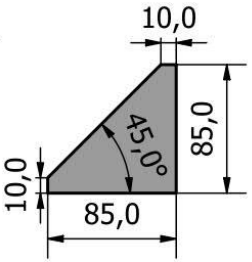

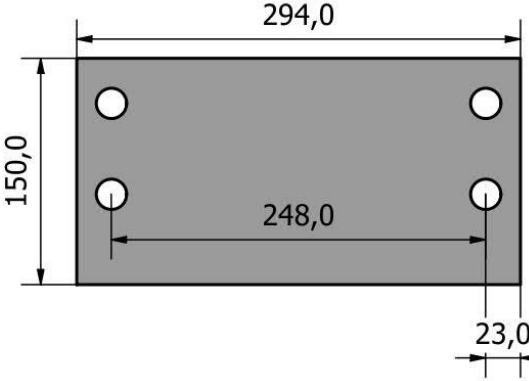

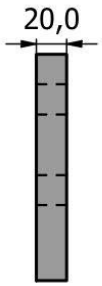

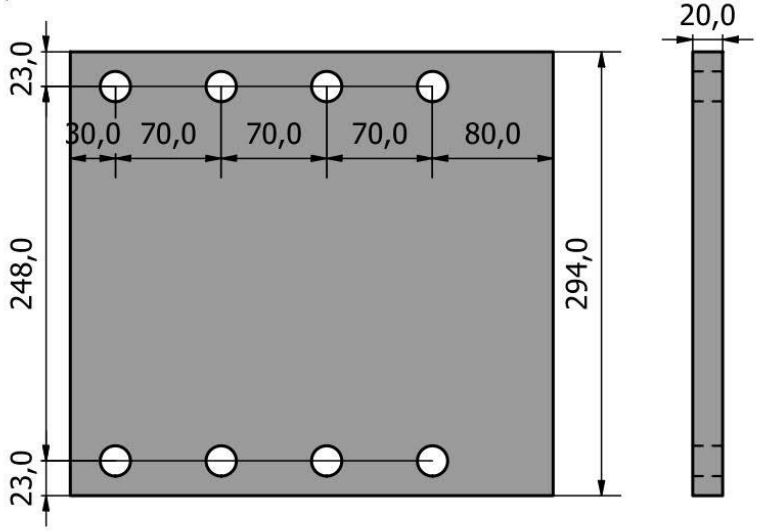

Notes:
1-Dimensions in mm with 0.1mm accuracy
2- Plates have Fy=350MPa and Fu=480MPa.
3- equal leg fillet weld with leg size of 8mm is used for welding.
4- Welding is for structural purposes (SP) with utilized weld metal: E48XX.
5-Required number of top gusset B is created by three plates and welding: 1

Designed by	Checked by	Approved by	Date
S. V.	P. Z.		6/25/2021

AUT University
School of Future Environment

Top gusset B

no: ST-006	Edition 2	Sheet 7 / 22

Top gusset C

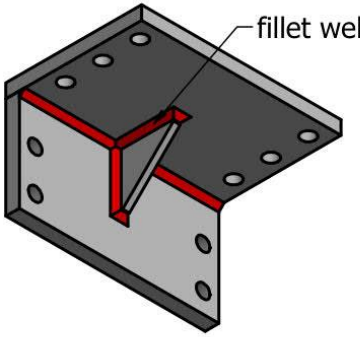

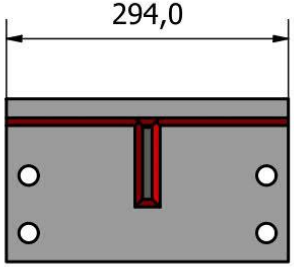

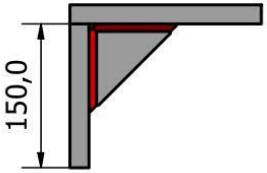

Notes:
1-Dimensions in mm with 0.1mm accuracy
2- Plates have Fy=350MPa and Fu=480MPa.
3- equal leg fillet weld with leg size of 8mm is used for welding.
4- Welding is for structural purposes (SP) with utilized weld metal: E48XX.
5-Required number of top gusset C is created by three plates and welding: **2**

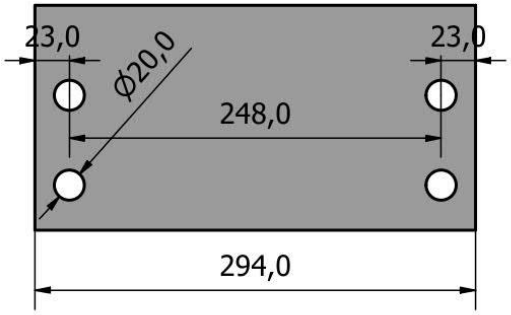

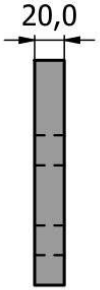

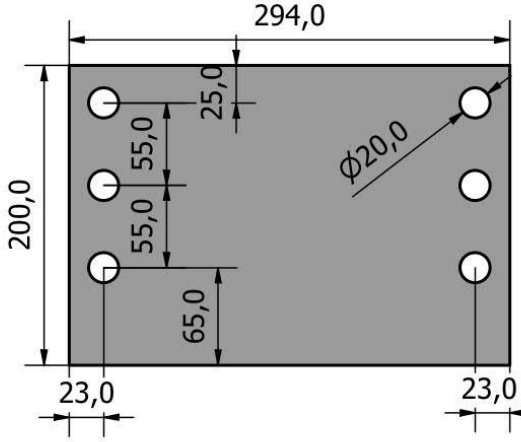

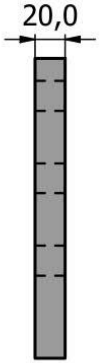

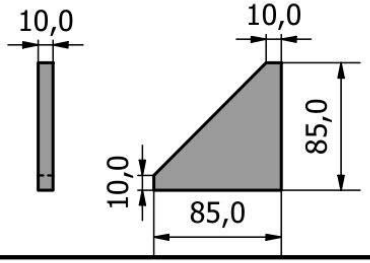

Designed by	Checked by	Approved by	Date
S. V.	P. Z.		6/25/2021

AUT University
School of Future Environment

Top gusset C

no: ST-007	Edition 2	Sheet 8 / 22

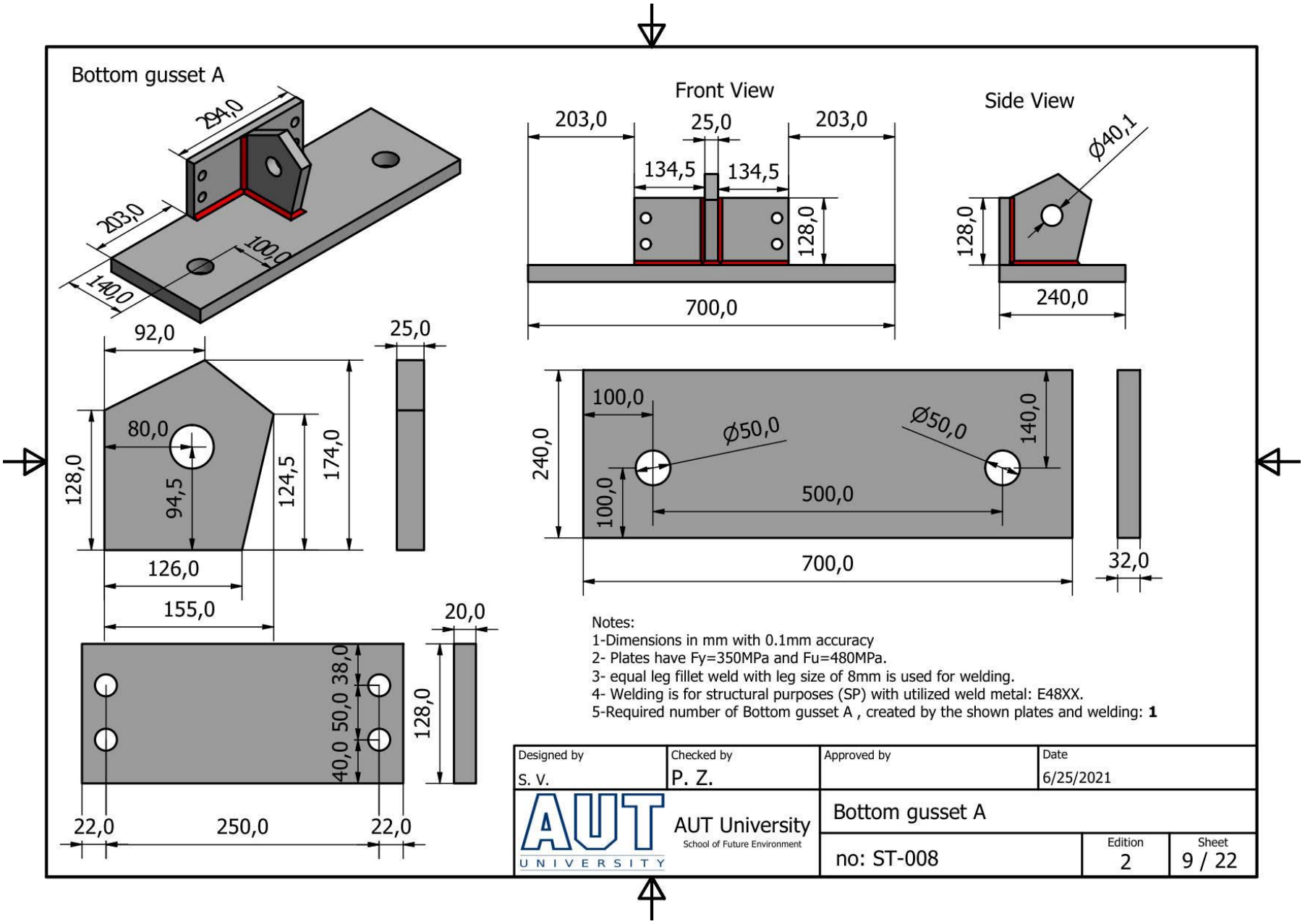
Bottom gusset A
294,0
203,0
100,0
140,0
Front View
203,0
25,0
203,0
134,5
134,5
128,0
700,0
Side View
Ø40,1
128,0
240,0
92,0
25,0
80,0
128,0
94,5
124,5
174,0
126,0
155,0
20,0
40,0
50,0
38,0
128,0
22,0
250,0
22,0
240,0
100,0
Ø50,0
Ø50,0
140,0
100,0
500,0
700,0
32,0
Notes:
1-Dimensions in mm with 0.1mm accuracy
2- Plates have Fy=350MPa and Fu=480MPa.
3- equal leg fillet weld with leg size of 8mm is used for welding.
4- Welding is for structural purposes (SP) with utilized weld metal: E48XX.
5-Required number of Bottom gusset A , created by the shown plates and welding: 1
Designed by
S. V.
Checked by
P. Z.
Approved by
Date
6/25/2021
AUT University
School of Future Environment
Bottom gusset A
no: ST-008
Edition
2
Sheet
9 / 22

Bottom gusset B

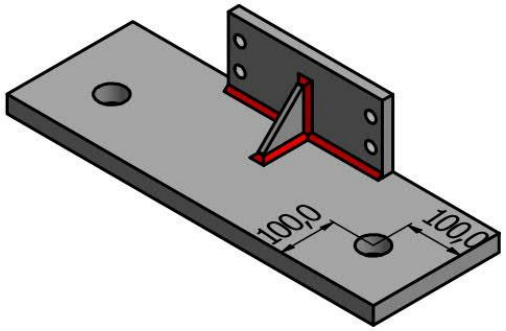

Side View

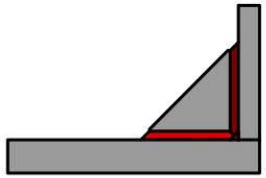

Front View

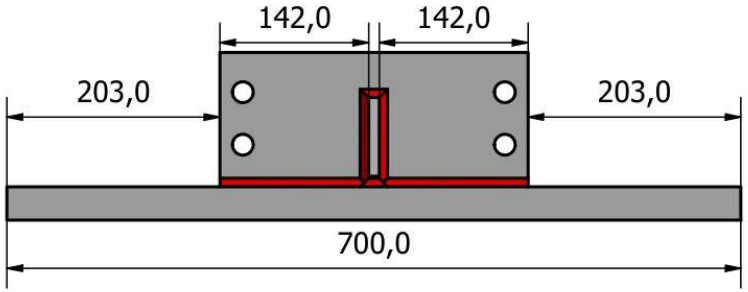

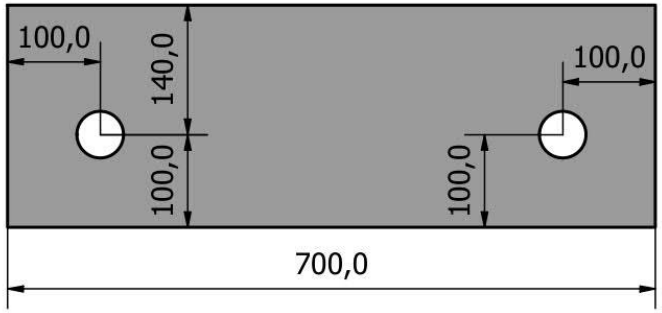

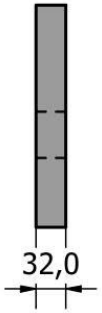

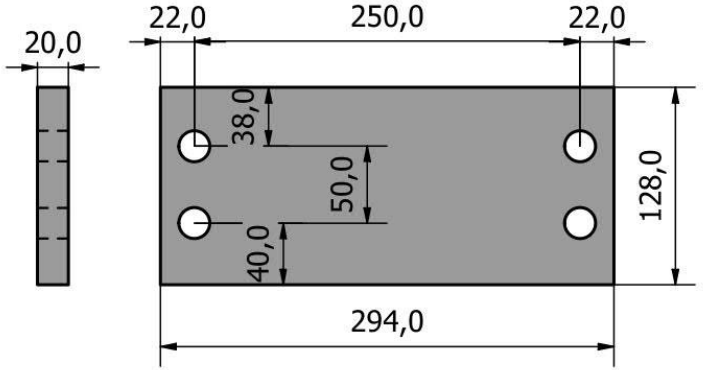

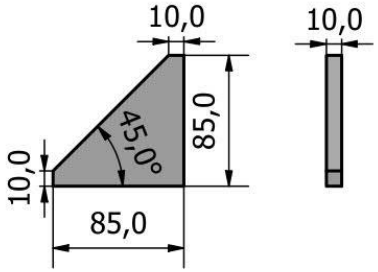

Notes:
1-Dimensions in mm with 0.1mm accuracy
2- Plates have Fy=350MPa and Fu=480MPa.
3- equal leg fillet weld with leg size of 8mm is used for welding.
4- Welding is for structural purposes (SP) with utilized weld metal: E48XX.
5-Required number of Bottom gusset B , created by the shown plates and welding: **1**

Designed by	Checked by	Approved by	Date
S. V.	P. Z.		6/25/2021

AUT University
School of Future Environment

Bottom gusset B

no: ST-009	Edition 2	Sheet 10 / 22

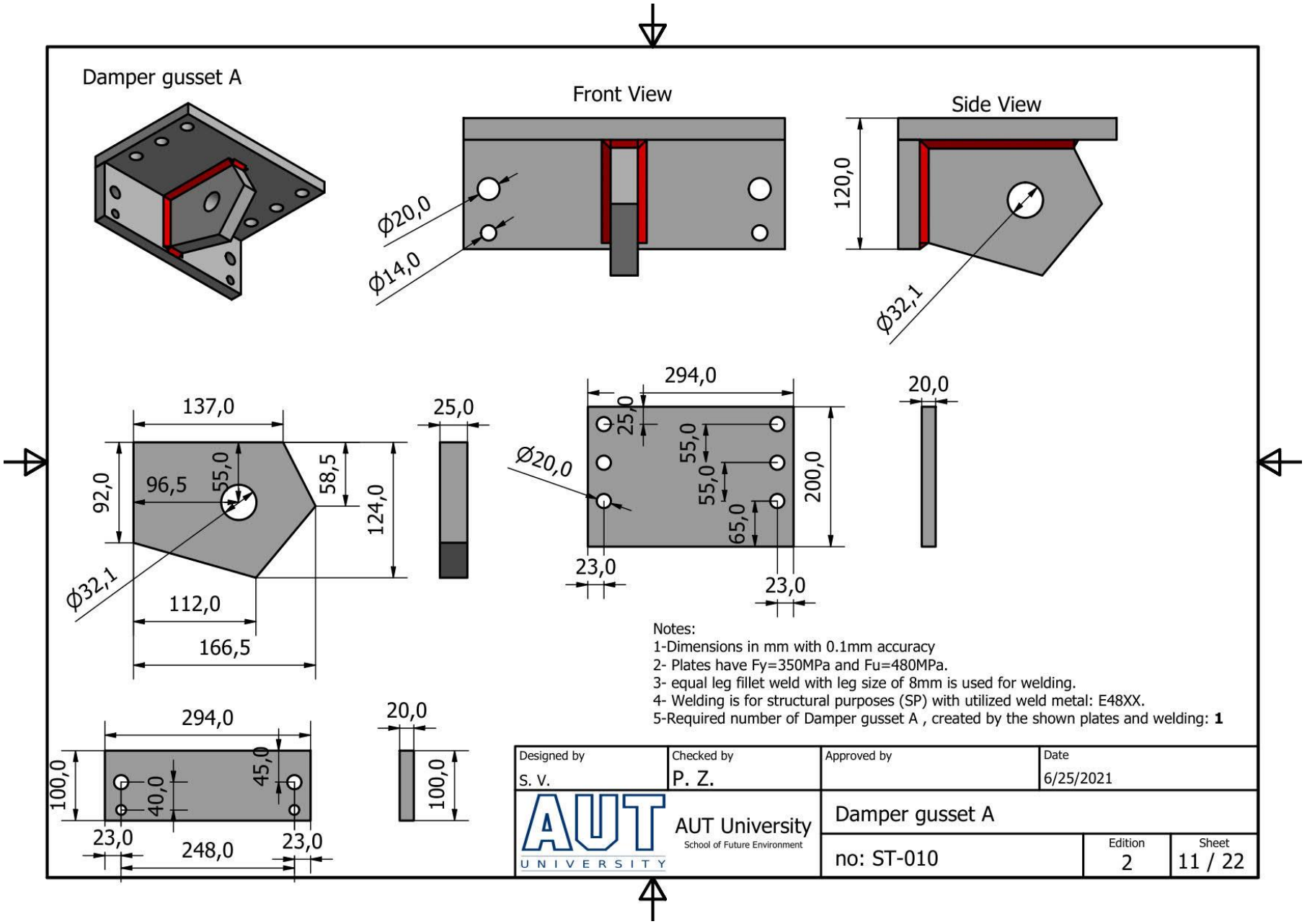
Damper gusset A
Front View
Side View
Ø20,0
Ø14,0
120,0
Ø32,1
137,0
25,0
92,0
96,5
55,0
58,5
124,0
Ø32,1
112,0
166,5
294,0
20,0
25,0
55,0
55,0
65,0
200,0
Ø20,0
23,0
23,0
294,0
20,0
100,0
40,0
45,0
100,0
23,0
248,0
23,0
Notes:
1-Dimensions in mm with 0.1mm accuracy
2- Plates have Fy=350MPa and Fu=480MPa.
3- equal leg fillet weld with leg size of 8mm is used for welding.
4- Welding is for structural purposes (SP) with utilized weld metal: E48XX.
5-Required number of Damper gusset A , created by the shown plates and welding: 1
Designed by
S. V.
Checked by
P. Z.
Approved by
Date
6/25/2021
AUT University
School of Future Environment
Damper gusset A
no: ST-010
Edition
2
Sheet
11 / 22

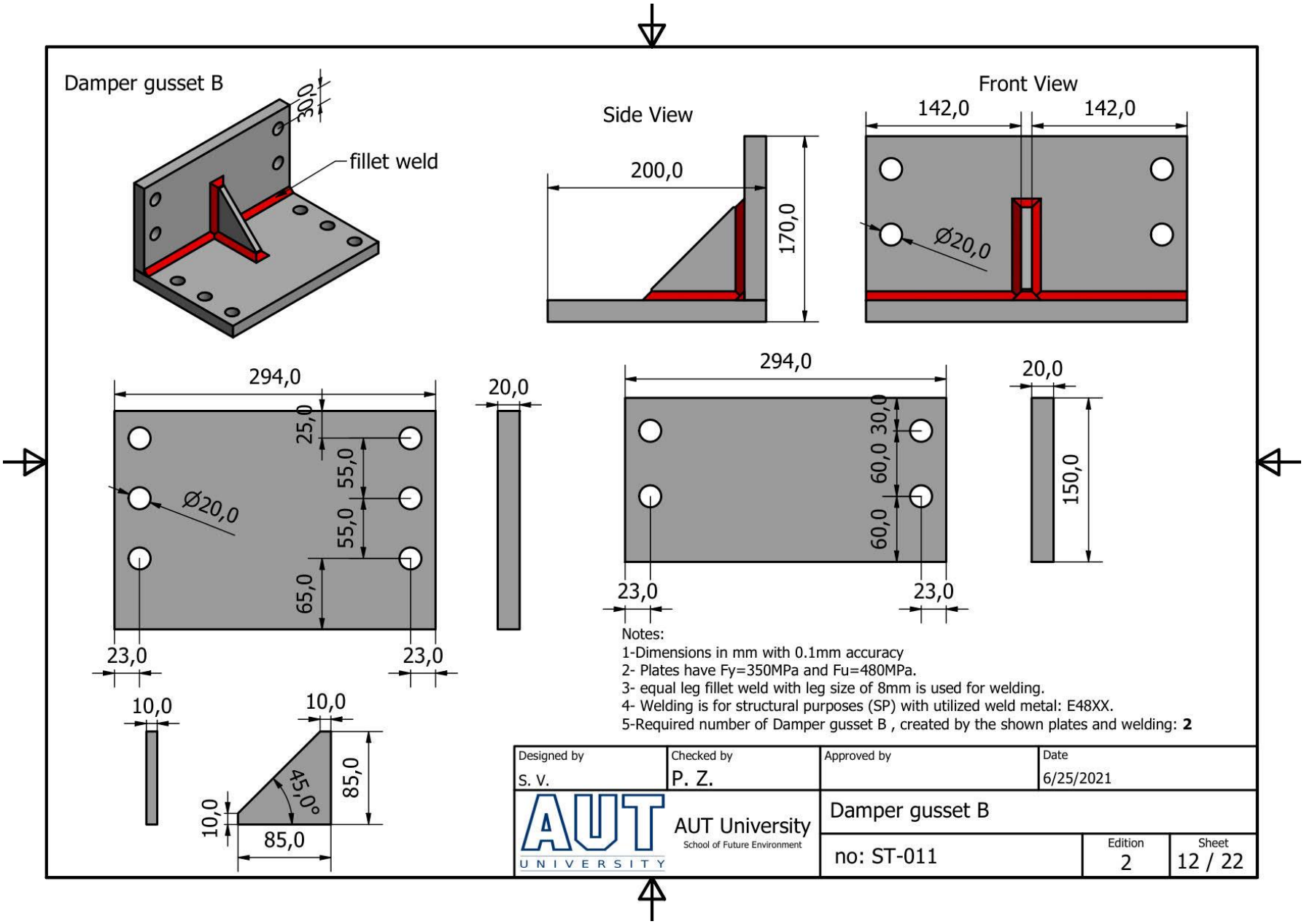
Damper gusset B
30,0
fillet weld
Side View
200,0
170,0
Front View
142,0
142,0
Ø20,0
294,0
25,0
55,0
55,0
65,0
Ø20,0
23,0
23,0
20,0
294,0
60,0
60,0
30,0
23,0
23,0
20,0
150,0
10,0
10,0
45,0°
85,0
10,0
85,0
Notes:
1-Dimensions in mm with 0.1mm accuracy
2- Plates have Fy=350MPa and Fu=480MPa.
3- equal leg fillet weld with leg size of 8mm is used for welding.
4- Welding is for structural purposes (SP) with utilized weld metal: E48XX.
5-Required number of Damper gusset B , created by the shown plates and welding: 2
Designed by
S. V.
Checked by
P. Z.
Approved by
Date
6/25/2021
AUT University
School of Future Environment
Damper gusset B
no: ST-011
Edition
2
Sheet
12 / 22

Damper Gusset C

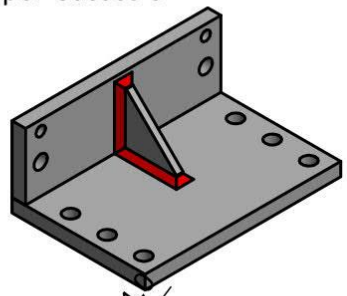

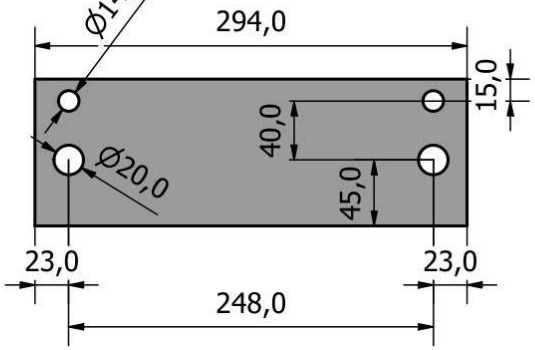

Side View

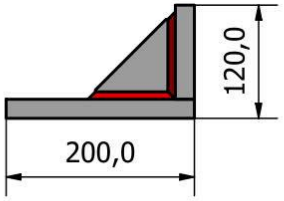

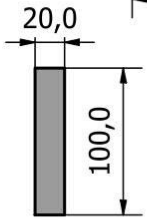

Front View

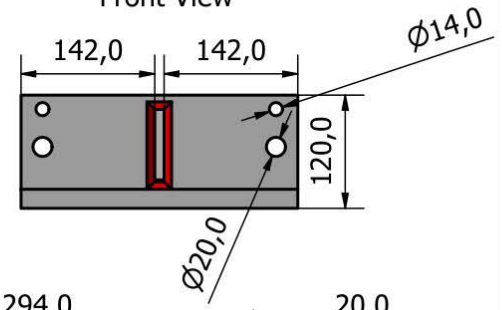

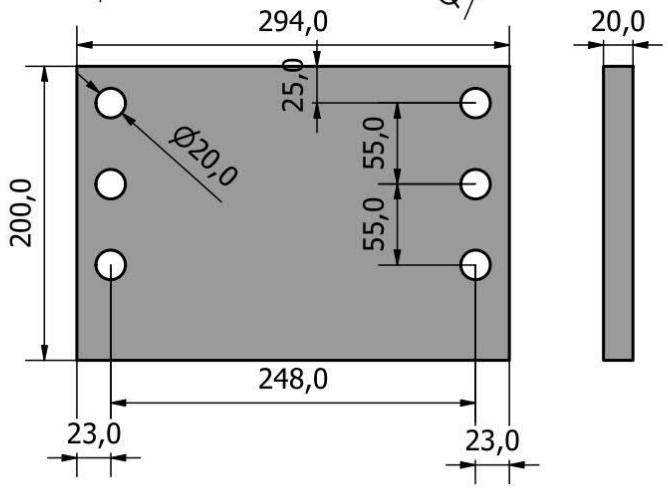

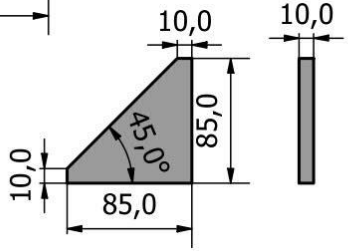

Notes:
1-Dimensions in mm with 0.1mm accuracy
2- Plates have Fy=350MPa and Fu=480MPa.
3- equal leg fillet weld with leg size of 8mm is used for welding.
4- Welding is for structural purposes (SP) with utilized weld metal: E48XX.
5-Required number of Damper gusset C , created by the shown plates and welding: **1**

Designed by	Checked by	Approved by	Date
S. V.	P. Z.		6/25/2021

AUT University
School of Future Environment

Damper gusset C

no: ST-012 | Edition 2 | Sheet 13 / 22

Bracket plate (for both sides of RC frame)

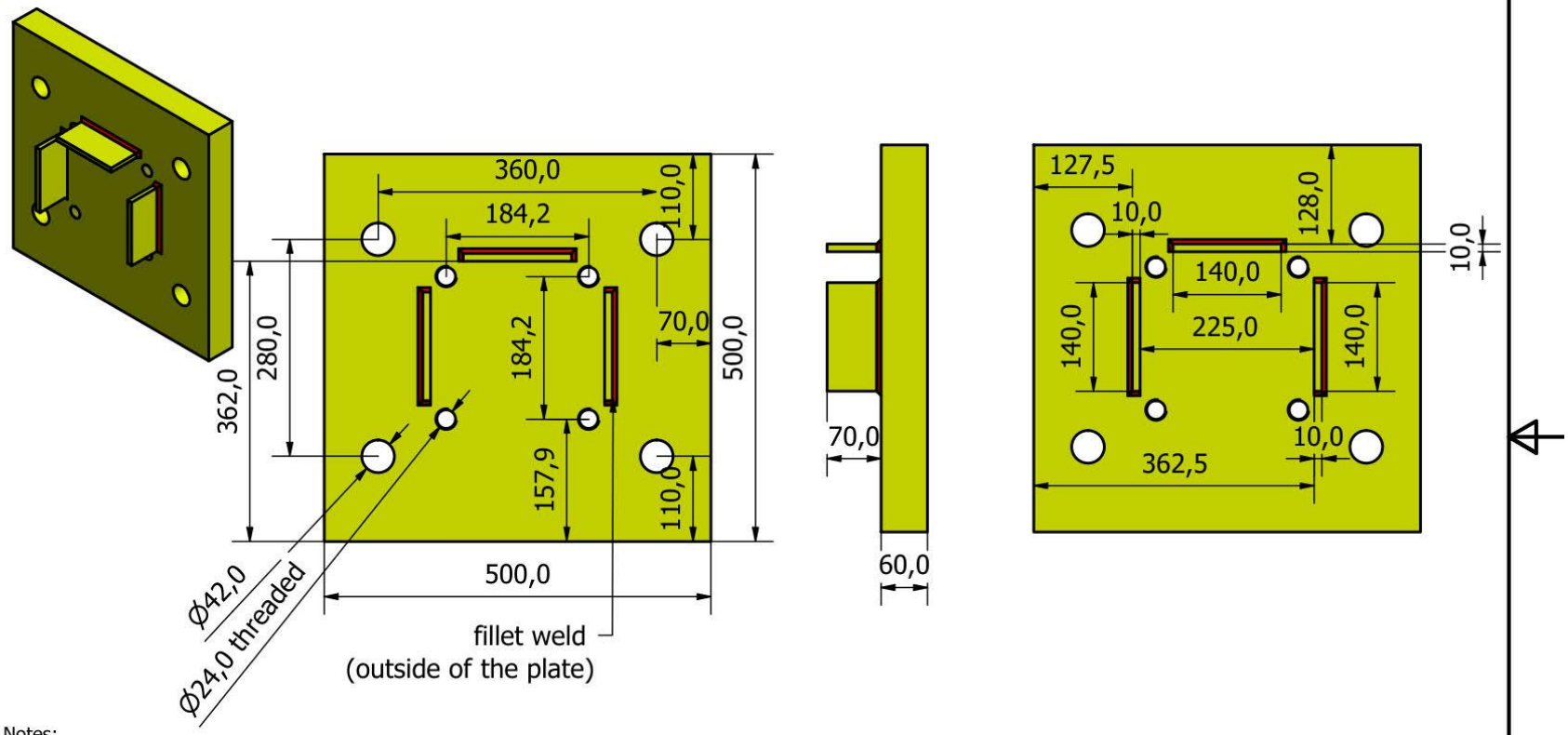

Notes:
1-Dimensions in mm.
2- Plates have at least Fy=350MPa and Fu=480MPa.
3- equal leg fillet weld with leg size of 6mm is used for welding. Welding is for the outside of the plates.
4- the M24 holes are threaded (threaded for M24 bolt).
5- Welding is for structural purposes (SP) with utilized weld metal: E48XX.
6-Required number of Yellow Plates: **2**

Designed by	Checked by	Approved by	Date
S. V.	P. Z.		6/25/2021
AUT University, School of Future Environment		bracket plate	
		no: ST-013	Edition 2 / Sheet 14 / 22

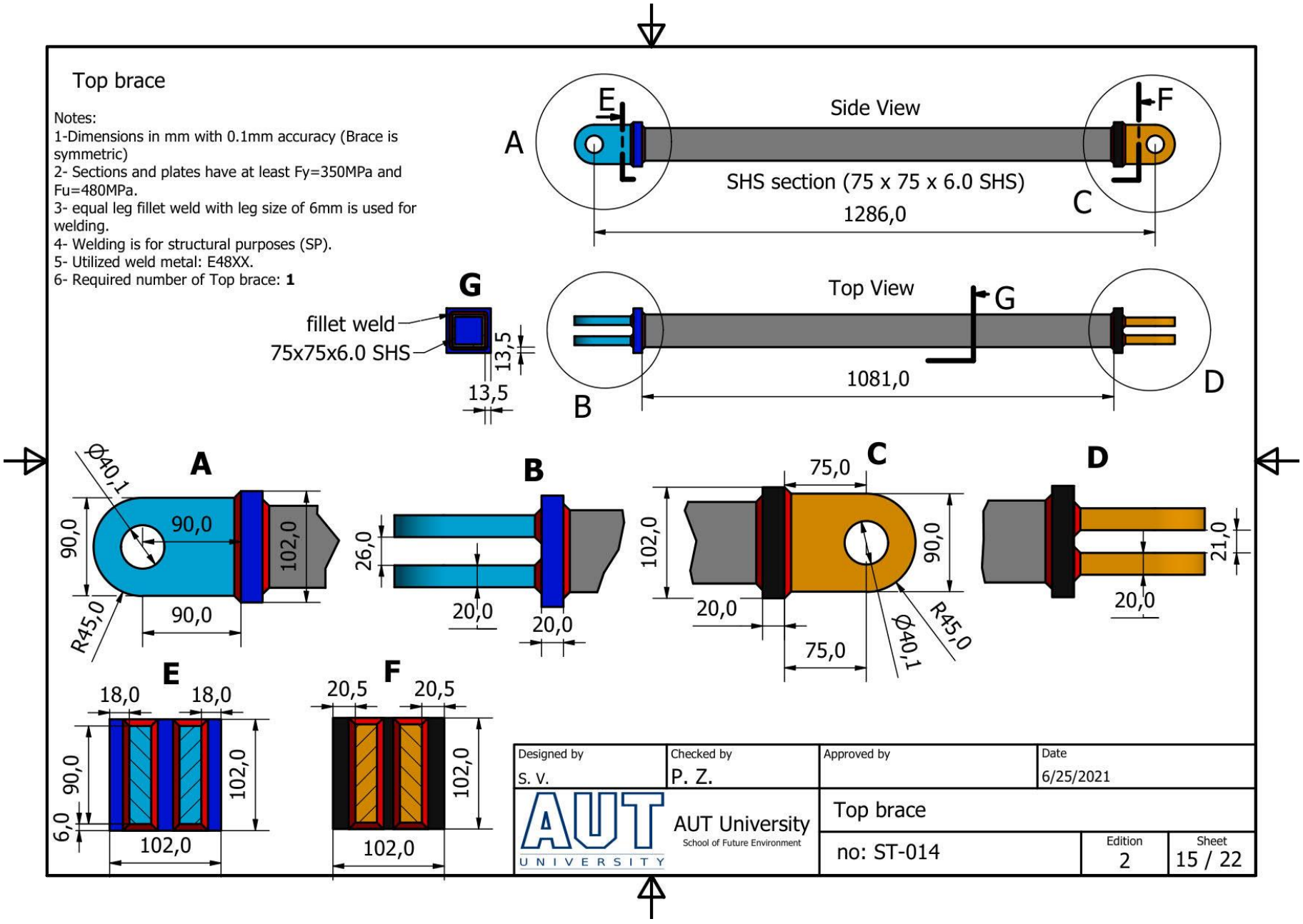
Top brace
Notes:
1-Dimensions in mm with 0.1mm accuracy (Brace is symmetric)
2- Sections and plates have at least Fy=350MPa and Fu=480MPa.
3- equal leg fillet weld with leg size of 6mm is used for welding.
4- Welding is for structural purposes (SP).
5- Utilized weld metal: E48XX.
6- Required number of Top brace: 1
Side View
SHS section (75 x 75 x 6.0 SHS)
1286,0
Top View
1081,0
fillet weld
75x75x6.0 SHS
13,5
13,5
A
B
C
D
E
F
G
Φ40,1
90,0
90,0
102,0
R45,0
26,0
20,0
20,0
75,0
102,0
90,0
20,0
75,0
21,0
20,0
18,0
18,0
6,0
20,5
20,5
Designed by
S. V.
Checked by
P. Z.
Approved by
Date
6/25/2021
AUT University
School of Future Environment
Top brace
no: ST-014
Edition
2
Sheet
15 / 22

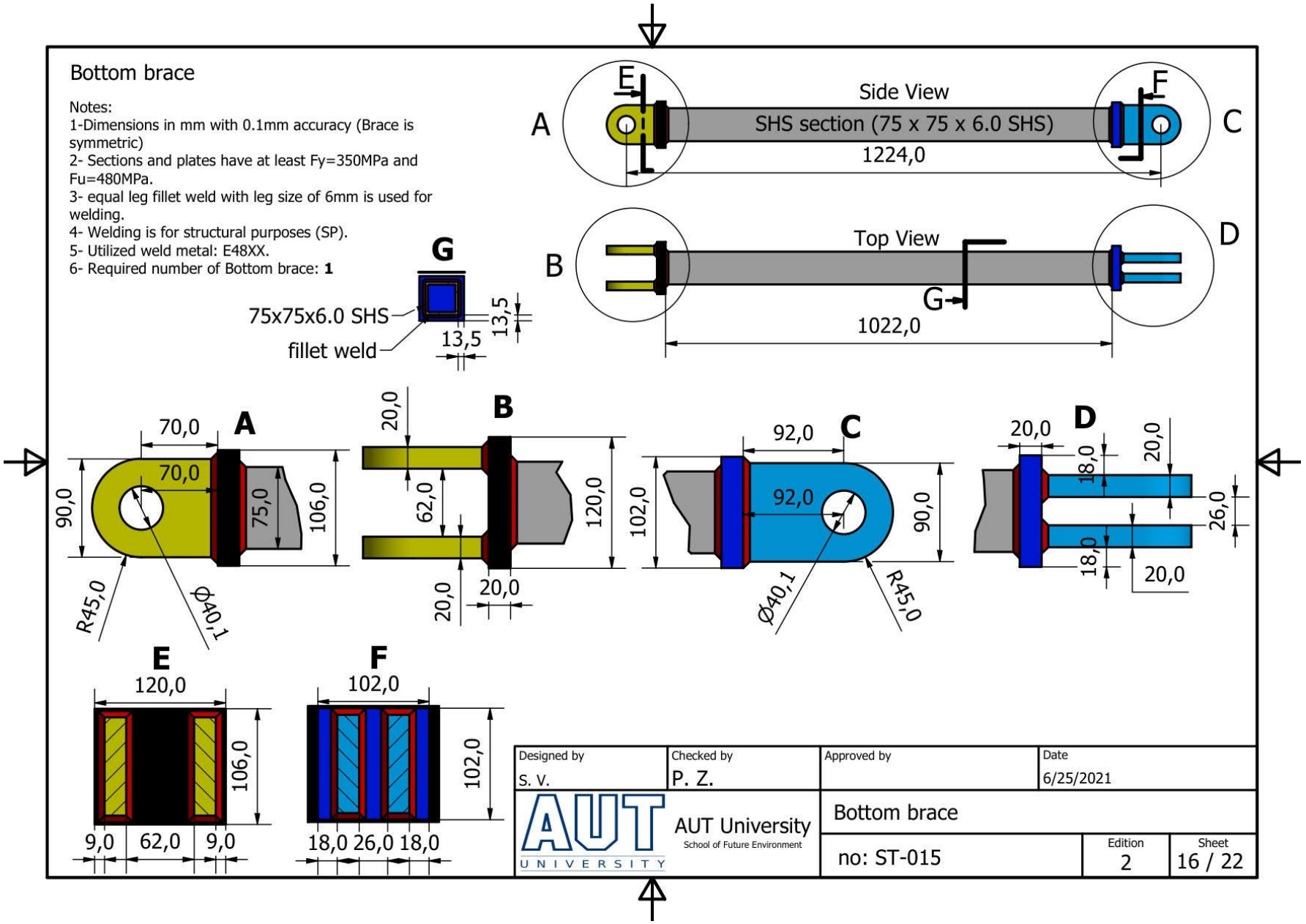
Bottom brace
Notes:
1-Dimensions in mm with 0.1mm accuracy (Brace is symmetric)
2- Sections and plates have at least Fy=350MPa and Fu=480MPa.
3- equal leg fillet weld with leg size of 6mm is used for welding.
4- Welding is for structural purposes (SP).
5- Utilized weld metal: E48XX.
6- Required number of Bottom brace: 1
Side View
SHS section (75 x 75 x 6.0 SHS)
1224,0
Top View
1022,0
75x75x6.0 SHS
fillet weld
13,5
A
B
C
D
E
F
G
70,0
90,0
75,0
106,0
R45,0
ϕ40,1
20,0
62,0
120,0
92,0
102,0
Ø40,1
R45,0
18,0
26,0
120,0
106,0
9,0
62,0
102,0
18,0 26,0 18,0
Designed by
S. V.
Checked by
P. Z.
Approved by
Date
6/25/2021
AUT University
School of Future Environment
Bottom brace
no: ST-015
Edition
2
Sheet
16 / 22

Damper Brace (Female part)

Notes:
1-Dimensions in mm with 0.1mm accuracy (Brace is symmetric)
2- Sections and plates have at least Fy=350MPa and Fu=480MPa.
3- Except for the female tube with fillet weld (leg size = 5mm), the rest have utilized equal leg fillet weld with leg size of 6mm.
4- Welding is for structural purposes (SP).
5- Utilized weld metal: E48XX.
6- Required number of damper brace (female part): **1**
7- The female CHS part would make a telescopic action with the male part, to form the RSFJ brace.

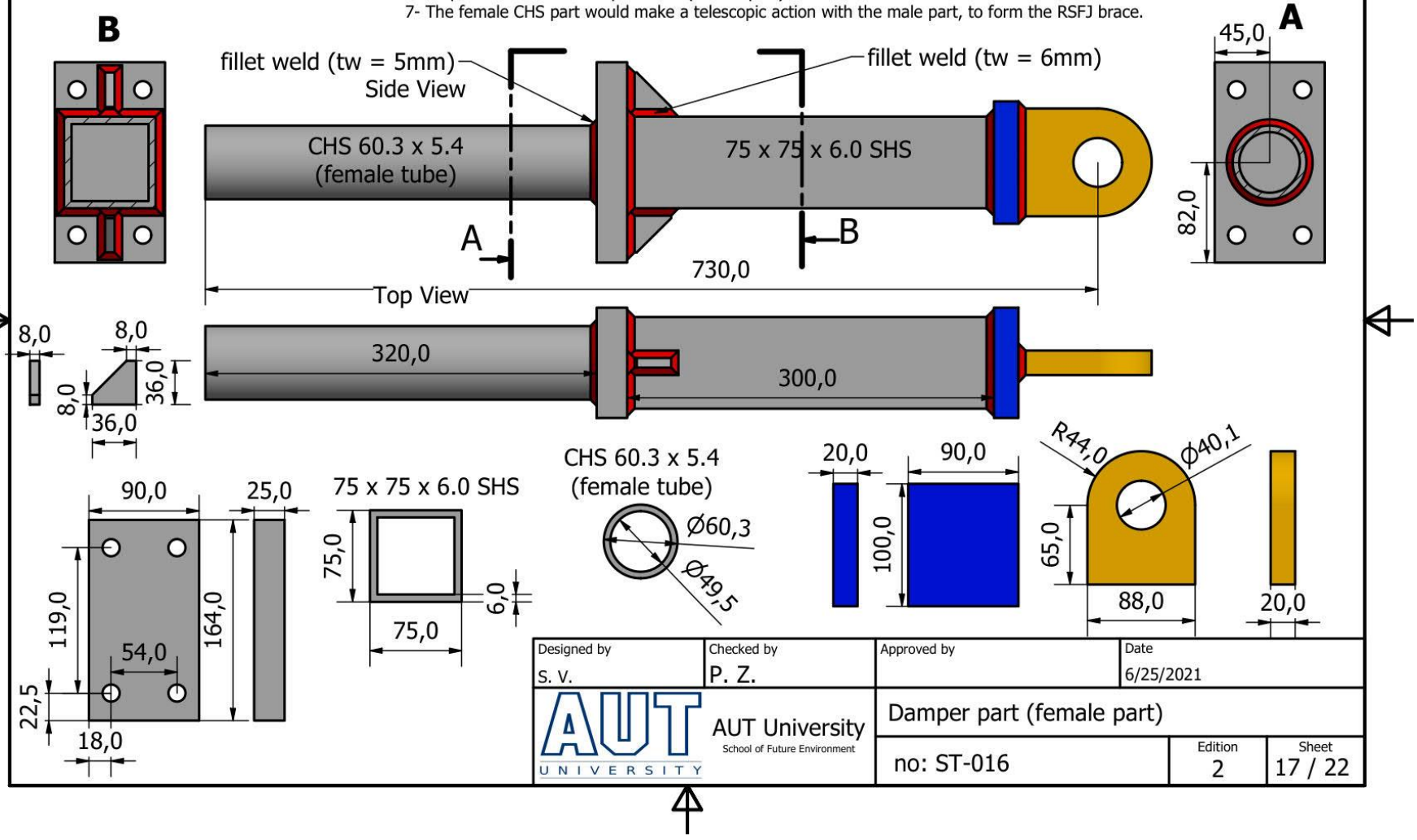

Designed by	Checked by	Approved by	Date
S. V.	P. Z.		6/25/2021

AUT University
School of Future Environment

Damper part (female part)

no: ST-016	Edition 2	Sheet 17 / 22

Damper Brace (Male part)

Notes:
1-Dimensions in mm with 0.1mm accuracy (Brace is symmetric)
2- Sections and plates have at least Fy=350MPa and Fu=480MPa.
3- Except for the male tube with fillet weld (leg size = 5mm), the rest have utilized equal leg fillet weld with leg size of 6mm.
4- Welding is for structural purposes (SP).
5- Utilized weld metal: E48XX.
6- Required number of damper brace (male part): **1**

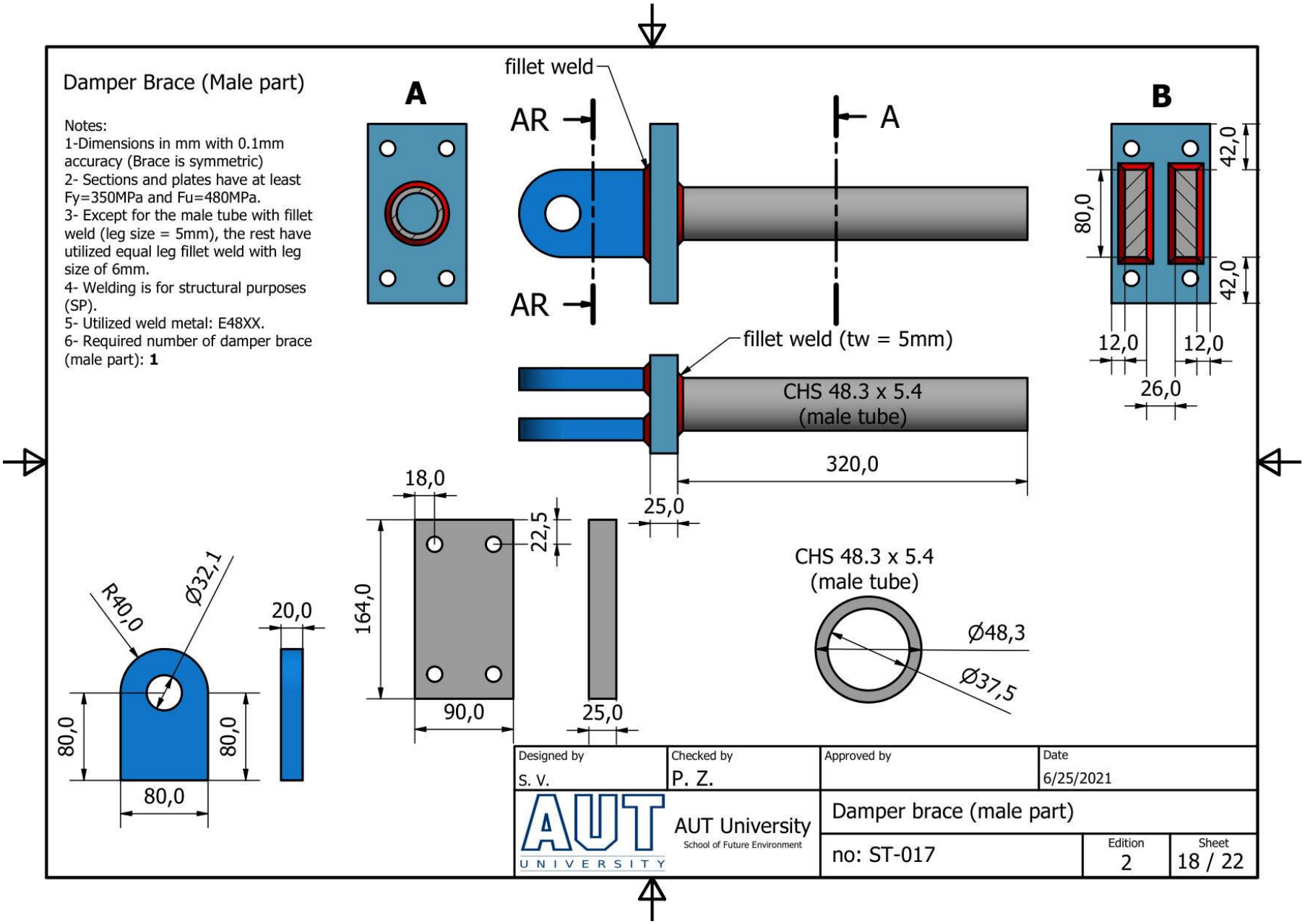

Designed by	Checked by	Approved by	Date
S. V.	P. Z.		6/25/2021

AUT University
School of Future Environment

Damper brace (male part)

no: ST-017	Edition 2	Sheet 18 / 22

Pins for the test setup

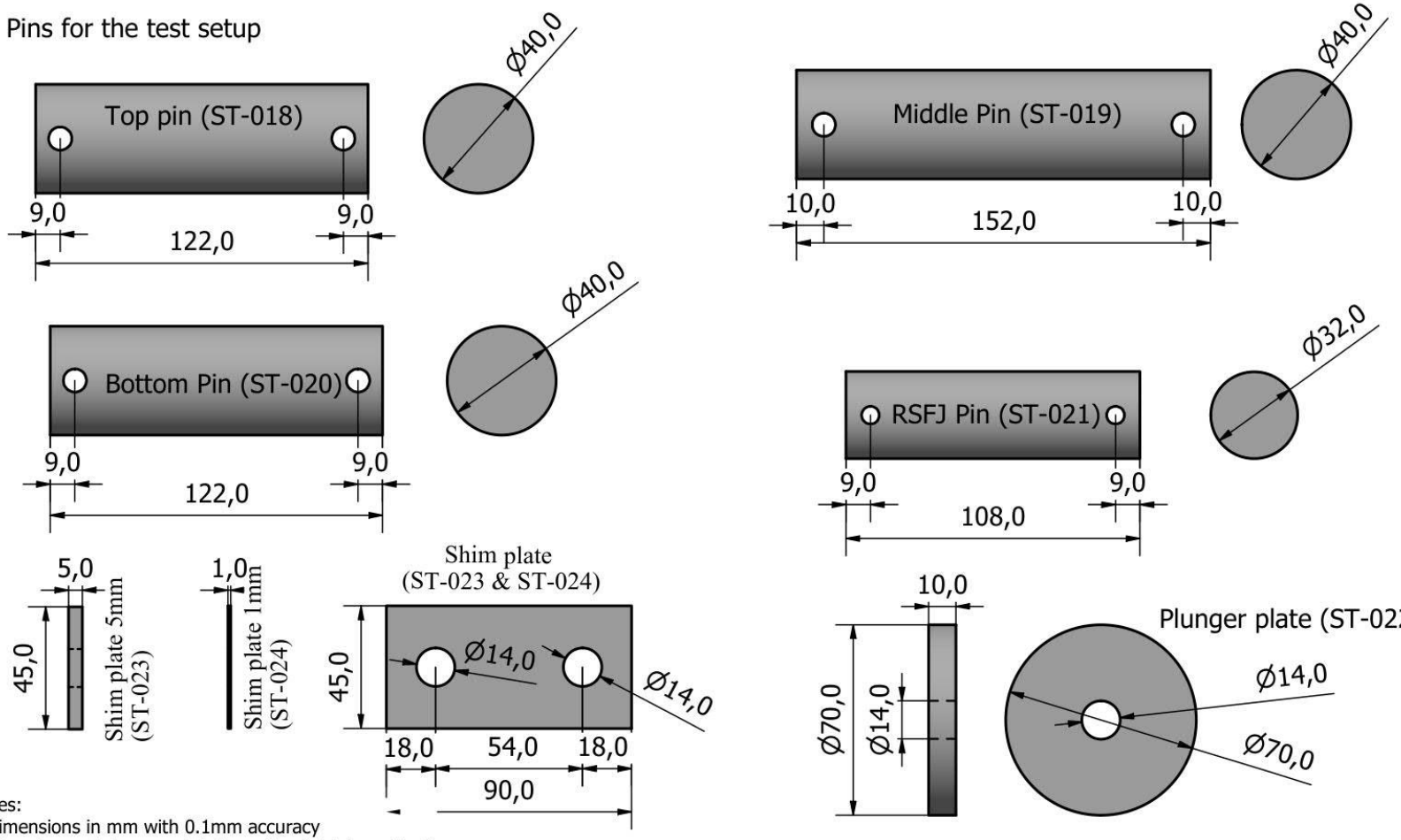

Notes:
1-Dimensions in mm with 0.1mm accuracy
2- The pins and plunger plate have the yield strength of Fy=700MPa.
3- Required number of each pin: **1**
4- Required number of plunger plate: **4**
5- For each pin, two Linchpin is required**.**
6-Shim plates have the same dimensions, with different thickness (1mm and 5mm)

Designed by	Checked by	Approved by	Date
S. V.	P. Z.		6/25/2021

AUT University
School of Future Environment

Pins and Plunger plate

no: ST-018~024	Edition	Sheet
	2	19 / 22

Damper Assembly
(The Resilient Slip Friction Joint)

Notes:
1-Dimensions in mm with 0.01mm accuracy (Damper is symmetric)
2- The cap plates (orange) and middle plates (black) have the yield strength of Fy=700MPa.
3- Required number of damper assembly: **2 (therefore, 4 middle plates and 4 cap plates are required)**
4- Due to complex shape of cap and middle plate, the current drawing cannot provide all the details of the damper, thus the solidwork file of the cap and middle plates will be provided for machining.

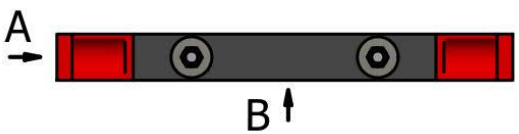

(A) Front view

(B) Top view

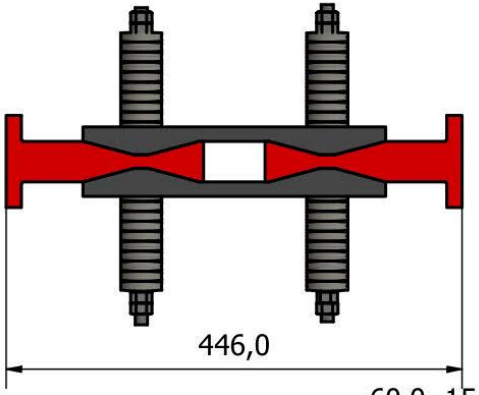

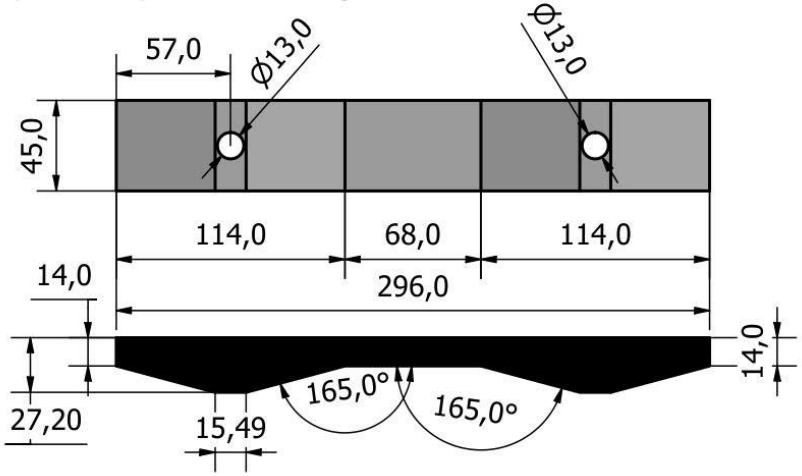

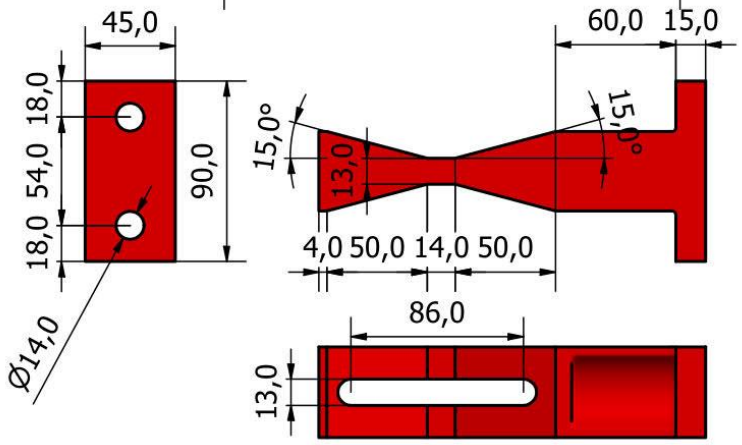

Designed by	Checked by	Approved by	Date
S. V.	P. Z.		6/25/2021

AUT University
School of Future Environment

RSFJ damper

no: ST-025	Edition 2	Sheet 20 / 22

Grip for UTM

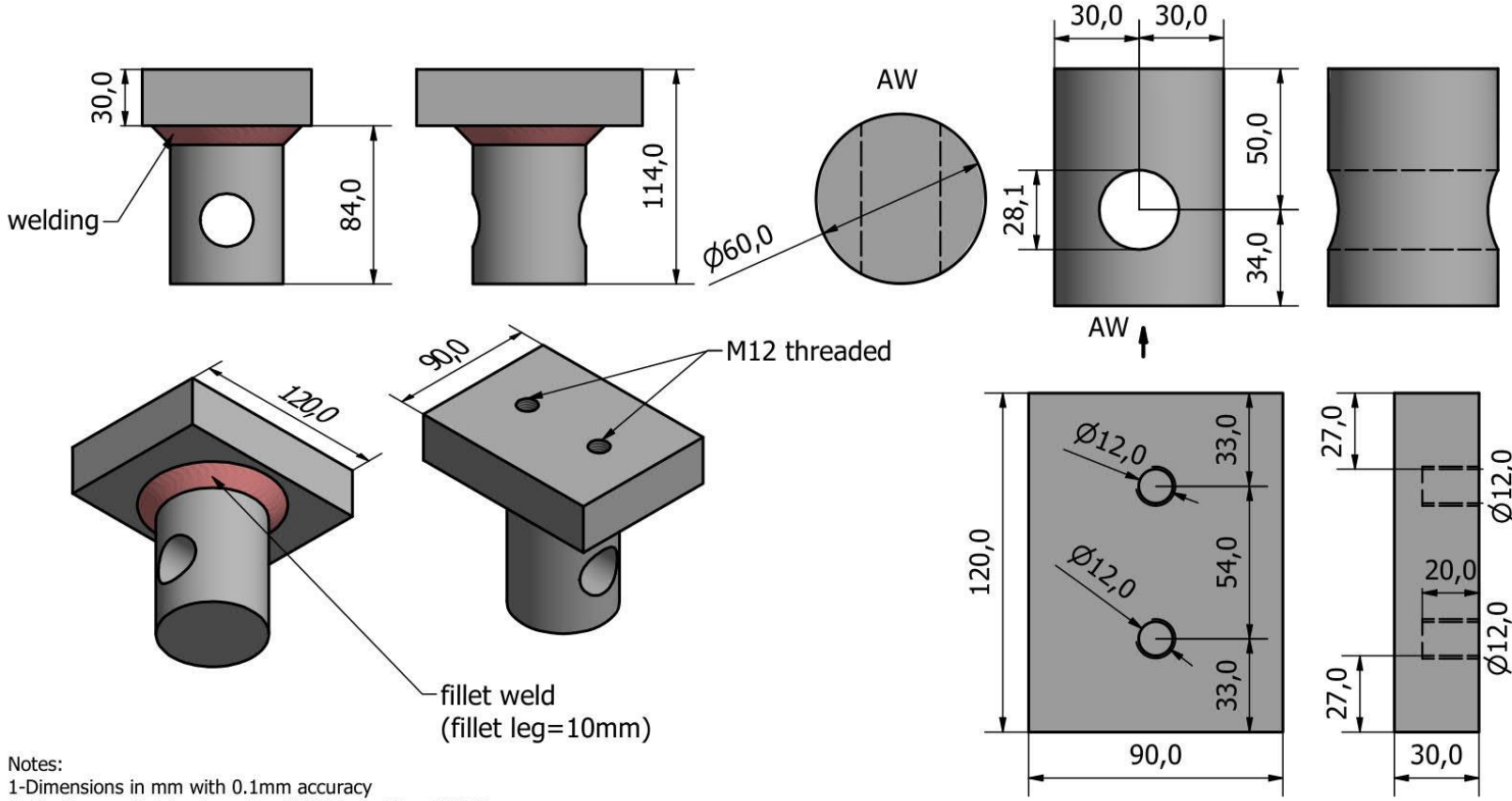

Notes:
1-Dimensions in mm with 0.1mm accuracy
2- Sections and plates have Fy=350MPa and Fu=480MPa.
3- equal leg fillet weld with leg size of 10mm is used for welding.
4- Welding is for structural purposes (SP).
5- Utilized weld metal: E48XX.
6- Grip assembly is consists of a cylinder part and a plate.
7- Required number of grip assembly: **2**

Designed by	Checked by	Approved by	Date
S. V.	P. Z.		6/25/2021

AUT University
School of Future Environment

Grip for UTM

no: ST-026	Edition 2	Sheet 21 / 22

RC frame overall dimension

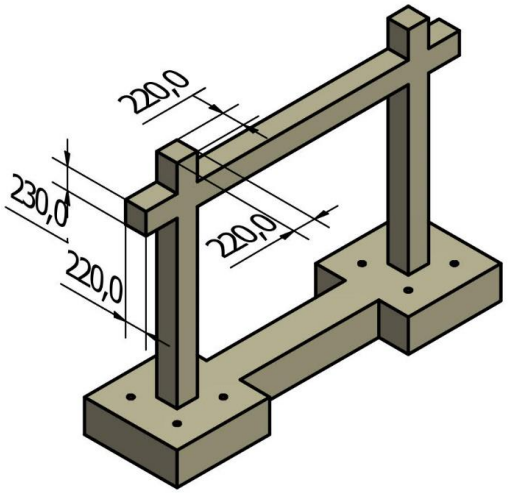

Front View

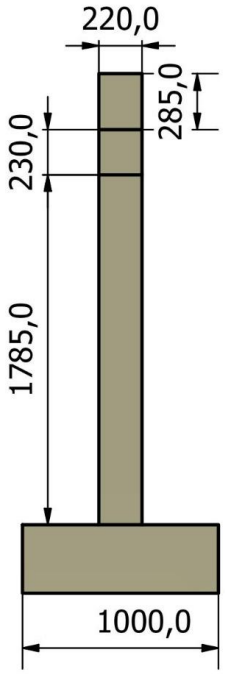

Side View

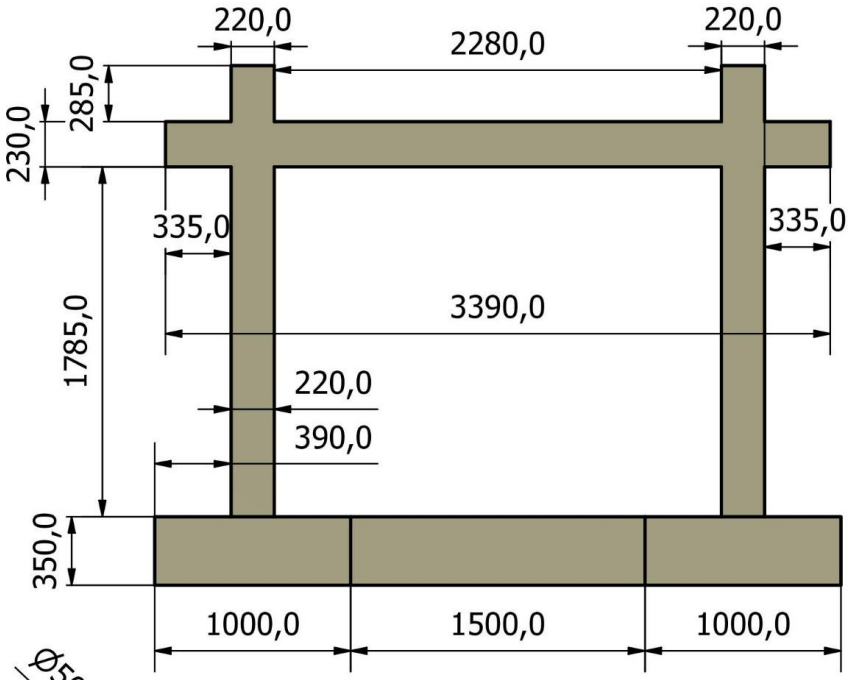

Top View

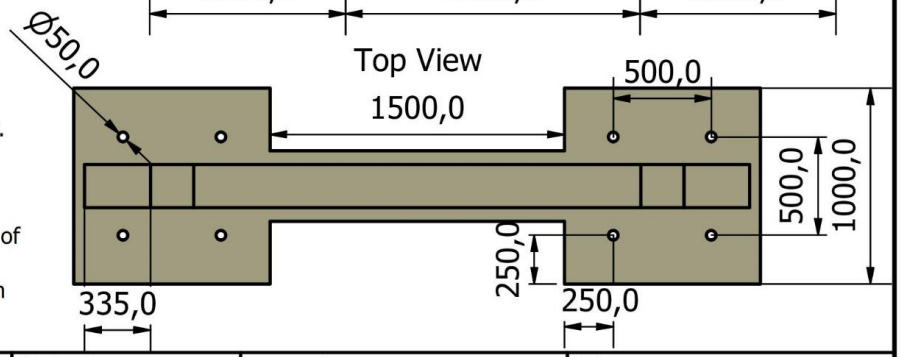

Note:

1- The rebar detailing and concrete specifications will be provided in a separate document.
2- f'c is 20 MPa (should not surpass 25MPa).
3- The rebar grade 300E deformed is utilized for reinforcement.
4-Please provide three concrete cylinder sample for each frame.
5-three sample of reinforcement rebar with the length of 300mm is required for each size of utilized rebar.
6-concrete cover (from center of main rebar to the surface) is assumed to be 35 to 38 mm
7- We required two RC frame for test.

Designed by	Checked by	Approved by	Date
S. V.	P. Z.		6/25/2021

AUT University
School of Future Environment

RC frame

no: ST-027	Edition 2	Sheet 22 / 22

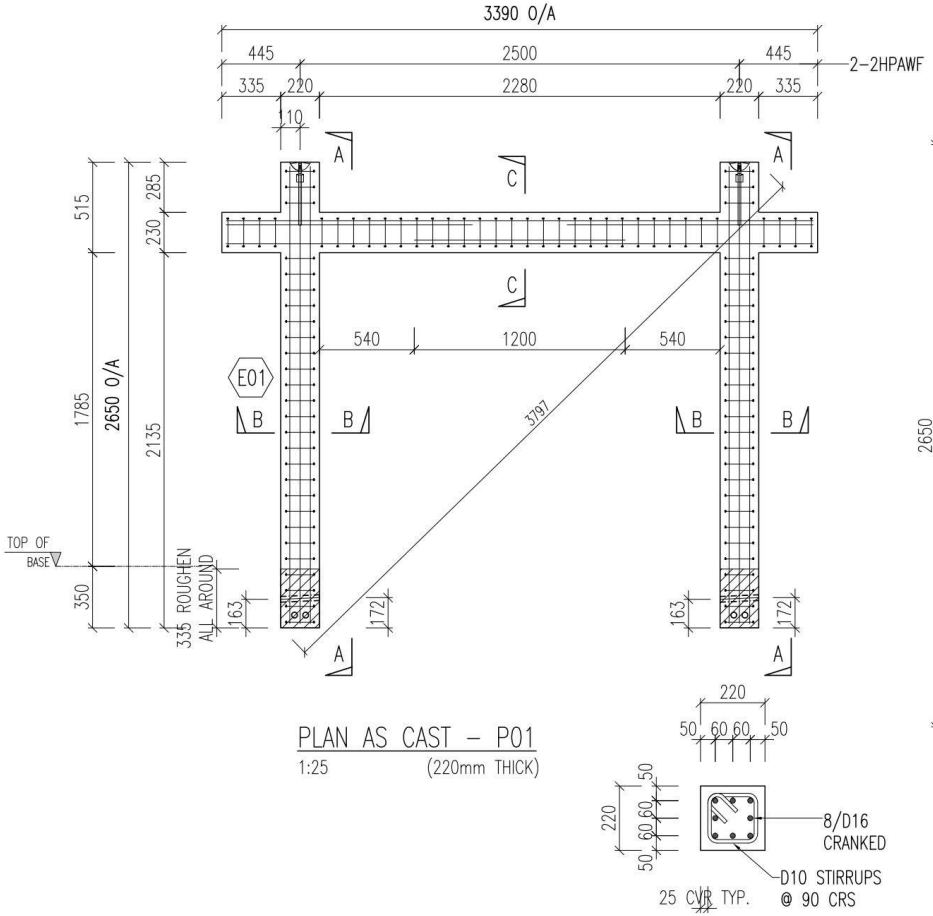

PLAN AS CAST – P01

1:25 (220mm THICK)

SECTION B–B

1:15

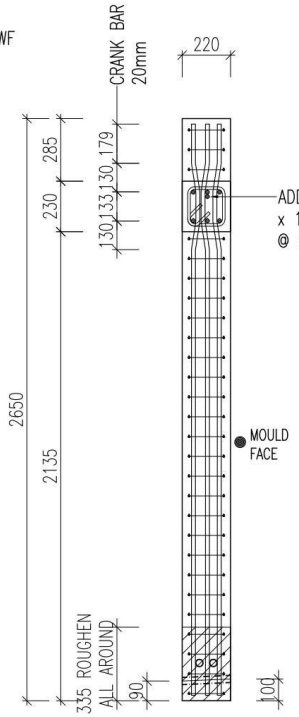

SECTION A–A

1:20

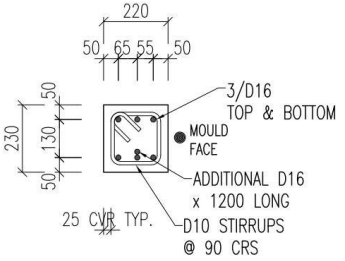

SECTION C–C

1:15

FIRST CASTING

25MPa - SPECIAL MIX

FOR APPROVAL ONLY
NOT FOR CONSTRUCTION

DRAWING ISSUE		
2	FOR APPROVAL	02.11.21
1	FOR APPROVAL	28.10.21
Check	PAUL	SCALE
Drawn	N.B.	1:10 U.N.O

CONCRETE NOTES		
MIX DESIGN	4013 CONTHE	
FINISHES	MOULD FACE	FS U.N.O.
	TOP FACE	U3 U.N.O.
	SIDES	FORMED U.N.O.
MIN. CONCRETE f'c AT 28 DAYS	25MPa	
MIN. CONC. STRENGTH AT LIFTING	20MPa	

REINFORCING NOTES

CONCRETE COVER = 25mm U. N. O.
HR=ROUND HIGH YEILD STEEL 500EMPA
HD=DEFORMED HIGH YEILD STEEL 500EMPA
D=DEFORMED MILD STEEL 300EMPA
R=ROUND MILD STEEL 300EMPA
REINFORCING TO AS/NZS 4671 MICRO ALLOY

LIFTING TYPE		PANEL DATA	
DEMOULD	CD1	GROSS AREA = 1.845	m^2
LOADING	CL1	VOLUME = 0.406	m^3
PLACING	P1	WEIGHT = 1.055	t
S = SPECIAL		A3 DENSITY = 2.6	t/m3

concreTec
NEW ZEALAND LIMITED
MANUFACTURERS OF PRECAST CONCRETE
587 Ridge Road, Pokeno - 09 275 9906 - www.concretec.co.nz

Project Title: AUT UNIVERSITY RC FRAME TEST

Drawing Title: DETAILS 220 THICK PANEL – P01

Job No. 6012 | Drg.No. P01 | Issue 2

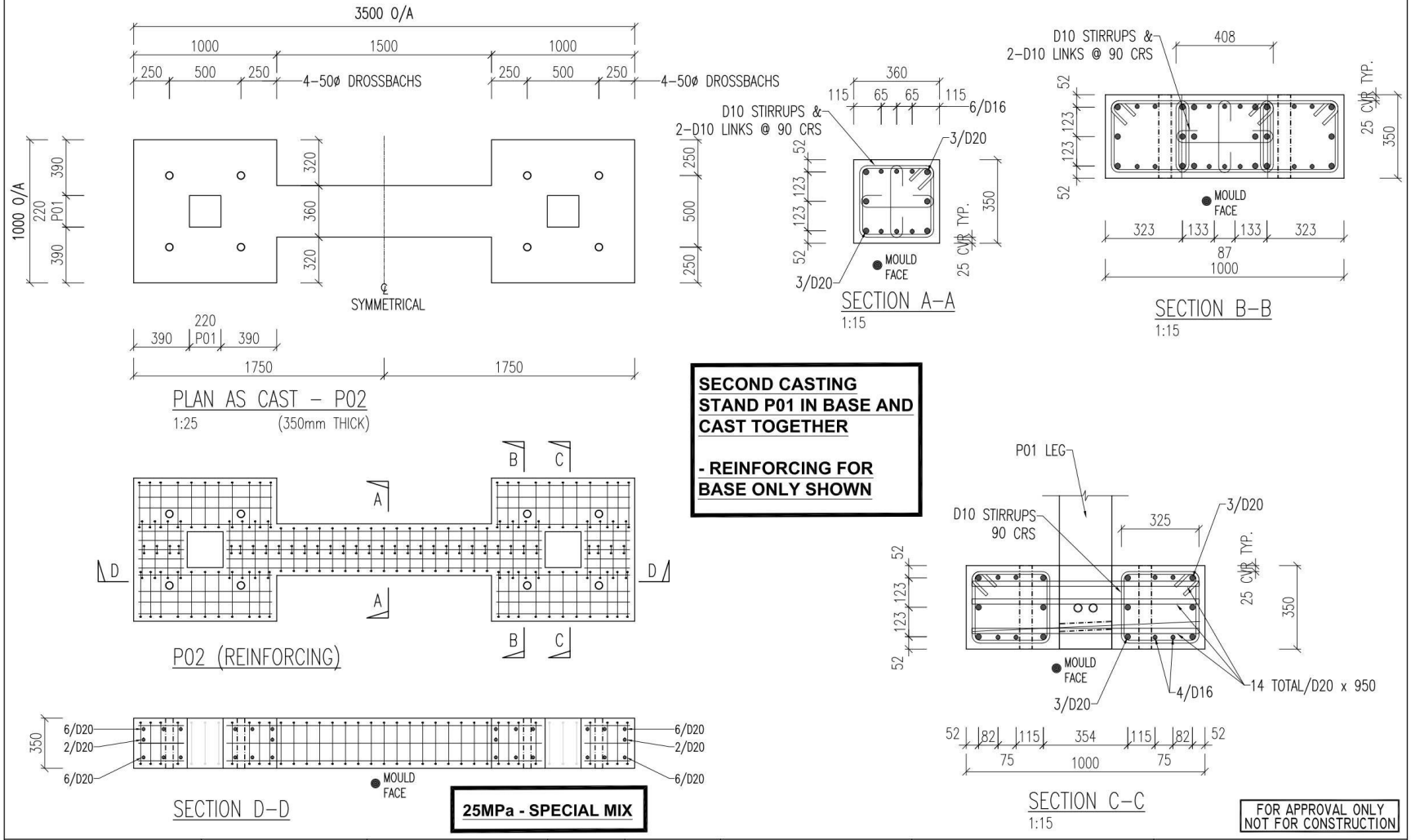

DRAWING ISSUE			CONCRETE NOTES			REINFORCING NOTES	LIFTING TYPE		PANEL DATA	
			MIX DESIGN	4013 CONTHE		CONCRETE COVER = 25mm U. N. O.	DEMOULD	CD5	GROSS AREA = 2.4	m^2
			FINISHES	MOULD FACE	F5 U.N.O.	HR=ROUND HIGH YEILD STEEL 500EMPA	LOADING	CL5	VOLUME = 0.84	m^3
2	FOR APPROVAL	02.11.21		TOP FACE	U3 U.N.O.	HD=DEFORMED HIGH YEILD STEEL 500EMPA	PLACING	P8	WEIGHT = 2.18	t
1	FOR APPROVAL	28.10.21		SIDES	FORMED U.N.O.	D=DEFORMED MILD STEEL 300EMPA	S = SPECIAL		A3 DENSITY = 2.6	t/m3
Check	PAUL	SCALE	MIN. CONCRETE f'c AT 28 DAYS 25MPa			R=ROUND MILD STEEL 300EMPA				
Drawn	N.B.	1:10 U.N.O	MIN. CONC. STRENGTH AT LIFTING 20MPa			REINFORCING TO AS/NZS 4671 MICRO ALLOY				

concreTec
NEW ZEALAND LIMITED
MANUFACTURERS OF PRECAST CONCRETE
587 Ridge Road, Pokeno - 09 275 9906 - www.concretec.co.nz

Project Title: AUT UNIVERSITY RC FRAME TEST

Drawing Title: BASE 350 THICK PANEL – P02

Job No. 6012 | Drg.No. P02 | Issue 2

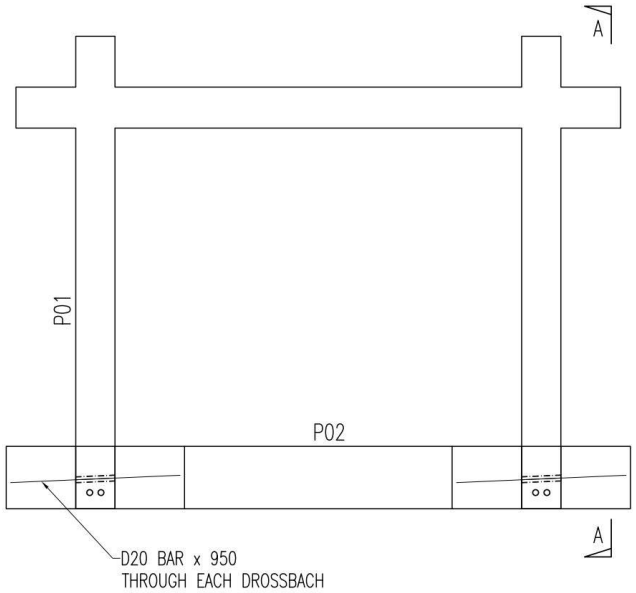

FRAME CAST AS ONE UNIT

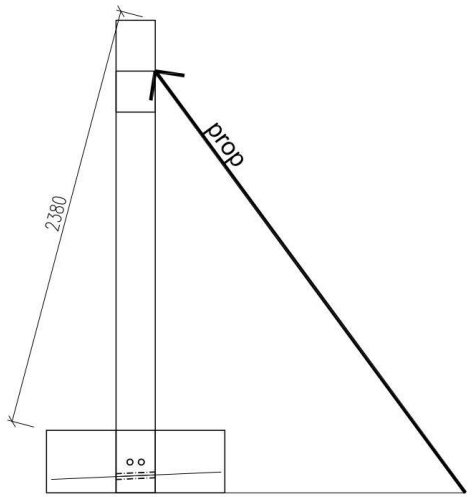

SECTION A–A

FRAME WIEGHT = 3.235T

FOR APPROVAL ONLY
NOT FOR CONSTRUCTION

DRAWING ISSUE		
1	FOR APPROVAL	02.11.21
Check	PAUL	SCALE
Drawn	N.B.	1:10 U.N.O

CONCRETE NOTES		
MIX DESIGN	4013 CONTHE	
FINISHES	MOULD FACE	F5 U.N.O.
	TOP FACE	U3 U.N.O.
	SIDES	FORMED U.N.O.
MIN. CONCRETE f'c AT 28 DAYS 25MPa		
MIN. CONC. STRENGTH AT LIFTING 20MPa		

REINFORCING NOTES
CONCRETE COVER = 25mm U. N. O.
HR=ROUND HIGH YEILD STEEL 500EMPA
HD=DEFORMED HIGH YEILD STEEL 500EMPA
D=DEFORMED MILD STEEL 300EMPA
R=ROUND MILD STEEL 300EMPA
REINFORCING TO AS/NZS 4671 MICRO ALLOY

LIFTING TYPE		PANEL DATA	
DEMOULD	–	GROSS AREA = –	m^2
LOADING	–	VOLUME = –	m^3
PLACING	–	WEIGHT = –	t
S = SPECIAL		A3 DENSITY = 2.6 t/m3	

concreTec
NEW ZEALAND LIMITED
MANUFACTURERS OF PRECAST CONCRETE
587 Ridge Road, Pokeno - 09 275 9906 - www.concretec.co.nz

Project Title: AUT UNIVERSITY RC FRAME TEST

Drawing Title: FRAME

Job No. 6012 | Drg.No. P03 | Issue 1